

Copyright

by

Stefano Freguia

2002

Modeling of CO₂ Removal from Flue Gases with Monoethanolamine

by

Stefano Freguia

Thesis

Presented to the Faculty of the Graduate School of
The University of Texas at Austin
in Partial Fullfillment
of the Requirements
of the Degree of

Master of Science in Engineering

The University of Texas at Austin
May, 2002

Modeling of CO₂ Removal from Flue Gases with Monoethanolamine

APPROVED BY

SUPERVISING COMMITTEE:

Supervisor:

Gary T. Rochelle

Thomas F. Edgar

Acknowledgments

I would like to thank Dr. Rochelle for his continuous support. He provided me with all the ideas that served to the accomplishment of this work.

I would also like to acknowledge those who financially supported me during these two years, in particular Fluor Daniel and the Texas Advanced Technology Program.

I would like to thank Dr. Ottmers, senior lecturer at The University of Texas at Austin, for the energy with which he helped me get into graduate school.

I would like to thank Satish Reddy, Carl Mariz and Ray Won at Fluor Daniel for the important information they provided to me for the accomplishment of this project. I also would like to thank Venkat Venkatamaran at Aspen Technology, for the helpful information he made available to me in order to use ASPEN PLUS at the highest level.

I want to express appreciation for all the graduate students that worked in Dr. Rochelle's group during the time I spent at the University of Texas. They certainly made my work as a graduate student a more pleasant experience.

Finally I would like to thank my parents for their emotional and financial support.

May 2002
Austin, TX

Modeling of CO₂ Removal from Flue Gases with Monoethanolamine

By

Stefano Freguia, M.S.E.

The University of Texas at Austin, 2002

SUPERVISOR: Dr. Gary T. Rochelle

The public interest in CO₂ removal from flue gases has recently increased, due to more restrictive regulations on emissions of greenhouse gases. The use of a classic absorption/stripping process downstream of power plants is the only option so far. Aqueous monoethanolamine is the most common solvent used to absorb CO₂. Its problem is that the energy required for solvent regeneration is high.

This work focuses on the creation of an ASPEN PLUS rate-based model of an absorption/stripping process for removal of CO₂ with 30 wt% aqueous monoethanolamine. The absorber was modeled with RATEFRAC and kinetic reactions, the stripper with RATEFRAC and equilibrium reactions. The rates of absorption follow the Interface-Pseudo-First-Order approximation, with rate constants adjusted to match experimental data (Dang, 2001). The equilibrium follows an Electrolyte-NRTL model, regressed using data from Jou et al. (1995).

The model was used to analyze the effects of process variables on energy requirement. The solvent circulation rate seems to be the most effective variable to adjust. Other process changes were analyzed, such as amine neutralization, stripper pressure decrease, split flow configuration, absorber intercooling. Even if the energy requirement is lowered by some options, the extent of the reduction is not large enough to make the process economic on a large scale power plant.

Table of Contents

List of Tables	ix
List of Figures.....	xii
Chapter 1 Introduction	1
1.1. Alkanolamines and their reactions with CO ₂	2
1.2. The absorption/stripping process for CO ₂ capture.....	5
1.3. Modeling of the process and scope of work	8
Chapter 2 Thermodynamic Model.....	11
2.1. Solution chemistry and equilibrium governing equations	11
2.2. Solubility data used in this work	13
2.3. System non-idealities.....	14
2.4. The Electrolyte-NRTL Model	15
2.4.1. Electrolyte-NRTL model applied to CO ₂ -amine systems	17
2.5. Regression.....	18
2.5.1. Reference states used in this work.....	19
2.5.2. Henry's constant	20
2.5.3. Regression results	21
Chapter 3 Rate Model	25
3.1. Rate data used in this work.....	26
3.2. Modeling of mass transfer in liquid boundary layer.....	28
3.2.1. Film theory.....	28
3.2.2. Eddy diffusivity theory	29
3.3. Mass transfer with fast chemical reaction	30
3.3.1. Pseudo first order models	30
3.3.2. IPFO model limitations: parallel reactions and rich conditions	34

3.4. Rigorous boundary layer integration: Bishnoi FORTRAN model	35
3.4.1. Simple equilibrium model and physical properties used in the Bishnoi FORTRAN model	36
3.4.2. Results with the Bishnoi model	38
3.5. RATEFRAC kinetic model	39
3.5.1. User kinetic subroutine	41
3.5.2. Results with the RATEFRAC model	42
3.6. Recommendations	46
Chapter 4 Integrated Modeling	47
4.1. Absorber models	49
4.1.1. RATEFRAC model	49
4.1.2. RADFRAC model	52
4.2. Stripper model and heat stable salts	58
4.2.1. Instantaneous reactions approximation and gas phase resistance	59
4.2.2. Heat stable salts	63
4.3. Combined absorber and stripper model	67
Chapter 5 Process Analysis and Optimization	71
5.1. Reboiler and heat requirements	71
5.2. Solvent rate optimization	73
5.3. Effects of the heights of the columns	80
5.3.1. Effect of absorber height, CO ₂ concentration and removal	81
5.3.2. Effect of stripper height	89
5.4. Effect of MEA concentration and MEA partial neutralization into heat stable salts	90
5.5. Effect of stripper pressure and the concept of lost work	93
5.6. Temperature effect on the absorber	98
5.6.1. Effect of solvent temperature	98
5.6.2. Intercooling effect	100
5.7. Split flow configuration	102
5.7.1. Effect of split feed extraction location	106
5.7.2. Effect of split flow rate	107
Chapter 6 Conclusions and Recommendations	111

6.1. Model: conclusions and recommendations.....	111
6.1. Process: conclusions and recommendations.....	112
APPENDIX A Regression Inputs and Results	115
APPENDIX B FORTRAN Kinetic Subroutine for RATEFRAC	119
APPENDIX C ASPEN PLUS Inputs and Results	128
C.1. Base case APEN PLUS input file	128
C.2. Input summary for base case.....	144
C.3. ASPEN PLUS process flow diagram.....	145
C.4. ASPEN PLUS simulation detailed results for 3% CO ₂ base case ...	146
C.5. Detailed results for 10% CO ₂ -90% removal case (Figures 5.18 and 5.19)	153
C.6. Hints on convergence of the model.....	159
APPENDIX D High CO₂ Base Case for Absorption/Stripping Model	161
APPENDIX E Detailed Simulation Results.....	173
Nomenclature	175
References	178
Vita	183

List of Tables

Table 2.1. Values of constants for T dependent expressions for equilibrium constants and Henry's constant for CO ₂ in H ₂ O.	13
Table 2.2. Reference states and their definitions.....	20
Table 2.3. Values of regressed interaction parameters for the CO ₂ -MEA-H ₂ O Electrolyte-NRTL model.....	21
Table 2.4. Comparison of VLE models and experimental data (Jou et al., 1995) at 60 °C and 120 °C.	23
Table 3.1. Some literature data on the reaction between CO ₂ and aqueous MEA. .	27
Table 3.2. Summary of inputs, unknowns, equations and boundary conditions for the rigorous integration of the boundary layer with the Bishnoi code. .	36
Table 3.3. RATEFRAC modeling results of Dang's data.....	43
Table 4.1. Analysis of importance of the kinetics at absorber and stripper temperature.	61
Table 4.2. Summary of results of simulation of Bellingham base case and test runs.	70
Table 5.1. Optimization of solvent flow rate, 3% mole CO ₂ in flue gas, 85 % removal, 0.1 mol HSS/mol MEA, reboiler duty normalized to moles of CO ₂ removed and divided by a typical industrial value in MJ/Kmol, stripper bottom pressure 1.7 atm.	74
Table 5.2. Results of absorber height analysis for the three cases of Figure 5. 9. ..	82
Table 5.3. Effect of stripper height on the reboiler duty; 3 mol% CO ₂ in flue gas, 85 % removal, 33.5 wt% MEA, 0.1 mol HSS/mol MEA _{tot} , solvent rate optimized.	89

Table 5.4. Effect of heat stable salt fraction of total MEA on specific reboiler duty, optimum L/G and loadings, at 3% CO ₂ , 85% removal.....	91
Table 5.5. Effect of reboiler pressure on relative specific reboiler duty, relative specific lost work and other operating parameters, 3% CO ₂ , 85 % removal, optimized L/G.....	97
Table 5.6. Comparison between intercooled and non-intercooled absorber, intercooler at half column, intercooler duty 1/3 reboiler duty, 10% CO ₂ , 90% removal, 0.1 mol HSS/mol MEA, optimized L/G.....	101
Table 5.7. Effect of extraction segment on the relative specific reboiler duty and other process variables, constant split flow of 5000 lbmol/hr, 10% CO ₂ , 90% removal, optimized L/G, 0.1 mol HSS/mol MEA.....	106
Table 5.8. Effect of split flow rate, split feed extracted at segment 17 and fed into segment 6, 10% CO ₂ , 90% removal, optimized L/G, 0.1 mol HSS/mol MEA.	107
Table 5.9. Effect of split flow rate, split feed extracted at segment 10 and fed into segment 6, 10% CO ₂ , 90% removal, optimized L/G, 0.1 mol HSS/mol MEA.	107
Table A.1. Input summary for experimental data used to regress Electrolyte-NRTL parameters with ASPEN PLUS DRS.	115
Table A.2. Results of ASPEN PLUS DRS regression, values and standard deviations of regressed parameters.....	116
Table A.3. Correlation matrix for regressed parameters.	116
Table A.4. Comparison of experimental values and values calculated with the regressed parameters.....	117
Table C.1. Detailed stream results for the base case run, 3.13 % CO ₂ , 0.1 mol HSS/mol MEA _{tot} , other conditions given in Table 4.2, first column, stream names refer to figure C.1.....	146
Table C.2. Absorber profiles for 3% CO ₂ base case.....	151

Table C.3. Stripper profiles for 3% CO ₂ base case.	151
Table C.4. Base case process heat exchanger duties, normalized to mass of CO ₂ removed and relative to the reference value in MJ/Kmol CO ₂	152
Table C.5. Detailed material and energy balance for 10% CO ₂ -90% removal case. McCabe-Thiele diagrams shown in figures 5.18 and 5.19, stream names refer to figure C.1, all other parameters same as 3.13% CO ₂ base case.	153
Table C.6. Absorber profiles for 10% CO ₂ -90% removal case.....	158
Table C.7. Stripper profiles for 10% CO ₂ -90% removal case.....	158
Table C.8. Process heat exchanger duties, normalized to mass of CO ₂ removed and relative to the reference value in MJ/Kmol CO ₂ , 10% CO ₂ -90% removal.	159
Table D.1. Input summary for the high CO ₂ base case.	162
Table D.2. Material and energy balance.....	164
Table D.3. Absorber profiles.	168
Table D.4. Stripper profiles.	169
Table D.5. Heat exchanger duties (values in KW).	169
Table D.6. Tabular data for Figures D.2 and D.3.....	171
Table E.1. Detailed simulation results for runs in Chapter 5.	173

List of Figures

Figure 1.1. Chemical structures of most common alkanolamines.	3
Figure 1.2. Schematic of absorption/stripping process for CO ₂ removal with alkanolamines.	6
Figure 1.3. Schematic of a split flow process for CO ₂ removal with alkanolamines.	10
Figure 2.1. Equilibrium partial pressure of CO ₂ at 60 °C for a 30wt% MEA solvent.	22
Figure 2.2. Equilibrium partial pressure of CO ₂ at 120°C for a 30wt% MEA solvent.....	23
Figure 3.1. Physical absorption representation with film theory	29
Figure 3.2. Representation of the PFO and IPFO approximations for absorption with fast chemical reaction.	31
Figure 3.3. Loading effects on diffusivity and Henry's constant of CO ₂ in 5 M aqueous MEA at 40° C.	37
Figure 3.4. Comparison of rigorous model, IPFO model and PFO model for kg' at 60°C.	38
Figure 3.5. Results of the RATEFRAC model at 40° C and loading of approximately 0.3.	44
Figure 3.6. Results of the RATEFRAC model at 60 °C and loading of approximately 0.3.	45
Figure 3.7. Results of RATEFRAC model at T=40°C and loading of approximately 0.5.	45
Figure 3.8. Results of the Retefrac model at 60° C and loading of approximately 0.5.	46

Figure 4.1. Base case absorption/stripping process with 30 wt% aqueous MEA (Bellingham plant).....	48
Figure 4.2. McCabe-Thiele diagram for Bellingham base case absorber, outlet gas P_{CO_2} compared to plant value, k_g^I adjusted, heat stable salts included in analysis.	51
Figure 4.3. Packing height assigned to a RADFRAC stage.	52
Figure 4.4. Block diagram of RADFRAC model of Bellingham absorber.	54
Figure 4.5. Liquid temperature, loading, efficiency profiles for the Bellingham absorber from the simulation with RADFRAC and the Bishnoi model, 3.13 % CO_2 , 30 wt% MEA, lean loading 0.16, heat stable salts not included in analysis.	55
Figure 4.6. Absorber liquid temperature profiles for 3.13 mol%-85% removal (base case) and 10.3 mol%-90% removal. RATEFRAC and RADFRAC results are compared.	57
Figure 4.7. Scheme of the RATEFRAC stripper model.....	58
Figure 4.8. Gas phase resistance, loading and vapor rate profiles for the base case stripper.	62
Figure 4.9. Isothermal stripper equilibrium lines at 120 °C at different HSS loadings and Bellingham operating line, fixed $(L/G)_{mass}=0.78$, fixed lean loading=0.16, HSS added to 30 wt% MEA.....	65
Figure 4.10. McCabe-Thiele diagrams for Bellingham stripper at $\beta=0$ and $\beta=0.1$. Results from rigorous RATEFRAC simulation, fixed $(L/G)_{mass}=0.78$, fixed lean loading=0.16, HSS added to 30 wt% MEA.....	67
Figure 4.11. Schematic of the absorption/stripping model.....	68
Figure 5.1. Optimization of solvent flow rate. 3% mole CO_2 in flue gas, 85 % removal, 0.1 mol HSS/mol MEA_{tot} , solvent rate normalized to flue gas rate, reboiler duty normalized to moles of CO_2 removed and divided by a typical industrial value in MJ/Kmol.	75

Figure 5.2. Absorber McCabe-Thiele diagram for low L/G case ($L/G_{\text{mass}}=0.63$). 3% CO ₂ in flue gas, 85 % removal, 33.5 wt% MEA, 0.1 mol HSS/mol MEA _{tot}	77
Figure 5.3. Stripper McCabe-Thiele diagram for low L/G case ($L/G_{\text{mass}} =0.63$). 3% CO ₂ in flue gas, 85 % removal, 33.5 wt% MEA, 0.1 mol HSS/mol MEA _{tot}	77
Figure 5.4. Absorber McCabe-Thiele diagram for optimum L/G case (L/G_{mass} $=0.86$). 3% CO ₂ in flue gas, 85 % removal, 33.5 wt% MEA, 0.1 mol HSS/mol MEA _{tot}	78
Figure 5.5. Stripper McCabe-Thiele diagram for optimum L/G case (L/G_{mass} $=0.86$). 3% CO ₂ in flue gas, 85 % removal, 33.5 wt% MEA, 0.1 mol HSS/mol MEA _{tot}	78
Figure 5.6. Absorber McCabe-Thiele diagram for high L/G case ($L/G_{\text{mass}} =1.77$). 3% CO ₂ in flue gas, 85 % removal, 33.5 wt% MEA, 0.1 mol HSS/mol MEA _{tot}	79
Figure 5.7. Stripper McCabe-Thiele diagram for high L/G case ($L/G_{\text{mass}} =1.77$). 3% CO ₂ in flue gas, 85 % removal, 33.5 wt% MEA, 0.1 mol HSS/mol MEA _{tot}	79
Figure 5.8. Stripper CO ₂ and H ₂ O mole fraction, loading and liquid T profiles, for high L/G case ($L/G_{\text{mass}} =1.77$). 3% CO ₂ in flue gas, 85 % removal, 33.5 wt% MEA, 0.1 mol HSS/mol MEA _{tot}	80
Figure 5.9. Effect of absorber height on reboiler duty per mole of CO ₂ removed, 33.5 wt% MEA, 0.1 mol HSS/mol MEA _{tot} , optimum solvent rate, reboiler duty normalized to total moles of CO ₂ removed and to typical industrial value.....	82
Figure 5.10. Effects of Figure 5.9, reboiler duty normalized by minimum heat duty.	83
Figure 5.11. Optimized solvent rate for the three cases of Figure 5.9.....	83

Figure 5.12. McCabe-Thiele diagram for the absorber; $Z_{\text{absorber}}/Z_{\text{Base case}}=0.6$, 33.5 wt% MEA, 0.1 mol HSS/mol MEA _{tot} , optimized solvent rate (L/G _{mass} =3.29), 3 mol% CO ₂ in flue gas, 85% removal.	85
Figure 5.13. McCabe-Thiele diagram for the stripper; $Z_{\text{absorber}}/Z_{\text{Base case}}=0.6$, 33.5 wt% MEA, 0.1 mol HSS/mol MEA _{tot} , optimized solvent rate (L/G _{mass} =3.29), 3 mol% CO ₂ in flue gas, 85% removal.	85
Figure 5.14. McCabe-Thiele diagram for the absorber; $Z_{\text{absorber}}/Z_{\text{Base case}}=1.6$, 33.5 wt% MEA, 0.1 mol HSS/mol MEA _{tot} , optimized solvent rate (L/G _{mass} =0.82), 3 mol% CO ₂ in flue gas, 85% removal.	86
Figure 5.15. McCabe-Thiele diagram for the stripper; $Z_{\text{absorber}}/Z_{\text{Base case}}=1.6$, 33.5 wt% MEA, 0.1 mol HSS/mol MEA _{tot} , optimized solvent rate (L/G _{mass} =0.82), 3 mol% CO ₂ in flue gas, 85% removal.	86
Figure 5.16. McCabe-Thiele diagram for the absorber; $Z_{\text{absorber}}/Z_{\text{Base case}}=1$, 33.5 wt% MEA, 0.1 mol HSS/mol MEA _{tot} , optimized solvent rate (L/G _{mass} =1.18), 3 mol% CO ₂ in flue gas, 90% removal.	87
Figure 5.17. McCabe-Thiele diagram for the stripper; $Z_{\text{absorber}}/Z_{\text{Base case}}=1$, 33.5 wt% MEA, 0.1 mol HSS/mol MEA _{tot} , optimized solvent rate (L/G _{mass} =1.18), 3 mol% CO ₂ in flue gas, 90% removal.	87
Figure 5.18. McCabe-Thiele diagram for the absorber; $Z_{\text{absorber}}/Z_{\text{Base case}}=1$, 33.5 wt% MEA, 0.1 mol HSS/mol MEA _{tot} , optimized solvent rate (L/G _{mass} =2.68), 10 mol% CO ₂ in flue gas, 90% removal.	88
Figure 5.19. McCabe-Thiele diagram for the stripper; $Z_{\text{absorber}}/Z_{\text{Base case}}=1$, 33.5 wt% MEA, 0.1 mol HSS/mol MEA _{tot} , optimized solvent rate (L/G _{mass} =2.68), 10 mol% CO ₂ in flue gas, 90% removal.	88
Figure 5.20. Effect of stripper height on the reboiler duty; 3 mol% CO ₂ in flue gas, 85 % removal, 33.5 wt% MEA, 0.1 mol HSS/mol MEA _{tot} , solvent rate optimized.	90

Figure 5.21. Effect of MEA concentration and of HSS loading on the reboiler duty, 3 mol% CO ₂ , 85% removal, optimum solvent rate.	92
Figure 5.22. Effect of stripper pressure on the reboiler duty and lost work, for a 3 mol % CO ₂ flue gas and 85% removal, 33.5 wt% MEA, 0.1 mol HSS/mol MEA _{tot} , L/G optimized.	96
Figure 5.23. McCabe-Thiele diagrams for strippers operating at 3.7 and 0.5 bar, 3 mol% CO ₂ , 85% removal, 33.5 wt% MEA, 0.1 mol HSS/mol MEA _{tot} , optimized L/G.	97
Figure 5.24. Effect of solvent temperature on the specific reboiler duty, 10 mol% CO ₂ , 33.5 wt% MEA, HSS loading=0.1, lean loading=0.19, solvent rate adjusted to keep removal at 90%.	99
Figure 5.25. Temperature profiles in the absorber for solvent inlet temperature 10 °C and 40 °C; 10 mol% CO ₂ , 33.5 wt% MEA, 0.1 mol HSS/mol MEA _{tot} , lean loading=0.19, solvent rate adjusted to keep removal at 90%.....	99
Figure 5.26. Comparison of liquid and gas temperature profiles for intercooled and non-intercooled absorber, intercooler at half column, intercooler duty 1/3 reboiler duty, 10% CO ₂ , 90% removal, 0.1 mol HSS/mol MEA, optimized L/G.	101
Figure 5.27. Comparison of absorber McCabe-Thiele diagrams for intercooled and non-intercooled absorber, intercooler at half column, intercooler duty 1/3 reboiler duty, 10% CO ₂ , 90% removal, 0.1 mol HSS/mol MEA, optimized L/G.	102
Figure 5.28. Schematic of the split flow configuration.	103
Figure 5.29. Qualitative McCabe-Thiele diagrams describing three possible effects of the split flow configuration; A: absorber cooling effect; B: loading discontinuity effect; C: stripper lean pinch effect.	105
Figure 5.30. Liquid and vapor temperature profiles in absorber with split flow injected at segment 6 (of 20), split flow rate 0.565 times the lean solvent	

rate, 10% CO ₂ , 90% removal, optimum L/G, 0.1 mol HSS/mol MEA.	108
Figure 5.31. Absorber McCabe-Thiele diagram, split flow injected at segment 6 (of 20), extracted from stage 10, split flow rate 0.565 times the lean solvent rate, 10% CO ₂ , 90% removal, optimum L/G, 0.1 mol HSS/mol MEA.	109
Figure 5.32. Stripper McCabe-Thiele diagram, split flow injected at segment 6 (of 20), extracted from stage 10, split flow rate 0.565 times the lean solvent rate, 10% CO ₂ , 90% removal, optimum L/G, 0.1 mol HSS/mol MEA.	109
Figure C.1. ASPEN PLUS process flow diagram for absorption/stripping process.	145
Figure D.1. ASPEN PLUS process flow diagram for absorption/stripping base case.	163
Figure D.2. Absorber McCabe-Thiele diagram.	170
Figure D.3. Stripper McCabe-Thiele diagram.	170
Figure D.4. Gas and liquid temperature profiles in the absorber.	172
Figure D.5. CO ₂ mole fraction profiles in absorber and stripper.	172

Chapter 1

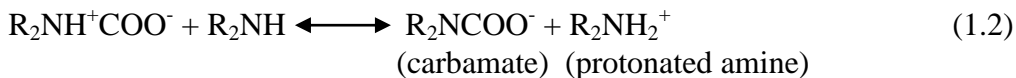
Introduction

Removal of carbon dioxide has been practiced industrially for several decades. Different processes need to have CO₂ removed. In natural gas processing CO₂ is removed to reduce the costs of compression and transportation. In ammonia manufacture CO₂ needs to be removed from the hydrogen stream, since it poisons the catalyst for the reaction between H₂ and N₂. Power plant flue gases are a new application of CO₂ removal processes, compared to the first two. In this case CO₂ is removed only to reduce greenhouse emissions. This issue is of increasing interest, because global warming is an important environmental and political issue. With the Kyoto protocol of 1997 forty-one industrialized countries agreed to cut the carbon dioxide emissions to approximately 5% less than the emissions in 1990, in a five year period going from 2008 to 2012. This situation makes CO₂ capture an important issue in the economies of most countries. It is a fact that a CO₂ removal facility is an expensive plant, and the operating costs are very high. For a power plant the removal of 90% of the CO₂ from the flue gas can use up to 30% of the energy produced by the plant (IEA Greenhouse Gas R&D Programme). This represents a heavy loss, and the focus of research in this field is to reduce the costs of removal, in particular reducing its energy requirements.

CO₂ has some uses and can be sold on the market. It is used mostly in enhanced oil recovery (EOR). CO₂ flooding represents one of the main methods for extracting the final amounts of recoverable oil from depleted reservoirs. CO₂ is also used in the food industry for carbonated beverages and brewing. It finds uses in smaller quantities as inert gas or as supercritical solvent. The problem of the CO₂ market is that many processes produce CO₂ as a by-product, and there is no need to buy from flue gas plants. In addition the amount of CO₂ needed for the aforementioned processes is much smaller than the amount that can be recovered from power plant flue gases.

1.1. Alkanolamines and their reactions with CO₂

CO₂ capture is typically done by absorption with alkanolamine-water solutions. The alkanolamines are bases, and they react with the acid species CO₂ to form different reaction products. They contain alcohol groups in order to become soluble in water. The first alkanolamine to be used industrially was monoethanolamine (MEA). This is the only amine that will be considered in this work. Its structure is shown in Figure 1.1, where it is compared to the structures of other common alkanolamines, such as methyldiethanolamine (MDEA), diethanolamine (DEA), triethanolamine (TEA), diglycolamine (DGA), and piperazine (PZ). The amines are distinguished as primary, secondary and tertiary, according to the number of organic groups attached to the alkaline nitrogens. MEA is a primary amine, DEA and PZ are secondary amines, and MDEA and TEA are tertiary amines. The different categories of amines differ on the type of mechanisms with which they react with CO₂, as well as the reaction products and the heats of reaction. Typically primary and secondary amines react forming a carbamate species, and the reaction may or may not proceed through an intermediate called the zwitterion.



Tertiary amines cannot form a carbamate species, because they do not have a hydrogen attached to the nitrogen atom. Typically the tertiary amines react according to equation 1.3.

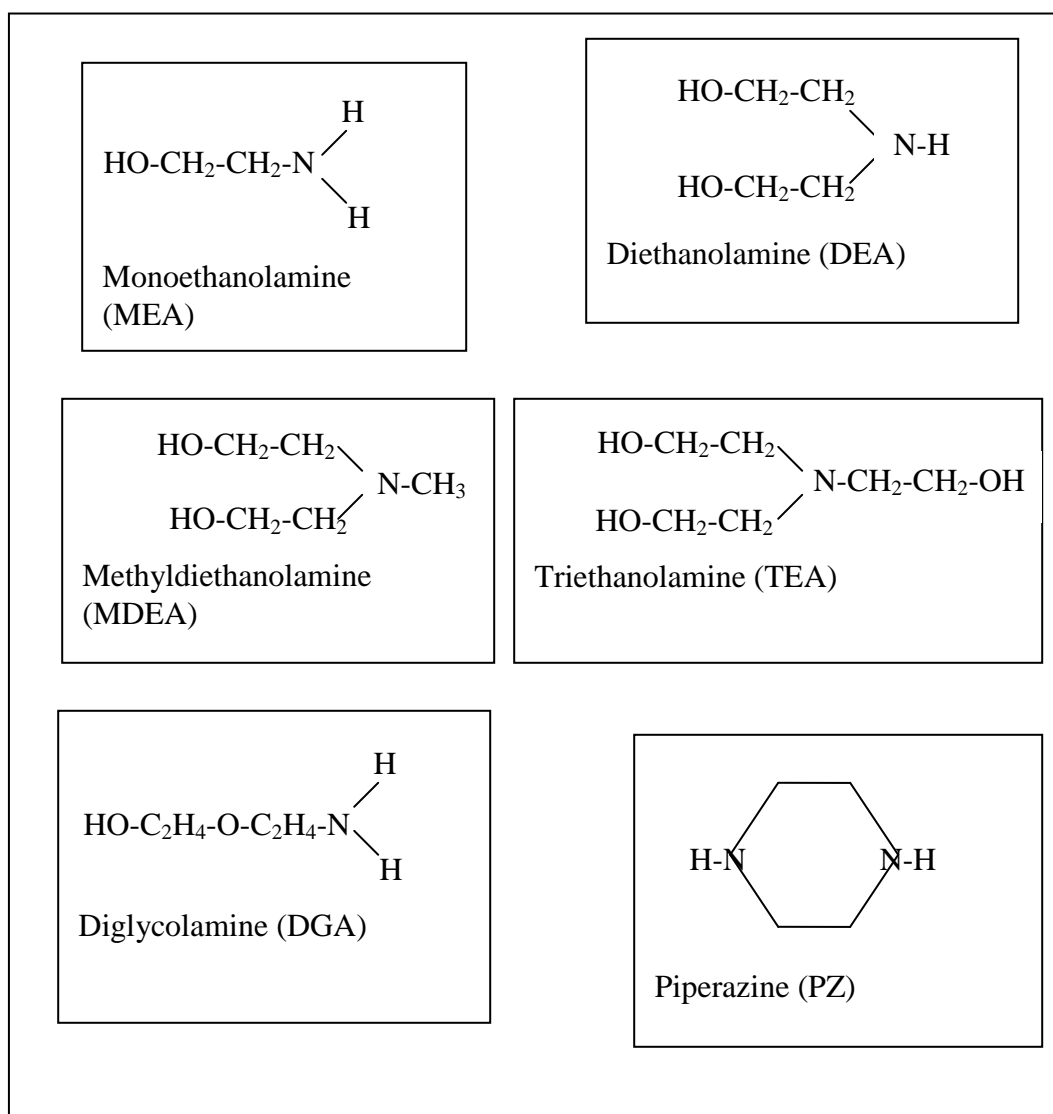
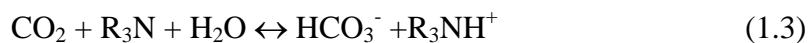


Figure 1.1. Chemical structures of most common alkanolamines.

Primary and secondary amines usually react faster than tertiary amines, and CO₂ has higher heats of absorption in these amines. Heats of reaction at 25⁰ C and unloaded conditions are approximately 20.3 kcal/mole for MEA and 14.8 kcal/mole for MDEA (Kohl and Nielsen, 1997).

A typical rate expression for amines that react according to 1.1 and 1.2 is equation 1.4 (Littel et al., 1991).

$$R_{CO_2} = \frac{[R_1R_2NH][CO_2]}{\frac{1}{k_2} + \frac{1}{k_{H_2O}[H_2O] + k_{R_1R_2NH}[R_1R_2NH] + k_B[B]}} \quad (1.4)$$

where [R₁R₂NH], [CO₂] and [H₂O] are the concentration of alkanolamine, CO₂ and water respectively, and B is any other base in solution that can extract a proton from the zwitterion.

For MEA the equation is particularly simple. The rate is dominated by the zwitterion formation, rather than by its reaction with another base. Therefore the rate expression becomes simply first order with respect to MEA.

$$R_{CO_2} = k_2 [CO_2] [MEA] \quad (1.5)$$

The advantage of a fast reacting amine is that the size of the separation equipment (absorbers) is smaller. The drawback is that more heat is required to reverse the reaction and regenerate the solvent. Solvent regeneration is the main obstacle to cost reduction of CO₂ capture.

The choice of a proper solvent is important. Some work has been done on mixed solvents. Bishnoi (2000) and Dang (2001) researched the properties of piperazine promoted MDEA and MEA respectively. Cullinane (2002) is currently studying the absorption into piperazine promoted potassium carbonate (K₂CO₃). Piperazine has very fast kinetics and can promote the absorption rates. MDEA, MEA and K₂CO₃ provide CO₂ capacity in the solvent and reduce the heat of regeneration, which would be otherwise too high if piperazine were to be used by

itself. These mixed solvents are being studied at bench scale, but they are not yet used in industry.

1.2. The absorption/stripping process for CO₂ capture

CO₂ removal is achieved industrially by a process based on a pair of columns, one absorber and one stripper. The purpose of the absorber is to capture the carbon dioxide, whereas the purpose of the stripper is to regenerate the solvent, so that it is ready to be recycled to the absorber. The cyclic process is shown in Figure 1.2. The absorber has two feeds; at the bottom the flue gas enters the column and flows upwards. The CO₂ content of the feed changes with the type of flue gas. Gas turbines produce flue gases with approximately 3 mole% CO₂. Natural gas and coal-fired power plants generate more CO₂, with flue gases containing 5-6% and 10-12% of CO₂ respectively.

The solvent is fed at the top, flowing down the column and contacting the gas phase. This solvent comes from the bottom of the stripper, and is called *lean*, because it has the lowest CO₂ content in the process. The solvent cannot be fully regenerated, because this would be too energy demanding. Nevertheless the regeneration needs to be almost complete, because the partial pressure of CO₂ allowed in the outlet gas streams can be as low as 50 mmHg. The CO₂ content of a liquid amine-water solution is usually expressed in terms of *loading* (total moles of CO₂/total moles of amine). In the absorber, during contact between the liquid and the gas phase, the CO₂ enters the liquid phase due to a concentration gradient. If there was no amine, there would be only physical absorption and the solvent would be quickly saturated with CO₂. The presence of MEA or other alkanolamines drives the CO₂ into the liquid phase due to a fast reaction. Besides providing CO₂ capacity, the amine enhances the absorption rates, which can be as much as one hundred times faster than in a physical solvent.

The most common way to provide contact area for mass transfer is the use of packing. The liquid phase forms a film around the packing, increasing the area of contact between the gas and liquid phases. Other ways to provide contact area are the use of sieve trays or sprays.

The gas coming off the top of the absorber is purified and can be discharged into the atmosphere. Because this gas usually does not need further processing, the absorber can operate at a pressure just above atmospheric, high enough to let the gas stream overcome the column pressure drop. From the bottom of the absorber, the exiting liquid phase takes the name of *rich* solvent, because it has the highest CO₂ loading. This is the stream that is fed to the stripper for regeneration. Typical values for lean and rich loading in aqueous MEA are 0.1-0.2 and 0.4-0.5 mol CO₂/mol MEA respectively.

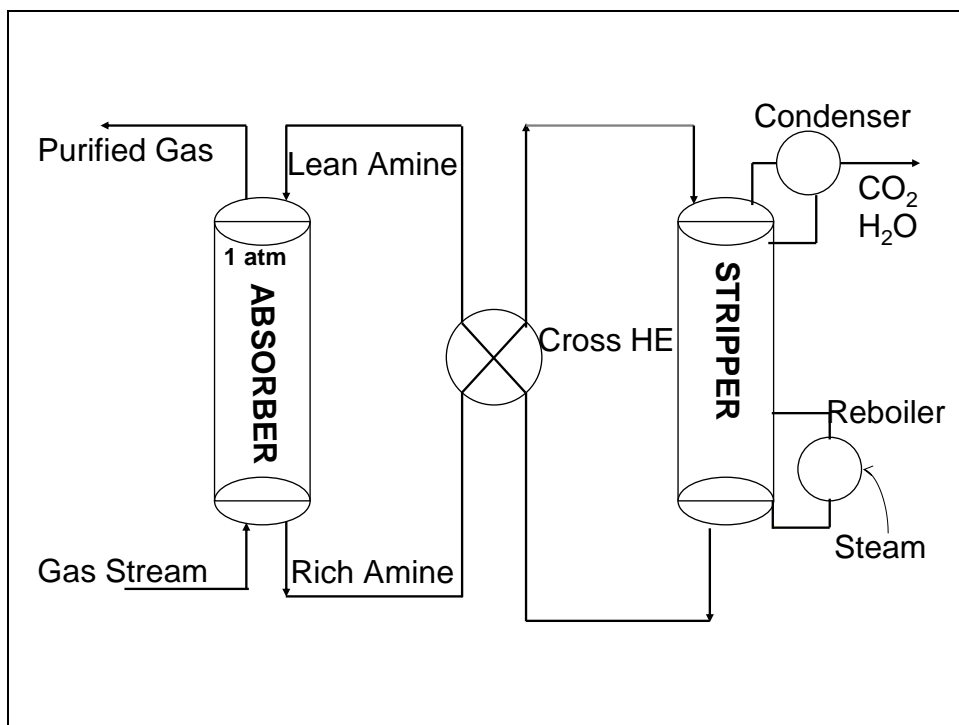


Figure 1.2. Schematic of absorption/stripping process for CO₂ removal with alkanolamines.

The stripper column operates by driving the CO₂ out of the solvent, through the generation of steam. Steam is generated in a reboiler at the bottom of the column. Energy is required in order to vaporize the liquid at the bottom of the stripper. This energy is usually provided by utility steam. The steam produced flows upwards and, having a low CO₂ content, can drive the mass transfer from the liquid to the gas phase. The energy requirement becomes higher as the purity of the lean solvent increases. An overhead partial condenser limits the amounts of water and amine eliminated with the top gas. The stripper usually operates at higher pressure (1.5-2 atm) than the absorber for two reasons. First, the purified CO₂ usually needs further processing or transportation, whether it is sold for enhanced oil recovery or disposed of in tanks. Secondly, the higher pressure implies higher temperatures (110-120⁰ C) and CO₂ has a heat of absorption in MEA approximately twice that of H₂O. As a consequence of the Clausius-Clapeyron thermodynamic relationship (1.6), the vapor pressure of CO₂ increases with temperature more rapidly than the vapor of pressure of water does. Thus the relative amount of CO₂ to H₂O in the gas phase increases as the temperature increases. In equation 1.6, P* is the vapor pressure of a component, R the universal gas constant, and ΔH_{l-v} is the heat of vaporization of water or the heat of desorption of CO₂. This pressure effect will be described in details in section 5.5.

$$\frac{d \ln P^*}{dT} = \frac{\Delta H_{l-v}}{RT^2} \quad (1.6)$$

A cross exchanger is used to heat up the rich amine and to cool down the lean amine. The rich amine needs to reach temperatures of approximately 110⁰ C, whereas the lean amine is cooled down to absorber temperature, approximately 40⁰ C. The cross exchanger uses the sensible heat of the hot stripper bottoms to heat up the absorber bottoms. This reduces the energy to be provided by the reboiler. The lean solvent usually needs to be further cooled with cooling water, before reaching absorber temperatures.

1.3. Modeling of the process and scope of work

Extensive experimental data have been collected in the past twenty years on the CO₂-MEA-H₂O system. These data cover thermodynamic equilibrium, rates of absorption and rates of reaction. Many thermodynamic models and rate models have been created in order to reproduce the experimental data. Among the thermodynamic models, the Kent and Eisenberg method (1976) must be cited for its simplicity. The currently most used model for this system is the electrolyte-NRTL, developed by Chen et al. (1979). It is a model to predict the excess Gibbs's energy of a mixture and will be described in details in chapter 2. This model successfully reproduces experimental data in a wide range of temperature and loadings.

The object of the present work is to create a model for an absorption/stripping process with MEA, based on the experimental data collected so far. The equilibrium data collected by Jou et al. (1995) are used to develop a rigorous electrolyte-NRTL thermodynamic model; the absorption rate data collected by Dang (2001) are used to develop a rate model. The model was developed in ASPEN PLUS, with the RATEFRACTM module. RATEFRAC is a rate based model used to simulate packed and tray columns. The mass transfer rates are calculated with an algorithm that uses film theory for the diffusion of the species in the liquid and gas phases and accounts for reaction rates in the calculation. The commercial version of RATEFRAC is not suitable to reproduce the experimental data for CO₂ absorption in MEA. This problem will be described in detail in chapter 3. It relates to the way RATEFRAC calculates the rates in the liquid boundary layer. A FORTRAN subroutine was written for the kinetics, in order to fix the problem. The RATEFRAC model was validated with field data provided by Fluor Daniel (Won et al., 1999), obtained from the commercial power plant in Bellingham, Massachusetts. This work represents the first successful model with RATEFRAC for acid gas treating with MEA.

Other models have been completed in the past, using either commercial software or language codes. TSWEET is an amine-gas sweetening computer program, which has been used since the early eighties for modeling of acid gas removal (called sweetening in the case of removal from natural gas). Model results with TSWEET can be found in the literature (Holmes et al., 1984).

Another software in use is AMSIM, which uses a rigorous non-equilibrium stage model (Zhang et al., 1996). Along with commercial packages, programs written in FORTRAN or Visual Basic have developed. These programs have the advantage of being specific for amine gas treating. They usually perform rigorous boundary layer integrations for the calculation of mass transfer rates. A model by Al-Baghli et al. (2001) uses this method. Although these rigorously integrated models provide a better insight on mass transfer with chemical reaction in the liquid boundary layer, they are usually slower, and present challenges in simulating the whole process. The purpose of this work is to understand how the design variables affect each other at the level of the whole process, not of the single absorber and stripper. ASPEN PLUS provides tools to perform analyses of this type. For this reason it was chosen as platform for this model.

The ultimate objective of the model is to find an optimum operating point for the process, characterized by a minimum energy requirement for a given CO₂ removal. This work wants to provide a tool for the design of CO₂ removal processes with lower costs. The main design parameters are heights of the two columns, solvent rate, temperature approach to equilibrium in the cross exchanger and operating pressure of the stripper.

Other configurations of the process are explored, that may lead to lower energy requirements. A split flow process was first proposed by Shoeld (1934), and its schematic is shown in Figure 1.3. General information on split flow effects is given in Kohl and Nielsen (1997). Applications on flue gas desulfurization were studied by Rochelle (1977), who proposed the configuration also for CO₂ removal. The

effect of split flow on H_2S removal from natural gas with MDEA was studied by Shethna et al. (1997), who showed that the split flow configuration can reduce energy requirements. In this work the effect of split flow on CO_2 removal from flue gases was studied. The split flow process will be described with more details and analyzed in section 5.6.

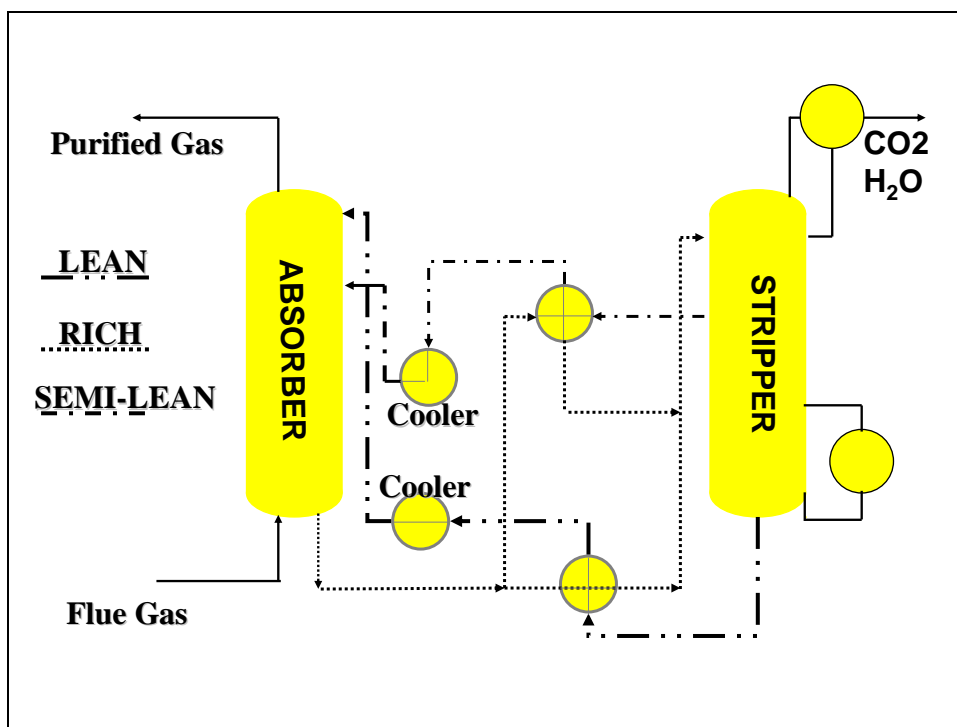


Figure 1.3. Schematic of a split flow process for CO_2 removal with alkanolamines.

In this modification of the absorption/stripping process a portion of the liquid phase flowing down the stripper is extracted from the column. This split stream (also called semi-lean amine) is cooled down to absorber temperatures through process heat exchange and extra-cooling, and is fed to an intermediate stage in the absorber.

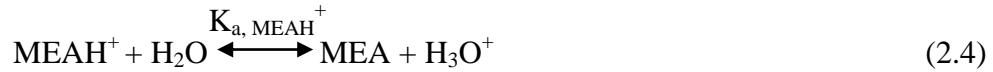
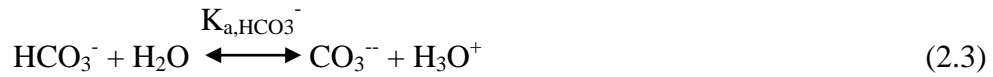
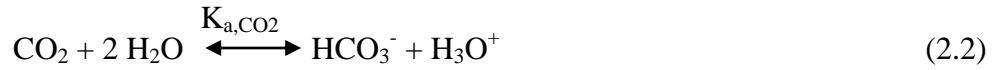
Chapter 2

Thermodynamic Model

A model of an absorption/stripping process requires the use of rigorous thermodynamics. Although CO₂ absorption is a non-equilibrium process, the knowledge of the equilibrium composition of the CO₂-MEA-H₂O system is required to determine liquid phase driving forces and solution speciation.

2.1. Solution chemistry and equilibrium governing equations

The following reversible reactions occur in the liquid phase when CO₂ is absorbed into an aqueous solution of MEA.



Every reaction represents an equilibrium constraint. Solving the thermodynamic problem for the solution of H₂O, MEA and CO₂ at a given temperature and pressure means finding the mole fractions of each of the components in both the liquid and the vapor phases. Because the ions are non-volatile, only CO₂, MEA and water are present in the vapor phase. Since there is a total of nine components, there are 12 unknowns in the problem, that require 12 equations. The known variables are total MEA concentration and CO₂ loading of the solution. The solving equations are the five equilibrium constraints (2.6), the CO₂ material balance (2.7), the MEA balance (2.8), the total material balance (2.9), electroneutrality (2.10) and the phase equilibrium relationships for CO₂, MEA and water (2.11-2.13).

$$K_j = \frac{\prod_{i=1}^{\text{prod}} (a_i)^{\nu_i}}{\prod_{i=1}^{\text{reactant}} (a_i)^{\nu_i}} \quad (2.6)$$

$$X_{\text{CO}_2\text{total}} = X_{\text{CO}_2} + X_{\text{HCO}_3^-} + X_{\text{CO}_3^{2-}} + X_{\text{MEACOO}^-} \quad (2.7)$$

$$X_{\text{MEA}_{\text{tot}}} = X_{\text{MEA}} + X_{\text{MEA}^+} + X_{\text{MEACOO}^-} \quad (2.8)$$

$$1 = X_{\text{CO}_2} + X_{\text{MEA}} + X_{\text{H}_2\text{O}} + X_{\text{HCO}_3^-} + X_{\text{CO}_3^{2-}} + X_{\text{MEACOO}^-} + X_{\text{MEA}^+} + X_{\text{H}_3\text{O}^+} + X_{\text{OH}^-} \quad (2.9)$$

$$0 = (X_{\text{HCO}_3^-} + X_{\text{MEACOO}^-} + X_{\text{OH}^-} + 2X_{\text{CO}_3^{2-}}) - (X_{\text{MEA}^+} + X_{\text{H}_3\text{O}^+}) \quad (2.10)$$

$$P_{y_{\text{CO}_2}} = \gamma_{\text{CO}_2}^* H_{\text{CO}_2} X_{\text{CO}_2} \quad (2.11)$$

$$P_{y_{\text{H}_2\text{O}}} = \gamma_{\text{H}_2\text{O}}^* P_{\text{H}_2\text{O}}^* X_{\text{H}_2\text{O}} \quad (2.12)$$

$$P_{y_{\text{MEA}}} = \gamma_{\text{MEA}}^* P_{\text{MEA}}^* X_{\text{MEA}} \quad (2.13)$$

In equation 2.6 a_i is the activity of component i in solution and ν_i is the stoichiometric coefficient of component i in reaction j . In equations 2.11 H_{CO_2} is the Henry's constant of CO₂ in the solvent. In equations 2.12 and 2.13 $P_{\text{H}_2\text{O}}^*$ and P_{MEA}^* are the vapor pressures of H₂O and MEA respectively.

The equilibrium constants are temperature dependent, according to equation 2.14, where T is in ⁰K.

$$\ln K_j = A + \frac{B}{T} + C \ln T + DT \quad (2.14)$$

The same temperature dependence is found for the Henry's constant of CO₂ in water. The values of the constants, from Austgen (1989), are reported in Table 2.1.

Table 2.1. Values of constants for T dependent expressions for equilibrium constants and Henry's constant for CO₂ in H₂O.

Parameter	Keq, reaction 2.1	Keq, reaction 2.2	Keq, reaction 2.3	Keq, reaction 2.4	Keq, Reaction 2.5	H _{CO₂,H₂O}
A	-0.52	231.46	216.05	-3.038	132.89	170.71
B	-2545.53	-12092.1	-12431.7	-7008.3	-13445.9	-8477.7
C	0	-36.78	-35.48	0	-22.47	-21.95
D	0	0	0	-0.00313	0	5.78E-3

2.2. Solubility data used in this work

Rochelle et al. (2001) and Dang (2000) have reviewed the extensive solubility data for the system CO₂-MEA-H₂O. Only the data collected by the Mather research group were used in this work. Lee et al. (1976) collected data at 1 to 5 M MEA, 25⁰C to 120⁰C, with 0.1 to 2 mol CO₂/mol MEA. Jou et al. (1995) collected data only in 30 wt% MEA, at 0⁰C to 150⁰C, with 0.001 to 1 mol CO₂/mol MEA.

The equilibrium model for CO₂ absorption in MEA developed by Austgen (1989) was based on the Lee data. The work of Jou, done 20 years later, pointed out that Lee's data were affected by a systematical error, a consequence of the experimental technique used to measure the CO₂ loading. In Lee's work the solution was acidified by adding H₂SO₄. The carbon dioxide evolved and was measured volumetrically. There is a small amount of CO₂ that remains in the acidic solution, and that seemed to be the cause of a systematical loading underprediction by approximately 0.04.

In Jou's work the CO₂ loading was measured using two different techniques, gas chromatography and precipitation of BaCO₃. The former was used for low loading, the latter for higher loading. A few points were measured with both methods, showing consistent measured values. The Jou data are considered the most reliable solubility measurements available in the literature. The vapor pressure of CO₂ varies over three orders of magnitude from unloaded solutions to loadings of 0.4-0.5.

The model developed here uses the Jou data for a development of an equilibrium model by the ASPEN PLUS Data Regression System (DRS), using the electrolyte-NRTL framework, developed by Chen et al. (1979).

2.3. System non-idealities

The mixture of CO₂, MEA and water is highly non-ideal in the liquid phase. The presence of ions and polar molecules creates significant thermal effects in solution. In order to predict equilibrium correctly, a good activity coefficient model is necessary.

The electrolyte-NRTL was chosen by Austgen (1989), Posey (1996) and Bishnoi (2000) as the most suitable model for the systems CO₂-amine-water. The present work starts from the model developed by Austgen and improves it including Jou's data in a parameter regression. Austgen had done his regression with data from several investigators, including Lee.

The gas phase does not present significant non-idealities, since the pressures of interest are not high (atmospheric to 4-5 atm). The thermodynamic model used in ASPEN PLUS uses the equation of Redlick-Kwan-Soave to treat vapor phase non-idealities, even if the calculated fugacity coefficients are always very close to one.

2.4. The Electrolyte-NRTL Model

The thermodynamic model developed in this work uses the electrolyte-NRTL theory developed by Chen and Evans (1979) and extended by Mock et al. (1986) for mixed solvent electrolyte systems. A short description of the theory will follow. More information on the model derivation can be found in Chen et al. (1979, 1982, 1986), Austgen (1989) and Bishnoi (1998, 2000).

The Electrolyte-NRTL model is a model for the excess Gibbs free energy of a solution. From background thermodynamics, it is known that the activity coefficients of every component of a mixture can be related to the excess Gibbs free energy by equation 2.15.

$$\ln \gamma_i = \frac{\partial}{\partial n_i} \left(\frac{G^E}{RT} \right)_{T, P, n_j \neq i} \quad (2.15)$$

γ_i is the activity coefficient of species i in solution, n_i is the number of moles of i , G^E is the excess Gibbs free energy, defined as

$$G^E = G - G^{id} \quad (2.16)$$

where G^{id} is the Gibbs free energy if the mixture were ideal. The excess Gibbs free energy is related to excess enthalpy and excess entropy of mixing (eq. 2.17)

$$G^E = H^E - TS^E \quad (2.17)$$

The excess enthalpy is determined by the fact that a component changes its interactions with the surrounding components when the composition changes. When ions are present in large amounts in the solution, they interact strongly with each other, and every molecule of CO_2 among them reduces the intensity of this interaction. For this reason the CO_2 is subject to the so called salting-out effect. It tends to leave the liquid phase when the solution has high ionic strength, because this reduces the total enthalpy of the solution. The excess entropy is due to a change in the randomness of the reciprocal position of the molecules in solution. The presence of ions creates a pseudo crystalline structure in the aqueous solution,

because water molecules tend to hydrate the ions. The electrolyte-NRTL model assumes that the non ideal entropy of mixing is negligible compared to the heat of mixing.

The electrolyte-NRTL model gives an analytical expression for the excess Gibbs free energy. In the model G^E is a sum of three terms, the long range ionic forces, the short range molecular forces and the Born correction (eq. 2.18).

$$G^E = G^{E, PDH} + G^{E, BORN} + G^{E, NRTL} \quad (2.18)$$

The long term ionic forces are described with the theory of Debye-Huckel, modified by Pitzer. The term depends heavily on the ionic strength of the solution I_x , defined in terms of mole fractions of the ions, like in equation 2.19, where z_i is the charge of ion i .

$$I_x = \frac{1}{2} \sum_i x_i z_i^2 \quad (2.19)$$

Documentation of this theory can be found in Chen et al. (1979). This term describes the interactions between ions. The Born correction is a term introduced by Scaufaire et al. (1989), in order to bring the reference states of all the ions to infinite dilution in water. The term $G^{E,PDH} + G^{E,BORN}$ represents the long range forces contribution with reference state of the ions at infinite dilution in water.

The short range molecular forces need to be included to account for hydrogen bonds and local interactions of molecules with molecules, molecules with ion pairs, and ion pairs with ion pairs. These interactions are described by the *non random two liquids* (NRTL) theory developed by Renon and Prausnitz (1968). The NRTL theory in the presence of ions uses two assumptions. The like-ion repulsion assumption states that the local compositions of cations around cations and anions around anions is zero. The local electroneutrality assumption states that the local charge is always zero. The NRTL term in the excess Gibbs free energy expression is a strong function of interaction parameters, defined in equation 2.20.

$$\tau_{ji, ki} = \frac{g_{ji} - g_{ki}}{RT} \quad (2.20)$$

g_{ji} and g_{ki} are the energies of interaction of species i with species j and k respectively. Equation 2.20 is the basis for the non-random distribution of species j and k around species i . The local mole fractions of j and k around i , X_{ji} and X_{ki} , are calculated according to equations 2.21 and 2.22, where $X_j = (x_j C_j)$, C_j is the charge for ions and unity for molecules, x_j is the total mole fraction of j in solution, and $\alpha_{ji, ki}$ is a parameter called nonrandomness factor. α is a symmetric parameter: $\alpha_{i,j} = \alpha_{j,i}$.

$$\frac{X_{ji}}{X_{ki}} = \left(\frac{X_j}{X_k} \right) G_{ji, ki} \quad (2.21)$$

$$G_{ji, ki} = e^{(-\alpha_{ji, ki} \tau_{ji, ki})} \quad (2.22)$$

The local composition around a species i , that can be a molecule, an anion or a cation, is determined by the relative energies of interaction of every species with species i . The τ values are impossible to measure and they have to be obtained by numerical regression. Normally they are assigned a temperature dependent expression (equation 2.23).

$$\tau = A + \frac{B}{T} \quad (2.23)$$

2.4.1. Electrolyte-NRTL model applied to CO₂-amine systems

Austgen (1989) applied the Electrolyte-NRTL model to the MEA-water-CO₂ system. He regressed τ parameters and the carbamate stability constants to match available experimental data. Based on Chen et al. (1986), he fixed all the τ 's for ionic pair-ionic pair to zero, and he set all the nonrandomness factors for molecule-molecule interactions and water-ion pair interaction to 0.2. As suggested by Mock et al. (1986), he set the nonrandomness factors for alkanolamine-ion pair and CO₂-ion pair to 0.1. These same values were used in this work. For the MEA-CO₂-H₂O

system, Austgen regressed the τ values for MEA-H₂O, H₂O-(MEACOO⁻MEA⁺), H₂O-(HCO₃⁻MEA⁺) and their reciprocal. All the other water-ion pair and ion pair-water parameters were set at fixed values of 8.0 and -4.0. The amine-ion pair/ion pair-amine parameters and the CO₂-ion pair/ion pair-CO₂ were set to 15.0 and -8.0. These values were reported by Chen and Evans (1986) and Mock et al. (1986) as average values of a large number of water-ion pair and organic solvent-ion pair parameters. All the values regressed by Austgen were used in this work, except the τ 's for H₂O-(MEACOO⁻MEA⁺), (MEACOO⁻MEA⁺)-H₂O, H₂O-(HCO₃⁻MEA⁺), and (HCO₃⁻MEA⁺)-H₂O.

Austgen used different sets of experimental data for his regression, including the data of Lee et al. (1976) mentioned above. The fact that this set of data was affected by systematic error produced regressed parameters that reproduce this error. In this work a new regression was performed, using the data of Jou et al. (1995) instead of those of Lee et al.

2.5. Regression

New interaction parameters were regressed in this work to make the model of Austgen match the experimental data of Jou et al. (1995). The regression was done using the Data Regression System (DRS) in ASPEN PLUS, the same tool used by Austgen. The regressed parameters are the τ values for the water-ion pairs H₂O-(MEACOO⁻MEA⁺), H₂O-(HCO₃⁻MEA⁺) and their reciprocal.

Jou reported partial pressures of CO₂ as a function of CO₂ loading and temperature. The DRS requires that temperature, pressure, liquid phase mole fractions and gas phase mole fractions are entered for every experimental point. Because the solution speciation is not known a priori, the apparent component approach was used. The vapor pressures of MEA and H₂O were estimated using a flash calculation in ASPEN PLUS. Their partial pressures were obtained with Raoult's law. The total pressure was obtained summing P_{CO_2} , P_{MEA} and $P_{\text{H}_2\text{O}}$. The

mole fractions were calculated dividing partial pressures by total pressure. Appendix A reports detailed inputs and results of the regression.

The DRS uses an algorithm developed by Deming (1943) called maximum likelihood. This algorithm treats all the experimental variables equally. Therefore temperature, pressure, liquid and gas phase mole fractions are all variables that contribute to a function to minimize. The function is given in equation 2.24 (Liu et al., 1999).

$$F = \sum_1^{ND} \sum_1^{NV} \left[\frac{(Z^{CAL} - Z^{EXP})}{\sigma} \right]^2 \quad (2.24)$$

The summation is over the total number of data points and the total number of variables. Z^{CAL} and Z^{EXP} are the calculated and experimental values, respectively. The standard deviation σ reflects the confidence of an experimental value. σ values for temperatures and pressures were set at lower values (higher confidence) than liquid phase mole fractions. The gas phase mole fractions of MEA were assigned a standard deviation of 100%, due to the large uncertainty of their values, which comes from the use of Raoult's law to calculate them. All the values for standard deviations can be viewed in Appendix A.

2.5.1. Reference states used in this work

The reference states for every component are those set by ASPEN PLUS. H₂O and MEA are both treated as solvents. Their reference state is the pure component. All the ions have a reference state of infinite dilution in water. The Henry components (CO₂, N₂ and O₂) have reference states at infinite dilution in the mixed solvent. Table 2.2 summarizes the reference states used and their meanings in terms of activity coefficients. This set of reference states was dictated by the defaults of ASPEN PLUS. As pointed out by Bishnoi (2000), there is a consistency problem with the reference state of infinite dilution in the mixed solvent for CO₂. $\gamma_{CO_2} \rightarrow 1.0$ as $x_{CO_2} \rightarrow 0.0$ in the mixed solvent. The problem is that ASPEN PLUS

sees the mixed solvent as the mixture of H₂O, MEA, and all the ions. The concentrations of MEA and ions change with loading, therefore the reference state is different as the loading changes. This would not be a problem if the Gibbs free energy of formation of CO₂ at the reference state changed accordingly; but the Gibbs free energy of formation is fixed, since the equilibrium constant is fixed. This creates a thermodynamic bug in ASPEN PLUS. It is not easy to quantify the effects of this bug. This inconsistency could not be removed, because it is built into the ASPEN PLUS code. The same inconsistency was present in the work of Austgen. Bishnoi (2000) removed the inconsistency by redefining the reference state of CO₂ as infinite dilution in water in a stand-alone FORTRAN code.

Table 2.2. Reference states and their definitions

Components	Activity coefficient definition
H ₂ O, MEA	Symmetric: $f_i = \gamma_i f_i^0 x_i$ $\gamma_i \rightarrow 1.0$ as $x_i \rightarrow 1.0$
Ions	Unsymmetric: $f_i = \gamma_i^* f_i^* x_i$ $\gamma_i^* \rightarrow 1.0$ as $x_i \rightarrow 0.0$ in pure water
CO ₂ , N ₂ , O ₂	Unsymmetric: $f_i = \gamma_i^* f_i^* x_i$ $\gamma_i^* \rightarrow 1.0$ as $x_i \rightarrow 0.0$ in mixed solvent

2.5.2. Henry's constant

The Henry's components in the mixture are CO₂, N₂, O₂. Nitrogen and oxygen are present as inert species. The values of their Henry's constant is not very important, because they are almost insoluble in the solvent. For CO₂, instead, the use of a good Henry's constant is required to regress a solid thermodynamic model. In ASPEN PLUS the problem is the way mixed solvents are treated. ASPEN PLUS calculates the Henry's constants in mixed solvents averaging the Henry's constant in pure solvents as in equations 2.25 through 2.27, as reported in the ASPEN PLUS manuals or in Liu et al. (1999).

$$\ln(H_{\text{CO}_2}/\gamma_{\text{CO}_2}^\infty) = \sum_A w_A \ln(H_{\text{CO}_2, A}/\gamma_{\text{CO}_2 A}^\infty) \quad (2.25)$$

$$\ln H_{\text{CO}_2, \text{A}}(T, p_A^*) = A + B/T + C \ln T + DT \quad (2.26)$$

$$H_{\text{CO}_2, \text{A}}(T, P) = H_{\text{CO}_2, \text{A}}(T, p_A^*) \exp \left(\frac{1}{RT} \int_{p_A^*}^P V_{\text{CO}_2, \text{A}}^{\infty} dp \right) \quad (2.27)$$

H_{iA} is the Henry's constant in pure solvent A, w_A is the weight fraction of solvent A, based on true solvent composition ratio (i.e. excluding all the components that are not solvents). γ_i^{∞} is the activity coefficient at infinite dilution in the mixed solvent, γ_{iA}^{∞} is the activity coefficient at infinite dilution in the pure solvent A. Equation 2.26 gives the Henry's constant in pure A at the vapor pressure of the mixture; equation 2.27 includes the Poynting correction, that brings the pressure up to the actual pressure of the solution. V_{iA}^{∞} is the infinite dilution partial molar volume of CO_2 in the mixture.

Based on the previous work of Austgen (1989), the Henry's constant of CO_2 in MEA was dropped. The values for the constant in equation 2.26 for $H_{\text{CO}_2, \text{H}_2\text{O}}$ are reported in Table 2.1.

Table 2.3. Values of regressed interaction parameters for the CO_2 -MEA- H_2O Electrolyte-NRTL model.

Parameter	Value	σ
$\tau_{\text{H}_2\text{O}-(\text{MEAH}^+\text{MEACOO}^-) \text{ A}}$	10.40	3.33
$\tau_{\text{H}_2\text{O}-(\text{MEAH}^+\text{MEACOO}^-) \text{ B}}$	-119.92	1055.66
$\tau_{(\text{MEAH}^+\text{MEACOO}^-)-\text{H}_2\text{O} \text{ A}}$	-5.963	1.30
$\tau_{(\text{MEAH}^+\text{MEACOO}^-)-\text{H}_2\text{O} \text{ B}}$	336.45	399.42
$\tau_{\text{H}_2\text{O}-(\text{MEAH}^+\text{HCO}_3^-) \text{ A}}$	6.88	19.91
$\tau_{\text{H}_2\text{O}-(\text{MEAH}^+\text{HCO}_3^-) \text{ B}}$	969.63	4107.75
$\tau_{(\text{MEAH}^+\text{HCO}_3^-)-\text{H}_2\text{O} \text{ A}}$	-3.89	6.99
$\tau_{(\text{MEAH}^+\text{HCO}_3^-)-\text{H}_2\text{O} \text{ B}}$	-91.35	1664.22

2.5.3. Regression results

Table 2.3 reports the values of the eight regressed parameters, along with their standard deviations. Except the regressed parameters, all the parameters were kept

at the values set by Austgen (1989). The standard deviations in the regressed parameters are all fairly high. This means that the confidence in each regressed parameter is low: the regression could have been done with a smaller number of parameters. The reason why eight parameters were used is that the same regression was performed by Won et al. (1999) with the same parameters, and this Electrolyte-NRTL model was built to reproduce the Won model.

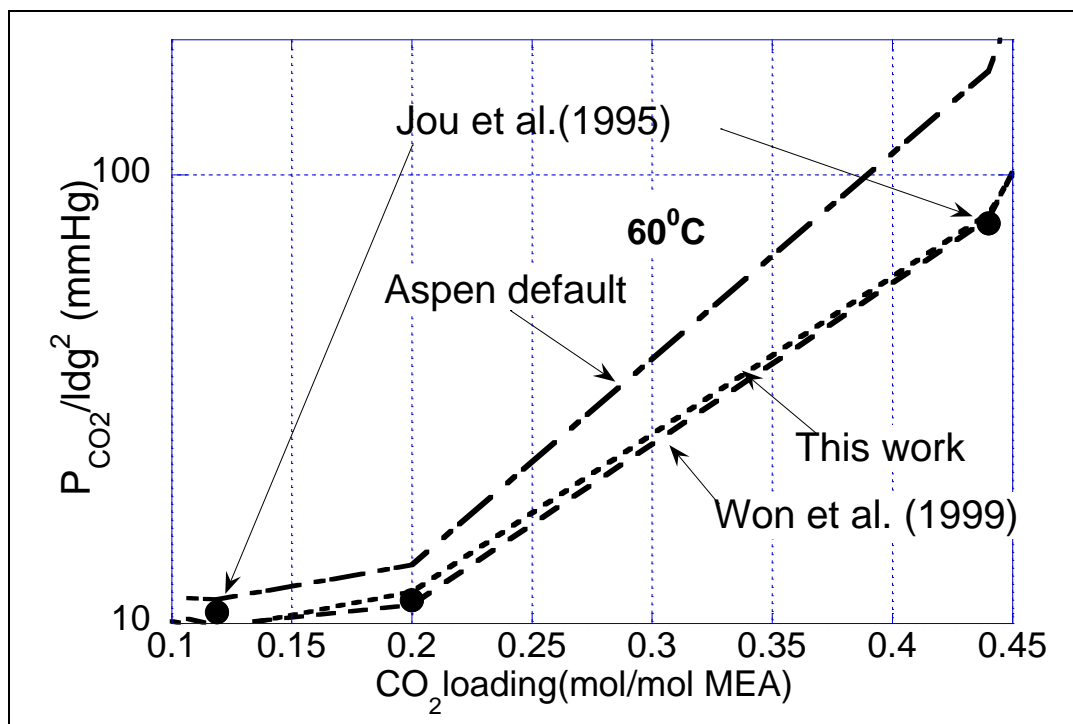


Figure 2.1. Equilibrium partial pressure of CO₂ at 60 °C for a 30wt% MEA solvent.

Figures 2.1 and 2.2 show the behavior at 60°C and 120°C respectively of the equilibrium partial pressure of CO₂. The partial pressure of CO₂ is reported as P_{CO_2} divided by the square of the loading. The curve generated by the model is compared to Jou's data points and with two other Electrolyte-NRTL models, the default of ASPEN PLUS and a model regressed by Won et al. (1999), which used the data of Jou et al. and a Henry's constant for CO₂ in MEA. The same data are tabulated in Table 2.4.

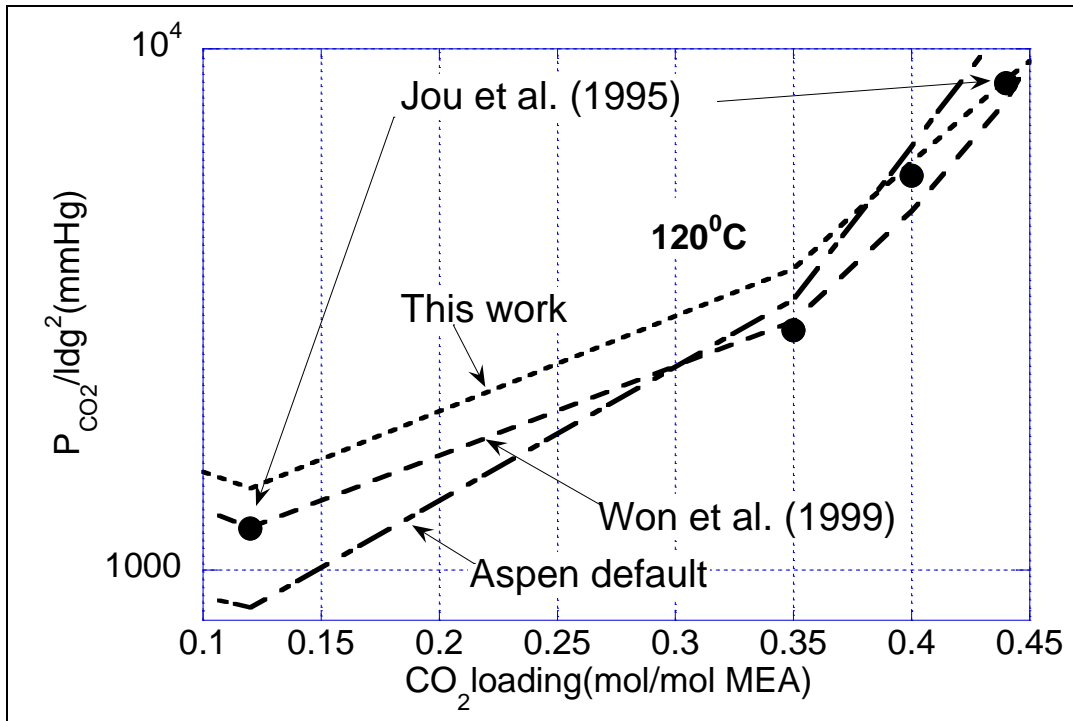


Figure 2.2. Equilibrium partial pressure of CO₂ at 120⁰C for a 30wt% MEA solvent.

Table 2.4. Comparison of VLE models and experimental data (Jou et al., 1995) at 60 °C and 120 °C.

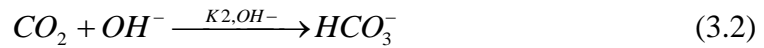
60⁰C							
	Loading	0.056	0.119	0.20	0.44	0.50	0.56
$P_{CO_2}^*$ mmHg	Jou (1995)	0.032	0.15	0.45	15.10	82.50	256
	Aspen	0.037	0.16	0.54	33	298	1961
	Won et al. (1999)	0.037	0.14	0.44	15.5	84.2	359
	This Work	0.035	0.137	0.47	15.86	70.16	226
120⁰C							
	Loading	0.025	0.12	0.35	0.40	0.44	0.47
$P_{CO_2}^*$ mmHg	Jou (1995)	0.738	17.30	353	915	1665	3165
	Aspen	0.661	12.20	405	1042	2172	3359
	Won et al. (1999)	1.1	17.39	368	782	1537	3035
	This Work	1.28	20.67	464	972	1695.7	2456

It can be noticed that both the model regressed in this work and the one regressed by Won et al. reproduce the experimental points much better than the default model provided by ASPEN PLUS. Since the work of Jou is considered of high quality, the model regressed in the present work can be applied with more confidence to the absorption/stripping modeling described in chapter 4.

Chapter 3

Rate Model

The absorption of carbon dioxide in monoethanolamine is a non-equilibrium process. The CO_2 reacts with MEA with finite rates. Even though the reaction is fast, it is generally not close to equilibrium at absorber conditions. Typical values for stage efficiencies in an absorber tray column are of the order of 0.1-0.2; for packed columns, efficiencies of 0.1 are typical for a height of packing of 2 or 3 feet. It is important to characterize the kinetics of the reactions in the system with rate expressions that contain temperature dependence and composition dependence. Two of the five reactions occurring (2.1 through 2.5), need a kinetic characterization. There are different possible ways to write these reactions, according to the possible equilibrium reactions incorporated in them. In this work the kinetic reactions are given by equations 3.1 and 3.2. These reactions are the two possible ways by which CO_2 can react directly in the mixture.



The rates can be both expressed with a second order expression.

$$R_{CO_2-MEA} = k_{2,MEA} [CO_2] [MEA] \quad (3.3)$$

$$R_{CO_2-OH^-} = k_{2,OH^-} [CO_2] [OH^-] \quad (3.4)$$

The rate constants $k_{2,MEA}$ and k_{2,OH^-} have Arrhenius expressions (equations 3.5).

$$k_2 = k_2^0 \exp\left(-\frac{E_A}{RT}\right) \quad (3.5)$$

Of the two mentioned reactions, only 3.1 contributes significantly to the absorption of CO₂. Even if the rate constant of reaction 3.2 is higher than that of 3.1, the former reaction is slow, because that the concentration of OH⁻ ions is always very small in solution. For most practical purposes, reaction 3.2 is not important. It can be non negligible only at rich conditions, when the CO₂+MEA reaction is slow.

3.1. Rate data used in this work

There are several researchers who have investigated the rates of reaction of CO₂ and MEA. A good summary of the work done so far on the subject can be found in Rochelle et al. (2001). A few representative experimental works are reported in Table 3.1. Five different experimental techniques have been used for the purpose of obtaining values for the rate constants: laminar jet, rapid mixing, wetted wall column, stirred cell and stopped flow. Most of the experiments agree on a value for the activation energy of approximately 41 kJ/mole. The rate expression chosen as a starting point for the model developed in this work was that of Hikita et al. (1977), given in equation 3.6. According to Blauwhoff et al. (1984) this expression well represents the rates between 5 and 80⁰ C; $k_{2,MEA}$ has units of liter/mol s.

$$\text{Log}_{10} k_{2,MEA} = 10.99 - \frac{2152}{T} \quad (3.6)$$

The concentration range of the data of Hikita is 0.015-0.18 M, much lower than the 5 M (approximately equal to 30 wt%) used industrially and studied in this work. This is a limitation to the validity of this model. Most of the other data are also at low amine concentration. The only investigator who analyzed higher MEA concentrations was Clarke (1964). The fact that the values are in relative agreement

with Hikita adds to the validity of the assumption that the rate constant is roughly independent of MEA concentration.

Table 3.1. Some literature data on the reaction between CO₂ and aqueous MEA.

Reference	T range (°K)	[MEA] (M)	k _{298 K}	E _A kJ/mol	Experimental technique
Clarke (1964)	298	1.6-4.8	7500		Laminar jet
Danckwerts And Sharma (1966)	291-308	1.0	7600, 6970	41.8	Laminar jet
Hikita et al. (1977)	278-315	0.015-0.18	5868	41.2	Rapid mixing
Alvarez-Fuster et al. (1980)	293	0.2-2.0	5750		Stopped flow
Penny and Ritter (1983)	278-303	0.009-0.06	4990	42.2	Stirred cell
Littel et al. (1992)	318-333		3703		

The kinetics of the reaction between CO₂ and OH⁻ have been correlated by Sherwood et al. (1975) (equation 3.7).

$$\ln k_{OH^-} = 31.396 - \frac{6658}{T} \quad (3.7)$$

This work took advantage of wetted wall column rate experiments done by Dang (2001). These experiments were run with the wetted wall column built by Mshewa (1995). The solution contained 5 M MEA and was loaded with CO₂ to 0.3-0.5 moles/mole MEA at 40⁰ C and 60⁰ C. These conditions are exactly the operating conditions of the absorber column modeled in this work. The rate data were used to correct the rate constant from the Hikita value. A comparison between the rate model developed in this work and the wetted wall data is shown later in this chapter.

3.2. Modeling of mass transfer in liquid boundary layer

The steady state diffusion of a species in the liquid phase due to a concentration gradient is governed by equation 3.8, obtained in rectangular coordinates, where x is the distance from the gas-liquid interface into the liquid phase and N is the flux of the species studied.

$$\frac{\partial N}{\partial x} = 0 \quad (3.8)$$

The flux of CO_2 can be expressed as a mass transfer coefficient times a driving force (equation 3.9).

$$N_{CO_2} = k_l^0 ([CO_2]_i - [CO_2]_{bulk}) \quad (3.9)$$

Different theories have developed to model mass transfer through a gas-liquid interface. The main mass transfer models are film theory, penetration theory, surface renewal theory and Eddy diffusivity theory. The two theories that were used in this work are film theory and Eddy diffusivity theory. They are both steady state theories, meaning that there are no time dependent variables in the models. Penetration theory and surface renewal theory are unsteady state theories and they will not be introduced here. A comparison between the four theories and the results obtained with them can be read in Bishnoi (2000).

3.2.1. Film theory

Film theory, introduced in 1924 by Lewis and Whitman, simply divides the liquid and gas phases into two regions, a bulk and a film. All the concentrations are assumed to change only in the film region. In the case of physical absorption (no chemical reactions occurring) the concentration profiles are linear in the film region and constant in the bulk region. Combining equations 3.8 and 3.9 with Fick's law, this theory predicts a mass transfer coefficient proportional to the diffusion

coefficient. This is not correct in most cases, where a square root dependence appears to be typical. Film theory is the simplest model for mass transfer and it is not able to represent well the absorption of CO₂ in aqueous MEA unless some changes are made.

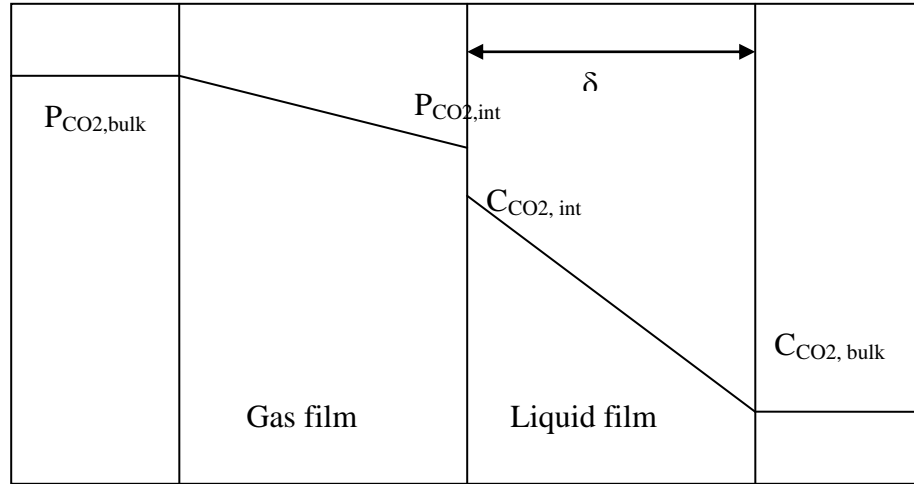


Figure 3.1. Physical absorption representation with film theory

3.2.2. Eddy diffusivity theory

This model was introduced by King (1966). It predicts a square root dependence of the mass transfer coefficient on diffusivity. This is achieved by the introduction of a square dependence of the diffusivities on the liquid depth (equation 3.10).

$$N_{CO_2} = -(D_{CO_2} + \epsilon x^2) \frac{\partial [CO_2]}{\partial x} \quad (3.10)$$

The expression for the mass transfer coefficient is given in equation 3.11.

$$k_l^0 = \frac{2}{\pi} \sqrt{D_{CO_2} \varepsilon} \quad (3.11)$$

The physical interpretation of this hypothesis is the presence of eddies in the liquid phase, that promote mass transfer as the distance from the surface increases.

3.3. Mass transfer with fast chemical reaction

When one or more reactions are present in the liquid phase, another term needs to be added to equation 3.8. Equation 3.12 represents the steady state diffusion-reaction equation when Eddy diffusivity theory is used.

$$\frac{\partial}{\partial x} \left[(D_{CO_2} + \varepsilon x^2) \frac{\partial [CO_2]}{\partial x} \right] - R_{CO_2} = 0 \quad (3.12)$$

The term R_{CO_2} contains all the kinetic (non equilibrium) reactions that CO_2 undergoes in the liquid phase. These include reactions 3.1 and 3.2 and their reverse.

The assumption that the chemical reaction is fast translates into the assumption that all the mass transfer is limited in a small region close to the gas-liquid interface, named boundary layer. This assumption is valid for the CO_2 -MEA reaction.

3.3.1. Pseudo first order models

The rigorous solution of the mass transfer with chemical reaction problem is rather complicated. It requires the solution of many simultaneous equations, as it is described later in this chapter. There are certain situations when it is not necessary to deal with the complicity of a large system of equations, if a few simplifying assumptions are satisfied. Assumptions 1 and 2 listed below lead to the pseudo first order (PFO) and interface pseudo first order (IPFO) approximations.

Assumption 1: the liquid phase driving force ($P_{CO_2, \text{interface}} - P_{CO_2, \text{bulk}}^*$) is small.

Assumption 2: the CO_2 +MEA reaction is fast enough that CO_2 reaches equilibrium with the rest of the solution, at its interface composition.

The IPFO approximation requires assumption 2; the PFO approximation requires assumption 1. In assumption 1 $P_{\text{CO}_2, \text{bulk}}^*$ is the partial pressure of CO_2 that would be in equilibrium with the bulk composition at the bulk temperature and loading. Small liquid phase driving force implies that the MEA is not significantly depleted at the interface and the reaction products do not build up at the interface. This assumption translates into the assumption that the concentrations of every component in solution, except CO_2 , can be considered constant in the liquid boundary layer. The assumption of small driving force is relative to the loading; at low loading there is a large amount of free MEA in solution, and a high driving force is necessary to break the validity of the assumption; at high loading there is little free MEA in solution: a very small driving force is required for the PFO assumption to be valid.

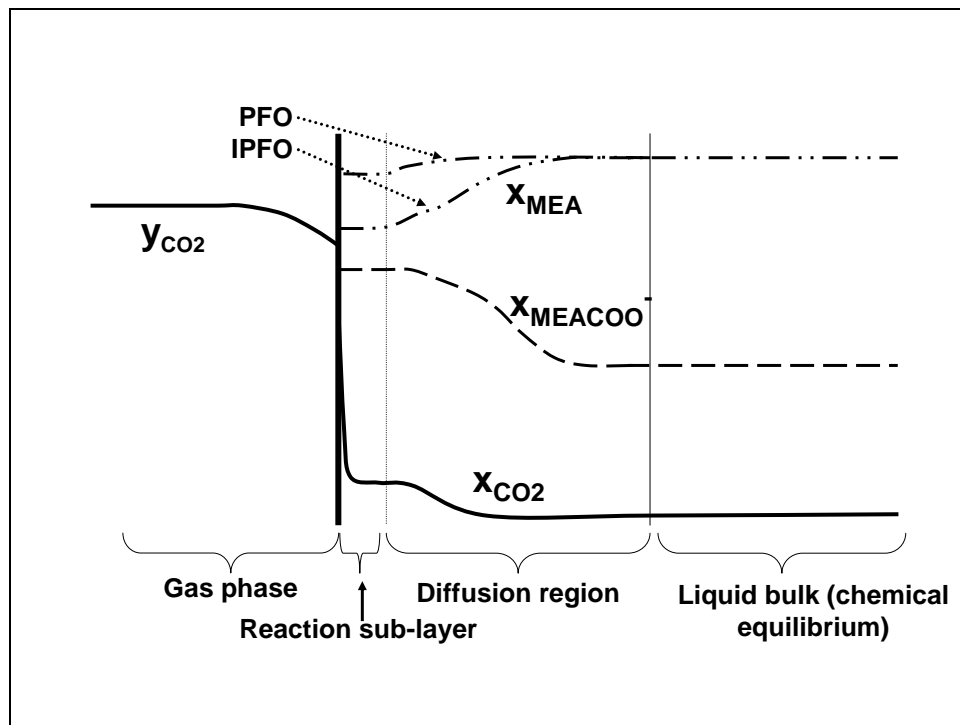


Figure 3.2. Representation of the PFO and IPFO approximations for absorption with fast chemical reaction.

Assumption 2 (IPFO) implies that all the reaction of CO_2 occurs in a small fraction of the boundary layer (that can be called reaction sub-layer), so that the CO_2 reaches equilibrium with the rest of the solution before the MEA and the other species in solution change significantly their concentrations from their values at the interface (CO_2 reaches an asymptote in this layer). The reaction sub-layer is controlled by the kinetics. In the diffusion region the MEA and the ions diffuse from and to the bulk; the CO_2 concentration changes, because it remains at equilibrium with all the other species.

Both the IPFO and PFO approximations assume that the concentration profiles of all the species in the reaction sub-layer, except CO_2 , are constant. The IPFO differs from the PFO approximation in that the profiles are assumed constant at their interface value, different from the bulk value. Figure 3.2 gives a graphical interpretation to the two assumptions.

The advantage of PFO and IPFO models is that the flux of CO_2 can be derived from the analytical solution of equation 3.12, when the two following boundary conditions are applied.

$$[\text{CO}_2] = [\text{CO}_2]_i \text{ @ } x=0 \text{ for PFO and IPFO} \quad (3.13)$$

$$[\text{CO}_2] = [\text{CO}_2]^*_{\text{bulk}} \text{ for PFO or}$$

$$[\text{CO}_2] = [\text{CO}_2]^*_i \text{ as } x \rightarrow \infty, \text{ for IPFO} \quad (3.14)$$

The x coordinate goes from the interface into the liquid bulk.

Applying phase equilibrium for CO_2 at the interface (equation 2.11), the analytical solutions for the CO_2 flux are equations 3.15 and 3.16, for PFO and IPFO respectively. In equations 3.15 and 3.16 the $\text{CO}_2 + \text{OH}^-$ reaction was neglected.

$$N_{\text{CO}_2} = \sqrt{k_{2,\text{MEA}}[\text{MEA}]_{\text{bulk}} D_{\text{CO}_2}} \frac{(P_{\text{CO}_2,i} - P_{\text{CO}_2,\text{bulk}}^*)}{(\gamma H)_{\text{CO}_2}} \quad (3.15)$$

$$N_{CO_2} = \sqrt{k_{2,MEA}[MEA]_i D_{CO_2}} \frac{(P_{CO_2,i} - P_{CO_2,i}^*)}{(\gamma H)_{CO_2}} \quad (3.16)$$

$P_{CO_2,i}^*$ is the partial pressure of CO_2 that would be in equilibrium with the composition at the interface.

The results are often reported as normalized flux k_g^I , defined by equation 3.17.

$$N_{CO_2} = k_g^I (P_{CO_2,i} - P_{CO_2,bulk}^*) \quad (3.17)$$

It is clear that equation 3.15 can be applied explicitly to calculate the flux, because $[MEA]_{bulk}$ can be calculated with an equilibrium model, like the one described in chapter 2. Equation 3.16 presents the problem that the concentration of MEA at the interface is not known a priori. Diffusion of reactants and products needs to be accounted for with mass transfer coefficients for those species. For example, for MEA an equation like 3.18 needs to be applied. Equation 3.18 represents in a simplified way the rate of mass transfer of MEA from the bulk to the interface, if a stoichiometric ratio of 1:1 holds for CO_2 and MEA.

$$[MEA]_{int} = [MEA]_{bulk} - \frac{N_{CO_2}}{k_{l,MEA}} \quad (3.18)$$

The knowledge of $k_{l,MEA}$ and of the mass transfer coefficients for the other species is required. Equations 3.16 and 3.18 need to be solved simultaneously.

If activity based kinetics are used, instead of concentration based kinetics, equation 3.16 turns into equation 3.19; the driving force is expressed in terms of activity and the Henry's constant of CO_2 is implicit in the activity of CO_2 . The activity coefficient that appears under the square root transforms the concentration based diffusivity into activity based diffusivity.

$$N_{CO_2} = \sqrt{k_{2,MEA}[MEA]_i \frac{D_{CO_2}}{\gamma_{CO_2}}} (a_{CO_2,i} - a_{CO_2,i}^*) \quad (3.19)$$

The activity of CO₂ at the gas-liquid interface can be calculated with equation 3.20, where $\gamma_{CO_2}^*$ is the unsymmetric activity coefficient of CO₂ and x_{CO_2} the mole fraction of CO₂.

$$a_{CO_2} = \gamma_{CO_2}^* x_{CO_2} \quad (3.20)$$

The activity $a_{CO_2,i}^*$ is the activity of CO₂ that would be in equilibrium with the interface composition. This is easy to define if a single kinetic reaction is considered; in this case $a_{CO_2,i}^*$ is calculated from the equilibrium equation for reaction 3.1:

$$a_{CO_2,i}^* = \left(\frac{x_{MEACOO^-} x_{H_3O^+}}{x_{MEA} x_{H_2O}} \frac{\gamma_{MEACOO^-} \gamma_{H_3O^+}}{\gamma_{MEA} \gamma_{H_2O}} \right)_i \quad (3.21)$$

3.3.2. IPFO model limitations: parallel reactions and rich conditions

If the reaction of CO₂ with hydroxide is included in the analysis done in the previous section, a few changes need to be made. Using activity based kinetics, the flux is represented by equation 3.22.

$$N_{CO_2} = \sqrt{\left(k_{2,MEA} [MEA]_i + k_{2,OH^-} [OH^-]_i \right) \frac{D_{CO_2}}{\gamma_{CO_2}}} (a_{CO_2,i} - a_{CO_2,i}^*) \quad (3.22)$$

The way $a_{CO_2,i}^*$ is calculated is no longer straight-forward. The term needs to contain both parallel reactions, in such a way that, at equilibrium, $a_{CO_2,i} = a_{CO_2,i}^*$. The expression chosen in this work is given by equation 3.23. The same type of problem is encountered if equation 3.16 is used to express the flux.

$$a_{CO_2,i}^* = \frac{\frac{k_{2,MEA}}{K_{CO_2-MEA}} \frac{a_{MEACOO^-} a_{H_3O^+}}{a_{H_2O} \gamma_{MEA}} + \frac{k_{2,OH^-}}{K_{CO_2-OH^-}} \frac{a_{HCO_3^-}}{\gamma_{OH^-}}}{k_{2,MEA} x_{MEA} + k_{2,OH^-} x_{OH^-}} \quad (3.23)$$

It can be shown that, if both reactions are at equilibrium, the right hand side is equal to the activity of CO₂. K_{CO_2-MEA} and $K_{CO_2-OH^-}$ are the equilibrium constants for reactions 3.1 and 3.2. Equation 3.22 is an arbitrary subdivision of the CO₂

reverse rate between reactions 3.1 and 3.2. This introduces a problem of the IPFO approximation; the representation of the reverse rates may not be accurate, when more reactions occur in parallel. In the case studied in this work, the rate of the $\text{CO}_2 + \text{OH}^-$ reaction is generally not important, but it is not negligible at high loading, when the $\text{CO}_2 + \text{MEA}$ reaction becomes slower. This problem is even more important in mixed amine solvents, where there are two fast reactions in parallel.

Another problem of the IPFO approximation is that its validity is questionable at high loading, when the rates of $\text{CO}_2 + \text{MEA}$ are reduced, because of the low concentration of free MEA. In this case it is possible that the CO_2 concentration profile does not reach equilibrium before the concentrations of MEA and reaction products change in the boundary layer, thus breaking the required assumption.

3.4. Rigorous boundary layer integration: Bishnoi FORTRAN model

A rigorous FORTRAN model was developed by Bishnoi (2000) for the interpretation of wetted wall column experiments with MDEA and piperazine. The code performs a rigorous integration of the boundary layer, in order to get concentration profiles for every species in solution. From the concentration profile the flux of CO_2 can be calculated. The mass transfer model used was the Eddy diffusivity theory.

The FORTRAN program was modified in this work in order to model the wetted wall column experimental data with MEA. Table 3.2 is a summary of the inputs and unknowns of the problem, the equations solved and their boundary conditions.

Table 3.2. Summary of inputs, unknowns, equations and boundary conditions for the rigorous integration of the boundary layer with the Bishnoi code.

Inputs	Unknowns	Equations	Boundary conditions
Temperature	$[\text{CO}_2](x)$	CO_2 overall material balance	@ $x=0$ $N_{\text{MEA}/\text{MEA}^+}=0$ $N_{\text{HCO}_3^-/\text{CO}_3^{2-}}=0$ $N_{\text{MEACOO}^-}=0$ Equilibrium relationships for reactions 2.3-2.4-2.5 $[\text{CO}_2]_i = [\text{CO}_2]_i^0$ Electroneutrality
MEA concentration	$[\text{MEA}](x)$	MEA overall material balance	
Loading (α)	$[\text{MEA}^+](x)$	Equilibrium for reaction 2.3	
P_{CO_2}	$[\text{MEACOO}^-](x)$	Equilibrium for reaction 2.4	
Liquid flow rate	$[\text{HCO}_3^-](x)$	Equilibrium for reaction 2.5	
	$[\text{CO}_3^{2-}](x)$	Electroneutrality	@ $x \rightarrow \infty$ $[i] = [i]_{\text{equilibrium}}$
	$[\text{H}_3\text{O}^+](x)$	Molecular CO_2 material balance	
	$[\text{OH}^-](x)$	MEACOO^- material balance	

3.4.1. Simple equilibrium model and physical properties used in the Bishnoi FORTRAN model

The density and viscosity were correlated using the empirical correlations of Weiland (1996). Both correlations account for temperature, MEA concentration and CO_2 loading effects. The diffusivity of CO_2 was related to the viscosity according to a Stokes-Einstein correlation (equation 3.24), used previously by Pacheco (1998).

$$D_{\text{CO}_2} = D_{\text{CO}_2, \text{water}} \left(\frac{\mu_{\text{water}}}{\mu_{\text{solution}}} \right)^{0.545} \quad (3.24)$$

The equilibrium model used in the FORTRAN code was not the rigorous Electrolyte-NRTL model described in Chapter 2, but a simple model where the activity coefficients were all defaulted to 1 and two adjustable parameters were

tuned to match equilibrium data. Due to the poor results in matching the experimental data, the model will not be described in details here.

The Henry's constant used is loading dependent (it corresponds to the term γH_{CO_2} in equation 2.11). The correlation used was developed by Weiland (1996).

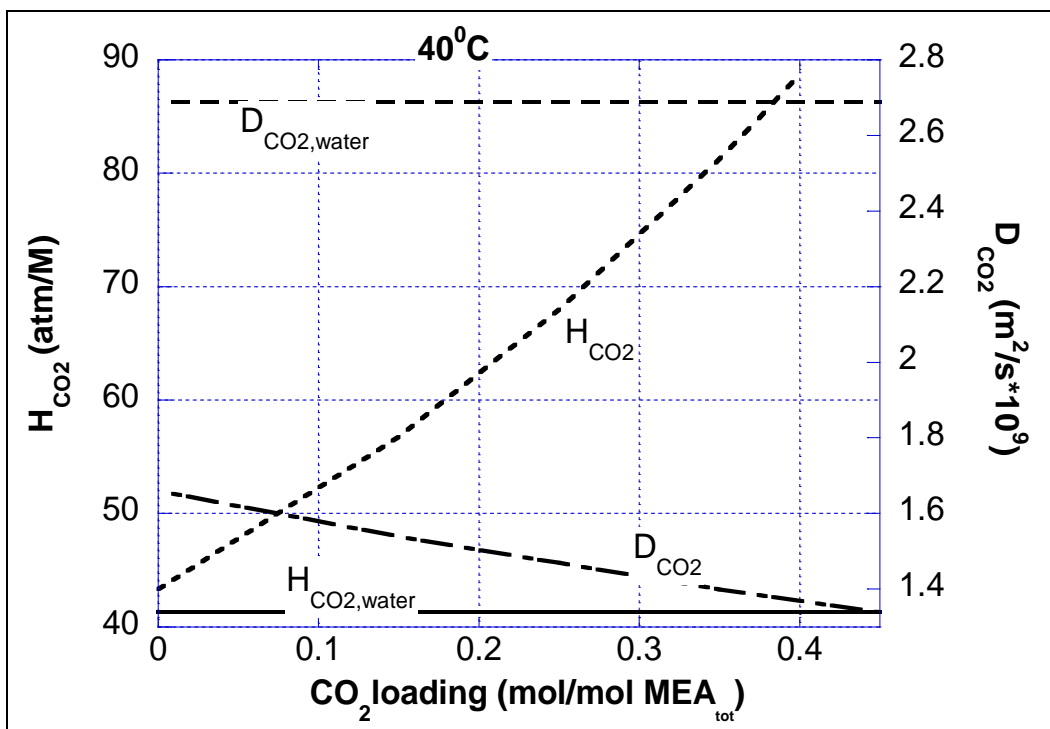


Figure 3.3. Loading effects on diffusivity and Henry's constant of CO₂ in 5 M aqueous MEA at 40° C.

Figure 3.3 shows that diffusivities and the Henry's constants are dependent on loading. The lines in Figure 3.3 are at 40° C, but the experimental loading dependences, obtained from the work of Weiland (1996), refer to a temperature of 25° C. At different temperatures these dependences are likely to change, especially for the Henry's constant. The loading dependence is an activity coefficient effect, thus it is related to liquid phase non-idealities described in Chapter 2.

There are no data available at higher temperature for CO₂ physical solubility in loaded solutions. It is recommended that measurements of physical solubility be

made in a range of temperatures from 40⁰ C to 60⁰ C, in order to be able to interpret the system non-idealities with confidence in an absorber integrated model.

3.4.2. Results with the Bishnoi model

Figure 3.4 reports the results of the attempt to reproduce the wetted wall column data (Dang, 2001). The Figure reports k_g^I at 60⁰ C. The model runs were made setting $P_{CO_2,i}$ to 10 times the $P_{CO_2}^*$. The experimental points are compared to the results generated with the rigorous Bishnoi model, with the PFO model and with the IPFO model. In the case of the IPFO model, the interface composition was calculated using the rigorous Bishnoi code.

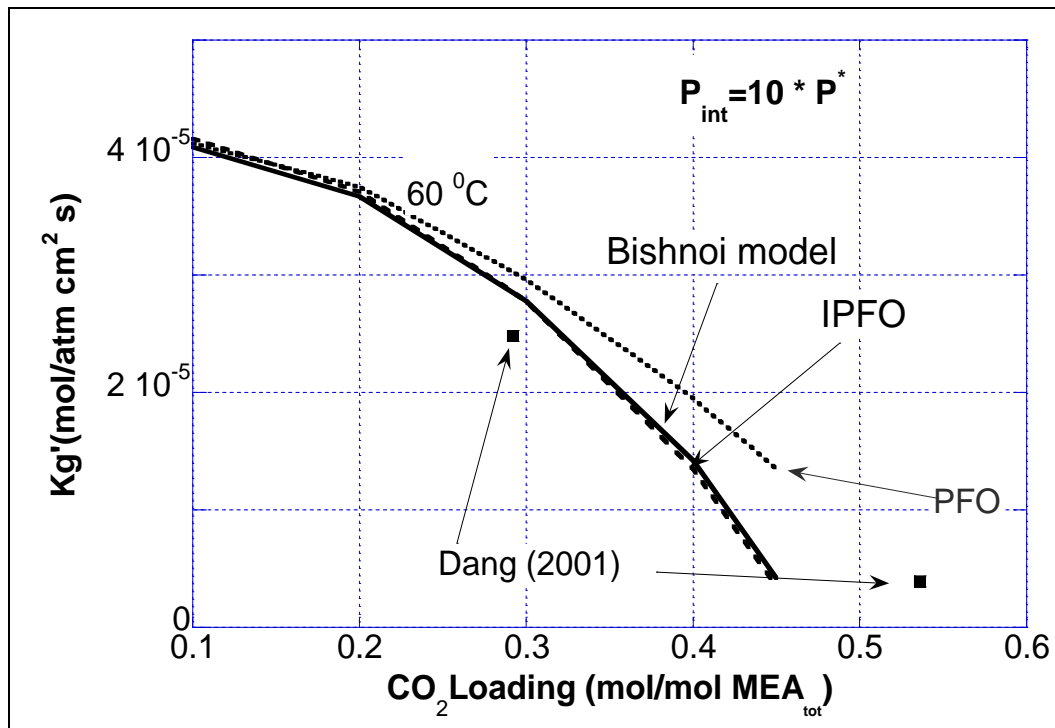


Figure 3.4. Comparison of rigorous model, IPFO model and PFO model for k_g' at 60⁰C.

The model does not match the experimental data well. This can be due to two reasons. First, the simple equilibrium model does not calculate reliable values for

the bulk equilibrium composition; secondly, the uncertainty on diffusivity of MEA and ions can explain the larger error at high loading, where there is a lot of MEA depletion at the interface and the diffusion of MEA and products is important.

The interesting result of the comparison is that the IPFO model reproduces very well the rigorous model. This means that, if the equilibrium model were reliable and the diffusivities of MEA and ions were correct, the IPFO model would match well the experimental data. The fact that the IPFO model reproduces the rigorous model results means that the assumption of reaction much faster than diffusion of MEA and products is verified. The knowledge of good values for the mentioned diffusivities would allow the use of the IPFO model, which has the advantage of converging faster than the rigorous integration.

From Figure 3.4, it can be seen that the PFO model follows the rigorous model well at low loading, as expected, whereas it overpredicts the k_g^I when the loading is higher than 0.2.

3.5. RATEFRAC kinetic model

A rate model was developed with RATEFRAC, the ASPEN PLUS module that solves packed or tray columns by rigorous rate calculations. Reaction kinetics, mass transfer coefficients and heat transfer coefficients are used to determine mass transfer rates and heat transfer rates. It is the most rigorous model that ASPEN PLUS provides for the solution of columns. The model was customized to reproduce the IPFO approximation.

The diffusivities of the MEA and the ions in solution are estimated by ASPEN PLUS. Binary mass transfer coefficients and heat transfer coefficients are calculated by ASPEN PLUS using the correlation of Onda et al. (1968).

RATEFRAC divides any packed column into a user defined number of segments, each corresponding to a given height. In this work the segments were defined to be well mixed in both the liquid and the gas phase. Given nominal

interfacial area for the packing, ASPEN PLUS uses the Onda correlation (Onda et al., 1968) to estimate wetted area per unit volume. With the specified column diameter and the height of a segment, ASPEN PLUS can estimate the wetted area per segment. For the wetted wall column modeling, the wetted area is fixed and known, thus the area routine was by-passed and a fixed value was assigned to the wetted area.

On every segment, RATEFRAC performs non-equilibrium material and energy balances on the liquid and the gas phases. When non-equilibrium reactions are present, ASPEN PLUS requires that a kinetic expression is provided, in order to calculate a value for the number of moles of each component reacted on the segment, which is then included by ASPEN PLUS into the material and energy balances.

ASPEN PLUS uses film theory to describe the liquid boundary layer. Unlike a rigorously integrated model, RATEFRAC does not calculate compositions between the interface and the bulk, but simply calculates the total amount of reaction on a segment, averaging the reaction rates at the interface and in the bulk, according to equation 3.25.

$$n_{CO_2} = \left(\frac{R_i + R_{bulk}}{2} \right) (holdup)_i + R_{bulk} (holdup)_{bulk} \quad (3.25)$$

n_{CO_2} is the number of moles reacted in a segment, R is the reaction rate, $holdup_{bulk}$ is the specified liquid holdup, $holdup_i$ is the volume of the boundary layer, calculated by ASPEN PLUS using equation 3.26, where δ is the thickness of the boundary layer, calculated by ASPEN PLUS, a_w is the wetted interfacial area per unit volume, S is the column diameter, and z is the height of the segment. For the wetted wall column, the term $a_w S z$ is known and constant.

$$(holdup)_i = \delta a_w S z \quad (3.26)$$

The bulk reaction term is usually negligible, because the reaction is fast enough that chemical equilibrium is reached within the boundary layer. Under this

assumption, if equation 3.25 is divided by $a_w S_z$, the flux is represented by equation 3.27.

$$N_{CO_2} = \frac{R_i}{2} \delta \quad (3.27)$$

3.5.1. User kinetic subroutine

Two bugs in the ASPEN PLUS algorithm needed to be fixed with a user kinetic subroutine. The subroutine code is provided in Appendix B for reference.

If a second order concentration based expression is used for k_2 (as in equation 3.3), the flux becomes

$$N_{CO_2} = \frac{\delta}{2} k_{2,MEA} [MEA]_i ([CO_2]_i - [CO_2]_i^*) \quad (3.28)$$

There are two problems with the formula represented by equation 3.28. The first is that there is a first order dependence on $k_{2,MEA}$ and $[MEA]_i$, whereas there should be a square root dependence, according to equation 3.16.

The second problem is that the RATEFRAC model does not have activity based kinetics as an option. The concentration driving force ($[CO_2]_i - [CO_2]_i^*$) is not consistent with the Electrolyte-NRTL equilibrium model. $[CO_2]_i^*$ is defined by equation 3.29.

$$[CO_2]_i^* = \frac{[MEACOO^-]_i [MEAH^+]_i}{[MEA]_i} \quad (3.29)$$

When this concentration driving force is zero, the interface is not necessarily at equilibrium. This can lead to wrong results if equilibrium is important in any part of the column. Activity based kinetics are required to solve this inconsistency.

Both problems were solved writing a FORTRAN kinetic subroutine for RATEFRAC. The routine computes a flux according to equation 3.22, which gives the right dependencies to $k_{2,MEA}$ and $[MEA]_i$, and uses activity based kinetics. The diffusivity of CO_2 , required in equation 3.22, was calculated in the subroutine, with the method described by equation 3.24. The viscosity was calculated with the

method of Weiland et al. (1996). Equation 3.23 was used to calculate $a_{CO_2,i}^*$. The interface composition is calculated by RATEFRAC iteratively, using built-in diffusivities for MEA and the ions. All the activity coefficients are calculated with the Electrolyte-NRTL model described in Chapter 2.

RATEFRAC requires that n_{CO_2} , the number of moles of CO_2 reacted in a segment, is returned to the program; n_{CO_2} is related to the flux N_{CO_2} through the wetted area, the column cross-sectional area and the segment height, according to equation 3.30.

$$n_{CO_2} = N_{CO_2} a_w S z \quad (3.30)$$

The wetted area is calculated in the subroutine, using the correlation of Onda et al. (1968).

3.5.2. Results with the RATEFRAC model

The FORTRAN subroutine discussed above was used to model the wetted wall column data of Dang (2001). The rate constant $k_{2,MEA}$ was adjusted in order to match the experimental k_g^I . The adjustment factor (AF) is defined in equation 3.31.

$$N_{CO_2,calc} = \sqrt{\left(AF k_{2,MEA} [MEA]_i + k_{2,OH^-} [OH^-]_i \right) \frac{D_{CO_2}}{\gamma_{CO_2}} (a_{CO_2,i} - a_{CO_2,i}^*)} \quad (3.31)$$

$k_{2,MEA}$ is the rate constant of Hikita et al. (1977). The normalized flux, not the flux was matched, so that equilibrium mismatch was not accounted for in the correction.

At low loading the normalized flux is almost independent of the diffusivities of MEA and reaction products (the PFO approximation is valid). The low loading data were used to adjust the k_g^I calculated with the Hikita kinetics. The adjustment factor corrects for uncertainties on the rate constant, the diffusivity of CO_2 , the activity coefficients and the Henry's constant. The adjustment factor takes the form of equation 3.32. The temperature dependence of AF reflects the need of different corrections at 40 and 60 °C. The data at higher loading were modeled with the adjusted k_g^I .

$$\ln AF = -11.32 + \frac{4050.6}{T(^{\circ}K)} \quad (3.32)$$

This correction translates into a factor of 5 at 40 $^{\circ}\text{C}$ and a factor of 2.3 at 60 $^{\circ}\text{C}$. This correction is significant and it can be attributed to the increased solution ionic strength in loaded solutions. This is consistent with the results of Pinsent et al. (1956), who showed that ionic strength as 1 M NaCl increased the reaction rate of CO_2 with ammonia by a factor of 3.

Table 3.3 reports the simulation results for the four data sets collected by Dang (2001). The temperature, loading and gas bulk P_{CO_2} were used as inputs; the driving force was calculated in ASPEN using the built-in correlation for gas phase mass transfer coefficient and the regressed Electrolyte-NRTL equilibrium model. Figures 3.5 through 3.9 show the results graphically.

It is important to reproduce the experimental temperature dependence of k_g^I , in order to build a reliable model for a non-isothermal absorber. As it can be seen from Table 3.3, k_g^I increases with temperature. The temperature dependence in the adjustment factor corrects for uncertainties in the temperature dependences of Henry's constant, CO_2 diffusivity and activity coefficient.

The plots show that the data at low loading are reproduced accurately by the model. This is expected, because the model was adjusted based on these data. The data at high loading, instead, are underpredicted by approximately 100%. Two reasons could be the cause of this problem. The first reason is related to the fact that, at 0.5 mol CO_2 /mol MEA, the diffusivity of MEA and ions determines the flux; if the diffusivities are underpredicted, the flux is underpredicted. The second reason relates to the reliability of the experimental data at high loading. It is difficult to measure high loading accurately, because of the high tendency of CO_2 to desorb.

Table 3.3. RATEFRAC modeling results of Dang's data.

	T ($^{\circ}\text{C}$)	Loading	($P_i - P_{\text{bulk}}^*$) (atm)	Flux _{exp} (mol/cm ² s)	k_g^I (mol/cm ² atm s)
--	--------------------------	---------	-------------------------------------	---	-------------------------------------

			Exp	Calc	Exp	Calc	Exp	Calc
40 °C $\alpha=0.3$	40	0.297	9.02E-04	9.47E-04	1.88E-08	1.92E-08	2.02E-5	2.00E-5
	40	0.297	1.10E-03	1.14E-03	2.16E-08	2.29E-08		
	40	0.297	1.24E-03	1.32E-03	2.55E-08	2.63E-08		
	40	0.297	1.41E-03	1.48E-03	2.84E-08	2.97E-08		
40 °C $\alpha=0.5$	40	0.521	3.27E-01	Not conv.	8.71E-07	Not conv.	3.56E-6	Not conv.
	40	0.514	2.99E-01	Not conv.	1.07E-06	Not conv.	3.83E-6	Not conv.
	40	0.512	2.78E-01	Not conv.	1.35E-06	Not conv.	4.50E-6	Not conv.
	40	0.509	2.45E-01	3.85E-01	1.50E-06	8.22E-07	4.59E-6	2.13E-06
60 °C $\alpha=0.3$	60	0.28	4.05E-03	4.96E-03	9.72E-08	1.25E-07	2.45E-5	2.48E-5
	60	0.287	5.07E-03	6.12E-03	1.23E-07	1.52E-07		
	60	0.291	6.04E-03	7.25E-03	1.50E-07	1.78E-07		
	60	0.292	7.13E-03	8.46E-03	1.76E-07	2.07E-07		
60 °C $\alpha=0.5$	60	0.536	1.56E-01	1.45E-01	6.10E-07	3.47E-07	3.90E-06	2.4E-06
	60	0.531	1.94E-01	1.97E-01	9.28E-07	4.96E-07	4.79E-06	2.5E-06
	60	0.529	2.22E-01	2.25E-01	9.51E-07	5.29E-07	4.28E-06	2.3E-06

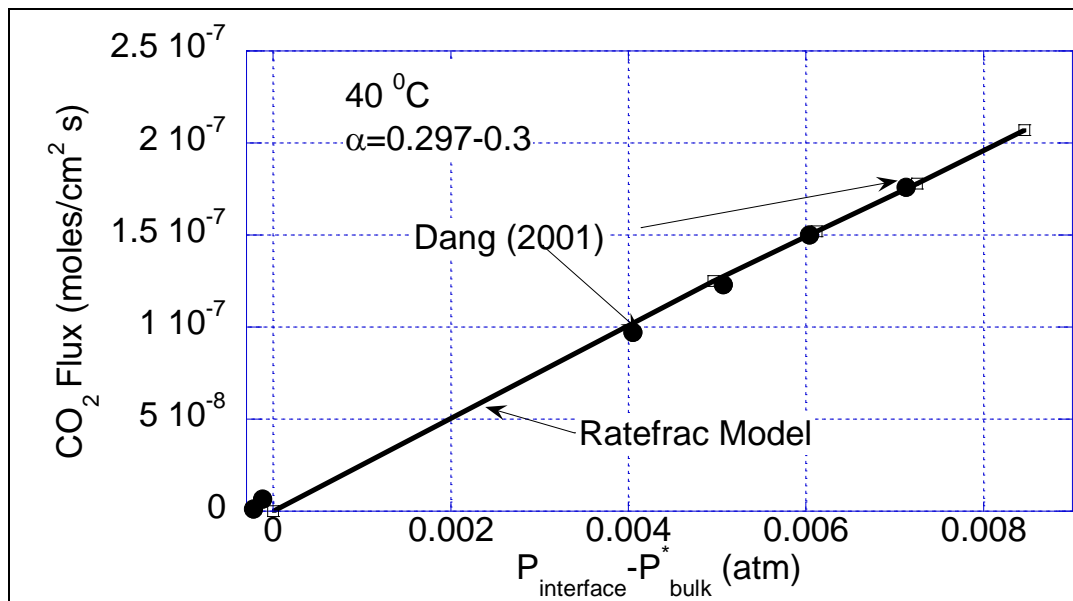


Figure 3.5. Results of the RATEFRAC model at 40° C and loading of approximately 0.3.

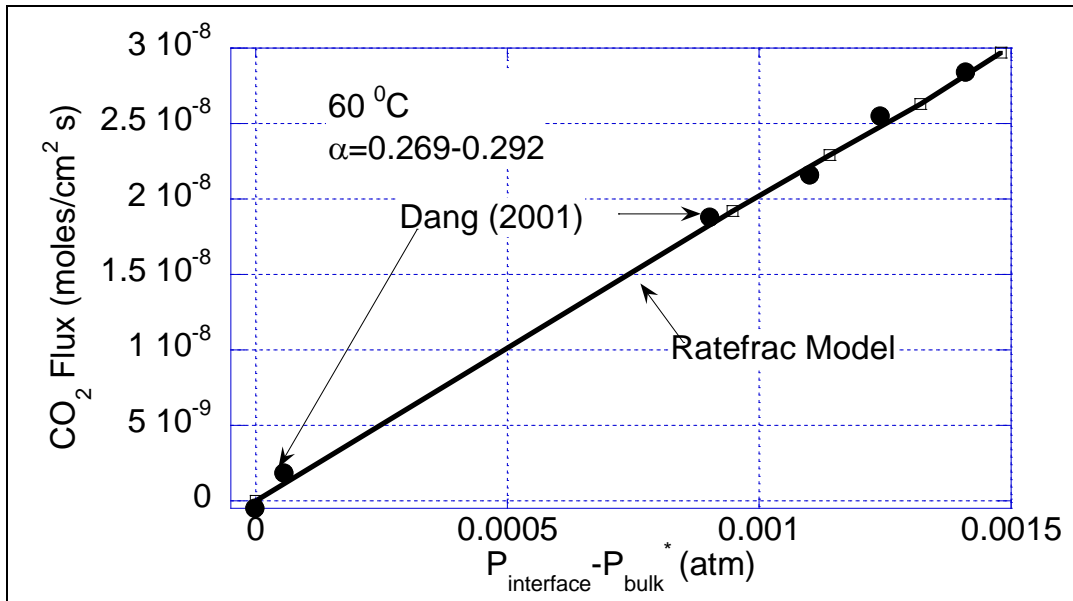


Figure 3.6. Results of the RATEFRAC model at 60 °C and loading of approximately 0.3.

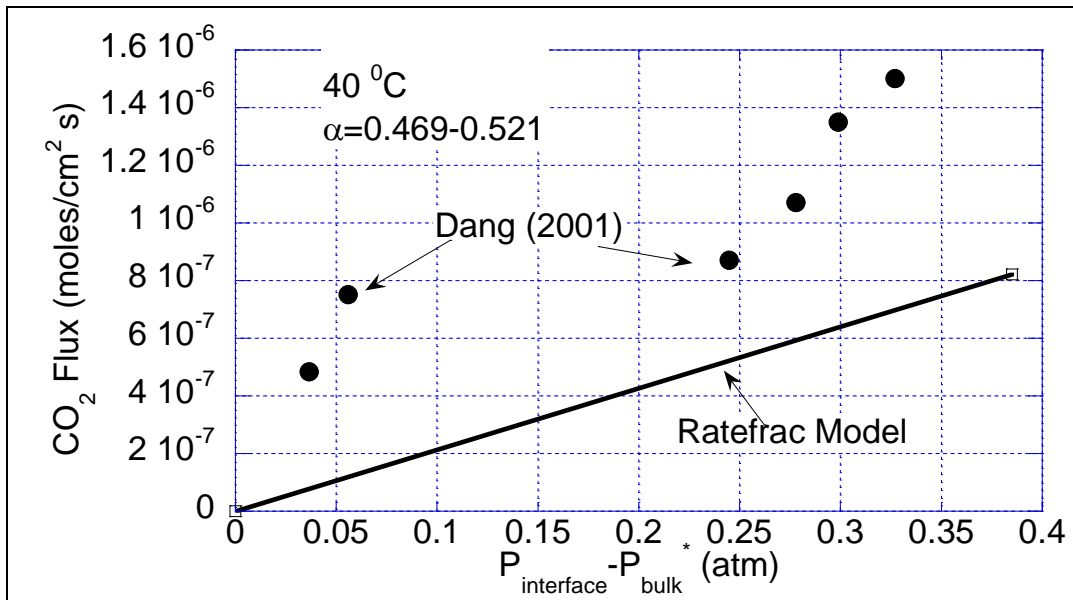


Figure 3.7. Results of RATEFRAC model at T=40°C and loading of approximately 0.5.

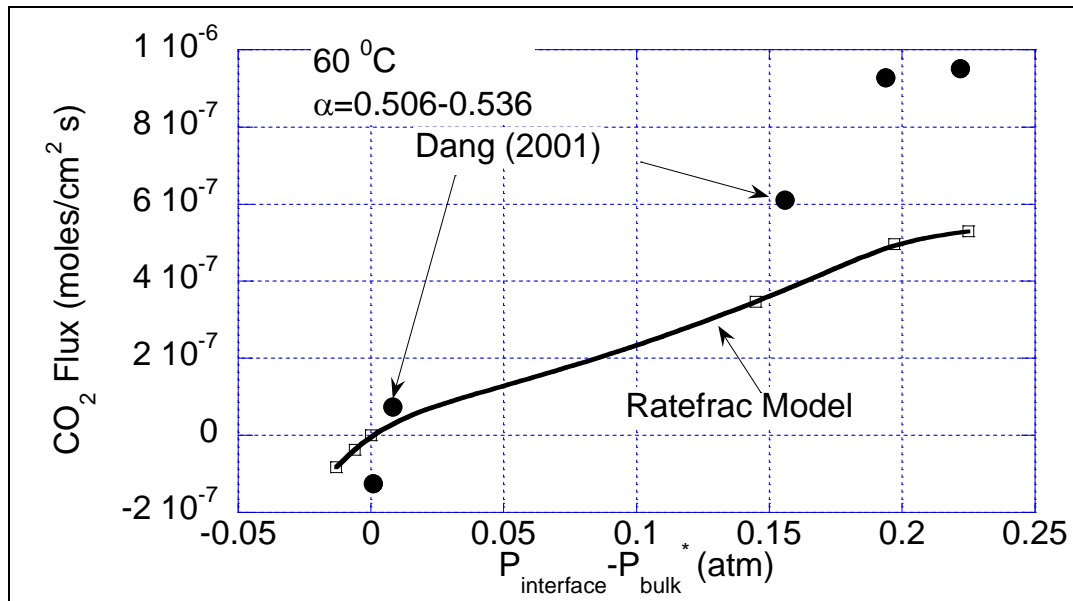


Figure 3.8. Results of the Retefrac model at 60⁰ C and loading of approximately 0.5.

3.6. Recommendations

The results shown in this chapter suggest that the rate model still needs improvements. The limited amount of experimental data does not allow a regression of parameters. More experiments with the wetted wall column and loaded 5 M MEA are recommended in order to regress the dependence of k_g^I on loading.

The fact that there are no data for physical solubility in loaded solutions at absorber temperature represents a weakness of the model. Measurements of CO₂ physical solubility in loaded solutions of aqueous MEA are therefore recommended.

The model also needs better values of MEA diffusivity in the aqueous solution. Wetted wall column experiments at high loading could be used to estimate the value of the diffusivity of MEA at different temperatures and loadings.

Chapter 4

Integrated Modeling

The thermodynamic model and the rate model described in chapters 2 and 3 were used to model the absorber and the stripper of the CO₂ removal process described in chapter 1. Figure 4.1 shows the absorption/stripping process. The values shown in the Figure were measured in a commercial plant (Bellingham), which was used as a base case. The values are reported in Won et al. (1999). The heights of the columns and the type of packing are not reported here, because they are proprietary information of Fluor Corp. The reboiler duty is reported normalized to the number of moles of CO₂ removed; the values are divided by a typical operating value, which will not be disclosed because of proprietary information of Fluor Corp. This reboiler duty will be referred to as relative specific reboiler duty and will be indicated with Q_{rel} .

The base case MEA concentration in the solvent is 30 wt% on an unloaded basis. A characteristic of the base case solvent is that, during the test days, it was partially degraded to heat stable salts. The heat stable salts will be defined and covered later in this chapter. The concentration of 30 wt% is considered heat stable salt free. The base case was run with 3.5 wt% heat stable salts.

The base case is a low CO₂ process (3.13 mol%), typical of gas turbine exhausts. The removal of CO₂ in the absorber is approximately 85%, leading to a CO₂ partial pressure in the vent of approximately 40 mmHg. The absorber operates

at 1 atm, with the inlet gas at 2 psig in order to overcome the pressure drop in the column. The flue gas coming from the turbine exhausts at 1 atm and 240 °F is cooled to 115 °F in a water saturator; it goes through a blower that compresses it to 2 psig and the temperature increases to 145°F. The absorber pressure is kept as close as possible to 1 atm, because the compression costs can be prohibitive at higher pressure.

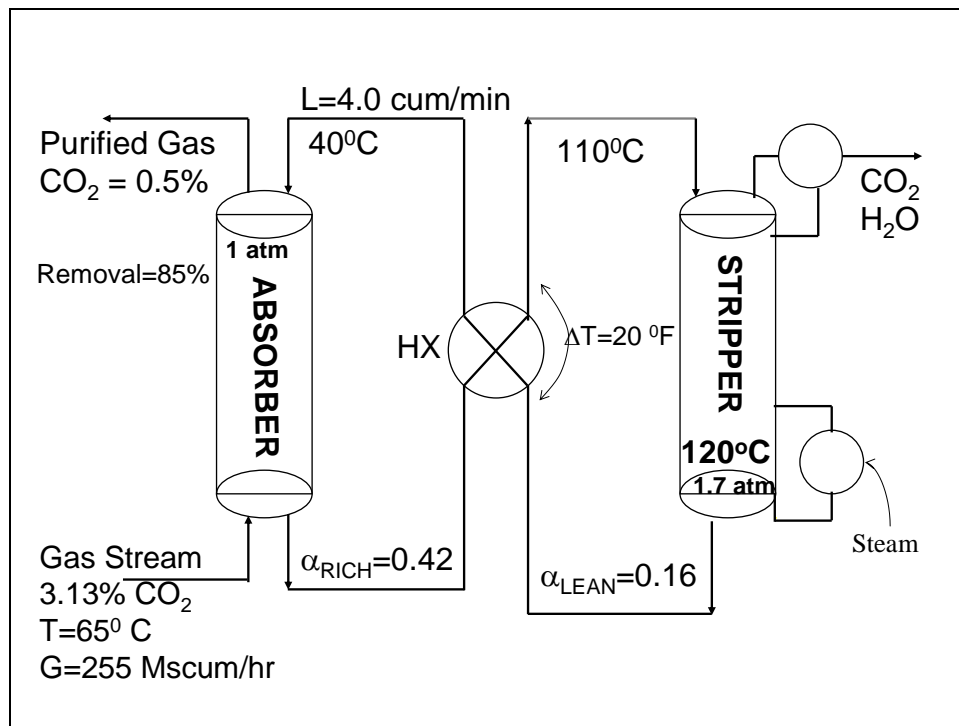


Figure 4.1. Base case absorption/stripping process with 30 wt% aqueous MEA (Bellingham plant).

As described in chapter 1, the stripper pressure is higher, because this increases the fraction of the heat duty that is used to desorb CO₂, compared to the fraction that goes into evaporation of water. The other reason for operating at higher pressure is that CO₂ needs to be sent to further processing or disposal. Operating at lower pressure would require more compression of CO₂ downstream.

Higher pressure requires higher temperatures. The cross heat exchanger heats the rich solvent to stripper temperature. The steam operated reboiler provides the remainder of the energy required to heat the solvent (sensible heat), along with the heat required to generate stripping steam and the heat required to reverse the $\text{CO}_2 + \text{MEA}$ reaction.

The absorber and stripper column models are now described separately.

4.1. Absorber models

The absorber column was modeled in two different ways. One way uses the RATEFRAC model developed for the wetted wall column (described in section 3.4). The second way uses ASPEN RADFRAC and stage efficiencies calculated with the Bishnoi FORTRAN model (described in section 3.3). Only RATEFRAC was used to model the overall process, but the RADFRAC model provides an interesting alternative way to represent the absorber, and it will be described in this chapter.

4.1.1. RATEFRAC model

The RATEFRAC model for the absorber column uses the same principles explained in section 3.4 for the wetted wall column model. The difference is that the gas-liquid interfacial area is not fixed for the column. The packing used was specified in the packing specification form in the RATEFRAC interface, and the interfacial area was calculated by ASPEN PLUS, using the correlation of Onda et al. (1968). Twenty segments were used to represent the packing. They were defined to be well mixed in both gas and liquid phases. The solvent enters the column at the first segment, the flue gas enters at the bottom segment.

The choice of 20 segments was based on an analysis done on the single base case absorber column. The number of segments was increased from 10 up to when the predicted CO_2 removal was not affected by the number of segments significantly. Going from 20 to 30 segments, the removal changed by 1 %. A

higher number of segments could give more accurate results, but the computation time would be too long.

The kinetic subroutine was the same used for the wetted wall model. An input file for the base case simulation (of the whole process) is included in Appendix C. It does not include the data that are proprietary to Fluor Corp.

Using the same kinetic constants as in the wetted wall column, the simulation did not match successfully the plant base case data. The performance was slightly underpredicted. The flux predicted by equation 3.22 was multiplied by an adjustment factor to reproduce the plant data. Two arguments can be used to explain the necessity of an adjustment factor.

1. The correlation of Onda et al. (1968) may not be satisfactory for this type of packing. The Onda model predicts a wetted area of approximately one half of the total area for the packing used. The adjustment factor would imply a wetted area greater than 50% of the total area. Measurements of wetted area are needed to prove this hypothesis.
2. The issue of wrong diffusivities for MEA and ions, described in section 3.4, can cause underprediction of absorption rates at high loading. The absorber bottom, in this base case, is at loading of 0.42. At this value of loading the diffusivities of MEA and reaction products can be important.

It is impossible to attribute the error to one specific reason, unless more measurements are made. All the results must be interpreted with caution: if the main cause of the error is wrong calculated wetted area, it is likely that, as the conditions change, the factor still holds and the results are reliable; if the main cause of the error is wrong diffusivities, then a constant correction factor is likely to overpredict performance at low loading and to underpredict performance at high

loading. This is because at low loading the diffusivities are unimportant, whereas they are rate controlling in absorbers that operate at high loading.

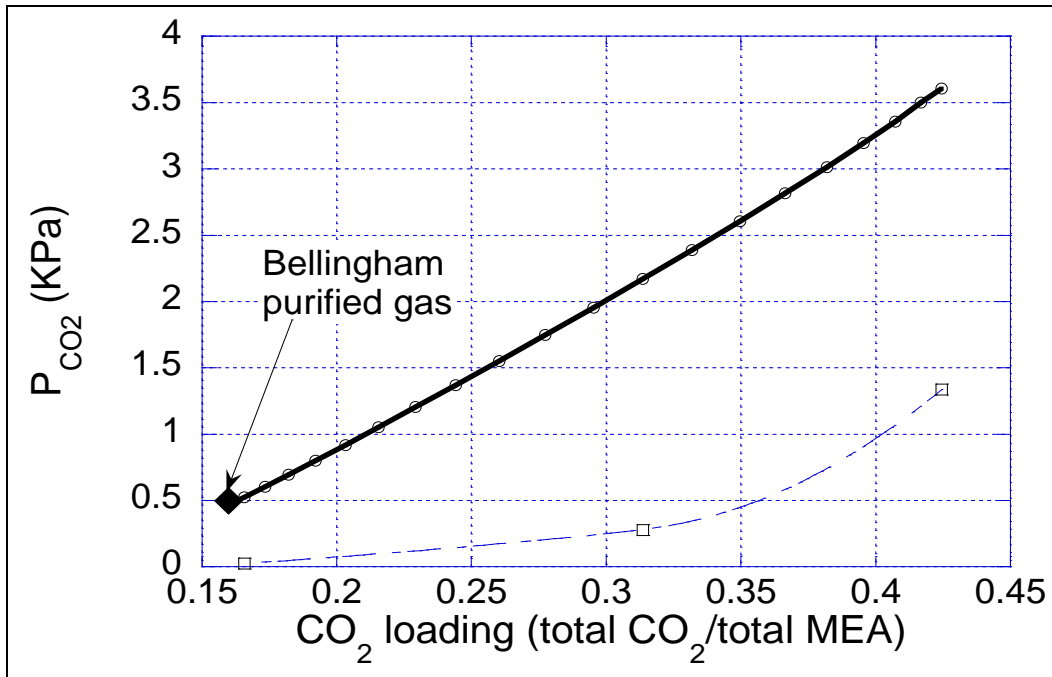


Figure 4.2. McCabe-Thiele diagram for Bellingham base case absorber, outlet gas P_{CO_2} compared to plant value, k_g^I adjusted, heat stable salts included in analysis.

Figure 4.2 is the McCabe-Thiele diagram derived for the base case absorber column with the RATEFRAC model. The point on the diagram represents the base case outlet CO_2 concentration, measured at the Bellingham plant. It can be observed that the absorber does not pinch in any point of the column. An equilibrium pinch is defined as a point in a column where the driving force is very small, and equilibrium and operating lines are close to each other. Pinches are often associated to several stages, or segments, that achieve little or no removal.

The equilibrium line in Figure 4.2, like those of all the McCabe-Thiele diagrams that will follow, was derived by calculating $P_{CO_2}^*$ with a bubble point

calculation, using the liquid temperature and composition of three segments in the column. A FLASH block in ASPEN PLUS was used to calculate the bubble point. The equilibrium model was the Electrolyte-NRTL model described in Chapter 2.

4.1.2. RADFRAC model

ASPEN RADFRAC is the ASPEN PLUS module that solves equilibrium stage columns. The absorber column in the CO₂ removal process is a packed column, and it has limited absorption rates. An equilibrium stage model cannot be applied directly to this process. Stage efficiencies need to be used, in order to account for finite rates. The transition packing-stage is done assigning a fixed height of packing to a stage, and treating that height of packing as well mixed in both gas and liquid phase (this assumption is followed also in RATEFRAC). The Murphree stage efficiency is defined as

$$eff = \frac{y_{out} - y_{in}}{y^* - y_{in}} \quad (4.1)$$

where y_{in} and y_{out} refer to Figure 4.3 and y^* is the gas phase mole fraction that would be in equilibrium with the liquid leaving the stage (x_{out}).

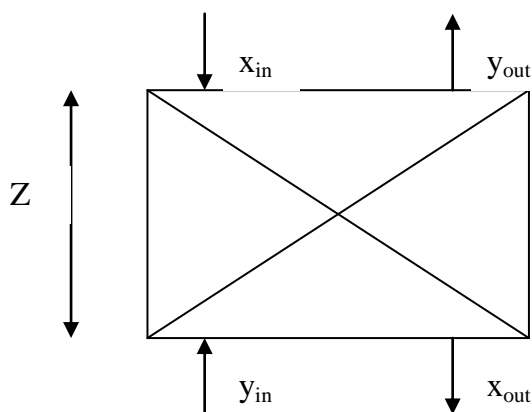


Figure 4.3. Packing height assigned to a RADFRAC stage.

More physically meaningful efficiencies were defined by Pacheco (1998) as modified Murphree efficiencies, given in terms of partial pressures (equation 4.2).

$$eff_m = \frac{P_{out} - P_{in}}{P^* - P_{in}} \quad (4.2)$$

The modified efficiency is more meaningful, because the driving forces are defined in terms of partial pressure, and the total pressure in equilibrium with the liquid is different from the total pressure of the stage. The modified efficiency can be expressed in terms of mole fractions, like in equation 4.3.

$$eff_m = \frac{y_{out} - y_{in}}{\frac{P_{eq}}{P} y^* - y_{in}} \quad (4.3)$$

P_{eq} is the total pressure in equilibrium with the liquid and P is the system total pressure. As described by Pacheco (1998) there are cases when these can be significantly different.

The modified efficiency defined by equation 4.2 can be calculated using the Bishnoi FORTRAN model, according to equations 4.4 and 4.5. Equation 4.4 can be derived with a differential material balance on the liquid phase.

$$eff_m = 1 - \exp\left(-\frac{K_g a_w S P z}{G}\right) \quad (4.4)$$

$$\frac{1}{K_g} = \frac{1}{k_g} - \frac{1}{k_g^I} \quad (4.5)$$

K_g is the overall mass transfer coefficient, k_g is the gas phase mass transfer coefficient, and k_g^I was defined by equation 3.17. In equation 4.4 a_w is the wetted area per unit volume, S is the column cross sectional area, P is the total pressure of the stage, z is the height of packing assigned to the stage, G is the gas mole flow rate.

The Bishnoi model provides k_g^I ; k_g and a_w are obtained from Onda's correlations (Onda et al., 1968). For this work Z was assigned an arbitrary value of 2.5 ft.

The modified efficiencies were provided to the ASPEN PLUS model, but ASPEN PLUS uses standard Murphree efficiencies (defined in equation 4.1). It is likely that the Bellingham model is not affected heavily by the error introduced, because this particular absorber is not pinched, which means that $P_{CO_2}^* < P_{CO_2}$ in every point of the column, and $eff_m \cong eff$.

The solution of the absorber column requires iterations on the RADFRAC model and the Bishnoi model, because the latter requires temperature and composition profiles in order to calculate efficiencies. Figure 4.4 shows the iterative process.

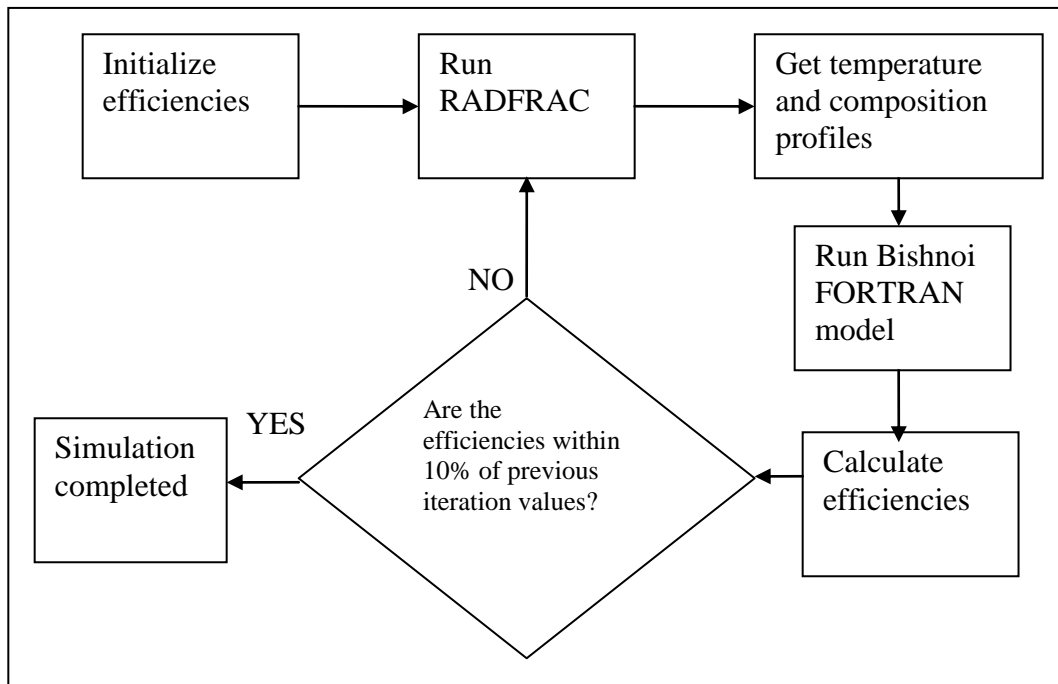


Figure 4.4. Block diagram of RADFRAC model of Bellingham absorber.

The heat stable salts were not included in the RADFRAC model. This could cause an overprediction of absorber performance (see section 4.2).

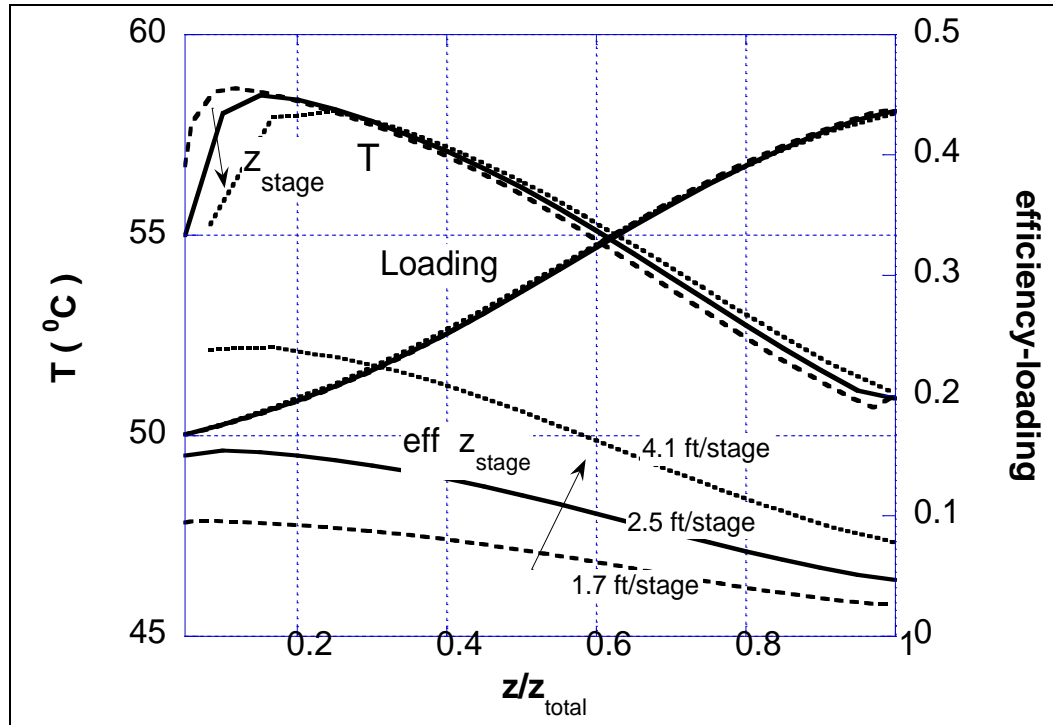


Figure 4.5. Liquid temperature, loading, efficiency profiles for the Bellingham absorber from the simulation with RADFRAC and the Bishnoi model, 3.13 % CO₂, 30 wt% MEA, lean loading 0.16, heat stable salts not included in analysis.

Figure 4.5 shows some results of the simulation of the Bellingham base case. Liquid temperature, loading and efficiency profiles are shown. The left end of the plot represents the top of the absorber. The lean loading and the lean solvent rate were fixed at the Bellingham base case values (0.16 and 4.0 cum/min respectively). The calculated removal is 88.7%. Three curves were plotted, for three different heights of packing assigned to a stage (1.7, 2.5 and 4.1 ft/stage). Intuitively the efficiency increases with the height of a segment (according to equation 4.4). The efficiency profile is decreasing going down the column. This is a consequence of

the fact that the CO₂ loading increases, reducing the free MEA in solution, thus reducing k_g^I and the efficiency.

The loading profile is smooth from lean end to rich end. Changes in the height of a stage do not affect the loading profile significantly.

The liquid temperature profile presents a typical bulge shape. This is due to the fact that the exothermic reaction produces heat and the heat is absorbed by the liquid and gas streams. The position of the bulge is, in this particular case, close to the top of the absorber. This means that the liquid absorbs most of the heat in the top stages. In fact, at low CO₂ content in the flue gas, the liquid flow in the column is relatively small, thus the liquid heat capacity is small. As a consequence the liquid temperature gradient at the top of the absorber is very steep. Even though the reaction occurs throughout the column, the temperature starts to decrease in the middle of the column, because the liquid is cooled by the flue gas flowing up the column.

From Figure 4.5 it is clear that the temperature profile is different for the three different heights of a stage. This is a consequence of the fact that RADFRAC assumes that the heat transfer efficiencies are 100%, even if the mass transfer efficiencies are limited. Under this assumption the heat transfer is overpredicted if the height of a stage is small. In the case of 1.7 ft/stage the temperature increases faster at the top of the column and the heat is dissipated faster at the bottom.

In Figure 4.6 a comparison between the RADFRAC and RATEFRAC predicted temperature bulges is presented, for the cases of 3.13 mol% CO₂ (base case) and 10.3 mol% CO₂. The 10.3 % case was run at 90% removal, with an $(L/G)_{\text{mass}}$ of 2.6. The difference between the two models is that RATEFRAC perform rigorous heat transfer calculations, whereas RADFRAC assumes thermal equilibrium on a stage. In both cases RATEFRAC predicts a larger temperature bulge, with a higher maximum and a slower dissipation at the bottom of the column. The 10% CO₂ case presents a wider temperature bulge than the 3% case. This can be explained with

the fact that, at higher CO₂ content, there is more reaction occurring; a higher liquid heat capacity absorbs the extra heat of reaction, but the gas rate is the same as the 3% CO₂ case, thus the cooling capacity of the gas is reduced.

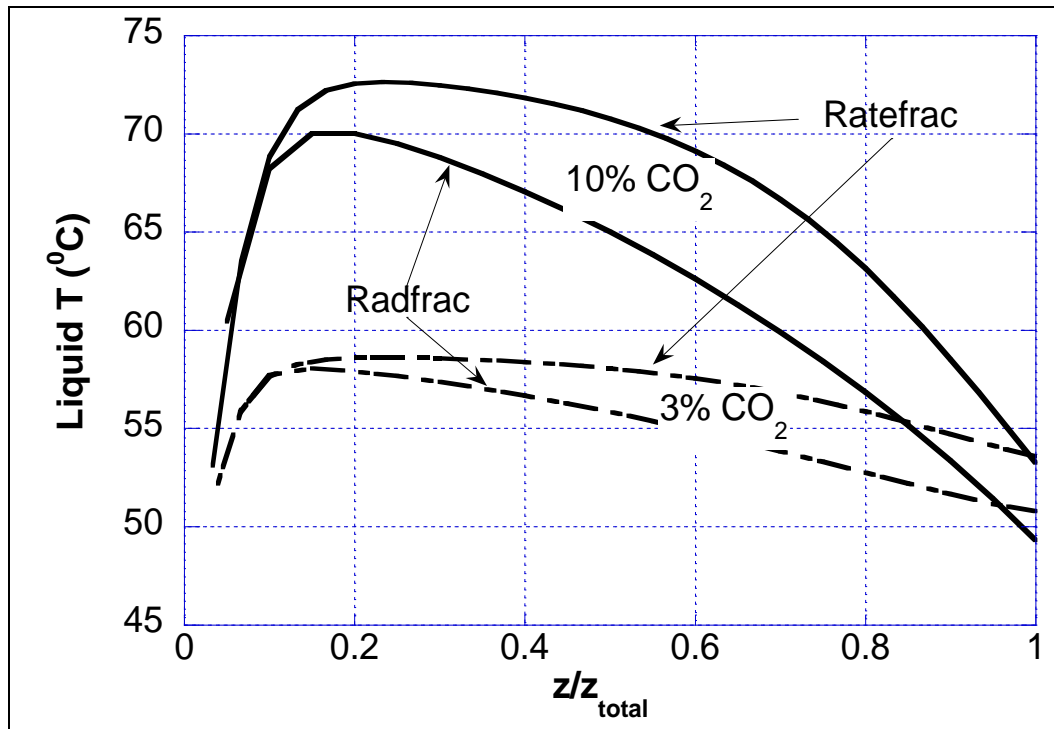


Figure 4.6. Absorber liquid temperature profiles for 3.13 mol%-85% removal (base case) and 10.3 mol%-90% removal. RATEFRAC and RADFRAC results are compared.

4.2. Stripper model and heat stable salts

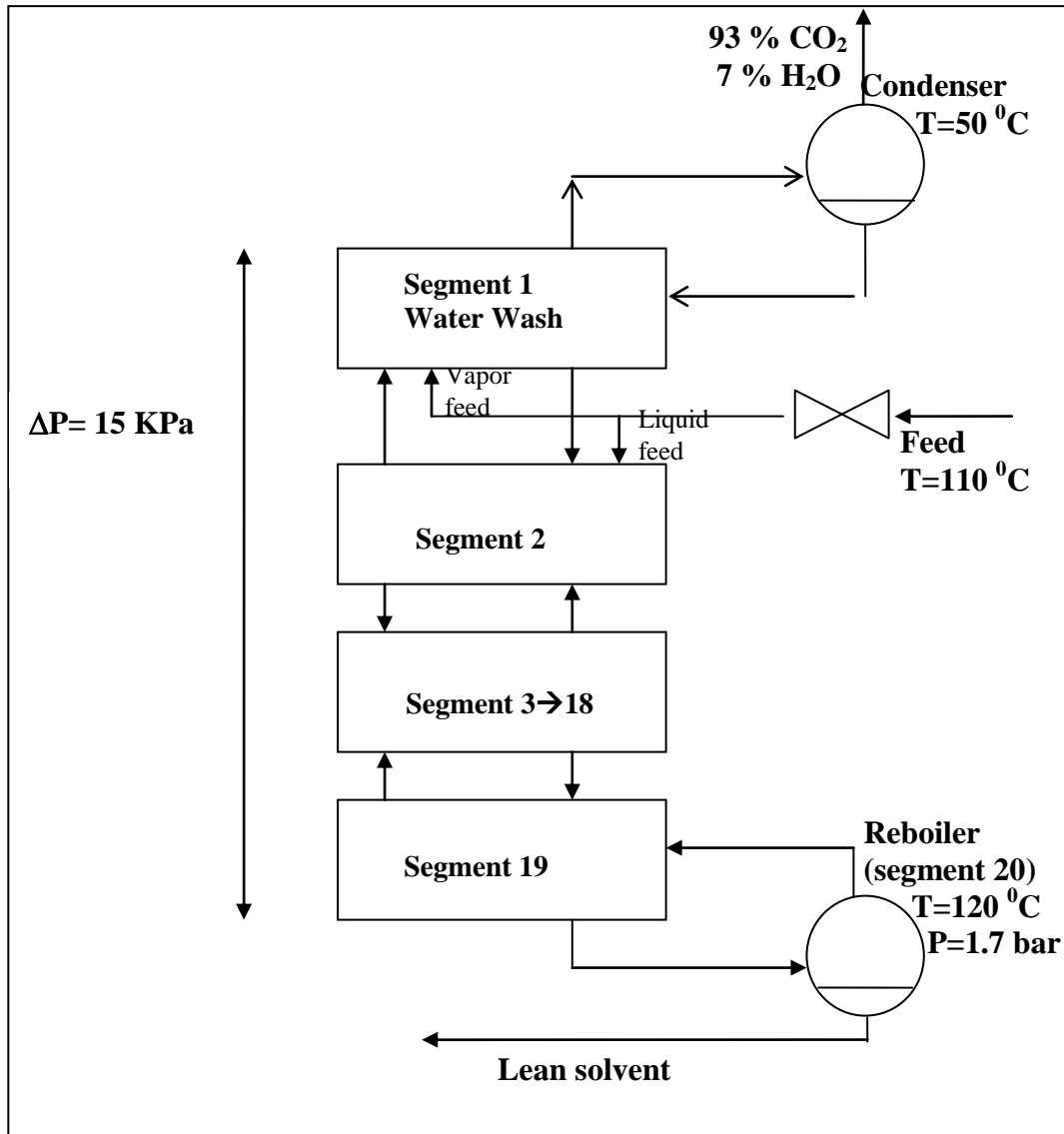


Figure 4.7. Scheme of the RATEFRAC stripper model.

The stripper was modeled with ASPEN RATEFRAC. A detailed scheme of the stripper is shown in Figure 4.7. Twenty segments were used to represent the packing. The number of twenty was chosen based on the same reasoning used for the absorber. Going from 20 to 30 stripper segments, the base case reboiler duty

changed by approximately 3 %. The reboiler, which was modeled as an equilibrium stage included in the RATEFRAC column, was set to operate with the heat duty necessary to obtain a specified lean loading. The partial condenser, modeled also as equilibrium stage but separately from the rest of the column, condenses part of the water present in the vapor at the top of the column and returns it to segment 1 of the column, which represents a water wash. The condenser is modeled as a heater at constant temperature of 120 °F (50 °C), which keeps the percentage of water in the gas stream leaving the column approximately at 7 mol%. The rich solvent is fed on top of segment 2 ('above stage' option in ASPEN PLUS) and is flashed by ASPEN PLUS at its temperature and at the pressure of segment 2, in order to calculate the feed vapor fraction and composition. The liquid fraction is fed into segment 2, the vapor fraction is fed into segment 1. Segments 2 through 19 represent the packing part of the column. The base case operates with a reboiler pressure of 1.7 bar and with a column pressure drop of 15 KPa.

4.2.1. Instantaneous reactions approximation and gas phase resistance

Kinetics were not used in the stripper, due to convergence problems in the kinetic algorithm at higher temperature. At the operating temperatures of the stripper (110 °C-120 °C) the reactions are faster, thus they were modeled as instantaneous. An analysis was done to estimate the error produced by this approximation. As explained in section 3.3.1, the IPFO approximation divides the boundary layer into two regions, one controlled by reaction rates and one controlled by diffusion of reactants and products. The liquid phase mass transfer resistance is determined by the resistances of the two regions in series (equation 4.6).

$$R_{liquid} = R_{IPFO} + R_{inst} \quad (4.6)$$

R_{IPFO} is the resistance of the reaction sub-layer, R_{inst} is the resistance of the diffusion region, where the reactions are instantaneous. Equation 4.6 turns into 4.7 when mass transfer coefficients are introduced.

$$\frac{1}{k_g^I} = \frac{1}{k_{g,IPFO}^I} + \frac{1}{k_{g,inst}^I} \quad (4.7)$$

The IPFO (kinetic controlled) term is given by equation 4.8, if concentration based kinetics are used.

$$k_{g,IPFO}^I = \frac{\sqrt{k_2[MEA]_i D_{CO_2}}}{H_{CO_2}} \quad (4.8)$$

All the symbols have been introduced in chapter 3.

The instantaneous coefficient can be calculated using equation 4.9, derived in Dang (2001), and valid for small driving forces.

$$k_{g,inst}^I = \frac{1}{\frac{\partial P_{CO_2}^*}{\partial [CO_2]^*}} k_{l,prod}^0 \quad (4.9)$$

The instantaneous coefficient depends on the partial derivative of the equilibrium partial pressure with respect to the CO_2 total concentration. It also depends on the physical mass transfer coefficient of the reaction products and MEA, $k_{l,prod}^0$. The derivative was obtained running the Electrolyte-NRTL model described in chapter 2; $k_{l,prod}^0$ was obtained from the correlation of Onda et al. (1968), using the diffusivity of MEA, as representative of that of all the reactants and products, and the values of liquid and vapor rates of the base case ($L=73.8$ Kg/s, $V=6.4$ Kg/s). The diffusivity of MEA was calculated from that of MDEA (Rowley, 1999), with a correction for molecular weight, multiplying by a factor of 1.5.

The error done by assuming equilibrium reactions in the stripper can be estimated by calculating the fractional resistance of the instantaneous term. The approximation is good if the fraction is close to 1.

$$fraction\ inst = \frac{k_g^I}{k_{g,inst}^I} \quad (4.10)$$

In the analysis some approximations were made. The loading dependences in equation 4.8 were neglected, and the values for Henry's constant and diffusivity of CO₂ were those in pure water. The correlations were those of Versteeg et al. (1998). The rate constant was that of Hikita (1977), multiplied by a constant value of 5 to represent the correction based on Dang (2001), described in chapter 2. Because equation 4.9 is valid only at small driving force, [MEA]_i was approximated with [MEA]_{bulk}. Table 4.1 shows the result of the analysis, done for 60 °C and 120 °C. At 60 °C the instantaneous resistance is always negligible. At 120 °C it is controlling at high loading, but at low loading the kinetic resistance accounts for almost 70% of the total resistance.

Table 4.1. Analysis of importance of the kinetics at absorber and stripper temperature.

T (°K)	Loading molCO ₂ /mol MEA	1/k _g ^I _{IPFO} cm ² s atm/mol	1/k _g ^I _{,inst} cm ² s atm/mol	Fraction instantaneous
333	0.2	1.87E+3	1.07E+1	5.71E-3
393	0.2	8.69E+2	4.04E+2	3.18E-1
333	0.4	3.91E+3	4.62E+2	1.06E-1
393	0.4	2.04E+3	1.07E+4	8.39E-1

The conclusion that can be drawn from this section is that the stripper model contains a source of error, that tends to overpredict the column performance, since part of the resistance is neglected. This problem becomes more important as the lean loading gets lower.

Since the reactions in the stripper are considered instantaneous, what limits the mass transfer in the stripper is the diffusion of reactants and products, along with the gas phase resistance.

The error introduced by the use of instantaneous reactions is higher if the gas phase resistance is smaller. The gas phase resistance in the stripper is between 50% and 70% in the base case stripper. This shows that the error is not negligible, because the mass transfer is not completely controlled by the gas phase.

Figure 4.8 shows the fractional resistance profile in the base case stripper, along with loading and vapor flow profiles. The gas phase resistance was calculated from the ASPEN PLUS simulation results of the base case.

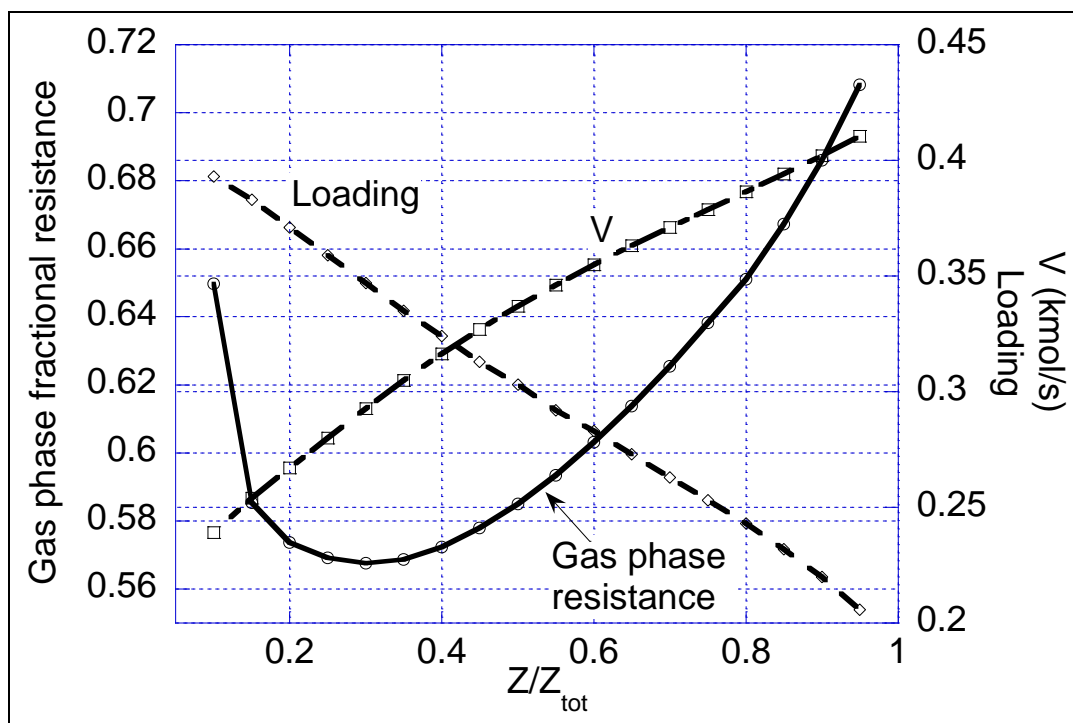


Figure 4.8. Gas phase resistance, loading and vapor rate profiles for the base case stripper.

The gas phase resistance tends to increase as the loading decreases. This is related to the fact that k_g^{-1} (equation 3.17) is higher at low loading, thus the liquid resistance due to reaction kinetics is smaller. The gas phase resistance tends to increase as the vapor flow rate decreases. This can explain the minimum seen in Figure 4.8, which is due to the combined effects of loading and vapor flow rate.

4.2.2. Heat stable salts

The regressed vapor-liquid equilibrium model described in chapter 2 becomes very important in the stripper model. The regressed VLE model is very sensitive to the presence, in solution, of heat stable salts (HSS). These are defined as any salts formed by neutralizing MEA with a strong acid. The fact that the acid is strong is what makes these salts stable. Once they are formed, they do not go back to MEA and acid unless a strong base is used. This means that, in a conventional absorption/stripping process, the heat stable salts keep circulating with the solvent once they are formed.

The heat stable salts are products of degradation, and can be present as sulfates or formates. In this model they were modeled as formates, formed according to equation 4.11.



The concentrations of HSS are normally reported as concentrations of neutralized MEA, because the anion is not known, and more anions could be present simultaneously. In this work the heat stable salts are reported as fraction of total MEA.

The presence of heat stable salts in solution is due to addition of a strong acid to it. The MEA becomes partially neutralized and therefore less effective for CO₂ removal: the absorber performance is reduced. In the stripper the reaction from carbamate to MEA and CO₂ is favored by the addition of an acid in solution: the stripper performance is enhanced. For a given total MEA concentration the equilibrium partial pressure of CO₂ is higher in the presence of heat stable salts, because equilibrium is shifted towards the acid species (such as CO₂).

In the presence of heat stable salts, the definition of loading is slightly different from the one seen so far. It is important to distinguish between total MEA and

active MEA, that is the portion of the total MEA that is not neutralized into heat stable salts.

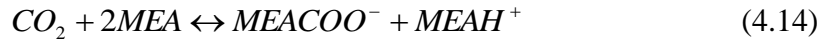
$$Loading = \alpha = \frac{[CO_2]}{[MEA]_{tot} - [HSS]} \quad (4.12)$$

A heat stable salt loading is defined:

$$\beta = \frac{[HSS]}{[MEA]_{tot}} \quad (4.13)$$

The base case was run with $\beta=0.1$.

In order to understand qualitatively how the heat stable salts can affect equilibrium, a simplified model was set up, where the only reaction occurring is 4.14:



At low loading this reaction can practically describe the speciation thoroughly, because the concentrations of all the other species, including bicarbonate, are negligible. If the equilibrium expression for reaction 4.14 is written and rearranged to give the partial pressure of CO_2 , equation 4.15 is generated.

$$P_{CO_2} \cong K(\alpha) \frac{\alpha(1-\beta)(\alpha(1-\beta)+\beta)}{(1-\beta-2\alpha(1-\beta))^2} \quad (4.15)$$

$K(\alpha)$ is a pseudo equilibrium constant, composition dependent. Its loading dependence can be derived from experimental data (Jou et al., 1995). At 120 °C, $K(\alpha)$ has the expression given by equation 4.16.

$$K(\alpha) = \frac{11.6}{\alpha} \text{ (KPa)} \quad (4.16)$$

Plotting P_{CO_2} versus CO_2 loading, at different HSS loadings, different isothermal equilibrium curves can be generated. Figure 4.8 shows three different isothermal equilibrium lines (120 °C), for $\beta=0, 0.1$ and 0.2 , at constant active MEA concentration: the heat stable salt was added on top of a 30 wt% MEA solution. Clearly the equilibrium lines are shifted up by the presence of heat stable salts. This

is intuitive: adding a strong acid to the solution, the CO_2 evolves into the gas phase. The points on the plot represent the experimental data of Jou et al. (1995) at 120°C . The straight line is an estimated operating line, derived from the reboiler duty.

$$\text{Slope of operating line} = L/V = \frac{L \Delta H_{\text{H}_2\text{O}}^{\text{vap}}}{Q_r} \quad (4.17)$$

The vapor mole flow generated in the reboiler (V) is proportional to the reboiler duty (Q_r); it is practically steam, so $\Delta H_{\text{H}_2\text{O}}^{\text{vap}}$ is the heat of vaporization of water at reboiler conditions. L is the liquid mole flow.

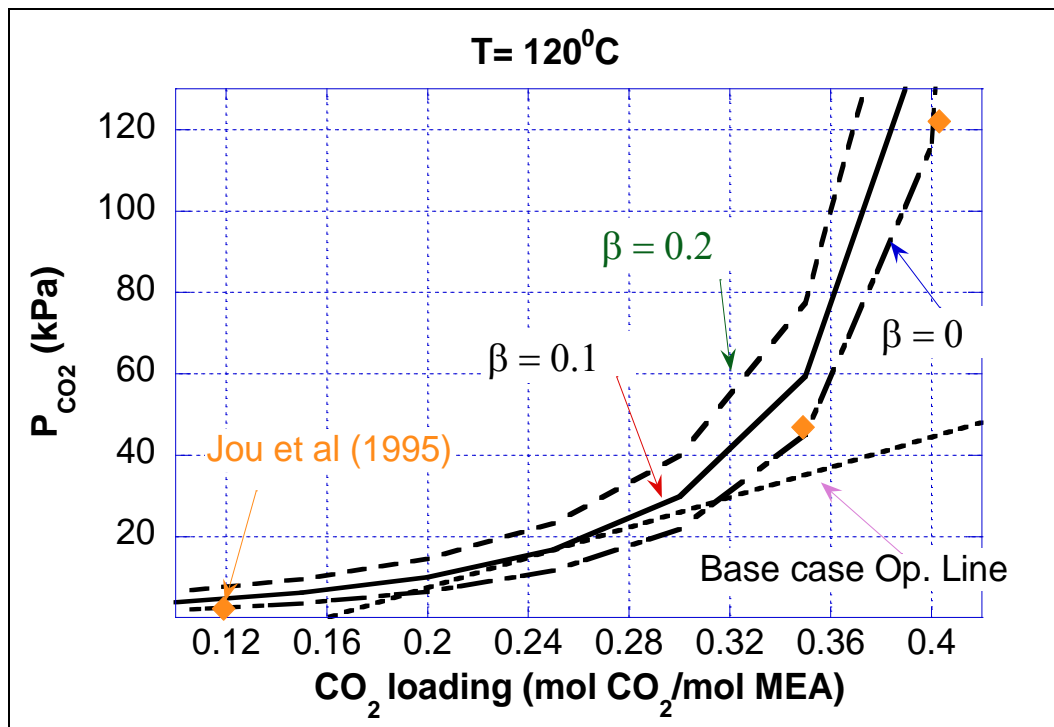


Figure 4.9. Isothermal stripper equilibrium lines at 120°C at different HSS loadings and Bellingham operating line, fixed $(L/G)_{\text{mass}}=0.78$, fixed lean loading=0.16, HSS added to 30 wt% MEA.

From Figure 4.9, it can be seen that the Bellingham operating line is not compatible with a solvent free of heat stable salts. The equilibrium curve with $\beta=0$ intersects the operating line. A higher reboiler duty (approximately 1.5 times)

would be required to lower the slope of the operating line, so that it stays below the operating line. The curve with $\beta=0.1$ is perfectly compatible with the operating line, with an equilibrium pinch at approximately 0.24 mol CO₂/mol MEA. At $\beta=0.2$, the equilibrium line is even higher. The reboiler duty could be lowered more, and still be compatible with the operating line.

Figure 4.9 shows only qualitatively why the Bellingham base case reboiler duty cannot be matched unless heat stable salts are accounted for. Figure 4.10 is the McCabe-Thiele diagram derived from a rigorous RATEFRAC run, where the heat stable salts are modeled as MEAH⁺HCOO⁻ and the Electrolyte-NRTL parameters of HCOO⁻ are arbitrarily set at the same values of MEACOO⁻ (reported in Table 2.3). In the Figure the McCabe-Thiele diagram is shown for both $\beta=0$ and $\beta=0.1$. The dashed lines are operating lines, the continuous lines are equilibrium lines. By adding 10% heat stable salts on top of a 30 wt% MEA solvent, at fixed solvent rate and lean loading, the reboiler duty is reduced by approximately 40%.

This hints that there can be benefits from adding acid to the solvent. Kohl and Nielsen (1997) showed that in gas purification processes acids have been added to enhance the stripping of amine solutions. Carey (1990) showed that partial neutralization of the amine with sulfuric acid can improve performance of an absorption/stripping system for H₂S. The combined effects of the heat stable salts on absorber and stripper will be analyzed in details in Chapter 5.

Another interesting result of the rigorous RATEFRAC simulation of the stripper is that, upon adding heat stable salts, not only does the equilibrium curve rise, but the equilibrium pinch is removed, with an operating line that follows the equilibrium line without becoming too close to it.

In Figure 4.10, like in all the stripper McCabe-Thiele diagrams in this work, the operating line is extrapolated to the point ($\alpha_{lean}, 0$), even though there is no vapor below the reboiler, and an operating line is not defined. The point ($\alpha_{lean}, 0$) is where the operating line tends, if linearly prolonged to the loading axis.

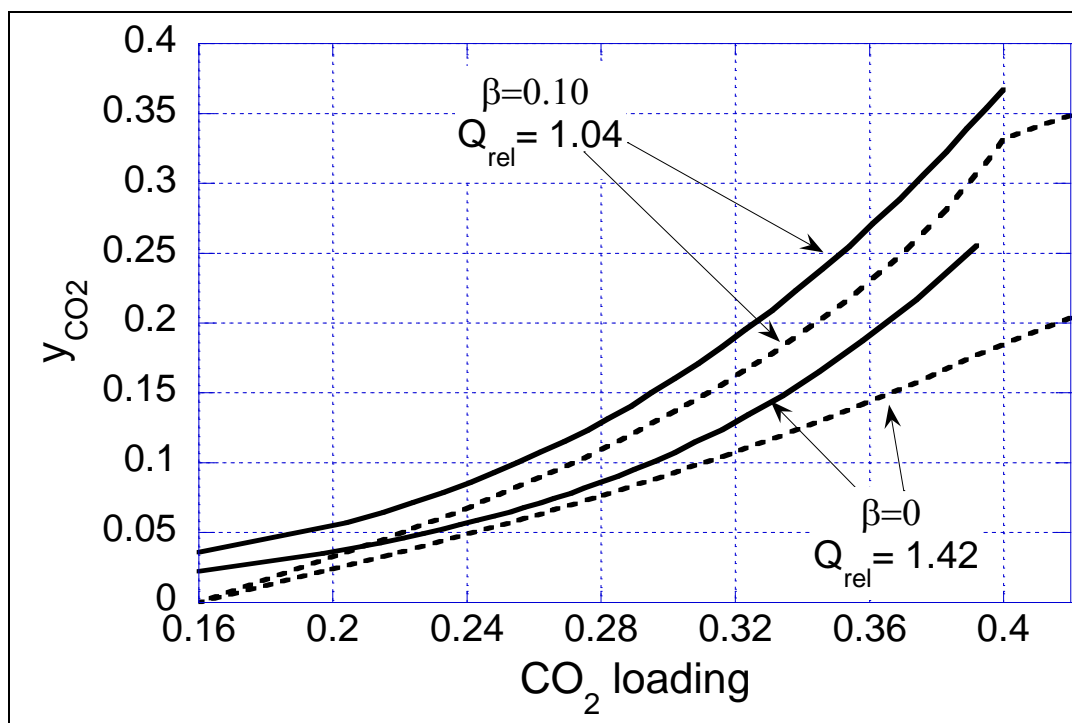


Figure 4.10. McCabe-Thiele diagrams for Bellingham stripper at $\beta=0$ and $\beta=0.1$. Results from rigorous RATEFRAC simulation, fixed $(L/G)_{mass}=0.78$, fixed lean loading=0.16, HSS added to 30 wt% MEA.

4.3. Combined absorber and stripper model

Figure 4.10 shows the schematic of how the absorber and stripper were combined in the ASPEN model.

The stream inputs are flow rate, temperature, pressure and composition of the flue gas and the lean solvent entering the absorber.

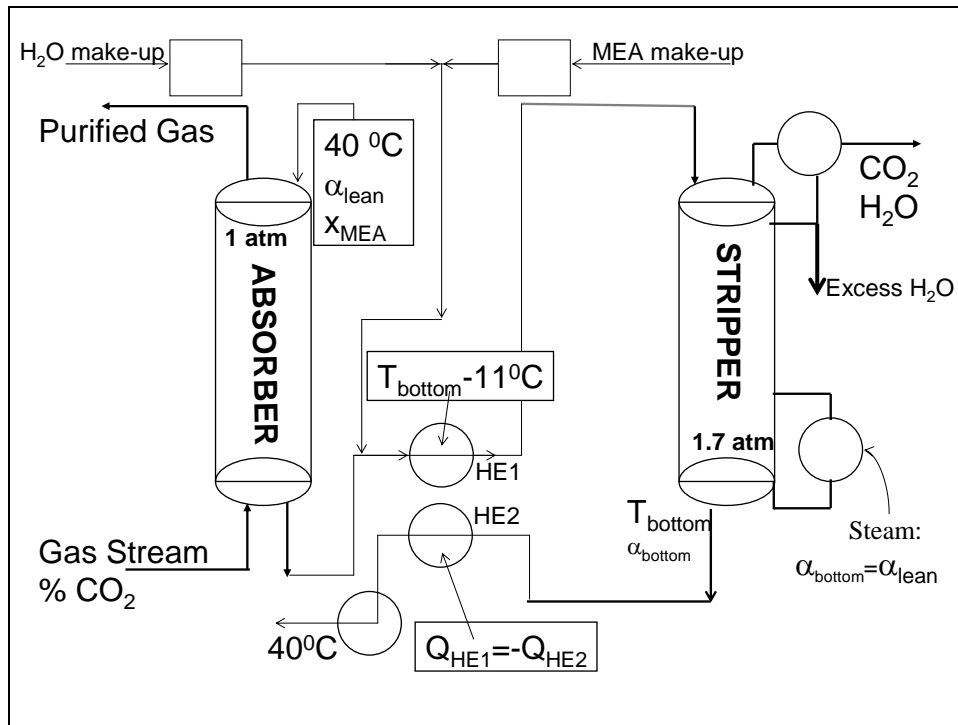


Figure 4.11. Schematic of the absorption/stripping model.

The cross heat exchanger was modeled with two separate HEATER blocks in ASPEN PLUS, HE1 and HE2. The specifications are shown in Figure 4.10 in the boxes. HE1 has a temperature specification, fixing the approach to equilibrium at 20 °F (11 °C). HE2 has a duty specification, such that the duties of HE1 and HE2 are matched.

The solvent loop is not closed in the model. In order to reduce the computation time, the lean stream was not connected from the stripper to the absorber. The lean stream into the absorber represents an input to the model. The lean stream coming from the stripper is forced to match the one entering the absorber, through DESIGN SPECIFICATIONS blocks and CALCULATOR blocks in ASPEN PLUS. The MEA material balance is closed with a design specification, which calculates the amount of make-up MEA required. The water balance is closed with a

CALCULATOR block, which computes the amount of water leaving in the “excess water” stream, arbitrarily taken from the stripper reflux stream. The CO₂ material balance is closed with a design specification on the reboiler duty, which is varied to match the lean loading at the stripper bottom with the one specified in the absorber solvent feed.

More details on the model can be found in Appendix C, where C.1 is an input file for the base case; C.2 is a summary of the input parameters necessary to run the model; C.3 shows the ASPEN PLUS process flow diagram; C.4 contains detailed results for the base case; C.5 contains detailed results for one of the high CO₂ cases described in chapter 5; C.6 gives hints on how to get the model to converge.

The model was used to simulate the Bellingham base case and three test runs done at the same plant. The results are summarized in Table 4.2, where the dark cells represent the process parameters that were fixed at the measured values. The most important outputs are the CO₂ removal and the reboiler duty. The removal is usually a specification and needs to be respected. The reboiler duty per mole of CO₂ recovered is the measure of the energy required to run the process. A CO₂ removal process downstream of a power plant can significantly reduce the power plant efficiency. It is important to be able to reproduce the correct reboiler duty with a model, if the goal of the model is to design a process with reduced energy requirements. In chapter 5 an optimization will be discussed, in order to keep the reboiler duty as low as possible at different operating conditions.

The results of Table 4.2 show that the reboiler duty is overpredicted by up to 10-15% in the base case and in test runs 1 and 3. In test 2 the overprediction approaches 50%. It can be guessed that wrong diffusivities calculated by ASPEN PLUS or wrong gas phase mass transfer coefficients can be the cause of a 10% overprediction of the reboiler duty. Another possible explanation is that the enthalpy of absorption calculated by ASPEN PLUS could be overestimated in the model. In test run 2 it is more likely that some measurements produced wrong

values, confirmed by the fact that the measured material balance does not close very well for this case (Won et al., 1999).

A base case for high CO₂ flue gases is reported in Appendix D. For this case the kinetics were left at the value adjusted from the data of Dang (2001).

Table 4.2. Summary of results of simulation of Bellingham base case and test runs.

	Ref.	model	Test Run 1	model	Test Run 2	model	Test Run 3	model
Flue Gas Flow, MSTDcum/hr	255		268		276		252	
CO ₂ mole % in feed, wet	3.13		2.87		3		2.86	
CO ₂ mole % in vent, wet	0.49	0.49	0.34	0.342	0.56	0.63	0.3	0.38
CO ₂ Recovery, %	85	85	88	87.9	81.5	78.6	89.7	85.5
Solvent Conc., wt % MEA	30		28.2		26.6		29	
Lean Solvent Rate, cum/min	4.0		3.63		3.63		3.63	
CO ₂ Loading, RICH AMINE	0.42	0.424	0.37	0.413	0.41	0.439	0.41	0.418
CO ₂ Loading, LEAN AMINE	0.16		0.109		0.129		0.147	
Q _r	0.99	1.035	1.125	1.515	1.02	1.20	0.995	1.135

Chapter 5

Process Analysis and Optimization

5.1. Reboiler and heat requirements

The RATEFRAC model described in chapter 4 for the absorption/stripping process was used to perform sensitivity analyses on the process variables and, ultimately, to optimize the process in terms of energy requirement. As pointed out in chapter one, the energy requirement is the main weakness of the CO₂ removal process. The goal of the analyses described in this chapter is to find operating conditions and process designs that permit CO₂ removal with a smaller energy input. All the runs done to perform the analyses described in this chapter develop from the base cases described in chapter 4 and appendix C, for 3% and 10% CO₂ respectively.

The process requires energy in two points, the stripper reboiler and the blower that pushes the flue gas into the absorber. The blower energy requirement is fixed, given by the flue gas flow rate and the absorber pressure drop. The reboiler duty, on the other hand, changes significantly with process conditions. The optimum operating point, in this work, is the point that operates at the minimum reboiler duty, for a given amount of CO₂ removed.

The process variables whose effects on the reboiler duty were analyzed in this work are the solvent rate, the heights of the columns, the CO₂ concentration in the flue gas, the ratio of heat stable salts to total MEA, and the stripper pressure.

Different operating conditions were compared at fixed CO₂ removal. The removal is usually a design specification, therefore it was not considered as an optimization variable in this work.

The reboiler is the focus of this energy minimization, thus some insight is needed to understand what affects it. Equations 5.1 and 5.2 represent the breakup of the reboiler duty, obtained from a simple energy balance across the stripper.

$$Q_r = Q_{des,CO_2} + Q_{steam\ generation} + Q_{sensible\ heat} \quad (5.1)$$

The heat, provided by condensing steam in the reboiler, is used to reverse the CO₂+MEA reaction (Q_{des, CO_2}), to generate steam in the reboiler ($Q_{steam\ generation}$), and to heat the solvent from the temperature at the inlet to the reboiler temperature ($Q_{sensible\ heat}$).

$$Q_r = -n_{CO_2}\Delta H_{abs,CO_2} + (V - n_{H_2O})\Delta H_{vap,H_2O} + Lc_p(T_{bottom} - T_{top}) \quad (5.2)$$

Q_r is the reboiler duty. $\Delta H_{abs,CO_2}$ is the heat of absorption of CO₂. $\Delta H_{vap,H_2O}$ is the heat of vaporization of water. n_{CO_2} is the number of moles of CO₂ desorbed in the stripper. n_{H_2O} is the number of moles of water that condense in the column, V is the vapor mole flow in the reboiler, L is the liquid mole flow in the reboiler, assumed to be approximately the same as the solvent feed rate. c_p is the liquid specific heat, and $T_{bottom}-T_{top}$ is the temperature difference between top and bottom of the stripper. Equation 5.2 accounts for the fact that water is condensing in the column. In this work the reboiler duty is always reported normalized to the moles of CO₂ recovered (equation 5.3)

$$\frac{Q_r}{n_{CO_2}} = -\Delta H_{abs,CO_2} + \frac{(V - n_{H_2O})}{n_{CO_2}}\Delta H_{vap,H_2O} + \frac{Lc_p}{n_{CO_2}}(T_{bottom} - T_{top}) \quad (5.3)$$

An energy balance around the reboiler generates equation 5.4.

$$Q_r = V\Delta H_{vap,H_2O} \quad (5.4)$$

Combining equations 5.2 and 5.4, equation 5.5 is obtained, showing that, in the column, the sensible heat and the heat to reverse the CO₂+MEA reaction are provided by condensing steam.

$$n_{H_2O}\Delta H_{vap,H_2O} = -n_{CO_2}\Delta H_{abs,CO_2} + Lc_p(T_{bottom} - T_{top}) \quad (5.5)$$

Equations 5.2 through 5.5 are approximations, because they assume that only water is vaporized in the reboiler. In reality there is also some CO₂ desorption.

In the sensible heat term the temperature at the bottom is set by the flash temperature of the liquid at the bottom pressure; the temperature at the top depends on how much heat is transferred through the cross heat exchanger. In this work the temperature approach to equilibrium in the cross heat exchanger was held constant at 20 °F (11 °C). For a stripper that operates at the pressure of the Bellingham base case (180 KPa at the reboiler), T_{bottom}=121 °C and T_{top}=110 °C.

In this chapter the reboiler duty is reported normalized to the moles of CO₂ removed. The values are made dimensionless in order not to disclose the base case value, proprietary to Fluor Corp.

The results of most of the runs presented in this chapter are reported in Appendix E.

5.2. Solvent rate optimization

The reboiler duty is very sensitive to the solvent rate. At very low solvent rates, the absorber performance is reduced; the solvent loads up quickly, reducing absorption rates. The way to keep the removal constant is to use a low lean loading. On the stripper side, low lean loading means that a lot of steam has to be produced to regenerate the solvent. At higher solvent rate, the wanted removal can be achieved even if higher lean loading is used. This reduces the energy required to regenerate the solvent in the stripper. At very high liquid rates the sensible heat becomes dominant, therefore the reboiler duty becomes higher. An optimum solvent rate is found, by plotting the results.

Table 5.1. Optimization of solvent flow rate, 3% mole CO₂ in flue gas, 85 % removal, 0.1 mol HSS/mol MEA, reboiler duty normalized to moles of CO₂ removed and divided by a typical industrial value in MJ/Kmol, stripper bottom pressure 1.7 atm.

Absorber L/G _{mass}	Optimum Lean loading	Optimum Rich loading	Q _{rel}
0.6326	0.11	0.4171	1.4900
0.6839	0.13	0.4152	1.2697
0.7351	0.15	0.4132	1.1451
0.7801	0.16	0.4115	1.0850
0.8628	0.18	0.4083	1.0505
0.9118	0.19	0.4064	1.0534
0.9678	0.20	0.4043	1.0636
1.0318	0.21	0.4020	1.0781
1.2991	0.24	0.3934	1.1439
1.7749	0.27	0.3829	1.2552

Figure 5.1 shows how the reboiler duty changes with solvent rate for the case of 3 mole % CO₂ in the flue gas and 85% CO₂ removal. For the runs the heat stable salts loading was kept at 0.1. Table 5.1 shows also the optimized L/G_{mass} and the optimum lean and rich loading.

The slopes of the reboiler duty curve are different on the two sides of the minimum. On the left side of the minimum, the heat increases approximately 10 times faster than on the right side. At low solvent rate steam generation accounts for most of the reboiler duty; at high solvent rate the sensible heat becomes more important. Because the CO₂ removal is kept constant, the term associated with heat of absorption is constant as the solvent rate changes.

Figures 5.2 through 5.7 show McCabe-Thiele diagrams for absorber and stripper at three different solvent rates. The absorber is never pinched. At high solvent rate the absorber tends to be more lean-pinched, whereas at low solvent rates the lean pinch becomes more loose. At very low solvent rate a rich pinch would be expected.

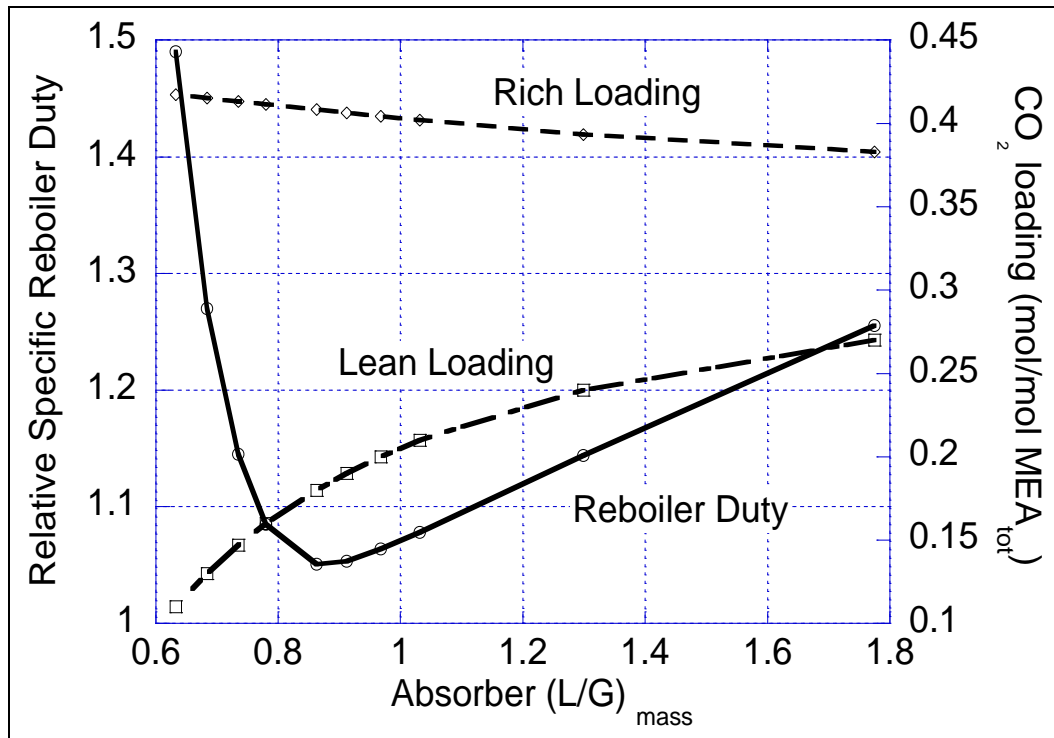


Figure 5.1. Optimization of solvent flow rate. 3% mole CO₂ in flue gas, 85 % removal, 0.1 mol HSS/mol MEA_{tot}, solvent rate normalized to flue gas rate, reboiler duty normalized to moles of CO₂ removed and divided by a typical industrial value in MJ/Kmol.

From the stripper McCabe-Thiele diagrams information can be obtained on the reboiler duty. Equation 5.4 states a direct proportionality between reboiler duty and slope of the operating line at the bottom of the stripper.

A tight lean pinch is observed when the solvent rate is low. The high steam requirement in the case of a lean pinch can be explained graphically. The equilibrium line is low at low loading; this constrains the operating line to have a low slope. Because the slope is proportional to L/V , V needs to be high, to keep the slope low.

At the optimum a rich pinch is observed in the stripper. At these conditions, the slope of the operating line can be high enough to keep V low. It can be noticed that the separation is well distributed among the 20 segments. A considerable

separation is achieved in the reboiler stage. This is a consequence of the fact that the reboiler was modeled as equilibrium segment. This assumption may be questionable when the model predicts a significant composition change in the reboiler.

At higher solvent rate the rich pinch is tighter. The stripping steam generation does not decrease, because the slope is constrained by the pinch. On the other hand sensible heat becomes important, and the reboiler duty increases as L increases.

At the rich end of the stripper it can be noticed that the loading may present a jump from the value in the feed to the value in the first segment of the column. In the low L/G and optimum L/G cases, the loading suddenly decreases from the feed to the first segment. In these cases the rich loading is sufficiently high that, at the stripper inlet temperature (approximately 110 °C) flashing occurs, with fast CO_2 vaporization.

The fact that CO_2 flashing is predicted introduces an uncertainty, due to the fact that the model sets the feed at vapor-liquid equilibrium. In the model the vapor coming into the column, result of flashing, is at equilibrium with the liquid. This represents reality only in the case that sufficiently small bubbles are formed in the liquid phase upon reducing the pressure of the feed to the stripper pressure.

In the high L/G case, the opposite happens. The loading increases from the feed to the first segment, and it keeps increasing in the top half of the column. The reason is that the solvent carries a high heat capacity, due to a high flow rate; therefore it does not heat up easily due to water condensation. Instead the vapor is cooled by the colder liquid, and more water condenses. This results in concentration of CO_2 in the gas phase, to the point that the CO_2 absorbs. Figure 5.8 shows the mole fraction profiles for CO_2 and H_2O in the column, along with loading and liquid temperature profiles. It can be seen that, in the top half of the column, a pinch is present, and the mole fraction of CO_2 slightly decreases going up the column.

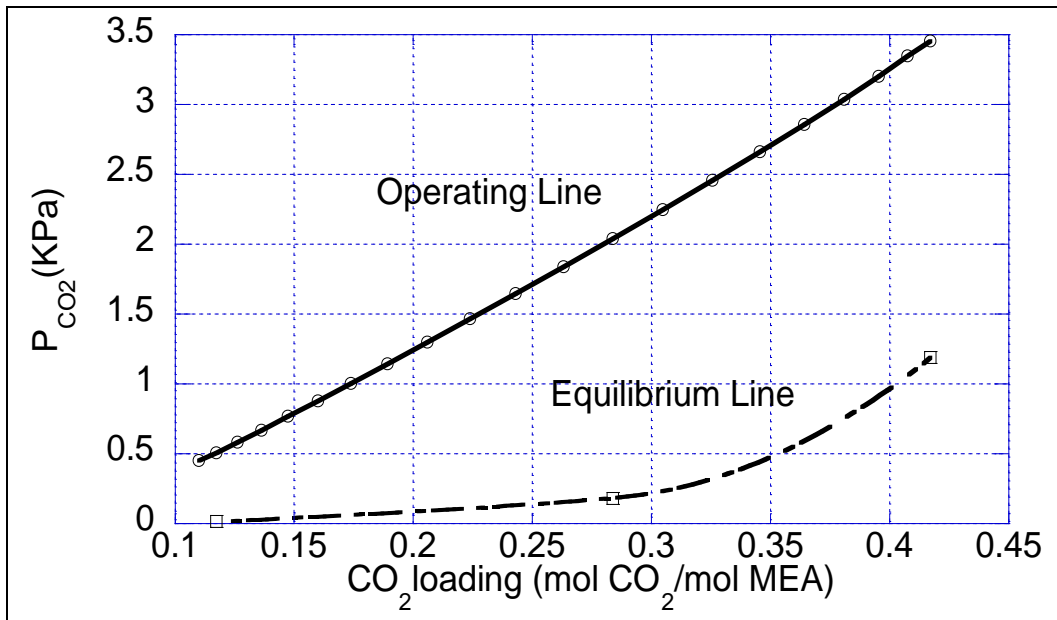


Figure 5.2. Absorber McCabe-Thiele diagram for low L/G case ($L/G_{\text{mass}}=0.63$). 3% CO₂ in flue gas, 85 % removal, 33.5 wt% MEA, 0.1 mol HSS/mol MEA_{tot}.

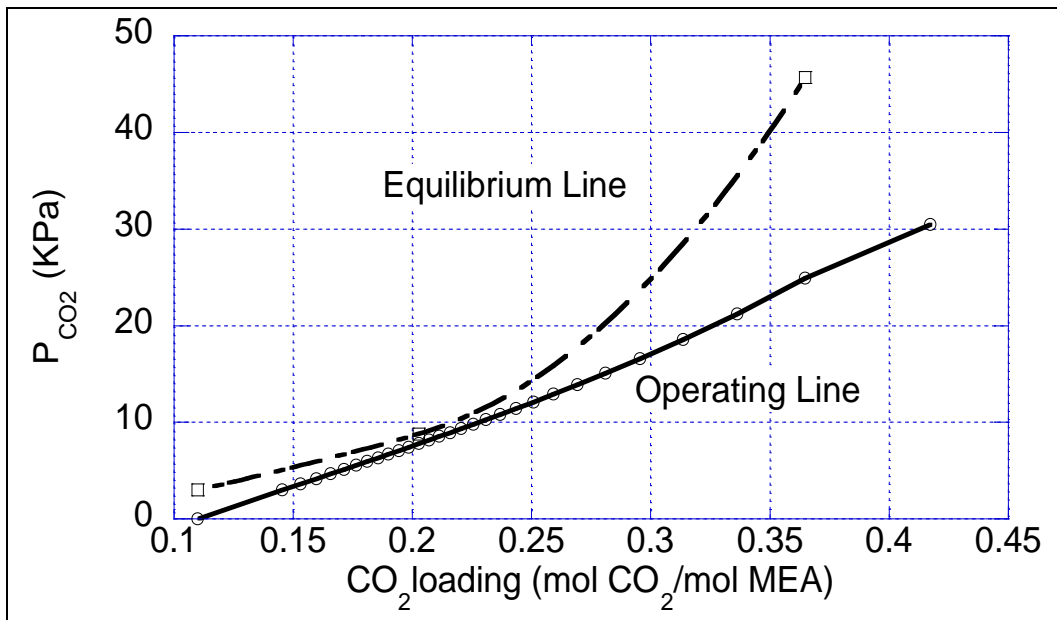


Figure 5.3. Stripper McCabe-Thiele diagram for low L/G case ($L/G_{\text{mass}} = 0.63$). 3% CO₂ in flue gas, 85 % removal, 33.5 wt% MEA, 0.1 mol HSS/mol MEA_{tot}.

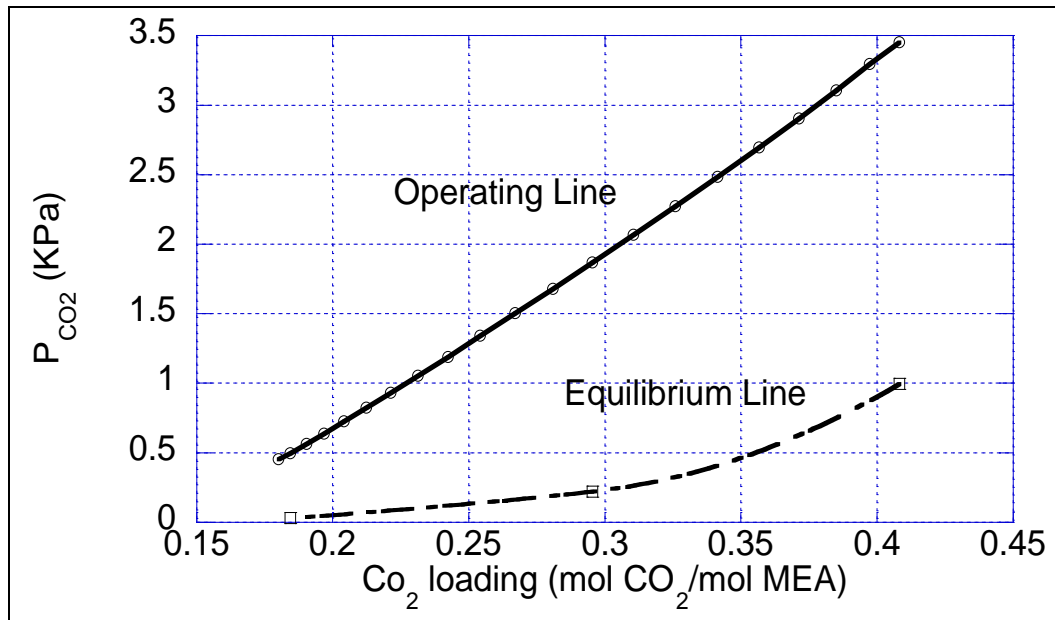


Figure 5.4. Absorber McCabe-Thiele diagram for optimum L/G case ($L/G_{\text{mass}} = 0.86$). 3% CO₂ in flue gas, 85 % removal, 33.5 wt% MEA, 0.1 mol HSS/mol MEA_{tot}.

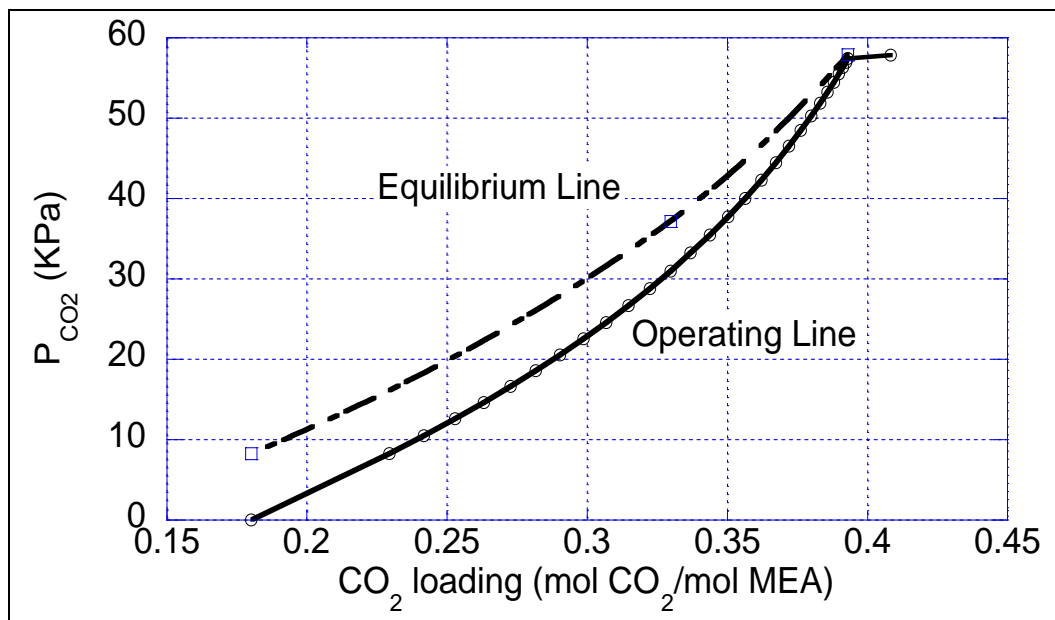


Figure 5.5. Stripper McCabe-Thiele diagram for optimum L/G case ($L/G_{\text{mass}} = 0.86$). 3% CO₂ in flue gas, 85 % removal, 33.5 wt% MEA, 0.1 mol HSS/mol MEA_{tot}.

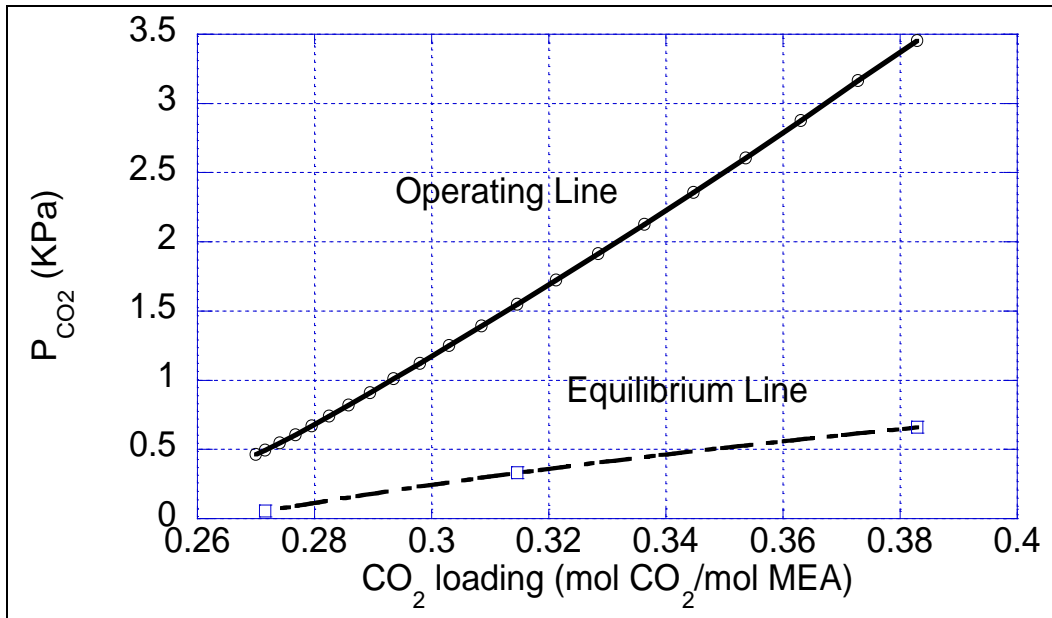


Figure 5.6. Absorber McCabe-Thiele diagram for high L/G case ($L/G_{\text{mass}} = 1.77$). 3% CO₂ in flue gas, 85 % removal, 33.5 wt% MEA, 0.1 mol HSS/mol MEA_{tot}.

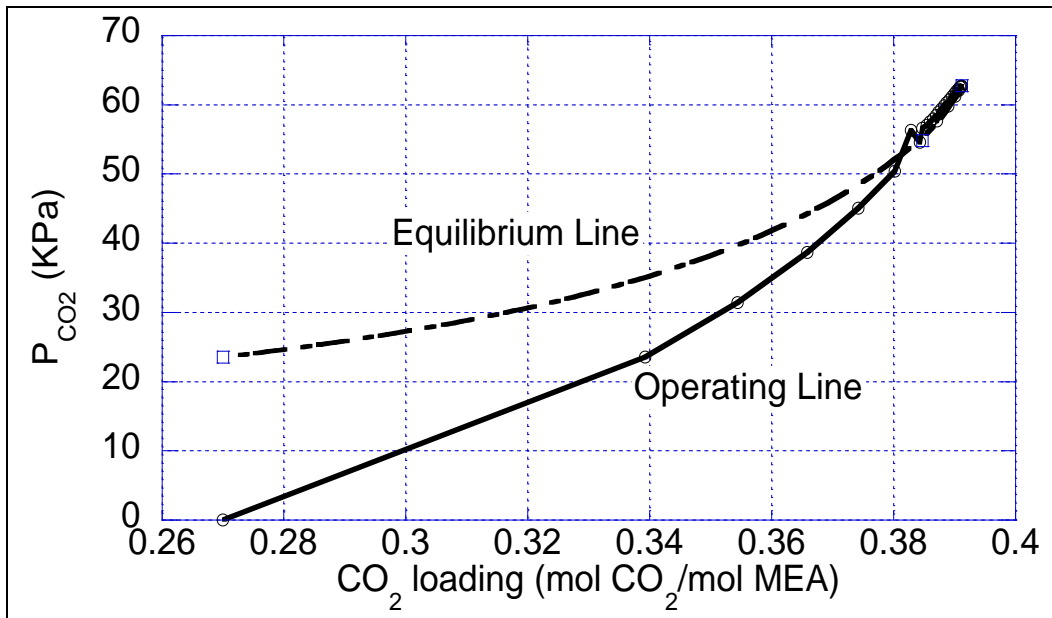


Figure 5.7. Stripper McCabe-Thiele diagram for high L/G case ($L/G_{\text{mass}} = 1.77$). 3% CO₂ in flue gas, 85 % removal, 33.5 wt% MEA, 0.1 mol HSS/mol MEA_{tot}.

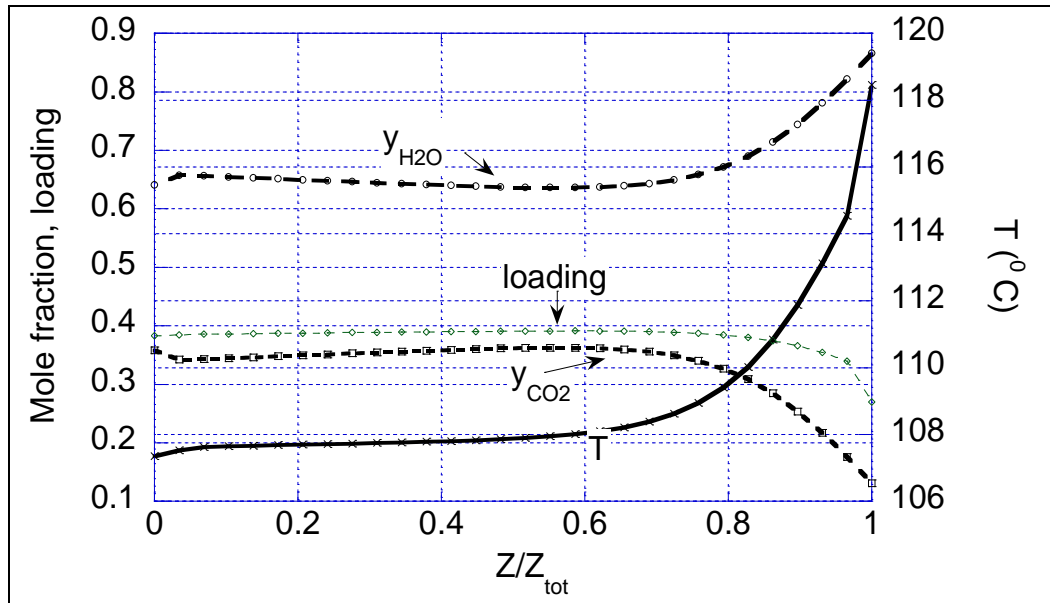


Figure 5.8. Stripper CO₂ and H₂O mole fraction, loading and liquid T profiles, for high L/G case ($L/G_{\text{mass}}=1.77$). 3% CO₂ in flue gas, 85 % removal, 33.5 wt% MEA, 0.1 mol HSS/mol MEA_{tot}.

5.3. Effects of the heights of the columns

The effect of absorber and stripper heights was analyzed in this work to determine to what extent they affect the performance of the process. It is intuitive that the performance of the process improves as the heights of the columns increase. Higher columns imply more area for mass transfer. The uncertainty on the wetted fraction of the total packing area is a source of uncertainty on the results of this sensitivity.

The stripper is usually pinched, therefore more area does not improve its performance significantly. In the absorber the mass transfer rates are slow, and more area would improve the performance more significantly. The problem of increasing the height of the absorber is that it implies high capital costs and higher pressure drop.

5.3.1. Effect of absorber height, CO₂ concentration and removal

The first sensitivity analysis involves only the absorber height. The column diameter was kept constant at the base case value. Three curves were generated, as shown in Figure 5.9. One curve refers to 3 mol% CO₂ in the flue gas and 85 % removal, one to 3% CO₂ and 90% removal and the last to 10 mol% CO₂ and 90% removal. Every point on the curves is optimized in the solvent rate. The absolute values of the heights were normalized to the height of the Bellingham absorber. Figure 5.10 shows the same results, but the reboiler duty is normalized to a minimum reboiler duty, which changes for every CO₂ concentration and removal and corresponds to infinite amount of packing. The minimum duty was calculated increasing the height of the absorber to the point where the reboiler duty stopped changing. For the three curves, the values of the minimum reboiler duties (relative to the reference arbitrary value) are 0.9425 (3% CO₂, 85% removal), 0.945 (3% CO₂, 90 % removal), and 0.891 (10% CO₂, 90% removal). It is interesting that, with a lot of packing, the removal practically does not affect the reboiler duty. In Figure 5.10 the normalized height is divided by $\ln(y_{in}/y_{out})$. The physical significance of this term is that, if K_g (overall mass transfer coefficient), G (gas flow rate) and P (total pressure) were constant along the column and equilibrium was not approached, the height of the column could be expressed by equation 5.6, which can be derived with the integration of a differential material balance.

$$Z = \frac{G}{K_g P a_w S} \ln \left(\frac{y_{in}}{y_{out}} \right) \quad (5.6)$$

Although only a rigorous costing analysis can optimize the absorber height, it can be noticed that, at 80% of the reference height, the process starts to perform poorly.

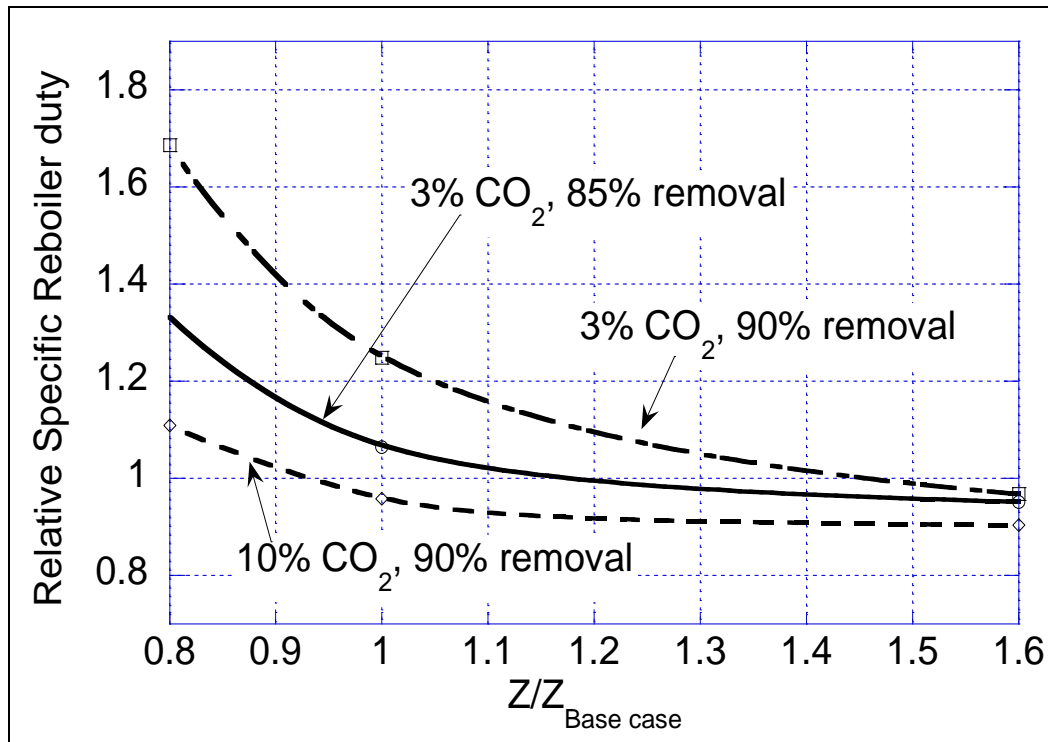


Figure 5.9. Effect of absorber height on reboiler duty per mole of CO₂ removed, 33.5 wt% MEA, 0.1 mol HSS/mol MEA_{tot}, optimum solvent rate, reboiler duty normalized to total moles of CO₂ removed and to typical industrial value.

Table 5.2. Results of absorber height analysis for the three cases of Figure 5. 9.

	$Z/Z_{\text{base case}}$	Q_{rel}	Optimum L/G_{mass}	Optimum lean loading	Optimum rich loading	minimum Q_{rel}
3% CO₂ 85% removal	0.6	1.87	3.29	0.26	0.321	0.942
	1.0	1.06	0.91	0.19	0.406	0.942
	1.6	0.95	0.82	0.20	0.440	0.942
3% CO₂ 90% removal	0.8	1.69	3.37	0.28	0.343	0.945
	1.0	1.25	1.18	0.19	0.368	0.945
	1.6	0.97	0.85	0.19	0.435	0.945
10% CO₂ 90% removal	0.8	1.11	5.42	0.29	0.417	0.891
	1.0	0.96	2.68	0.19	0.442	0.891
	1.6	0.90	2.61	0.20	0.460	0.891

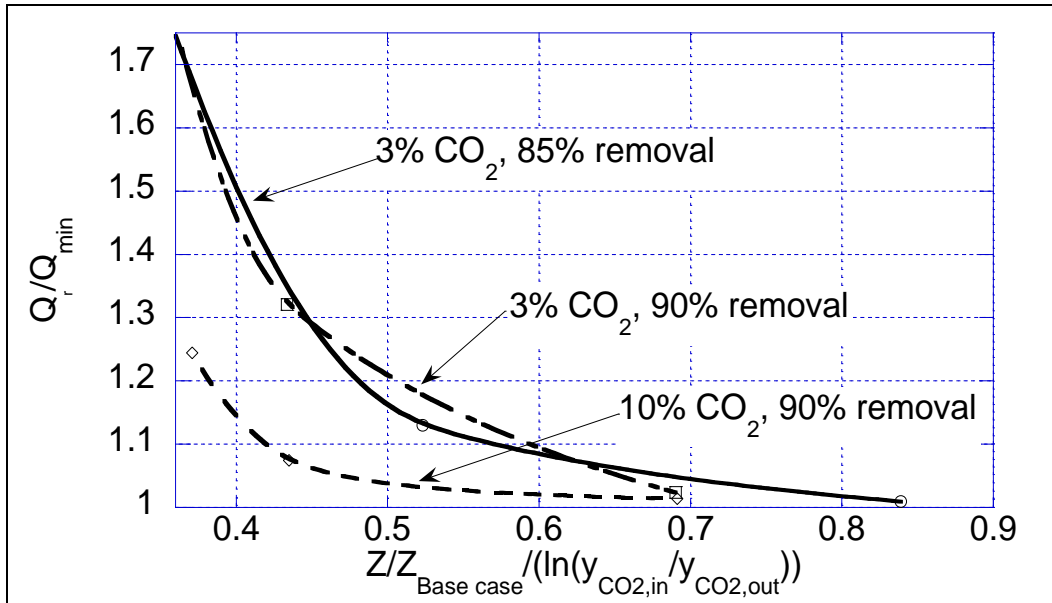


Figure 5.10. Effects of Figure 5.9, reboiler duty normalized by minimum heat duty.

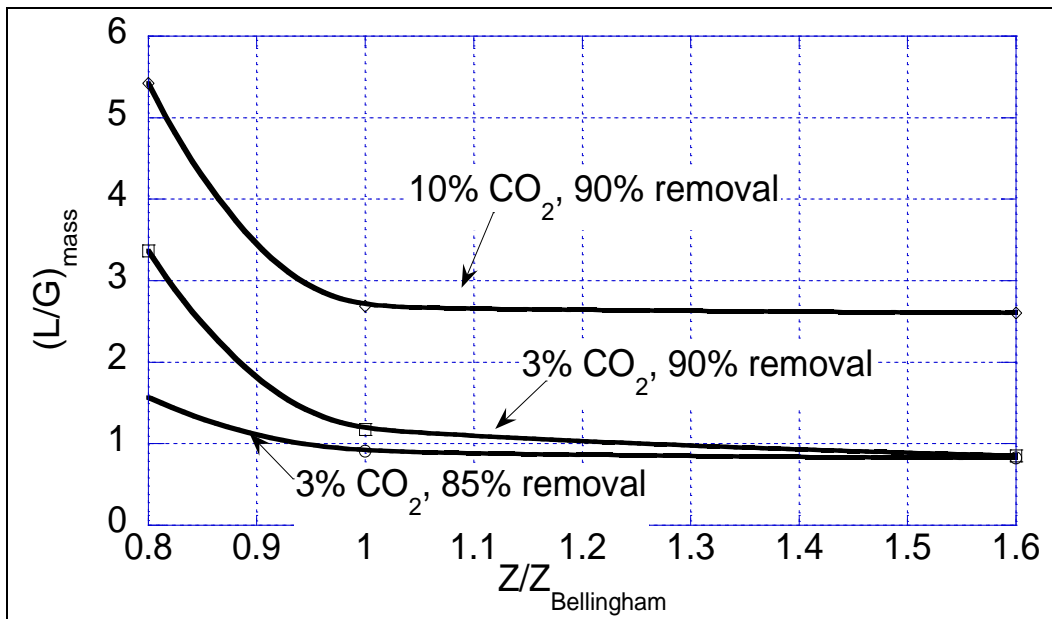


Figure 5.11. Optimized solvent rate for the three cases of Figure 5.9.

Figure 5.11 shows how the optimum solvent rate (normalized to the gas rate) decreases as the height of the absorber increases. Shorter columns require higher

flow rates, in order to keep the removal constant. Table 5.2 shows the reboiler duty, optimum L/G_{mass} , and optimum loadings for every point in Figure 5.9.

Intuitively, a higher solvent rate is required to increase removal at a given flue gas CO_2 concentration, or to keep the removal constant when the flue gas concentration increases. At constant CO_2 concentration in the flue gas, the higher the removal, the higher the reboiler duty. This is a consequence of the fact that the optimum solvent rate increases as the removal increases. This increases the sensible heat requirement and causes CO_2 absorption at the stripper top.

At constant removal, the normalized reboiler duty increases as the CO_2 concentration in the flue gas decreases. Even though the absolute reboiler duty is higher for the 10% CO_2 case than the 3% CO_2 case, the reboiler duty normalized to the total number of moles recovered is lower. A simple explanation can be found if the minimum thermodynamic work required for the process is calculated at isothermal conditions (equation 5.7).

$$\frac{W_{\min}}{n_{\text{CO}_2}} = \Delta G_{T,P} = RT \ln \frac{P_{\text{CO}_2,\text{out}}}{P_{\text{CO}_2,\text{in}}} \quad (5.7)$$

For the case of 3 mol% of CO_2 in the flue gas, $P_{\text{CO}_2,\text{in}}=0.03$ atm; for the 10% case, $P_{\text{CO}_2}=0.1$ atm. Assuming a stripper outlet pressure of 2 atm, the minimum work required to compress the CO_2 from the absorber inlet condition to the stripper outlet condition is $\ln(2/0.03)/\ln(2/0.1)=1.4$ times higher in the low CO_2 case.

Figures 5.12 through 5.19 show McCabe-Thiele diagrams for some of the cases discussed above. A difference between the optimized 3% and 10% CO_2 cases is that the stripper McCabe-Thiele diagram shows a rich pinch in the 3% CO_2 case, but it does not in the 10% CO_2 case. This is due to the fact that the high CO_2 case has 3.3 times more CO_2 to desorb, but the stripper size is the same. The higher liquid and vapor rates in the high CO_2 case increase the mass transfer coefficients k_{La} and k_{Ga} , but not proportionally to the CO_2 content. The consequence is that the column is not large enough to reach equilibrium at the rich end.

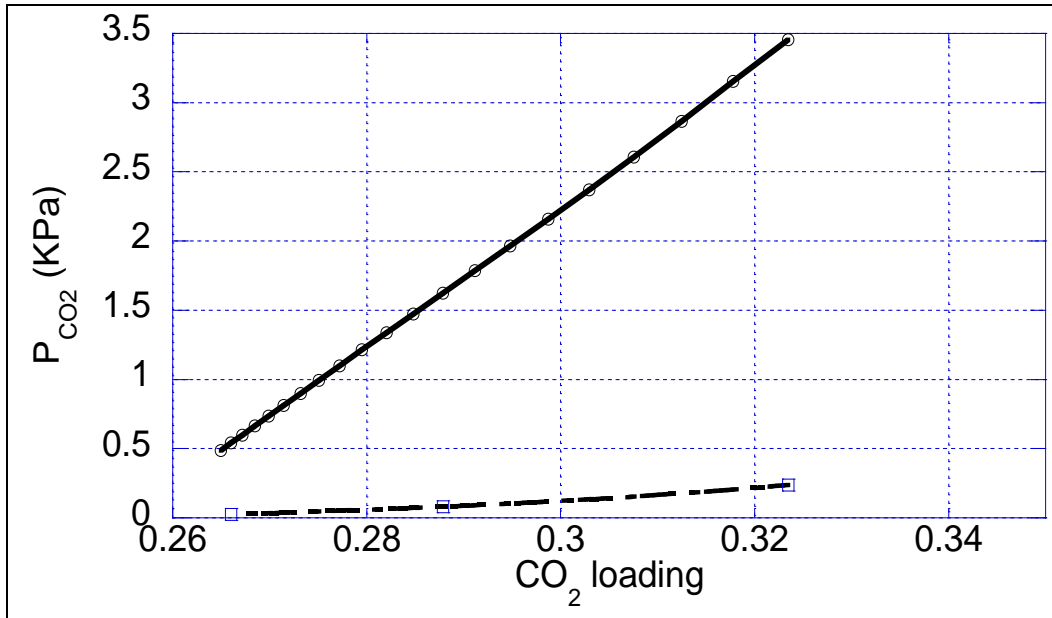


Figure 5.12. McCabe-Thiele diagram for the absorber; $Z_{\text{absorber}}/Z_{\text{Base case}}=0.6$, 33.5 wt% MEA, 0.1 mol HSS/mol MEA_{tot} , optimized solvent rate ($L/G_{\text{mass}}=3.29$), 3 mol% CO_2 in flue gas, 85% removal.

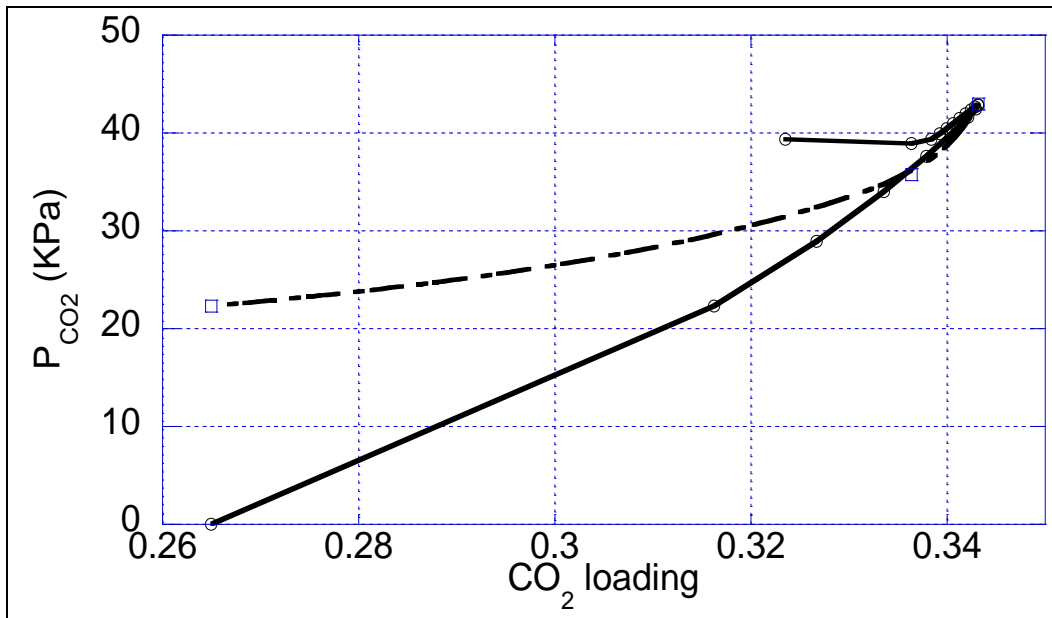


Figure 5.13. McCabe-Thiele diagram for the stripper; $Z_{\text{absorber}}/Z_{\text{Base case}}=0.6$, 33.5 wt% MEA, 0.1 mol HSS/mol MEA_{tot} , optimized solvent rate ($L/G_{\text{mass}}=3.29$), 3 mol% CO_2 in flue gas, 85% removal.

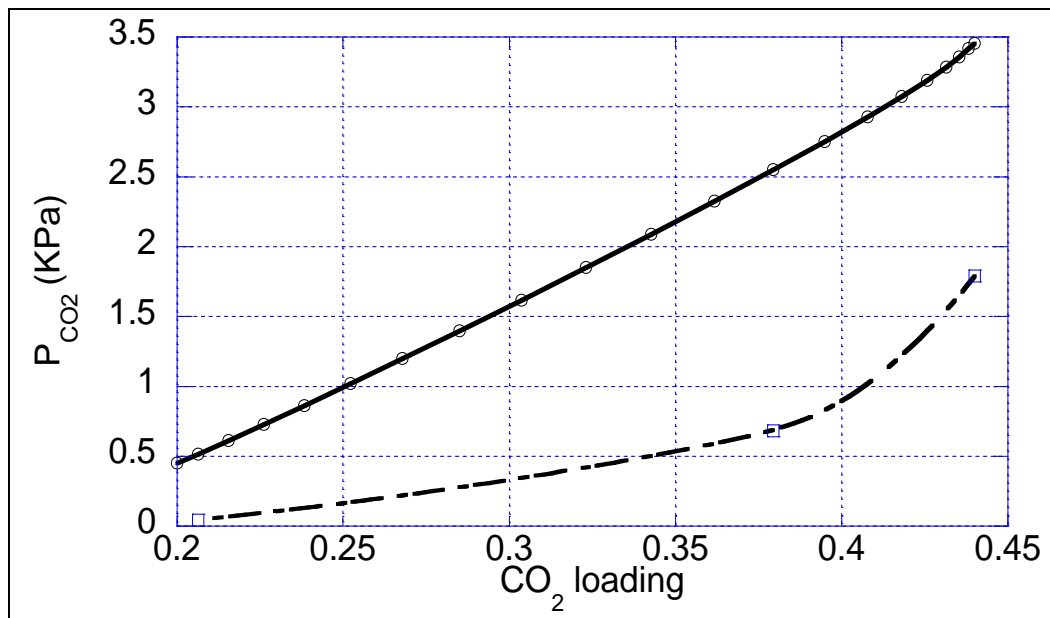


Figure 5.14. McCabe-Thiele diagram for the absorber; $Z_{\text{absorber}}/Z_{\text{Base case}}=1.6$, 33.5 wt% MEA, 0.1 mol HSS/mol MEA_{tot} , optimized solvent rate ($L/G_{\text{mass}}=0.82$), 3 mol% CO_2 in flue gas, 85% removal.

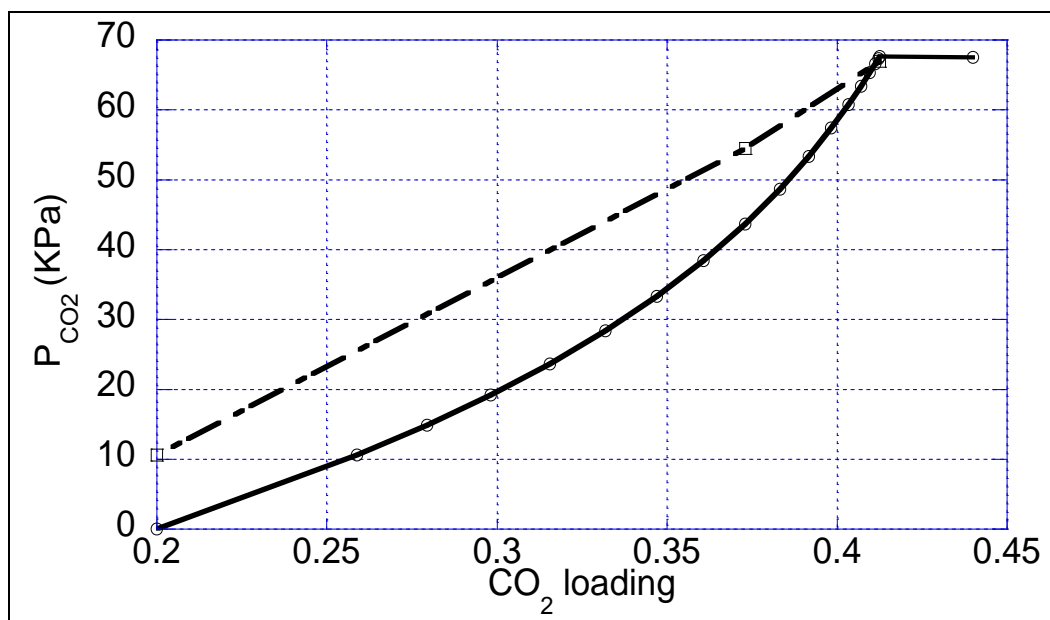


Figure 5.15. McCabe-Thiele diagram for the stripper; $Z_{\text{absorber}}/Z_{\text{Base case}}=1.6$, 33.5 wt% MEA, 0.1 mol HSS/mol MEA_{tot} , optimized solvent rate ($L/G_{\text{mass}}=0.82$), 3 mol% CO_2 in flue gas, 85% removal.

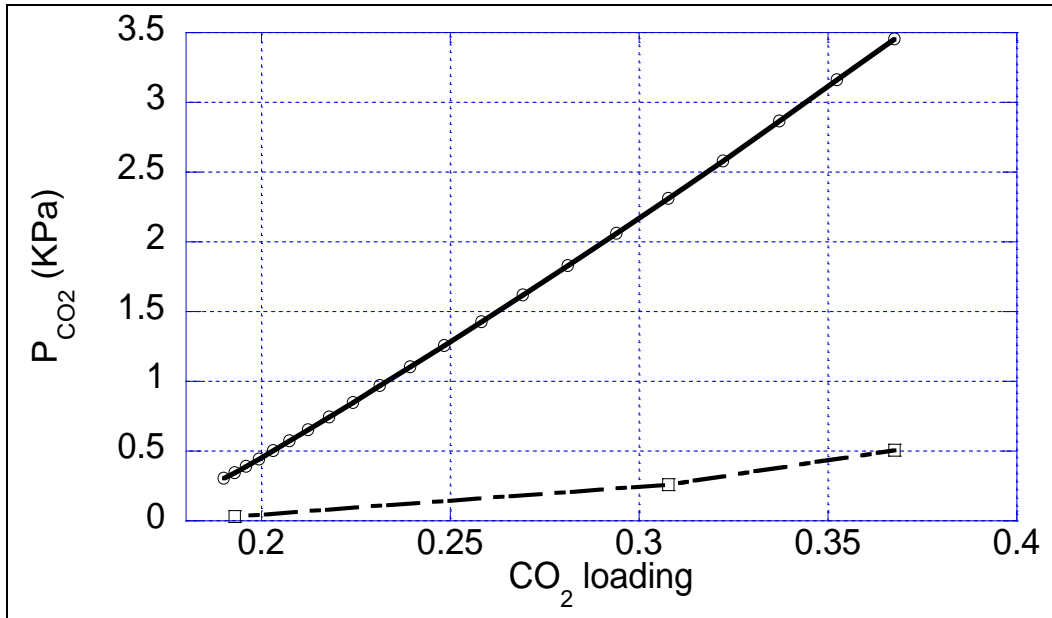


Figure 5.16. McCabe-Thiele diagram for the absorber; $Z_{\text{absorber}}/Z_{\text{Base case}}=1$, 33.5 wt% MEA, 0.1 mol HSS/mol MEA_{tot}, optimized solvent rate ($L/G_{\text{mass}}=1.18$), 3 mol% CO₂ in flue gas, 90% removal.

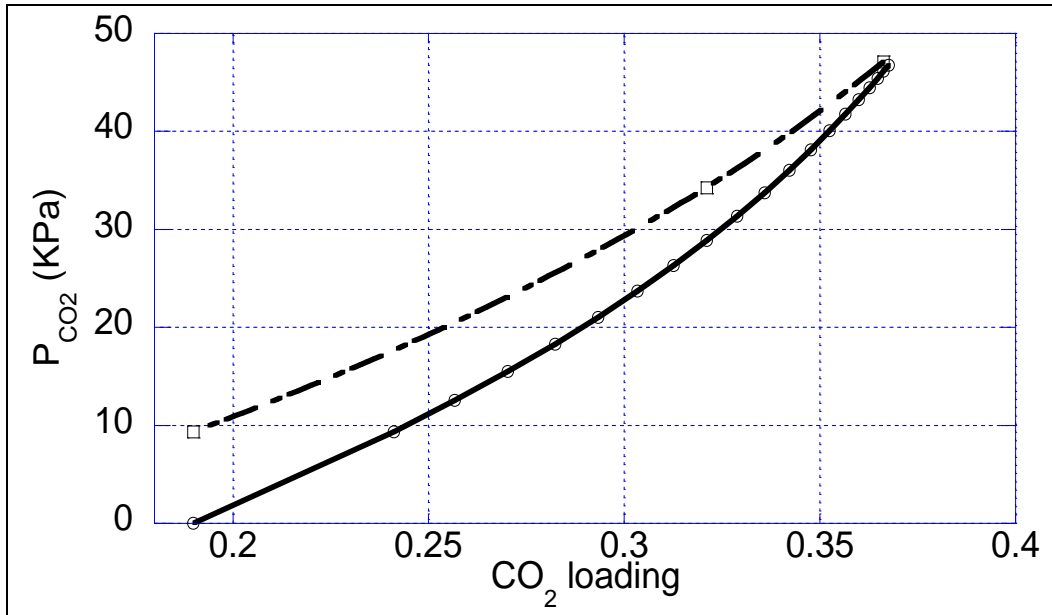


Figure 5.17. McCabe-Thiele diagram for the stripper; $Z_{\text{absorber}}/Z_{\text{Base case}}=1$, 33.5 wt% MEA, 0.1 mol HSS/mol MEA_{tot}, optimized solvent rate ($L/G_{\text{mass}}=1.18$), 3 mol% CO₂ in flue gas, 90% removal.

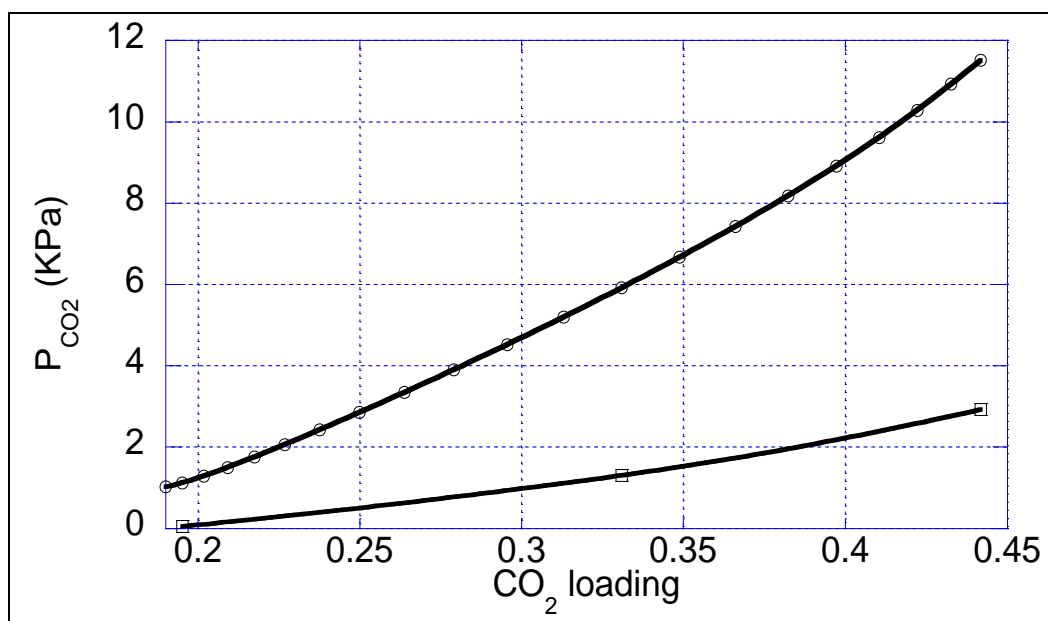


Figure 5.18. McCabe-Thiele diagram for the absorber; $Z_{\text{absorber}}/Z_{\text{Base case}}=1$, 33.5 wt% MEA, 0.1 mol HSS/mol MEA_{tot}, optimized solvent rate ($L/G_{\text{mass}}=2.68$), 10 mol% CO₂ in flue gas, 90% removal.

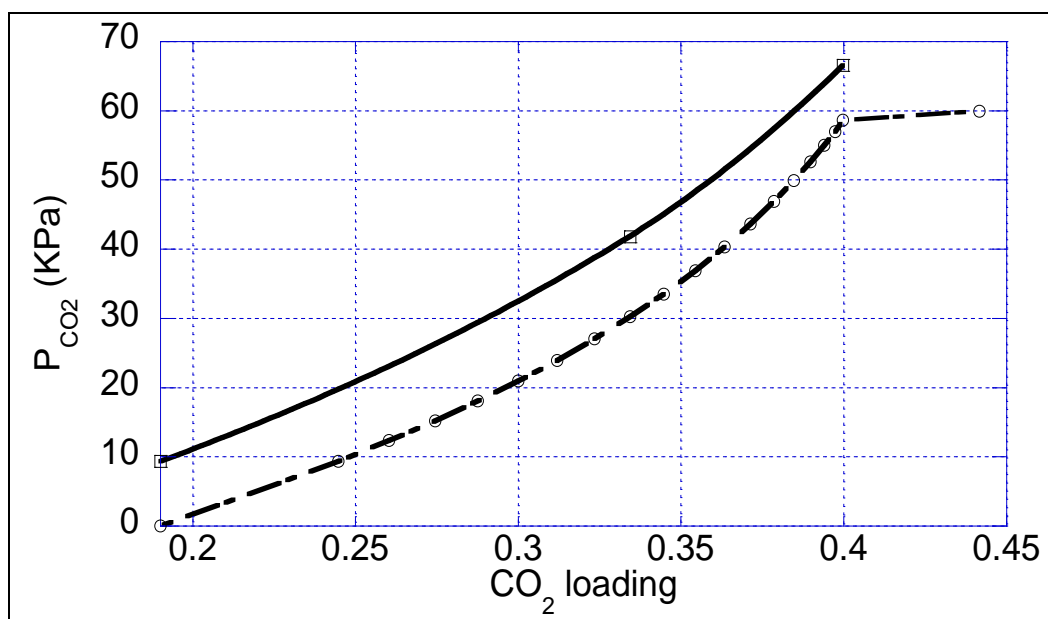


Figure 5.19. McCabe-Thiele diagram for the stripper; $Z_{\text{absorber}}/Z_{\text{Base case}}=1$, 33.5 wt% MEA, 0.1 mol HSS/mol MEA_{tot}, optimized solvent rate ($L/G_{\text{mass}}=2.68$), 10 mol% CO₂ in flue gas, 90% removal.

5.3.2. Effect of stripper height

An analysis was completed to determine the effect of stripper height on the performance of the process. The stripper diameter was kept constant. In this analysis it is important to remember that the liquid phase mass transfer performance in the stripper is overpredicted by the model, due to the use of instantaneous reactions (see section 4.2.1). The performance predicted by the model with a given height of packing requires a higher height for a real stripper. The fact that the reboiler is modeled as an equilibrium segment also goes in the direction of performance overprediction.

Figure 5.20 shows how the relative specific reboiler duty changes, as the stripper height changes, for the case of 3 mol% CO₂ and 85% removal, keeping the solvent rate optimized. The optimized L/G_{mass} values are also shown in the Figure. For this analysis the height was normalized to the height of the base case stripper. Table 5.3 shows also the optimum lean and rich loading.

It is clear that the stripper height affects the heat requirement less dramatically than the absorber height. This means that a stripper as high as the base case stripper is oversized. A column half as high could perform almost as well, with a reboiler duty less than 4% higher. This conclusion is valid only for the 3% CO₂ case. As pointed out in section 5.3.1, the 10% CO₂ case requires a larger stripper size in order to perform optimally.

Table 5.3. Effect of stripper height on the reboiler duty; 3 mol% CO₂ in flue gas, 85 % removal, 33.5 wt% MEA, 0.1 mol HSS/mol MEA_{tot}, solvent rate optimized.

$Z/Z_{\text{Base case}}$	Q_{rel}	L/G _{mass}	Optimum Lean loading	Optimum rich loading
0.285	1.142	1.174	0.23	0.399
0.428	1.110	1.031	0.21	0.402
0.714	1.079	0.967	0.2	0.404
1	1.064	0.912	0.19	0.406

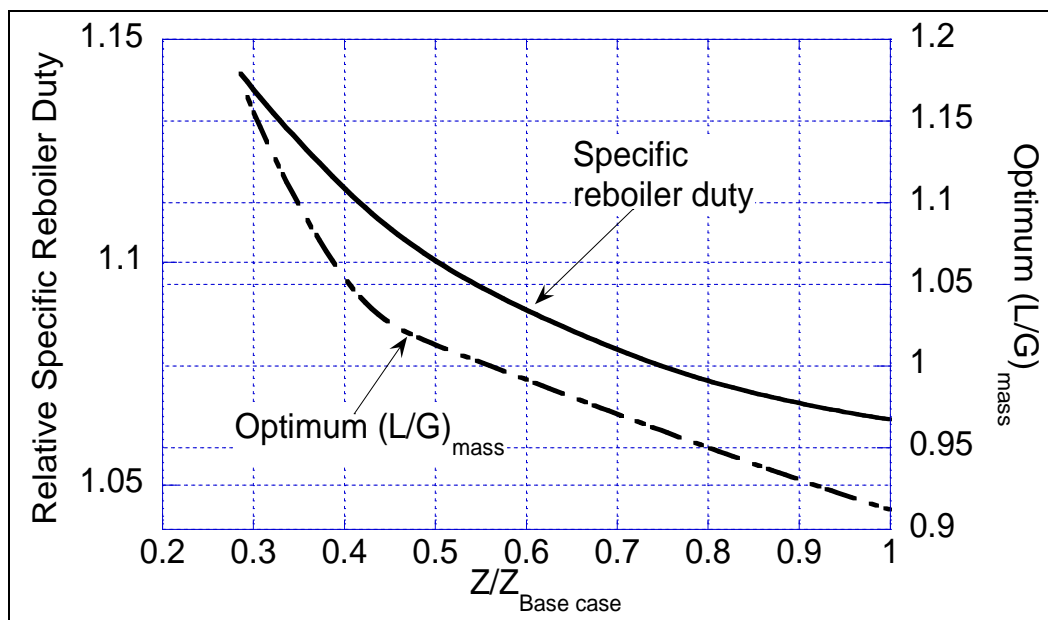


Figure 5.20. Effect of stripper height on the reboiler duty; 3 mol% CO₂ in flue gas, 85 % removal, 33.5 wt% MEA, 0.1 mol HSS/mol MEA_{tot}, solvent rate optimized.

5.4. Effect of MEA concentration and MEA partial neutralization into heat stable salts

As described in chapter 4, the presence of heat stable salts can affect the process performance significantly. By adding 10% heat stable salts to a 30 wt% MEA aqueous solution at a given L/G, it was shown (Figure 4.9) that the reboiler duty can be reduced by 40%. In this chapter a more detailed analysis is described. The goal of this analysis is to determine if it is possible to take advantage of the properties of the heat stable salts to reduce energy requirements.

The model was run at different total MEA concentrations and different HSS loadings (β). In all the runs the solvent rate was optimized. The results are shown in

Figure 5.9. Table 5.4 also shows the optimized L/G_{mass} and the corresponding optimum loadings.

Table 5.4. Effect of heat stable salt fraction of total MEA on specific reboiler duty, optimum L/G and loadings, at 3% CO₂, 85% removal.

wt % MEA	X _{HSS} /X _{MEA} _{tot}	0.000	0.050	0.100	0.150	0.200	0.250
20%	Q _{rel}	1.201	1.197	1.196	1.195	1.198	1.203
	lean loading	0.220	0.210	0.200	0.180	0.160	0.150
	Rich loading	0.451	0.448	0.444	0.441	0.437	0.432
	L/G _{mass}	1.250	1.279	1.321	1.314	1.319	1.390
30%	Q _{rel}	1.093	1.084	1.074	1.067	1.063	1.066
	lean loading	0.230	0.210	0.200	0.180	0.160	0.140
	Rich loading	0.431	0.427	0.421	0.416	0.410	0.402
	L/G _{mass}	0.970	0.951	0.990	0.988	0.996	1.021
36%	Q _{rel}	1.087	1.069	1.053	1.043	1.040	1.033
	lean loading	0.230	0.200	0.190	0.180	0.140	0.120
	Rich loading	0.407	0.402	0.396	0.387	0.381	0.372
	L/G _{mass}	0.928	0.860	0.896	0.951	0.871	0.894

The plot shows that the reboiler duty decreases as the total MEA concentration increases. This can be explained with equation 3.16. Higher [MEA] implies higher rates of absorption and a more efficient absorber. The improvement that comes from a higher MEA concentration vanishes at concentrations higher than 35%, because the viscosity of the solution increases to the point that the diffusivity of CO₂ (equation 3.18) drops and the rates start decreasing, according to equation 3.16. Another reason why the process is never operated at concentration higher than 35 wt% is that MEA is very corrosive when concentrated.

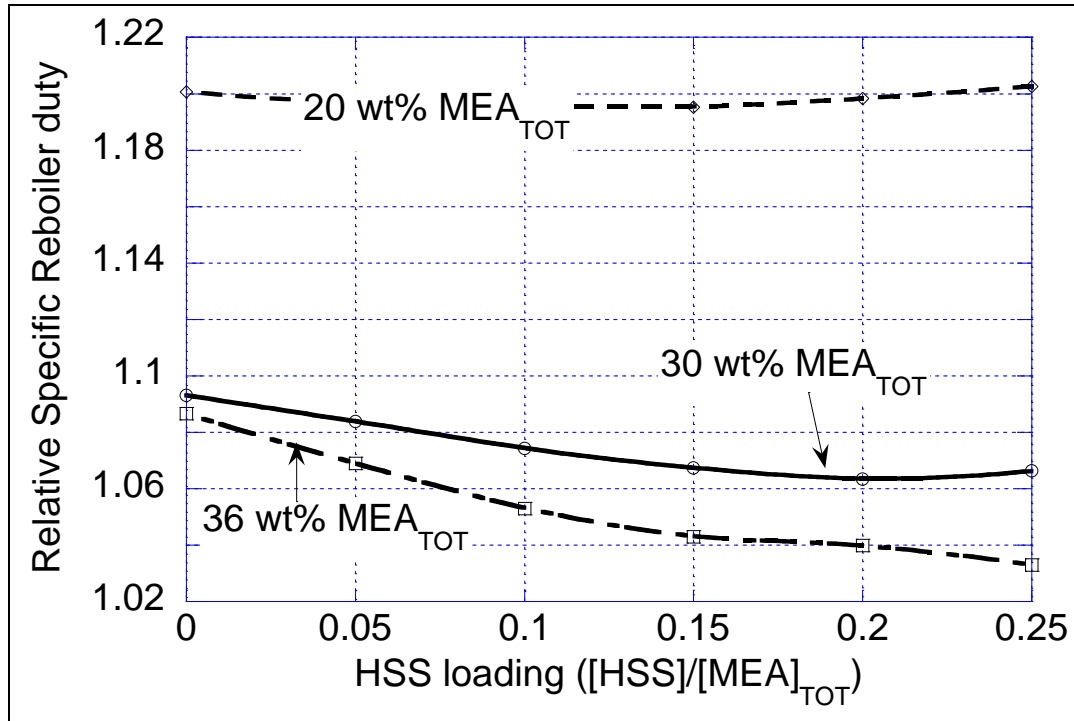


Figure 5.21. Effect of MEA concentration and of HSS loading on the reboiler duty, 3 mol% CO₂, 85% removal, optimum solvent rate.

The reason of the lower steam requirements at $\beta=0.1-0.2$ is that, with heat stable salts in solution, the equilibrium curves in the absorber and stripper tend to become straight at low loading. Straight equilibrium lines tend to generate higher driving forces throughout the columns.

Equation 4.15 can explain why the equilibrium line tends to become straight. Equation 5.8 describes the equilibrium line for $\beta=0$ and $\alpha \rightarrow 0$, and equation 5.9 for $\beta \neq 0$ and $\alpha \rightarrow 0$. Equations 5.8 and 5.9 are derived directly from 4.15.

$$P_{\text{CO}_2} = K \alpha^2 \quad (5.8)$$

$$P_{\text{CO}_2} = K \frac{\alpha(1-\beta)\beta}{(1-\beta)^2} \quad (5.9)$$

From the equation it is clear that the equilibrium line is straight at low loading, if some heat stable salts are present. Without heat stable salts, the equilibrium curve is quadratic at low loading.

When the heat stable salt concentration becomes too high, a low lean loading is no longer enough to keep the removal constant; a high solvent rate is necessary. This requires higher sensible heat in the stripper, and the reboiler duty increases.

The result of this analysis is that, although the heat stable salts cannot appreciably reduce the energy requirement for CO₂ removal, they are not harmful, as long as the solvent rate is optimized.

5.5. Effect of stripper pressure and the concept of lost work

In chapter 1 it was mentioned that the stripper pressure is kept above atmospheric, because this reduces the heat used to generate stripping steam. The heat required by the reboiler is provided by condensing steam. In general the steam is taken from the power plant upstream of the CO₂ removal process. This steam becomes no longer available to produce power. It is meaningful to think about the heat requirement as lost work, which is the work that could be produced if the steam was expanded in a turbine.

With this point of view, it makes a difference whether the steam is extracted at low or high pressure: high pressure steam can produce more work and represents a bigger loss for the power plant than low pressure steam.

As pointed out earlier, the reboiler duty decreases with pressure, because the relative amount of CO₂ and H₂O increases with temperature in the gas phase. Writing the equation of Clausius-Clapeyron (1.6) for both CO₂ and H₂O, and combining them, equation 5.10 and 5.11 are obtained.

$$\frac{d \ln P_{CO_2}^{sat}}{d \ln P_{H_2O}^{sat}} = \frac{-\Delta H_{abs, CO_2}}{\Delta H_{vap, H_2O}} \approx 2 \quad (5.10)$$

$$P_{CO_2}^{sat} \propto P_{H_2O}^{sat\ 2} \quad (5.11)$$

That means that the vapor pressure of CO₂ increases with temperature faster than that of water. The higher the pressure, the higher the temperature and the ratio $P_{CO_2}^{sat}/P_{H_2O}^{sat}$. As the total pressure gets higher, less stripping steam is necessary to drive the CO₂ into the gas phase. At lower pressure, a smaller amount of CO₂ can saturate the CO₂-H₂O gas mixture: more stripping steam is necessary to carry out the separation. The factor of 2 in equation 5.10 makes the energy requirement increase significantly at low pressure.

As a consequence of the aforementioned considerations a minimum is expected in the lost work as a function of stripper pressure. Compression work must also be added if the pressure of the stripper is lower than atmospheric.

A lost work analysis was performed in this work, varying the reboiler pressure from 0.5 bar to 3.7 bar. The stripper model used is that described in chapter 4.2. Because the reactions were all set to equilibrium, the error introduced at lower pressure is larger, since the temperature is also lower and the reaction rates are smaller. Additional sources of error are related to modeling the reboiler as an equilibrium stage and considering the feed at vapor-liquid equilibrium (see chapter 4.2).

When the pressure is lowered, the gas density becomes lower; as a consequence the gas superficial velocity is increased, and this increases the approach to flooding. To avoid that, the column diameter was changed, in order to keep the gas velocity within 80% of the flooding velocity. The pressure drop in the column was changed proportionally to the pressure of the reboiler.

Power cycles are usually complicated; therefore it is not possible to give an exact value for the lost work. In this analysis the lost work was estimated by calculating the thermodynamic maximum work of a cycle where the heat input equals the reboiler duty. Equation 5.12 is the expression of a Carnot cycle, where T_{low} was set to 313⁰K. Q_{in} is the reboiler duty.

$$W_{\max} = Q_{in} \left(1 - \frac{T_{low}}{T_{steam}} \right) \quad (5.12)$$

T_{steam} is the temperature, in Kelvin, at which the steam condenses, where a 20 °F (11 °C) temperature approach to equilibrium in the reboiler is assumed. The values of the lost work are normalized to the moles of CO₂ removed in the process and to the same fixed value introduced in chapter 4.2. The analysis was done for the case of a flue gas with 3 mol% CO₂ and removal kept constant at 85%. The solvent rate was kept optimized for the different runs. The temperature approach to equilibrium in the cross heat exchanger was held constant to 20 °F (11 °C). This analysis does not account for CO₂ compression work.

Figure 5.22 shows the effect of stripper bottom pressure on the reboiler duty and the corresponding lost work. The minimum in the lost work is found approximately at 2 atm, not far from where the base case Bellingham stripper is operated. The slope of the lost work line is steep going to lower pressure, whereas is almost flat at pressure higher than the optimum. The reboiler duty drops quickly at low pressure, tending to reach an asymptote at high pressure. The asymptote represents a minimum heat requirement, when there is no stripping steam generated and the vapor is pure CO₂.

The results can be viewed in tabular form in Table 5.5. Figure 5.23 shows the McCabe-Thiele diagrams for the strippers operated at 3.7 bar and 0.5 bar.

It is evident that, using aqueous MEA as solvent, it is not convenient to reduce the stripper pressure. Not only does the lost work increase, but also there is extra work required for compression of CO₂. Operation at pressure higher than 2 atm is not advised, because the temperature of the column becomes too high and polymerization degradation of MEA becomes important (Rochelle et al., 2001).

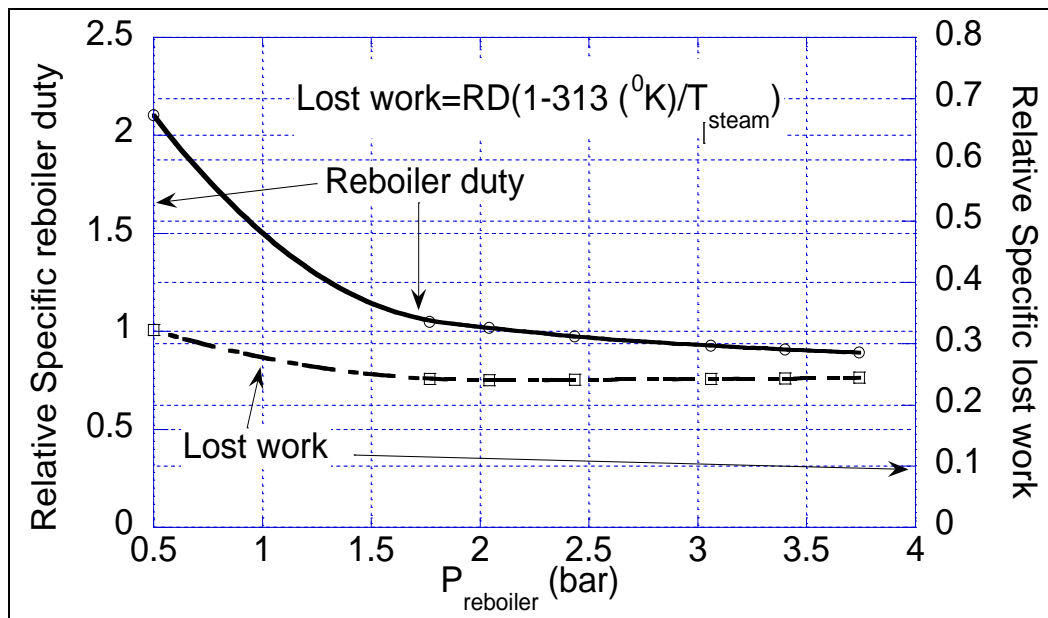


Figure 5.22. Effect of stripper pressure on the reboiler duty and lost work, for a 3 mol % CO₂ flue gas and 85% removal, 33.5 wt% MEA, 0.1 mol HSS/mol MEA_{tot}, L/G optimized.

The high heat of absorption of CO₂ is what makes MEA not attractive for low pressure stripper operation. Other solvents, with lower heat of absorption, could be much more attractive on this aspect.

For a solvent with the ratio $-\Delta H_{\text{abs,CO}_2}/\Delta H_{\text{vap,H}_2\text{O}}$ equal to 1, the stripper pressure would not affect the reboiler duty. The stripper could be run at low pressure with lower lost work. The compression cost would be part of the pressure optimization. Another advantage would be a lower amine degradation rate, due to lower operating temperature. Extensive work is underway to study solvents with lower heat of absorption than MEA, such as piperazine promoted K₂CO₃ (Cullinane, 2002).

Table 5.5. Effect of reboiler pressure on relative specific reboiler duty, relative specific lost work and other operating parameters, 3% CO₂, 85 % removal, optimized L/G.

P_{reboiler} (atm)	0.500	1.769	2.041	2.435	3.061	3.401	3.741
T_{reboiler} (°C)	85.39	121.00	125.53	131.47	139.34	143.10	146.61
T_{steam} (°C)	96.39	132.00	136.53	142.47	150.34	154.10	157.61
P_{steam} (atm)	0.881	2.835	3.236	3.829	4.746	5.244	5.743
Q_{rel}	2.102	1.050	1.019	0.974	0.928	0.909	0.892
Relative lost work	0.322	0.243	0.240	0.241	0.243	0.244	0.244
Optimum L/G_{mass}	1.930	0.863	0.810	0.780	0.710	0.680	0.660
lean loading	0.280	0.180	0.170	0.160	0.140	0.130	0.120
rich loading	0.384	0.408	0.411	0.413	0.415	0.416	0.417
Pressure drop (Kpa)	4.136	15.164	17.232	20.679	26.193	28.950	31.71
Normalized diameter (d/d_{base case})	1.529	1.000	0.824	0.824	0.765	0.765	0.765

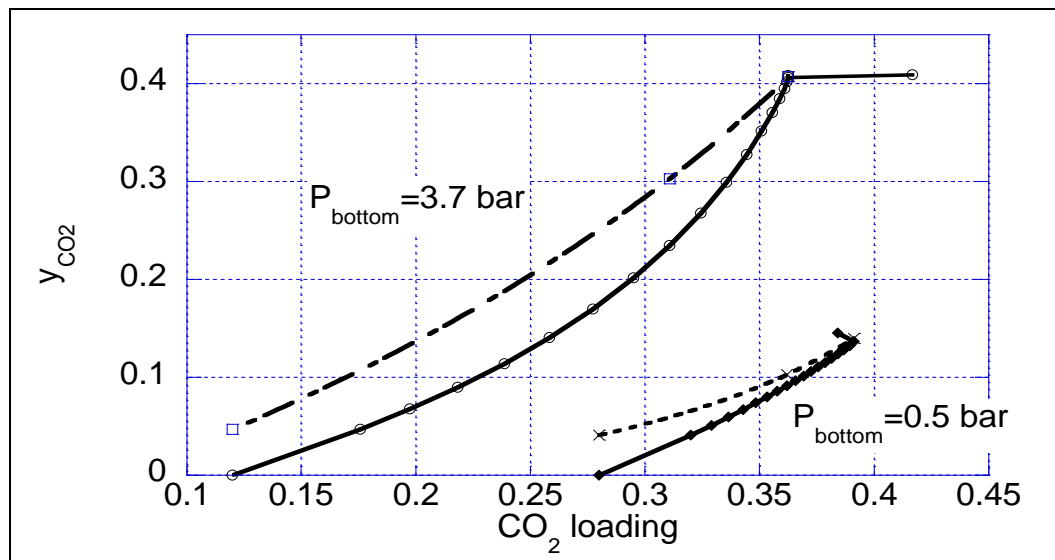


Figure 5.23. McCabe-Thiele diagrams for strippers operating at 3.7 and 0.5 bar, 3 mol% CO₂, 85% removal, 33.5 wt% MEA, 0.1 mol HSS/mol MEA_{tot}, optimized L/G.

5.6. Temperature effect on the absorber

Temperature affects strongly the rates of absorption of CO₂. Equation 3.19 shows that k_g^I and the driving force ($P_i - P_{\text{bulk}}^*$) contribute to determine the absorption rate. The temperature dependence of the two factors is opposite, since k_g^I increases with temperature and the driving force decreases with temperature, at a given CO₂ loading. An analysis was performed to show that it is more efficient that the absorber operates at lower temperature.

5.6.1. Effect of solvent temperature

The temperature of the solvent entering the absorber was varied from 10 °C to 40 °C. Figure 5.24 shows the effect of the lean solvent temperature on the reboiler duty, for a 10% CO₂ flue gas, at constant removal of 90%. The absorber performance is not very sensitive to solvent temperature. A 30 °C change produces a change of less than 2% on the reboiler duty. Even if the effect is not strong, it is clear that lower absorber temperatures are better.

The reason of the weak effect is that the solvent temperature does not affect the temperature of the whole column, because the solvent heat capacity is small and the solvent heats up due to the exothermic reaction.

In Figure 5.25 the temperature profile in the absorber is shown, for solvent temperature of 10 °C and 40 °C. The profiles are different at the top of the column; but the effect vanishes soon, when the heat of reaction and the gas cooling effect act on the solvent flowing down the column.

A strong effect on the absorber performance might be achieved if the whole column was cooled. This could be achieved using alternative designs, that involve cooling coils or small intercooled columns.

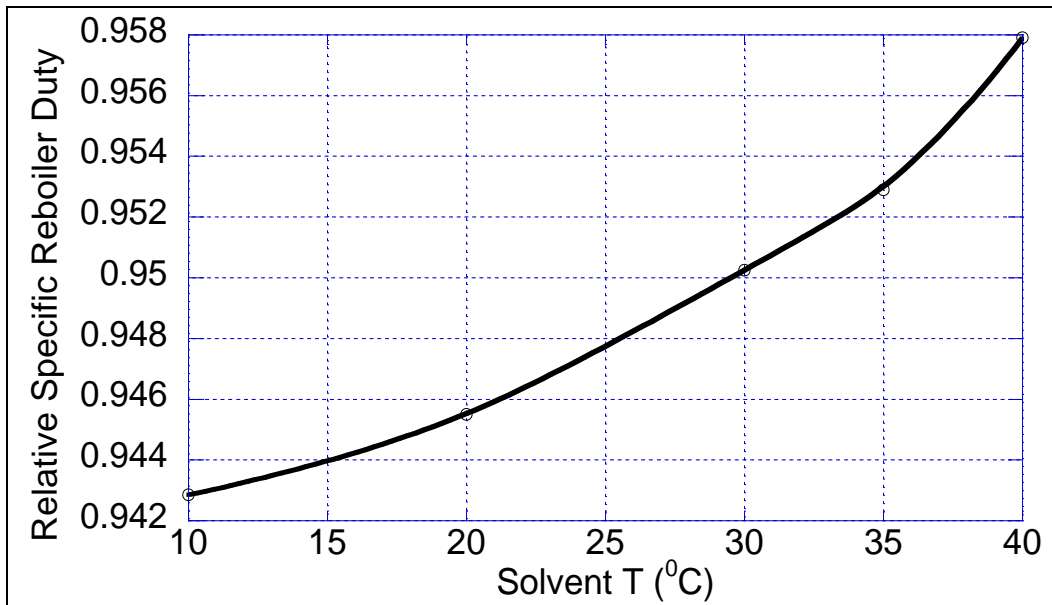


Figure 5.24. Effect of solvent temperature on the specific reboiler duty, 10 mol% CO₂, 33.5 wt% MEA, HSS loading=0.1, lean loading=0.19, solvent rate adjusted to keep removal at 90%.

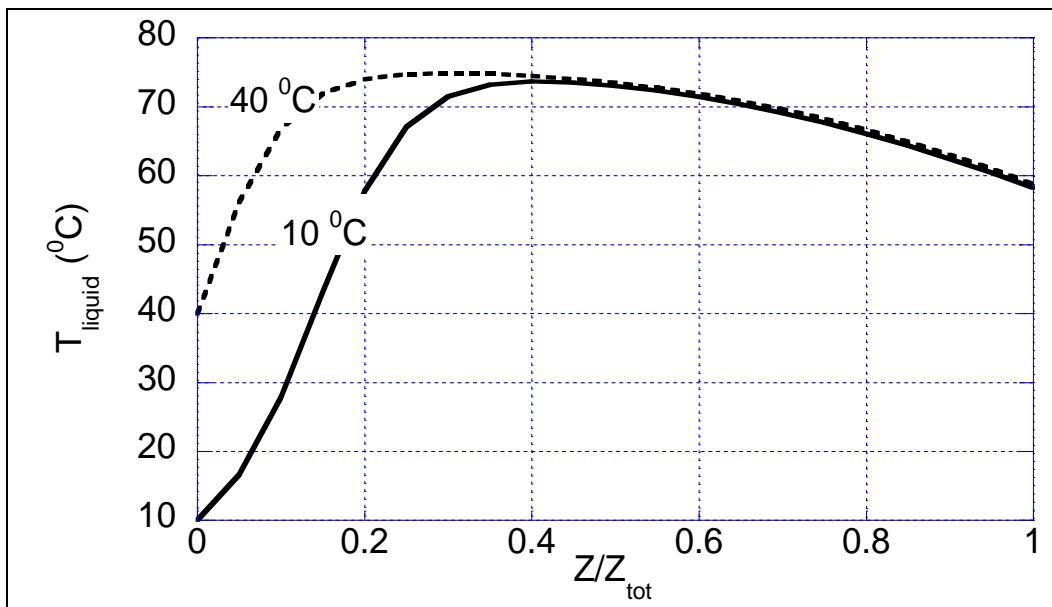


Figure 5.25. Temperature profiles in the absorber for solvent inlet temperature 10 °C and 40 °C; 10 mol% CO₂, 33.5 wt% MEA, 0.1 mol HSS/mol MEA_{tot}, lean loading=0.19, solvent rate adjusted to keep removal at 90%.

5.6.2. Intercooling effect

In order to take full advantage of the benefit derived from operating the absorber at lower temperature, the use of intercoolers is recommended.

The effect of absorber intercoolers on the performance of the process was analyzed, for a 10% CO₂-90% removal case. The intercoolers were modeled with the ASPEN RATEFRAC feature “Heaters Coolers Specifications”, which requires a duty specification, the phase from which heat is taken and a location in the column. The heat was always taken from the liquid phase. The case analyzed was with a cooler located at segment 10 of the absorber, exactly in the middle of the column. The duty was chosen at a value based on a minimum liquid temperature of 40 °C. The value selected for the cooling duty was one third of the reboiler duty. The solvent rate was optimized and the removal was kept constant at 90%. The result was that the reboiler duty was reduced by approximately 3.8%. The results are shown in Table 5.6. Figure 5.26 shows the temperature profile for the liquid and the gas phases, compared to the profile for the non cooled case. Figure 5.27 compares the absorber McCabe-Thiele diagrams for the cooled and non cooled cases. The equilibrium line is lower for the cooled case, increasing the driving forces throughout the column and thus improving the absorber performance. Table 5.6 shows the results of the simulation.

It must be noted that the effect of intercooling, like the effect of solvent temperature, is more important for high CO₂ flue gases. The fact that the absorber temperatures are higher allows a bigger impact of cooling.

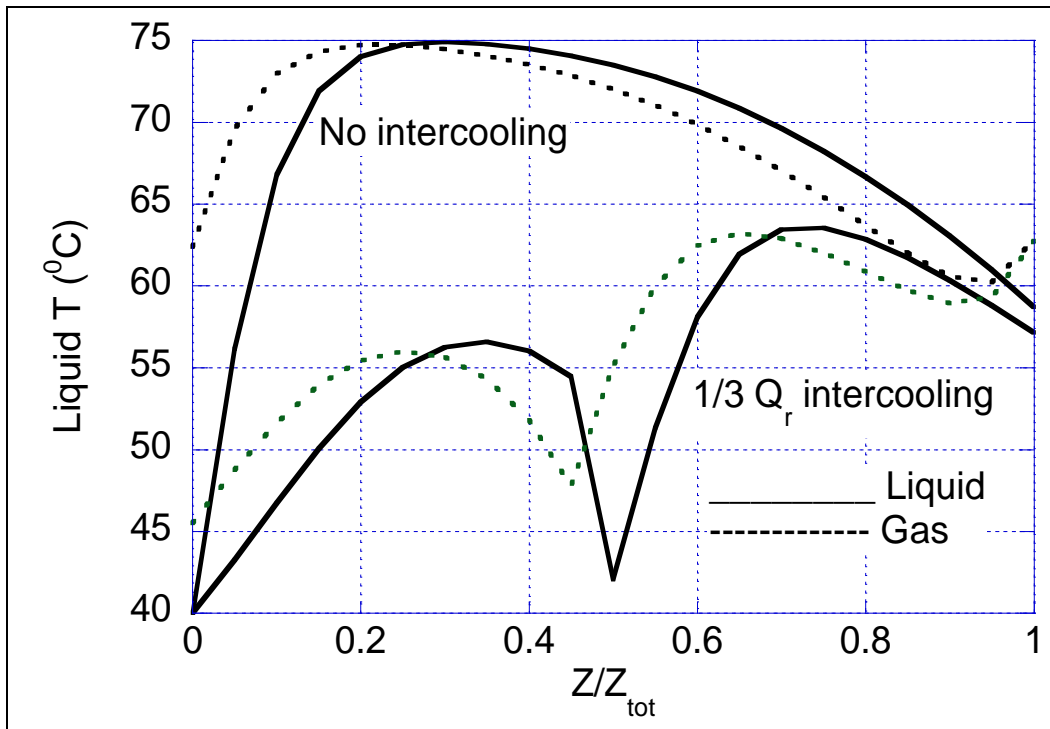


Figure 5.26. Comparison of liquid and gas temperature profiles for intercooled and non-intercooled absorber, intercooler at half column, intercooler duty 1/3 reboiler duty, 10% CO₂, 90% removal, 0.1 mol HSS/mol MEA, optimized L/G.

Table 5.6. Comparison between intercooled and non-intercooled absorber, intercooler at half column, intercooler duty 1/3 reboiler duty, 10% CO₂, 90% removal, 0.1 mol HSS/mol MEA, optimized L/G.

Cooling duty (relative)	lean loading	rich loading	L/G _{mass}	Q _{rel}
0.307	0.20	0.452	2.674	0.921
0	0.19	0.441	2.684	0.957

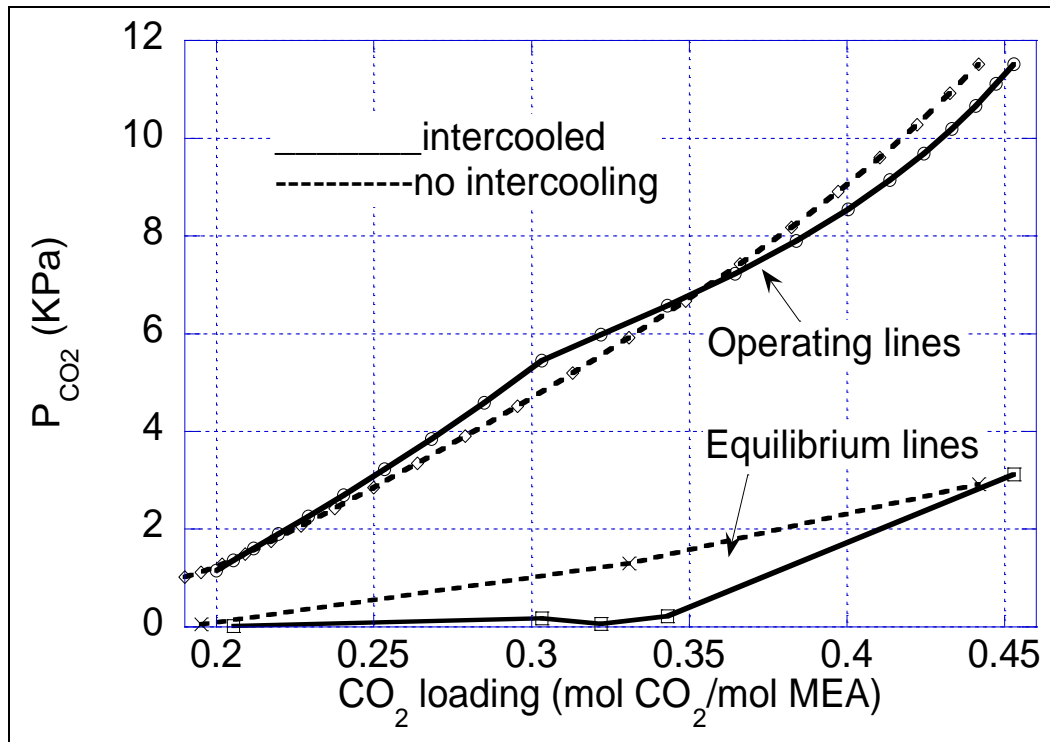


Figure 5.27. Comparison of absorber McCabe-Thiele diagrams for intercooled and non-intercooled absorber, intercooler at half column, intercooler duty 1/3 reboiler duty, 10% CO₂, 90% removal, 0.1 mol HSS/mol MEA, optimized L/G.

5.7. Split flow configuration

The fact that the process performance is improved at lower temperature suggests a simpler way to cool down the absorber. If the solvent is fed at two different points in the column, rather than only at the top, the temperature bulge should be more limited, therefore improving performance. The split flow idea consists of taking a stream of solvent (called semi-lean) from an intermediate segment of the stripper and feeding it to an intermediate segment of the absorber. The configuration is shown schematically in Figure 5.28. The Figure shows also the new optimum cross heat exchanger configuration, which is different from the simple one used in the standard process, because the semi-lean stream is colder

than the stripper bottom. This configuration was proposed by Rochelle (1977) for SO_2 and CO_2 removal, without the solvent coolers, which were added here to get the benefit of a colder absorber.

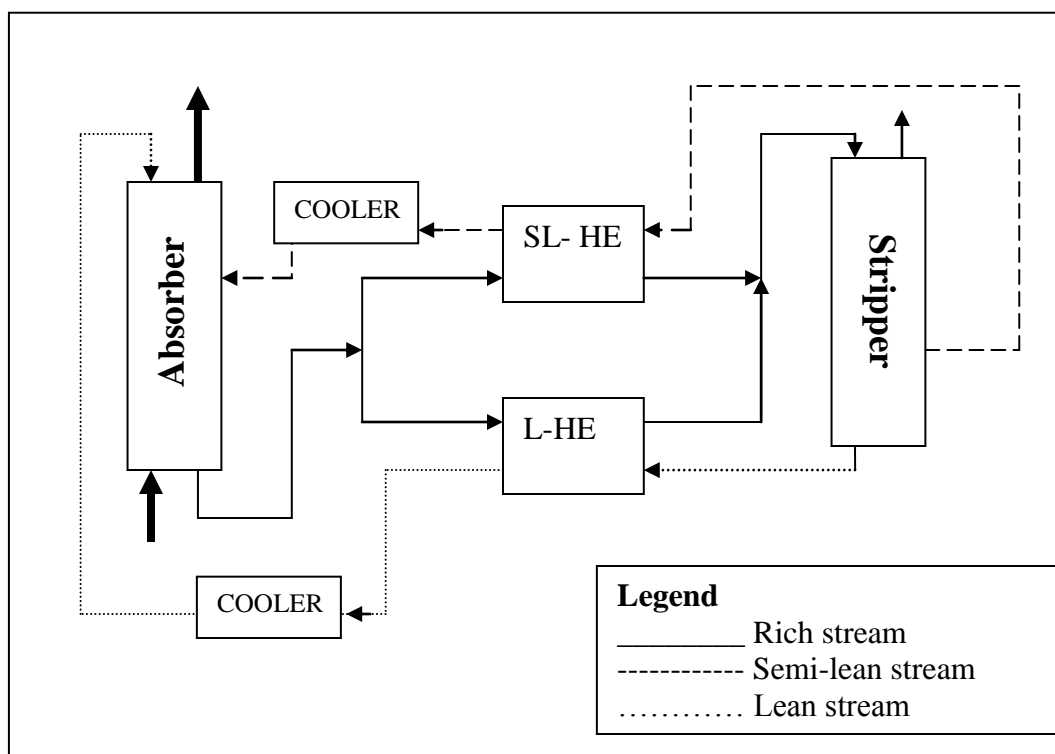


Figure 5.28. Schematic of the split flow configuration.

In the ASPEN PLUS model, the split flow was modeled like the standard model, with a few changes. The new heat exchange network was reproduced, using HEATER blocks and CALCULATOR blocks to match the heat duties (see Figure 4.10), while keeping the temperature approaches to 20 °F. The split feed was treated like the lean feed. The semi-lean loop was not closed. The convergence was obtained in this case with manual iterations.

Several considerations must be considered in order to understand the multiple effects that a split flow configuration has on the process performance.

- A. The absorber is cooled by the semi-lean stream; this increases the driving force for absorption and improves absorber performance.
- B. If the split feed loading does not match that of the injection point in the absorber, a gap is created that tends to reduce the driving force for absorption.
- C. If the stripper is lean pinch limited, then the split flow can by-pass the stripper lean pinch, reducing the stripping steam required to regenerate the solvent.
- D. The fact that the semi-lean stream is extracted from an intermediate segment prevents the semi-lean stream from being thoroughly regenerated; more CO_2 remains in the solvent, tending to reduce driving forces in the absorber.
- E. The lower the extraction stage in the stripper, the higher the temperature of the semi-lean stream. The sensible heat provided by the reboiler is reduced.

Some of these considerations tend to improve the process performance, others tend to reduce it. An analysis is necessary to find out what the effect of split flow on the reboiler duty is.

Figure 5.29 shows qualitative McCabe-Thiele diagrams that can help to understand considerations A, B and C. Continuous lines describe the standard configuration, dashed lines describe the split flow configuration.

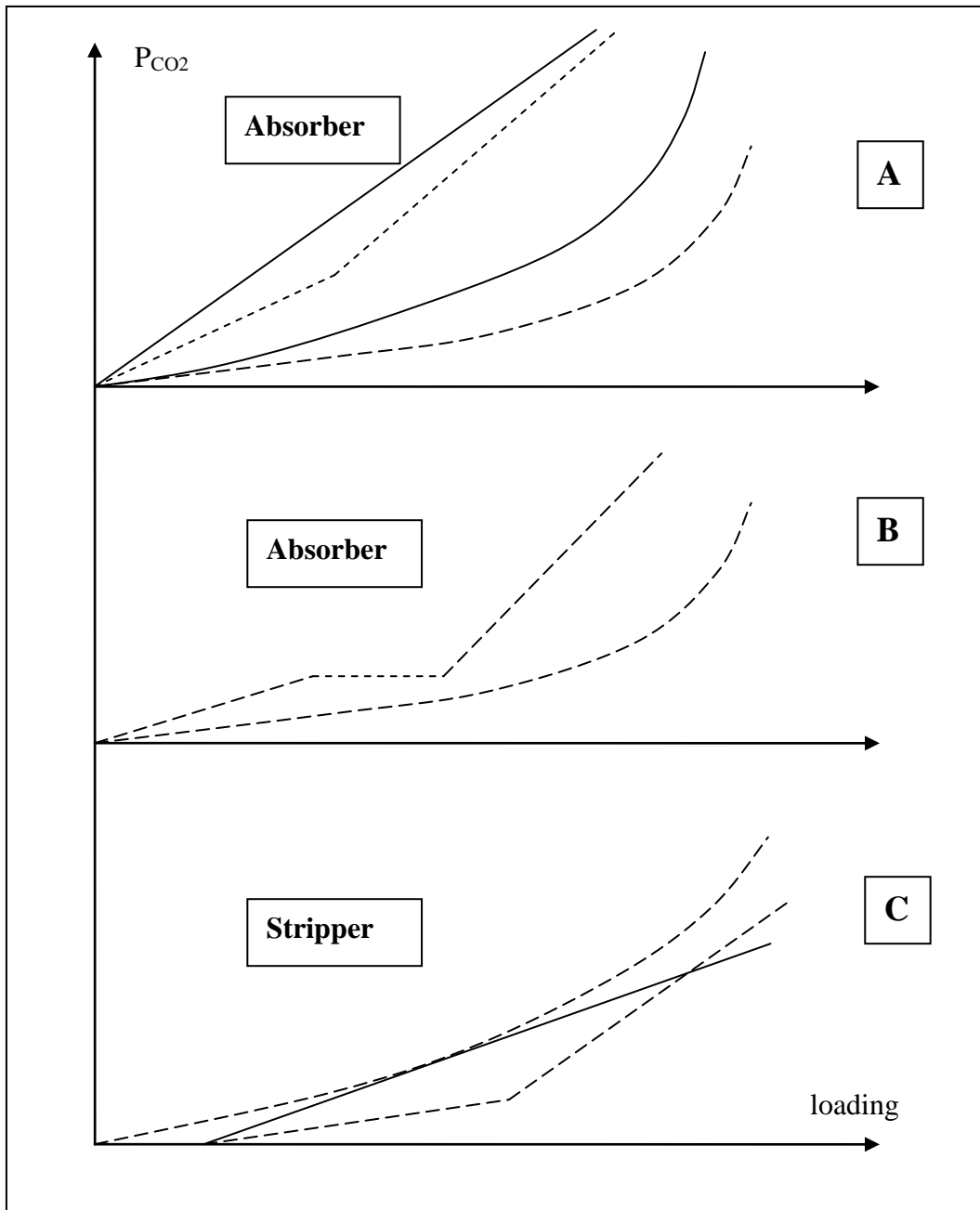


Figure 5.29. Qualitative McCabe-Thiele diagrams describing three possible effects of the split flow configuration; A: absorber cooling effect; B: loading discontinuity effect; C: stripper lean pinch effect.

5.7.1. Effect of split feed extraction location

The effect of split flow location and flow rate was studied. An analysis was completed for a 10% CO₂ case, at constant removal of 90%. The split flow was fixed at a small value (approximately 5% of the lean solvent flow). The injection point in the absorber was fixed at segment 10 (center of the column) and the extraction point in the stripper was varied over the whole column. The small split flow rate does not affect optimum L/G and loadings significantly, therefore the lean loading was kept constant at 0.2 mol CO₂/mol MEA. The lean solvent rate was adjusted to keep the removal constant. The purpose of this analysis was to understand whether the split flow reduces or increases the heat requirement of the process. Table 5.7 shows the results of the analysis.

Table 5.7. Effect of extraction segment on the relative specific reboiler duty and other process variables, constant split flow of 5000 lbmol/hr, 10% CO₂, 90% removal, optimized L/G, 0.1 mol HSS/mol MEA.

Injection segment	Extraction segment	Q_{rel}	lean loading	rich loading	semi-lean loading	L_{lean}/L_{sl}	$(L_{rich}/G)_{mole}$
10	18	1.050	0.200	0.424	0.276	0.060	3.530
10	16	1.051	0.200	0.424	0.300	0.059	3.561
10	15	1.051	0.200	0.423	0.311	0.059	3.570
10	14	1.051	0.200	0.423	0.322	0.059	3.578
10	13	1.051	0.200	0.423	0.332	0.059	3.587
10	12	1.051	0.200	0.423	0.342	0.059	3.595
10	11	1.051	0.200	0.423	0.352	0.059	3.602
10	10	1.051	0.200	0.423	0.360	0.058	3.609
10	9	1.050	0.200	0.424	0.368	0.058	3.613
10	8	1.049	0.200	0.424	0.376	0.058	3.612
10	7	1.052	0.200	0.423	0.383	0.058	3.627
10	6	1.052	0.200	0.423	0.389	0.058	3.632
10	5	1.053	0.200	0.423	0.389	0.058	3.636
		1.047	0.200	0.420		0	3.679

The analysis shows that, for all the extraction segments tested, the reboiler duty increases, compared to the value in the case without split flow. The effect of split flow is a reduction of the overall process performance, at small split flow rates.

5.7.2. Effect of split flow rate

The effect of split flow rate was analyzed for two particular cases, to verify that the effect observed at low split flows does not reverse at high split flows. The cases picked have 10% CO₂, 90% removal, optimized L/G. In Table 5.8 the split stream is extracted from segment 17 of the stripper and fed into segment 6 of the absorber, in Table 5.9 the stream goes from segment 10 to 6. This last case was analyzed up to very high split flow rates.

Table 5.8. Effect of split flow rate, split feed extracted at segment 17 and fed into segment 6, 10% CO₂, 90% removal, optimized L/G, 0.1 mol HSS/mol MEA.

Split Flow rate (lbmol/hr)	$(L_{sl}/L_{lean})_{mole}$	Q_{rel}	lean loading	rich loading	semi-lean loading	$(L_{rich}/G)_{mole}$
0	0	1.046	0.21	0.420		3.679
10000	0.121	1.053	0.2	0.422	0.291	3.664
30000	0.440	1.057	0.19	0.424	0.292	3.906
40000	0.565	1.066	0.2	0.420	0.313	4.411

Table 5.9. Effect of split flow rate, split feed extracted at segment 10 and fed into segment 6, 10% CO₂, 90% removal, optimized L/G, 0.1 mol HSS/mol MEA.

Split Flow rate (lbmol/hr)	$(L_{sl}/L_{lean})_{mole}$	Q_{rel}	lean loading	rich loading	semi-lean loading	$(L_{rich}/G)_{mole}$
0	0	1.045	0.21	0.420276		3.679
60000	0.691	1.105	0.225	0.427757	0.396165	6.14304
120000	2.39	1.132	0.17	0.440923	0.38829	7.038451

From Tables 5.8 and 5.9 it is clear that the split flow effect of increasing the reboiler duty increases with the amount of flow extracted. As it can be seen from the last column in the tables, the total flow required to keep the removal at 90% becomes very high at high split flow rates. The sensible heat becomes the main energy sink.

It can be noticed that the impact of split flow on the reboiler duty is not very large. Increasing the split flow rate from zero to twice the lean solvent rate increases the reboiler duty by approximately 10%.

Figures 5.30 through 5.33 show more detailed results for the case defined by the last line of Table 5.8. Figure 5.30 is the absorber temperature profile, Figure 5.31 is the absorber McCabe-Thiele diagram, Figure 5.32 is the stripper McCabe-Thiele diagram.

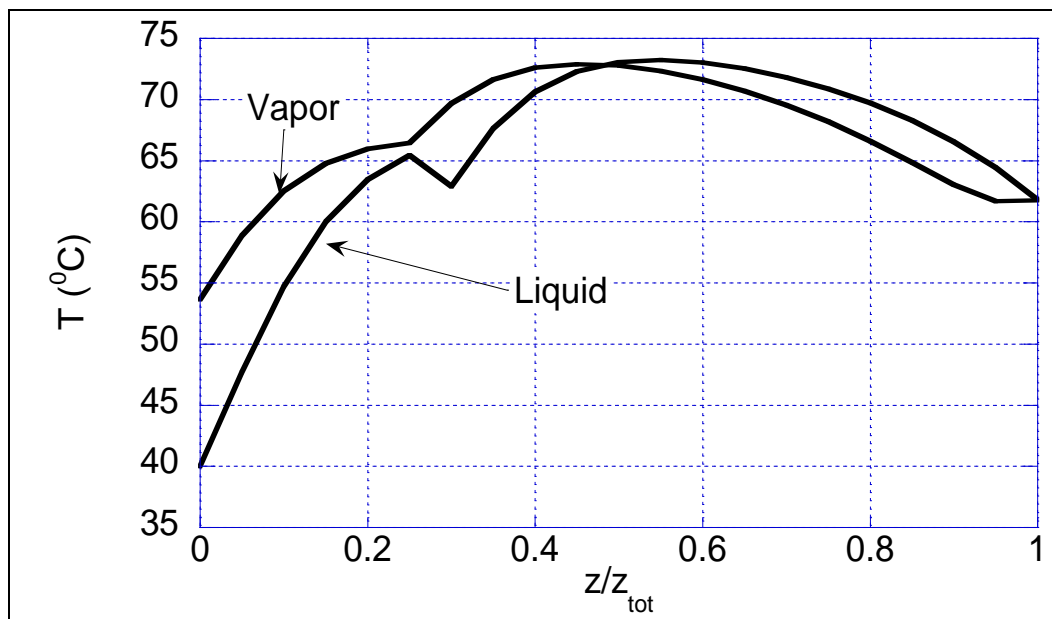


Figure 5.30. Liquid and vapor temperature profiles in absorber with split flow injected at segment 6 (of 20), split flow rate 0.565 times the lean solvent rate, 10% CO₂, 90% removal, optimum L/G, 0.1 mol HSS/mol MEA.

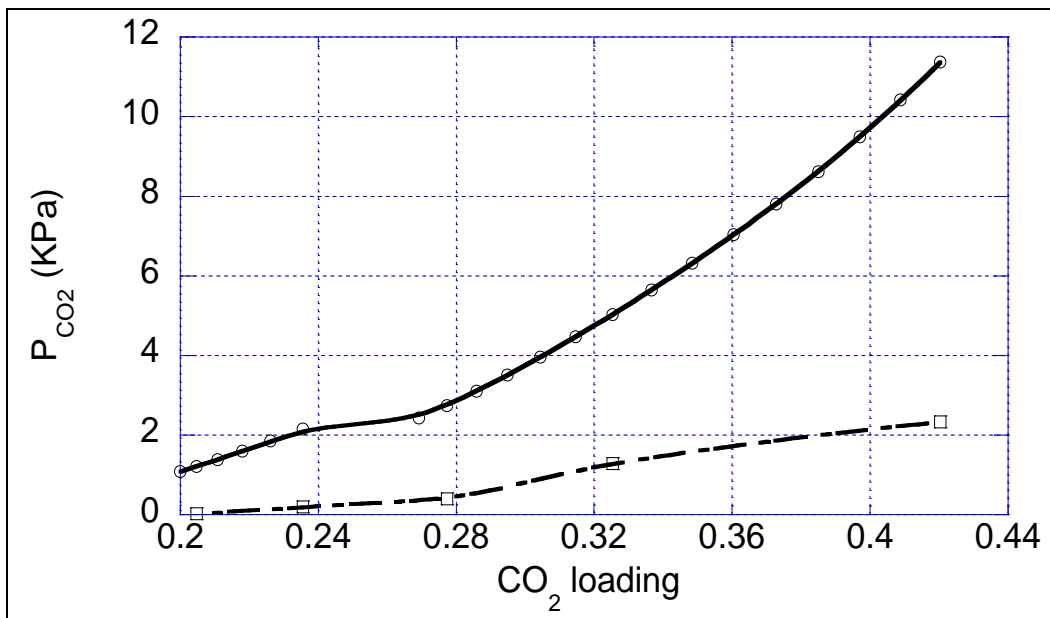


Figure 5.31. Absorber McCabe-Thiele diagram, split flow injected at segment 6 (of 20), extracted from stage 10, split flow rate 0.565 times the lean solvent rate, 10% CO₂, 90% removal, optimum L/G, 0.1 mol HSS/mol MEA.

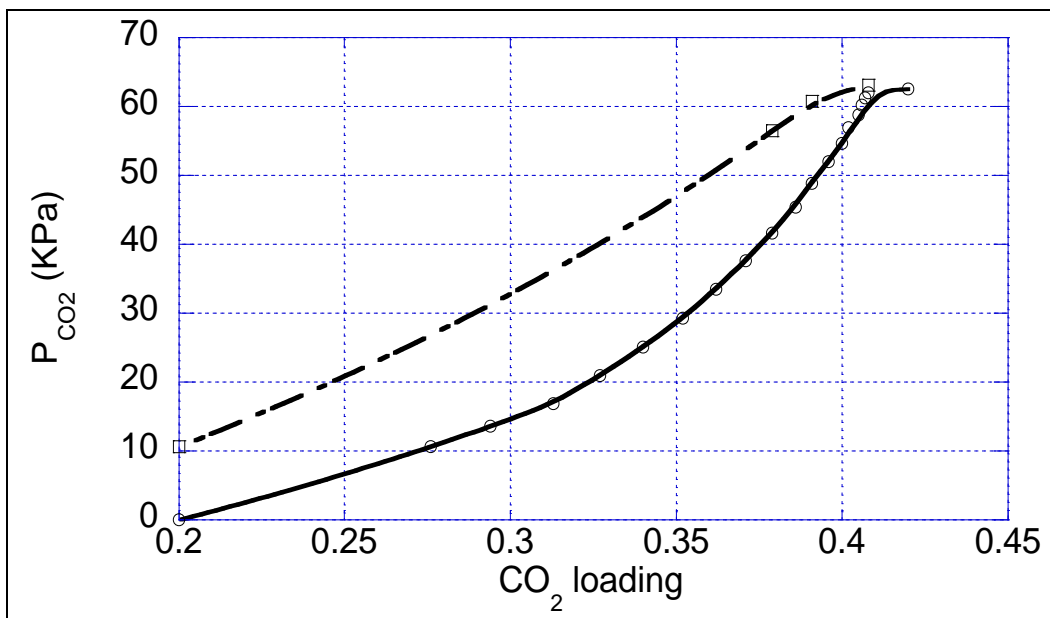


Figure 5.32. Stripper McCabe-Thiele diagram, split flow injected at segment 6 (of 20), extracted from stage 10, split flow rate 0.565 times the lean solvent rate, 10% CO₂, 90% removal, optimum L/G, 0.1 mol HSS/mol MEA.

From Figure 5.30 it can be noticed that, at split flow rate of about half the lean solvent rate, the temperature effect is not very important. As a consequence there is no great benefit from absorber lower temperature. As the split flow becomes higher, the temperature effect is expected to be more important. However, from Table 5.9, it can be noticed that the total flow becomes very high. This implies high sensible heat effect, which requires high reboiler duty. The conclusion is that at no flow rate the split flow is of any benefit to the CO₂ removal process.

Figure 5.31 shows that the absorber, in the particular case shown, presents a small loading discontinuity. It can be noticed how the discontinuity tends to keep the driving force small at low and medium loading.

Figure 5.32 shows that the stripper presents a minor rich pinch, typical of the processes operated at optimum solvent rate (section 5.2). The stripper cannot take advantage of the potential benefit that split flow would give if the stripper was operated at lean pinch conditions.

Chapter 6

Conclusions and Recommendations

6.1. Model: conclusions and recommendations

The ASPEN PLUS model developed for the absorption/stripping process is able to reproduce some plant data, if a correction is applied to the kinetics of the CO_2 +MEA reaction obtained from the data of Dang (2001). The model uses kinetics to represent the mass transfer in the absorber. The stripper model uses equilibrium reactions, since the temperature is higher. Equilibrium is represented with a regressed Electrolyte-NRTL model, based on the experimental work of Jou et al. (1995). The equilibrium model is very important to predict stripper performance, and the heat requirement of the process. The user kinetic subroutine developed for the absorber makes the kinetics consistent with a valid model for mass transfer with chemical reaction (the interface-pseudo-first-order model) and with the regressed equilibrium model.

The model can be improved on several aspects. The following list summarizes the points where the model should be improved.

1. The adjusted kinetics are based on four wetted wall column experiments and a test run on a commercial plant. The validity of the model is

closely related to the quality and accuracy of those data. More wetted wall column data would allow for the regression of a more reliable rate constant.

2. The model used the Henry's constant of CO₂ in water. More physical solubility data would allow for a better estimate of the Henry's constant, which is needed both in the equilibrium and in the rate models.
3. The mass transfer rates in the absorber and, more importantly, in the stripper, are affected by the diffusivity of MEA and the ions in solution. The values for these properties are retrieved by ASPEN PLUS. An improved model would require that better values for diffusivities be supplied to ASPEN PLUS.
4. The mass transfer in the stripper and, in some cases, in the absorber, can be controlled by gas phase resistance. The correlation of Onda et al. (1968) for k_g is very general, thus it cannot be very accurate for every type of packing and every flow range. The values of k_g should be verified and the correlation improved.
5. The estimation of the wetted area in the columns is based on a correlation of Onda et al. (1966). More area measurements are necessary for a better model.
6. The use of kinetic reactions in the stripper could give more accurate results, especially when the stripper is run at pressure lower than 1.5 atm. Also, the hypothesis of equilibrium reboiler may not well describe the reality.

6.1. Process: conclusions and recommendations

The process for the removal of CO₂ from flue gases with aqueous MEA was analyzed and optimized in this work. The main focus of the analysis is the heat

required by the process to regenerate the solvent in the stripper. This heat duty can account for 30% of the energy output of a power plant. Different operating conditions and process configurations have been studied, in order to find working conditions at a lower energy requirement.

The solvent circulation rate is the main variable to control, to keep the process at an optimum. It was shown that the heat requirement of a 3% CO₂ process can increase by 50% if the solvent circulation rate is 30% smaller than the optimum or by 25 % if it is twice the optimum (Figure 5.1). This result shows that the loss of performance is much higher when the solvent rate is low. Practically it is recommended to operate at a solvent rate slightly higher than the optimum. In fact, if the process is exactly at the optimum, a small decrease in the solvent rate causes a high increase in the heat requirement.

The presence of heat stable salts as products of acid neutralization of MEA was analyzed, showing that, if the design does not account for these products, the process may require up to 50% more steam. The key in handling a process with heat stable salts is to re-optimize the solvent rate. If the solvent rate is kept at an optimum, it is even possible to slightly reduce the heat requirement when heat stable salts are present (Figure 5.21), although the solvent may be more corrosive.

The stripper pressure affects the reboiler duty and the lost work of the power plant. It was shown that, for an aqueous MEA solvent, the optimum stripper pressure is approximately 2 atm. However, the effect of stripper pressure on lost work is small, so it may be attractive to operate the stripper at any convenient pressure.

It is possible to improve performance by increasing the height of packing in the absorber, up to a minimum value of reboiler duty. Capital cost considerations need to be included, in order to truly optimize the height of the absorber.

The height of the stripper seems to affect the performance less dramatically than that of the absorber. This conclusion depends on the validity of the assumption of considering the reactions in the stripper to be instantaneous.

Temperature effects on the absorber show that the process is more efficient when the absorber is cooled down. This is valid especially for high CO₂ flue gases, where the temperature bulge is larger, and cooling produces a more significant effect. The design of intercooled absorbers seems to be the only way to reduce significantly the heat requirements, when MEA is used as solvent.

A split flow configuration was analyzed. The result was that, when the solvent rate is kept optimized, there is no benefit from this modified configuration. The reboiler duty is even higher than the basic single-loop process.

The recommendation, for a CO₂ removal unit operating with MEA, is to control carefully the solvent rate, keeping it close to the optimum. By doing this, the effect of all the other operating parameters is damped.

In order to reduce heat requirements significantly, the MEA solvent needs to be replaced with more attractive ones, such as piperazine promoted K₂CO₃, which combine low heat of reaction with fast rates.

APPENDIX A

Regression Inputs and Results

This Appendix reports the summary of inputs and results for the regression of Electrolyte-NRTL parameters by the APEN PLUS DRS, for the CO₂-MEA-H₂O system. The Tables include data points (A.1), regressed values and standard deviations (A.2), correlation matrix (A.3) and a comparison between experimental and calculated values (A.4).

Table A.1. Input summary for experimental data used to regress Electrolyte-NRTL parameters with ASPEN PLUS DRS.

	T	P	X	X	X	Y	Y	Y
USE	(°C)	(Pa)	CO ₂	MEA	H ₂ O	CO ₂	MEA	H ₂ O
STD-DEV	0	0.10%	0.10%	0.10%	0	0.10%	100%	0
DATA	40	6555.017	0.010	0.111	0.879	0.000	0.003	0.997
DATA	40	6480.334	0.022	0.110	0.868	0.001	0.003	0.996
DATA	40	6425.978	0.039	0.108	0.853	0.011	0.003	0.987
DATA	40	6897.105	0.049	0.107	0.844	0.088	0.002	0.910
DATA	40	8828.358	0.054	0.106	0.839	0.291	0.002	0.707
DATA	60	17667.93	0.013	0.111	0.876	0.001	0.004	0.995
DATA	60	17538.00	0.023	0.110	0.868	0.003	0.004	0.993
DATA	60	17663.90	0.042	0.108	0.851	0.030	0.004	0.966
DATA	60	19056.03	0.047	0.107	0.846	0.105	0.004	0.891
DATA	60	27926.45	0.054	0.106	0.840	0.394	0.002	0.604
DATA	80	42735.87	0.013	0.111	0.876	0.002	0.006	0.992
DATA	80	42591.09	0.021	0.110	0.869	0.007	0.006	0.988
DATA	80	44246.83	0.038	0.108	0.854	0.060	0.005	0.934
DATA	80	57079.58	0.049	0.107	0.844	0.280	0.004	0.716
DATA	80	96831.05	0.055	0.106	0.839	0.578	0.002	0.419
DATA	100	94466.26	0.021	0.110	0.869	0.015	0.008	0.977
DATA	100	110102.5	0.041	0.108	0.851	0.173	0.006	0.821
DATA	100	129702.0	0.045	0.107	0.848	0.301	0.005	0.694
DATA	100	159170.3	0.051	0.107	0.843	0.433	0.004	0.562
DATA	100	199131.8	0.051	0.107	0.842	0.547	0.003	0.449
DATA	120	192683.6	0.013	0.111	0.876	0.012	0.010	0.978
DATA	120	232461.4	0.038	0.108	0.854	0.201	0.008	0.790
DATA	120	306584.3	0.043	0.107	0.849	0.398	0.006	0.596
DATA	120	405774.8	0.047	0.107	0.846	0.547	0.005	0.448
DATA	120	605206.5	0.050	0.107	0.843	0.697	0.003	0.300

Table A.2. Results of ASPEN PLUS DRS regression, values and standard deviations of regressed parameters.

	Parameter	Component i	Component j	Value (SI units)	Stdev
1	GMELCC/1	H2O	(MEA+,HCO ₃ ⁻)	6.885	19.920
2	GMELCC/1	H2O	(MEA+,MEACOO ⁻)	10.407	3.331
3	GMELCC/1	(MEA+,HCO ₃ ⁻)	H2O	-3.899	6.991
4	GMELCC/1	(MEA+,MEACOO ⁻)	H2O	-5.963	1.309
5	GMELCD/1	H2O	(MEA+,HCO ₃ ⁻)	969.636	4107.759
6	GMELCD/1	H2O	(MEA+,MEACOO ⁻)	-119.927	1055.668
7	GMELCD/1	(MEA+,HCO ₃ ⁻)	H2O	-91.347	1664.222
8	GMELCD/1	(MEA+,MEACOO ⁻)	H2O	336.452	399.424

Table A.3. Correlation matrix for regressed parameters.

	1	2	3	4	5	6	7	8
1	1							
2	-0.4068	1						
3	-0.9595	0.3129	1					
4	0.6560	-0.9165	-0.5857	1				
5	-0.8481	0.3895	0.8953	-0.5414	1			
6	0.3480	-0.9918	-0.2630	0.8866	-0.3683	1		
7	0.4317	-0.1239	-0.6238	0.2099	-0.807	0.1400	1	
8	-0.5986	0.928	0.5349	-0.9920	0.5155	-0.9137	-0.216	1

Table A.4. Comparison of experimental values and values calculated with the regressed parameters.

Exp PRES	Est PRES	Exp	Est	Exp	Est	Exp	Est	Exp	Est
		X CO2	X CO2	X MEA	X MEA	X H2O	X H2O	Y CO2	Y CO2
N/sqm	N/sqm								
6555.017	6408.548	0.010	0.010	0.111	0.113	0.879	0.877	0.000	0.000
6480.333	6473.279	0.022	0.022	0.110	0.109	0.868	0.869	0.001	0.001
6425.979	6526.027	0.039	0.039	0.108	0.109	0.853	0.852	0.011	0.011
6897.108	7062.114	0.049	0.050	0.107	0.106	0.844	0.844	0.088	0.087
8828.358	9026.968	0.054	0.055	0.106	0.106	0.839	0.839	0.291	0.288
17667.933	17442.447	0.013	0.013	0.111	0.108	0.876	0.878	0.001	0.001
17538.001	17425.844	0.023	0.022	0.110	0.110	0.868	0.867	0.003	0.003
17663.906	17784.909	0.042	0.041	0.108	0.111	0.851	0.849	0.030	0.030
19056.034	19290.683	0.047	0.047	0.107	0.107	0.846	0.846	0.105	0.105
27926.456	28212.568	0.054	0.054	0.106	0.106	0.840	0.840	0.394	0.391
42735.878	41381.223	0.013	0.013	0.111	0.110	0.876	0.877	0.002	0.002
42591.095	41540.803	0.021	0.021	0.110	0.109	0.869	0.870	0.007	0.007
44246.829	43683.266	0.038	0.038	0.108	0.107	0.854	0.855	0.060	0.060
57079.586	56554.668	0.049	0.049	0.107	0.107	0.844	0.844	0.280	0.282
96831.075	96542.529	0.055	0.055	0.106	0.106	0.839	0.839	0.578	0.580
94466.242	89516.910	0.021	0.021	0.110	0.108	0.869	0.871	0.015	0.015
110102.518	105449.522	0.041	0.041	0.108	0.108	0.851	0.852	0.173	0.174
129702.037	125038.217	0.045	0.045	0.107	0.107	0.848	0.848	0.301	0.306
159170.299	155291.240	0.051	0.049	0.107	0.109	0.843	0.842	0.433	0.445
199131.899	195928.939	0.051	0.051	0.107	0.106	0.842	0.843	0.547	0.558
192683.715	175346.641	0.013	0.013	0.111	0.107	0.876	0.879	0.012	0.012
232461.501	214806.027	0.038	0.037	0.108	0.109	0.854	0.855	0.201	0.206
306584.348	289963.777	0.043	0.043	0.107	0.106	0.849	0.850	0.398	0.412
405774.809	393237.175	0.047	0.048	0.107	0.106	0.846	0.846	0.547	0.567
605206.492	592244.141	0.050	0.052	0.107	0.103	0.843	0.844	0.697	0.704

Exp	Est	Exp	Est	Exp	Est	Exp	Est	Exp	Est
Y	Y	Y	Y	Y/X	Y/X	Y/X	Y/X	Y/X	Y/X
MEA	MEA	H2O	H2O	CO2	CO2	MEA	MEA	H2O	H2O
0.003	0.001	0.997	0.999	-0.010	-0.009	-0.109	-0.112	0.118	0.121
0.003	0.001	0.996	0.998	-0.021	-0.021	-0.107	-0.108	0.128	0.129
0.003	0.000	0.987	0.989	-0.029	-0.029	-0.105	-0.108	0.134	0.137
0.002	0.000	0.910	0.913	0.038	0.038	-0.104	-0.106	0.066	0.069
0.002	0.000	0.707	0.712	0.237	0.233	-0.104	-0.106	-0.132	-0.127
0.004	0.001	0.995	0.998	-0.012	-0.012	-0.107	-0.107	0.119	0.119
0.004	0.001	0.993	0.996	-0.019	-0.019	-0.106	-0.109	0.125	0.128
0.004	0.001	0.966	0.969	-0.012	-0.011	-0.104	-0.110	0.116	0.121
0.004	0.000	0.891	0.894	0.059	0.058	-0.104	-0.107	0.045	0.049
0.002	0.000	0.604	0.609	0.340	0.337	-0.104	-0.106	-0.236	-0.231
0.006	0.002	0.992	0.996	-0.011	-0.011	-0.105	-0.108	0.116	0.118
0.006	0.002	0.988	0.992	-0.014	-0.014	-0.104	-0.107	0.118	0.121
0.005	0.001	0.934	0.939	0.023	0.022	-0.103	-0.106	0.080	0.084
0.004	0.000	0.716	0.718	0.231	0.233	-0.103	-0.107	-0.128	-0.126
0.002	0.000	0.419	0.420	0.523	0.525	-0.104	-0.106	-0.420	-0.420
0.008	0.002	0.977	0.983	-0.006	-0.006	-0.102	-0.106	0.108	0.112
0.006	0.001	0.821	0.824	0.132	0.134	-0.101	-0.107	-0.030	-0.027
0.005	0.001	0.694	0.694	0.255	0.261	-0.102	-0.106	-0.154	-0.154
0.004	0.000	0.562	0.555	0.383	0.395	-0.102	-0.108	-0.280	-0.287
0.003	0.000	0.449	0.442	0.496	0.507	-0.103	-0.106	-0.393	-0.401
0.010	0.004	0.978	0.985	-0.001	-0.002	-0.101	-0.104	0.102	0.105
0.008	0.002	0.790	0.792	0.164	0.170	-0.100	-0.107	-0.064	-0.063
0.006	0.001	0.596	0.587	0.355	0.369	-0.101	-0.105	-0.253	-0.264
0.005	0.001	0.448	0.433	0.500	0.519	-0.102	-0.105	-0.397	-0.414
0.003	0.000	0.300	0.295	0.647	0.652	-0.104	-0.103	-0.543	-0.549

APPENDIX B

FORTRAN Kinetic Subroutine for RATEFRAC

This Appendix reports the complete FORTRAN code for the kinetic subroutine that integrates RATEFRAC in the calculation of the flux of CO₂, due to reactions with MEA and OH⁻ and diffusion in the boundary layer.

```

C*****
C-----
C
c    KINETIC SUBROUTINE WRITTEN BY STEFANO FREGUIA,
C    THE UNIVERSITY OF TEXAS AT AUSTIN, 2002
C    FOR CALCULATION OF RATES FOR MEA-CO2 REACTION
C
      SUBROUTINE KIN(NSTAGE, NCOMP, NR,  NRL,  NRV,
2         T,  TLIQ, TVAP, P,  PHFRAC,
3         F,  X,  Y,  IDX,  NBOPST,
4         KDIAG, STOIC, IHLBAS, HLDLIQ, TIMLIQ,
5         IHVBAS, HLDVAP, TIMVAP, NINT,  INT,
6         NREAL, REAL,  RATES, RATEL, RATEV,
7         NINTB, INTB,  NREALB, REALB, NIWORK,
8         IWORK, NWORK,  WORK)
C
C  VARIABLES IN ARGUMENT LIST
C
C  VARIABLE I/O TYPE  DIMENSION  DESCRIPTION AND RANGE
C  NSTAGE  I  I      -    STAGE NUMBER
C  NCOMP   I  I      -    NUMBER OF COMPONENTS
C  NR      I  I      -    TOTAL NUMBER OF KINETIC
C                          REACTIONS
C  NRL     I  I      -    NUMBER OF LIQUID PHASE
C                          KINETIC REACTIONS
C  NRV     I  I      -    NUMBER OF VAPOR PHASE
C                          KINETIC REACTIONS
C  T       I  R      -    STAGE TEMPERATURE (K)
C  TLIQ    I  R      -    LIQUID TEMPERATURE (K)
C                          * USED ONLY BY RATEFRAC **
C  TVAP    I  R      -    VAPOR TEMPERATURE (K)

```

```

C          * USED ONLY BY RATEFRAC **
C  P      I  R      -      STAGE PRESSURE (N/SQ.M)
C  VF     I  R      3      VAPOR FRACTION
C  F      I  R      -      TOTAL FLOW ON STAGE
C                          (VAPOR+LIQUID) (KMOL/SEC)
C  X      I  R      NCOMP,3  LIQUID MOLE FRACTION
C  Y      I  R      NCOMP    VAPOR MOLE FRACTION
C  IDX    I  I      NCOMP    COMPONENT INDEX VECTOR
C  NBOPST I  I      6        OPTION SET BEAD POINTER
C  KDIAG  I  I      -        LOCAL DIAGNOSTIC LEVEL
C  STOIC  I  R      NCOMP,NR  REACTION STOICHIOMETRY
C  IHLBAS I  I      -        BASIS FOR LIQUID
C                          HOLDUP SPECIFICATION
C                          1:VOLUME,2:MASS,3:MOLE
C  HLDLIQ I  R      -        LIQUID HOLDUP
C                          IHLBAS  UNITS
C                          1      CU.M.
C                          2      KG
C                          3      KMOL
C  TIMLIQ I  R      -        LIQUID RESIDENCE TIME
C                          (SEC)
C  IHVBAS I  I      -        BASIS FOR VAPOR
C                          HOLDUP SPECIFICATION
C                          1:VOLUME,2:MASS,3:MOLE
C  HLDVAP I  R      -        VAPOR HOLDUP
C                          IHVBAS  UNITS
C                          1      CU.M.
C                          2      KG
C                          3      KMOL
C  TIMVAP I  R      -        VAPOR RESIDENCE TIME (SEC)
C  NINT   I  I      -        LENGTH OF INTEGER VECTOR
C  INT    I/O I      NINT     INTEGER VECTOR
C  NREAL  I  I      -        LENGTH OF REAL VECTOR
C  REAL   I/O R      NREAL     REAL VECTOR
C  RATES  O  R      NCOMP     COMPONENT REACTION RATES
C                          (KMOL/SEC)
C  RATEL  O  R      NRL       INDIVIDUAL REACTION RATES
C                          IN THE LIQUID PHASE
C                          (KMOL/SEC)
C          * USED ONLY BY RATEFRAC **
C  RATEV  O  R      NRV       INDIVIDUAL REACTION RATES
C                          IN THE VAPOR PHASE

```

```

C          (KMOL/SEC)
C          * USED ONLY BY RATEFRAC **
C  NINTB   I  I   -   LENGTH OF INTEGER VECTOR
C          (FROM UOS BLOCK)
C  INTB    I/O I   NINTB   INTEGER VECTOR
C          (FROM UOS BLOCK)
C  NREALB  I  I   -   LENGTH OF REAL VECTOR
C          (FROM UOS BLOCK)
C  REALB   I/O R   NREALB  REAL VECTOR
C          (FROM UOS BLOCK)
C  NIWORK  I  I   -   LENGTH OF INTEGER WORK
C          VECTOR
C  IWORK   I/O I   NIWORK  INTEGER WORK VECTOR
C  NWORK   I  I   -   LENGTH OF REAL WORK VECTOR
C  WORK    I/O R   NWORK   REAL WORK VECTOR
C
C*****
C*****
C
C  IMPLICIT NONE
C
C  DECLARE VARIABLES USED IN DIMENSIONING
C
C  INTEGER NCOMP, NR,  NRL,  NRV,  NINT,
+  NINTB, NREALB, NIWORK, NWORK, N_COMP
C
C  DECLARE PARAMETERS & VARIABLES USED IN PARAMETERS
C
C  INTEGER K_CO2, K_MEA, K_H2O, K_MEAH, K_MEACOO, K_HCO3,
K_CO3, K_H3O
C  INTEGER K_OH, K_N2, K_O2
C  integer dms_kccidc, kvector(ncomp),i

C  DECLARE ARGUMENTS
C
C  INTEGER IDX(NCOMP), NBOPST(6), INT(NINT),
+  INTB(NINTB), IWORK(NIWORK), NSTAGE,
+  KDIAG, IHLBAS, IHVBAS, NREAL, KPHI,
+  KER
C  REAL*8 X(NCOMP,3), Y(NCOMP),
+  STOIC(NCOMP,NR),  RATES(NCOMP),

```

```

+   RATEL(NRL), RATEV(NRV),
+   REALB(NREALB),WORK(NWORK), B(1), T,
+   TLIQ, TVAP, P, PHFRAC(3), F
REAL*8 HLDLIQ,TIMLIQ,HLDVAP,TIMVAP
C
C   DECLARE LOCAL VARIABLES
C
INTEGER IMISS, L_GAMMA, J, KV, LMW,I,L_GAMMA1
REAL*8 REAL(NREAL), RMISS
REAL*8 PHI(NCOMP)
REAL*8 DPHI(NCOMP)
REAL*8 GAMMA(NCOMP)
REAL*8 R1, R2, R3, R4, LNKEQ1, KEQ1, LNKEQ2, KEQ2, k1,k2
REAL*8 VMX, DVMX, VISC, delta, aco2,aco2s,ctot, dco2
real*8 dco2w,viscw,aw, atot, area, pi, Lm, Gm, Lf, Gf
real*8 g, rel, frl, wel, sigma, sigmac,SRFTEN, dens, mwl,mwv
real*8 XMW(NCOMP), FF,holdup, IS, A, gam, xmeat,henry, R, henrya
real*8 mend, pco2s,pco2,C,Vam,Vh20,Vstar,vco2,v,xco2,xmea,xwat
real*8 totmass,alpha,par1,par2,wfam ,visc2
c
C
#include "ppexec_user.cmn"
EQUIVALENCE (RMISS, USER_RUMISS)
EQUIVALENCE (IMISS, USER_IUMISS)
C
C

#include "dms_plex.cmn"
C
EQUIVALENCE(B(1),IB(1))
C
#include "dms_maxwrt.cmn"

#include "dms_ipoff1.cmn"

#include "dms_ipoff3.cmn"

#include "ppbase_snbops.cmn"

c      Some extra passed parameters are needed in realb
c
c

```

```

c
c      realb(1)=total packing area per unit volume, in 1/m
c
c      realb(2)=column diameter, in m
c
c      realb(3)=stage height, in m. Play with this if convergence is difficult
c
c      realb(4)=packing surface tension, in dyne/cm
c
c      realb(5)=liquid rate, changes during simulation
c
c      realb(6)=adjustable parameter for rate constant
c
c      realb(7)=adjustable parameter for wetted area
c
c      EXECUTABLE CODE

      NBOPST(1)=SNBOPS_NBOPSS
      NBOPST(2)=SNBOPS_NBHNRY
      NBOPST(3)=SNBOPS_NBCHEM
      NBOPST(4)=SNBOPS_IXTRUE
      NBOPST(5)=SNBOPS_NBFREE
      NBOPST(6)=SNBOPS_IXSOLU

      xco2=x(2,1)+x(7,1)+x(8,1)+x(9,1)
*      +x(12,1)
      xmea=x(3,1)+x(6,1)+x(7,1)
      xwat=1.0-xco2-xmea

c      Density with Weiland correlation

      Vam=61.09/(-(5.35162e-7)*tliq*tliq-(4.51417e-4)*tliq+1.19451)
      Vh20=1000.0/55.556  ! Basically constant at 0-40 C
      Vstar=-1.8218
      Vco2=0.04747
      V=xmea*Vam+xco2*Vco2+xwat*Vh20+xmea*xwat*Vstar
      totmass=xmea*61.09+xwat*18.02+xco2*44.01
      dens=totmass/V*1000.0

c      Get molecular weights of both phases

C      Molecular weights of components

```

```

LMW = IPOFF1_IPOFF1(306)
DO I = 1,NCOMP
  XMW(I) = B(LMW+IDX(I))
END DO

```

c Molecular weights

```

      mwl=0.0
      mwv=0.0
      do 1 i=1,ncomp
        mwl=mwl+xmw(i)*x(i,1)
        mwv=mwv+xmw(i)*y(i)
1      continue

```

c Molar density

```

      ctot=dens/mwl      ! gmol/liter

```

c Viscosity with Weiland correlation

```

      alpha=xco2/xmea    !It's a loading that includes heat stable salts

      viscw=exp(-24.71+4209.0/tliq+0.04527*tliq-0.00003376*tliq*tliq)

      wfam=xmea/(18.0/61.0+(1.0-18.0/61.0)*xmea)

      par1=21.186*wfam*100.0+2373.0
      par2=0.01015*wfam*100.0+0.0093*tliq-2.2589

      visc=viscw*exp(par1*(alpha*par2+1.0)*wfam*100.0/(tliq*tliq)) !mPa*s

```

C USE STOKES-EINSTEIN TO DETERMINE DCO2 (m²/s) (from Pacheco)

```

      dco2w=(2.35e-6)*exp(-2119.0/tliq)

      dco2=dco2w*(viscw/visc)**0.545

```

```

c      write(maxwrt_maxbuf(1),FMT='((G10.4))')dco2
c      call dms_wrtrm(1)

```

c RATE CONSTANTS:

$k1=4.3152e13*\text{dexp}(-13249.0/1.987/\text{tliq})*\text{ctot}*\text{ctot} \text{ ! mole/liter/s}$

$k2=\text{realb}(6)*5858.51*\text{ctot}*\text{ctot}*\text{dexp}(-41177.38/8.31*$
 $*(1.0/\text{tliq}-1.0/298.0))$

c Correction to match Dang's points: it corrects k2, Henry, and gamma

$A=1.206e-5*\text{dexp}(4050.6/\text{tliq}) \text{ ! mole/liter/s}$
 $k2=k2*A$

C EQUILIBRIUM CONSTANTS:

$\text{LNKEQ1}=98.566+1353.8/\text{TLIQ}-14.304*\text{LOG}(\text{TLIQ})$
 $\text{KEQ1}=\text{DEXP}(\text{LNKEQ1})$
 $\text{LNKEQ2}=231.98-9546.57/\text{TLIQ}-36.7816*\text{LOG}(\text{TLIQ})$
 $\text{KEQ2}=\text{DEXP}(\text{LNKEQ2})$

C calculate fugacity coefficient
 $\text{KPHI}=1$

C fugacity coefficient of components in the mixture

$\text{CALL PPMON_FUGLY}(T,P,X$
 $+ \text{ ,Y,NCOMP,IDX,NBOPST,KDIAG,KPHI,PHI,DPHI,KER})$

c

C set offset to get activity coefficients

C (see vol5, p 11-11 and asp\$or search for 'GAMMAL')

$\text{L_GAMMA}=\text{IPOFF3_IPOFF3}(24)$
 $\text{L_GAMMA1}=\text{IPOFF3_IPOFF3}(29)$

C calculate activities for plex data

$\text{DO J}=1,\text{NCOMP}$
 $\text{GAMMA}(\text{J})=\text{dexp}(\text{B}(\text{L_GAMMA}+\text{J}))$
 END DO
 $\text{GAMMA}(2)=\text{dexp}(\text{B}(\text{L_GAMMA1}+2))$

C CALCULATE ACO2 AND ACO2*

$\text{aco2}=\text{gamma}(2)*\text{x}(2,1)$

```

aco2s=(k2/keq2*gamma(7)*x(7,1)*gamma(10)*x(10,1)/gamma(3)/gamma(
1)
* /x(1,1)+k1/keq1*gamma(8)*x(8,1)/gamma(11))/
* (k1*x(11,1)+k2*x(3,1))

c    THICKNESS OF BOUNDARY LAYER ACCORDING TO ASPEN PLUS
c    Use Onda's correlation for wet area

pi=3.14159
atot=realb(1)      ! 1/m
area=(pi/4.0)*realb(2)*realb(2)  !m^2

FF=F
holdup=hldliq
if((F.lt.1.0).or.(F.gt.1.01))then
realb(5)=FF
c    atot=atot/10000.0
else
FF=realb(5)
endif

Lm=FF*(1.0-phfrac(1))*MWL

Gm=FF*phfrac(1)*MWV

Lf=Lm/area
Gf=Gm/area
g=9.81  ! m/s^2

c    Reynold's number
rel=Lf/atot/visc*1.0e3

c    Fraud's number
frl=Lf*Lf*atot/((dens**2.0)*g)

c    Get surface tension of mixture
call ppmon_srftny (t,p,x,y,ncomp,idx,nbopst,kdiag,
*                  srften,ker)
sigma=srften  !N/m

c    Weber number
wel=Lf*Lf/atot/dens/sigma

```



```

    sigmac=realb(4) ! dyne/cm (surface tension of packing)
    sigmac=sigmac*1.0e-3 !N/m

    aw=atot*(1-exp(-1.45*((sigmac/sigma)**0.75)*(rel**0.1)
*      *(frl**(-0.05))*(wel**0.2)))) !1/m

c    aw=atot ! For wetted wall column

    aw=realb(7)*aw

    delta=holdup/(aw*area*realb(3))

    gam=gamma(2)

    R1=2.0/delta*k1*x(11,1)*sqrt(dco2*ctot/gam)/
*    sqrt(k2*x(3,1)+k1*x(11,1))*aco2

    R2=2.0/delta*k1*x(11,1)*sqrt(dco2*ctot/gam)/
*    sqrt(k2*x(3,1)+k1*x(11,1))*aco2s

    R3=2.0/delta*k2*x(3,1)*sqrt(dco2*ctot/gam)/
*    sqrt(k2*x(3,1)+k1*x(11,1))*aco2

    R4=2.0/delta*k2*x(3,1)*sqrt(dco2*ctot/gam)/
*    sqrt(k2*x(3,1)+k1*x(11,1))*aco2s

    RATEL(1)=R1*holdup
    RATEL(2)=R2*holdup
    RATEL(3)=R3*holdup
    RATEL(4)=R4*holdup

    RATES(1)=-ratel(3)+ratel(4)
    RATES(2)=-ratel(1)+ratel(2)-ratel(3)+ratel(4)
    RATES(3)=-ratel(3)+ratel(4)
    RATES(7)=ratel(3)-ratel(4)
    RATES(8)=ratel(1)-ratel(2)
    RATES(10)=ratel(3)-ratel(4)
    RATES(11)=-ratel(1)+ratel(2)

5  RETURN
END

```

APPENDIX C

ASPEN PLUS Inputs and Results

This Appendix reports the required inputs to run the base case absorption/stripping model with ASPEN PLUS. C.1 is the ASPEN PLUS Input File; C.2 is the summary of all the inputs parameters required to run the model; C.3 is the ASPEN PLUS process flow diagram; C.4 and C.5 contain detailed results for the base case and for a 10% CO₂ case; C.6 contains hints on model convergence.

This Appendix contains proprietary information of Fluor Corp.

Confidential information: the relative values for the reboiler duties must be multiplied by 200 in order to get the normalized reboiler duty in MJ/Kmol CO₂.

C.1. Base case APEN PLUS input file

```
;  
;Input Summary created by ASPEN PLUS Rel. 10.2.1 at 11:01:25 Mon Apr 15,  
2002  
;Directory C:\My thesis simulations Filename  
C:\DOCUME~1\Stefano\LOCALS~1\Temp\~ap6ba.tmp  
;  
  
;  
;Input Summary created by ASPEN PLUS Rel. 10.2.1 at 10:05:31 Wed Jan 23, 200  
;Directory C:\My thesis simulations Filename C:\My thesis simulations\strp-  
;  
;  
;Input Summary created by ASPEN PLUS Rel. 10.2.1 at 16:18:14 Tue Jan 22, 200  
;Directory C:\My Simulations Filename C:\My Simulations\strp-hss-kin.inp  
;
```

IN-UNITS ENG

DEF-STREAMS CONVEN ALL

DESCRIPTION "

BLANK TEMPLATE FOR SIMULATION "

DATABANKS PURE10 / AQUEOUS / SOLIDS / INORGANIC / &
NOASPEN PLUSPCD

PROP-SOURCES PURE10 / AQUEOUS / SOLIDS / INORGANIC

COMPONENTS

H2O H2O /
CO2 CO2 /
MEA C2H7NO /
N2 N2 /
O2 O2 /
MEA+ C2H8NO+ /
MEACOO- C3H6NO3- /
HCO3- HCO3- /
CO3-- CO3-2 /
H3O+ H3O+ /
OH- OH- /
HCOO- CHO2-

HENRY-COMPS HC-1 CO2 N2 O2

CHEMISTRY C-1

STOIC 1 H2O -2.0 / H3O+ 1.0 / OH- 1.0
STOIC 2 CO2 -1.0 / H2O -2.0 / HCO3- 1.0 / H3O+ 1.0
STOIC 3 HCO3- -1.0 / H2O -1.0 / CO3-- 1.0 / H3O+ 1.0
STOIC 4 MEA+ -1.0 / H2O -1.0 / MEA 1.0 / H3O+ 1.0
STOIC 5 MEACOO- -1.0 / H2O -1.0 / MEA 1.0 / HCO3- 1.0
K-STOIC 1 A=132.898880 B=-13445.90 C=-22.47730
K-STOIC 2 A=231.465439 B=-12092.10 C=-36.78160
K-STOIC 3 A=216.050430 B=-12431.70 C=-35.48190
K-STOIC 4 A=-3.0383250 B=-7008.3570 D=-.00313480
K-STOIC 5 A=-.521350 B=-2545.530

FLOWSHEET

BLOCK STRP IN=REFLUX RICH OUT=CO2 LEAN

BLOCK COND IN=CO2 OUT=PCO2 S2
 BLOCK PUMP IN=S2 OUT=13
 BLOCK HE1 IN=BOT-MIX OUT=RICH
 BLOCK HE-2 IN=LEAN OUT=TO-ABS
 BLOCK ABSORBER IN=LEANIN FLUEGAS OUT=PUREGAS RICHOUT
 BLOCK FLA1 IN=PUREGAS WMAKEUP OUT=OUT 10
 BLOCK MIX IN=10 M-MEA RICHOUT OUT=BOT-MIX
 BLOCK B6 IN=13 OUT=REFLUX XSH2O
 BLOCK CALC-SEP IN=XSH2O OUT=S-1 S-3
 BLOCK COOLER IN=TO-ABS OUT=LEANOUT

PROPERTIES ELECNRTL HENRY-COMPS=HC-1 CHEMISTRY=C-1

PROP-DATA HENRY-1

IN-UNITS ENG
 PROP-LIST HENRY
 BPVAL CO2 H2O 174.78036780 -15259.879680 -21.957430 &
 .003211526690 31.730003750 440.33000050
 BPVAL N2 H2O 180.33998820 -15178.985880 -21.5580 -.00468680 &
 31.730003750 163.13000270
 BPVAL O2 H2O 157.89622970 -13995.107890 -18.39740 &
 -.00524641120 33.530003730 166.73000270

PROP-DATA NRTL-1

IN-UNITS ENG
 PROP-LIST NRTL
 BPVAL H2O CO2 10.0640 -5882.6429530 .20 0.0 0.0 0.0 &
 32.000003740 392.00000090
 BPVAL CO2 H2O 10.0640 -5882.6429530 .20 0.0 0.0 0.0 &
 32.000003740 392.00000090
 BPVAL H2O MEA 1.4384980 178.23787060 .20 0.0 0.0 0.0 &
 77.000003380 302.00000160
 BPVAL MEA H2O -1.0466020 -607.58207510 .20 0.0 0.0 0.0 &
 77.000003380 302.00000160

PROP-DATA VLCLK-1

IN-UNITS ENG
 PROP-LIST VLCLK
 BPVAL MEA+ OH- -6.2631455230 16.018463450

PROP-DATA GMELCC-1

IN-UNITS ENG

PROP-LIST GMELCC

PPVAL H2O (MEA+ MEACOO-) 10.4070
PPVAL (MEA+ MEACOO-) H2O -5.9630
PPVAL H2O (MEA+ HCO3-) 6.8850
PPVAL (MEA+ HCO3-) H2O -3.8980
PPVAL H2O (H3O+ HCO3-) 8.0450
PPVAL (H3O+ HCO3-) H2O -4.0720
PPVAL H2O (H3O+ CO3--) 8.0450
PPVAL (H3O+ CO3--) H2O -4.0720
PPVAL H2O (H3O+ OH-) 8.0450
PPVAL (H3O+ OH-) H2O -4.0720
PPVAL CO2 (MEA+ MEACOO-) 15.0
PPVAL (MEA+ MEACOO-) CO2 -8.0
PPVAL CO2 (MEA+ HCO3-) 15.0
PPVAL (MEA+ HCO3-) CO2 -8.0
PPVAL CO2 (MEA+ CO3--) 15.0
PPVAL (MEA+ CO3--) CO2 -8.0
PPVAL CO2 (MEA+ OH-) 15.0
PPVAL (MEA+ OH-) CO2 -8.0
PPVAL CO2 (H3O+ MEACOO-) 15.0
PPVAL (H3O+ MEACOO-) CO2 -8.0
PPVAL CO2 (H3O+ HCO3-) 15.0
PPVAL (H3O+ HCO3-) CO2 -8.0
PPVAL CO2 (H3O+ CO3--) 15.0
PPVAL (H3O+ CO3--) CO2 -8.0
PPVAL CO2 (H3O+ OH-) 15.0
PPVAL (H3O+ OH-) CO2 -8.0
PPVAL MEA (MEA+ MEACOO-) 15.0
PPVAL (MEA+ MEACOO-) MEA -8.0
PPVAL MEA (MEA+ HCO3-) 15.0
PPVAL (MEA+ HCO3-) MEA -8.0
PPVAL MEA (MEA+ CO3--) 15.0
PPVAL (MEA+ CO3--) MEA -8.0
PPVAL MEA (MEA+ OH-) 15.0
PPVAL (MEA+ OH-) MEA -8.0
PPVAL MEA (H3O+ MEACOO-) 15.0
PPVAL (H3O+ MEACOO-) MEA -8.0
PPVAL MEA (H3O+ HCO3-) 15.0
PPVAL (H3O+ HCO3-) MEA -8.0
PPVAL MEA (H3O+ CO3--) 15.0
PPVAL (H3O+ CO3--) MEA -8.0
PPVAL MEA (H3O+ OH-) 15.0

PPVAL (H3O+ OH-) MEA -8.0
 PPVAL H2O (MEA+ HCOO-) 10.4070
 PPVAL (MEA+ HCOO-) H2O -5.9630
 PPVAL CO2 (MEA+ HCOO-) 15.0
 PPVAL (MEA+ HCOO-) CO2 -8.0
 PPVAL MEA (MEA+ HCOO-) 15.0
 PPVAL (MEA+ HCOO-) MEA -8.0
 PPVAL H2O (H3O+ HCOO-) 8.0450
 PPVAL (H3O+ HCOO-) H2O -4.0720
 PPVAL CO2 (H3O+ HCOO-) 15.0
 PPVAL (H3O+ HCOO-) CO2 -8.0
 PPVAL MEA (H3O+ HCOO-) 15.0
 PPVAL (H3O+ HCOO-) MEA -8.0

PROP-DATA GMELCD-1

IN-UNITS ENG TEMPERATURE=K
 PROP-LIST GMELCD
 PPVAL H2O (MEA+ MEACOO-) -119.920
 PPVAL (MEA+ MEACOO-) H2O 336.450
 PPVAL H2O (MEA+ HCO3-) 969.630
 PPVAL (MEA+ HCO3-) H2O -91.350
 PPVAL CO2 (MEA+ MEACOO-) 0.0
 PPVAL (MEA+ MEACOO-) CO2 0.0
 PPVAL CO2 (MEA+ HCO3-) 0.0
 PPVAL (MEA+ HCO3-) CO2 0.0
 PPVAL CO2 (MEA+ CO3--) 0.0
 PPVAL (MEA+ CO3--) CO2 0.0
 PPVAL CO2 (MEA+ OH-) 0.0
 PPVAL (MEA+ OH-) CO2 0.0
 PPVAL CO2 (H3O+ MEACOO-) 0.0
 PPVAL (H3O+ MEACOO-) CO2 0.0
 PPVAL CO2 (H3O+ HCO3-) 0.0
 PPVAL (H3O+ HCO3-) CO2 0.0
 PPVAL CO2 (H3O+ CO3--) 0.0
 PPVAL (H3O+ CO3--) CO2 0.0
 PPVAL CO2 (H3O+ OH-) 0.0
 PPVAL (H3O+ OH-) CO2 0.0
 PPVAL MEA (MEA+ MEACOO-) 0.0
 PPVAL (MEA+ MEACOO-) MEA 0.0
 PPVAL MEA (MEA+ HCO3-) 0.0
 PPVAL (MEA+ HCO3-) MEA 0.0
 PPVAL MEA (MEA+ CO3--) 0.0

PPVAL (MEA+ CO3--) MEA 0.0
 PPVAL MEA (MEA+ OH-) 0.0
 PPVAL (MEA+ OH-) MEA 0.0
 PPVAL MEA (H3O+ MEACOO-) 0.0
 PPVAL (H3O+ MEACOO-) MEA 0.0
 PPVAL MEA (H3O+ HCO3-) 0.0
 PPVAL (H3O+ HCO3-) MEA 0.0
 PPVAL MEA (H3O+ CO3--) 0.0
 PPVAL (H3O+ CO3--) MEA 0.0
 PPVAL MEA (H3O+ OH-) 0.0
 PPVAL (H3O+ OH-) MEA 0.0
 PPVAL H2O (MEA+ HCOO-) -119.920
 PPVAL (MEA+ HCOO-) H2O 336.450
 PPVAL CO2 (MEA+ HCOO-) 0.0
 PPVAL (MEA+ HCOO-) CO2 0.0
 PPVAL MEA (MEA+ HCOO-) 0.0
 PPVAL (MEA+ HCOO-) MEA 0.0
 PPVAL H2O (H3O+ HCOO-) 0.0
 PPVAL (H3O+ HCOO-) H2O 0.0
 PPVAL CO2 (H3O+ HCOO-) 0.0
 PPVAL (H3O+ HCOO-) CO2 0.0
 PPVAL MEA (H3O+ HCOO-) 0.0
 PPVAL (H3O+ HCOO-) MEA 0.0

PROP-DATA GMELCE-1

IN-UNITS ENG

PROP-LIST GMELCE

PPVAL CO2 (MEA+ MEACOO-) 0.0
 PPVAL (MEA+ MEACOO-) CO2 0.0
 PPVAL CO2 (MEA+ HCO3-) 0.0
 PPVAL (MEA+ HCO3-) CO2 0.0
 PPVAL CO2 (MEA+ CO3--) 0.0
 PPVAL (MEA+ CO3--) CO2 0.0
 PPVAL CO2 (MEA+ OH-) 0.0
 PPVAL (MEA+ OH-) CO2 0.0
 PPVAL CO2 (H3O+ MEACOO-) 0.0
 PPVAL (H3O+ MEACOO-) CO2 0.0
 PPVAL CO2 (H3O+ HCO3-) 0.0
 PPVAL (H3O+ HCO3-) CO2 0.0
 PPVAL CO2 (H3O+ CO3--) 0.0
 PPVAL (H3O+ CO3--) CO2 0.0
 PPVAL CO2 (H3O+ OH-) 0.0

PPVAL (H3O+ OH-) CO2 0.0
 PPVAL MEA (MEA+ MEACOO-) 0.0
 PPVAL (MEA+ MEACOO-) MEA 0.0
 PPVAL MEA (MEA+ HCO3-) 0.0
 PPVAL (MEA+ HCO3-) MEA 0.0
 PPVAL MEA (MEA+ CO3--) 0.0
 PPVAL (MEA+ CO3--) MEA 0.0
 PPVAL MEA (MEA+ OH-) 0.0
 PPVAL (MEA+ OH-) MEA 0.0
 PPVAL MEA (H3O+ MEACOO-) 0.0
 PPVAL (H3O+ MEACOO-) MEA 0.0
 PPVAL MEA (H3O+ HCO3-) 0.0
 PPVAL (H3O+ HCO3-) MEA 0.0
 PPVAL MEA (H3O+ CO3--) 0.0
 PPVAL (H3O+ CO3--) MEA 0.0
 PPVAL MEA (H3O+ OH-) 0.0
 PPVAL (H3O+ OH-) MEA 0.0

PROP-DATA GMELCN-1

IN-UNITS ENG
 PROP-LIST GMELCN
 PPVAL CO2 (MEA+ MEACOO-) .10
 PPVAL CO2 (MEA+ HCO3-) .10
 PPVAL CO2 (MEA+ CO3--) .10
 PPVAL CO2 (MEA+ OH-) .10
 PPVAL CO2 (H3O+ MEACOO-) .10
 PPVAL CO2 (H3O+ HCO3-) .10
 PPVAL CO2 (H3O+ CO3--) .10
 PPVAL CO2 (H3O+ OH-) .10
 PPVAL MEA (MEA+ MEACOO-) .10
 PPVAL MEA (MEA+ HCO3-) .10
 PPVAL MEA (MEA+ CO3--) .10
 PPVAL MEA (MEA+ OH-) .10
 PPVAL MEA (H3O+ MEACOO-) .10
 PPVAL MEA (H3O+ HCO3-) .10
 PPVAL MEA (H3O+ CO3--) .10
 PPVAL MEA (H3O+ OH-) .10
 PPVAL H2O (MEA+ MEACOO-) .20
 PPVAL H2O (MEA+ HCO3-) .20
 PPVAL H2O (MEA+ CO3--) .20
 PPVAL H2O (MEA+ OH-) .20
 PPVAL H2O (H3O+ MEACOO-) .20

PPVAL H2O (H3O+ HCO3-) .20
PPVAL H2O (H3O+ CO3--) .20
PPVAL H2O (H3O+ OH-) .20
PPVAL H2O (MEA+ HCOO-) .20
PPVAL H2O (H3O+ HCOO-) .20
PPVAL CO2 (MEA+ HCOO-) .10
PPVAL CO2 (H3O+ HCOO-) .10
PPVAL MEA (MEA+ HCOO-) .10
PPVAL MEA (H3O+ HCOO-) .10

PROP-SET PS-1 MWMX SUBSTREAM=MIXED PHASE=L

STREAM FLUEGAS

SUBSTREAM MIXED TEMP=145. PRES=16.7 &
MOLE-FLOW=11377.42122 <kmol/hr>
MOLE-FRAC H2O 0.1 / CO2 0.0313 / N2 0.7487 / O2 0.12

STREAM LEAN

SUBSTREAM MIXED TEMP=250.520323 PRES=26
MOLE-FLOW H2O 19294.9565 / CO2 0.672292168 / MEA &
1736.08292 / MEA+ 697.851456 / MEACOO- 379.183813 / &
HCO3- 22.2479651 / CO3-- 0.833367795 / H3O+ &
7.890951E-006 / OH- 0.0749869148 / HCOO- 294.677966

STREAM LEANIN

SUBSTREAM MIXED TEMP=40. <C> PRES=20. &
MASS-FLOW=250985.952 <kg/hr>
MOLE-FRAC H2O 0.86142 / CO2 0.017962578 / MEA &
0.112266112 / MEA+ 0.01314 / HCOO- 0.01314

STREAM M-MEA

SUBSTREAM MIXED TEMP=100. PRES=25.
MOLE-FLOW MEA 0.01923923

STREAM REFLUX

SUBSTREAM MIXED TEMP=120.00956 PRES=23.8
MOLE-FLOW H2O 975.867413 / CO2 0.478541667 / MEA &
0.00442495016 / N2 1.107002E-006 / O2 6.013399E-007 / &
MEA+ 1.18712472 / MEACOO- 0.00564022543 / HCO3- &
1.18035562 / CO3-- 0.00056570386 / H3O+ 6.597995E-006 &
/ OH- 4.066158E-006

STREAM RICH

SUBSTREAM MIXED TEMP=228 PRES=100

MOLE-FLOW H2O 20024.7108 / CO2 12.2683184 / MEA &
600.304699 / N2 0.0701790357 / O2 0.0205750107 / &
MEA+ 1380.04241 / MEACOO- 929.924656 / HCO3- &
141.801214 / CO3-- 1.72321442 / H3O+ 1.895644E-005 / &
OH- 0.0150878793 / HCOO- 304.855009

STREAM WMAKEUP

SUBSTREAM MIXED TEMP=100. PRES=25.
MOLE-FLOW H2O 420.

STREAM XSH2O

SUBSTREAM MIXED TEMP=100. PRES=23.8
MOLE-FLOW H2O 100.

BLOCK MIX MIXER

BLOCK B6 FSPLIT

MOLE-FLOW XSH2O 100.

BLOCK COOLER HEATER

PARAM TEMP=40. <C> PRES=20.

BLOCK HE-2 HEATER

PARAM PRES=0. DUTY=45. <MMBtu/hr>

BLOCK HE1 HEATER

PARAM TEMP=228.0 PRES=100.0

BLOCK CALC-SEP FLASH2

PARAM TEMP=120. VFRAC=1.

BLOCK COND FLASH2

PARAM TEMP=120.0 PRES=-2.0

BLOCK FLA1 FLASH2

PARAM TEMP=118.6 PRES=14.7

BLOCK ABSORBER RATEFRAC

PARAM NCOL=1 MAX-ITER=30 TOT-SEGMENT=20
COL-CONFIG 1 20 CONDENSER=NO REBOILER=NO

PACK-SPECS 1 1 20 HTPACK=50. PACK-ARRANGE=RANDOM &
 PACK-TYPE=CMR PACK-MAT=METAL PACK-DIM="NO-2P" &
 PACK-SIZE=.1405833 SPAREA=43.89173 PACK-FACTOR=26.00000 &
 PACK-TENSION=75.00000 COL-DIAM=20. PERCENT-LHLD=0.01 &
 VOID-FRACTIO=0.971
 FEEDS LEANIN 1 1 ABOVE-SEGMENT / FLUEGAS 1 20 &
 ON-SEGMENT
 PRODUCTS PUREGAS 1 1 V / RICHOUT 1 20 L
 P-SPEC 1 1 14.7
 COL-SPECS 1 MOLE-RDV=1.0 Q1=0.0 QN=0.0 DP-COL=2.
 REAC-SEGMENT 1 1 20 MEA-CO2
 KIN-USER-VEC NREAL=7
 REALK VALUES=143.907 6.1 0.7625 75. 2. 1. 1.3

BLOCK STRP RATEFRAC

PARAM NCOL=1 MAX-ITER=10 INIT-OPTION=STANDARD TOT-
 SEGMENT= &
 20
 COL-CONFIG 1 20 CONDENSER=NO
 PACK-SPECS 1 1 19 HTPACK=35.0 PACK-ARRANGE=RANDOM &
 PACK-TYPE=CMR PACK-MAT=METAL PACK-DIM="NO-2P" &
 PACK-SIZE=.14058330 SPAREA=43.891730 PACK-FACTOR=26.0 &
 PACK-TENSION=75.0 COL-DIAM=8.50 PERCENT-LHLD=4.0 &
 VOID-FRACTIO=.9710
 FEEDS REFLUX 1 1 ABOVE-SEGMENT / RICH 1 2
 PRODUCTS CO2 1 1 V / LEAN 1 20 L
 P-SPEC 1 1 23.80
 COL-SPECS 1 MOLE-RDV=1.0 Q1=0.0 QN=6.0220E+07 DP-COL=2.20
 REPORT INT-PROFILE HEAT-COEFF
 SEGMENT-REPO PROPERTIES=PS-1 COMP-EFF=YES
 REAC-SEGMENT 1 1 20 EQUIL
 HOLD-UP 1 REBOILER VOL-LIQUID=35.3146662

BLOCK PUMP PUMP

PARAM DELP=2.0

DESIGN-SPEC LEANL

DEFINE LEANL PARAMETER 1
 DEFINE MEA MOLE-FLOW STREAM=LEAN SUBSTREAM=MIXED &
 COMPONENT=MEA
 DEFINE MEAH MOLE-FLOW STREAM=LEAN SUBSTREAM=MIXED &
 COMPONENT=MEA+

```

DEFINE MEACOO MOLE-FLOW STREAM=LEAN SUBSTREAM=MIXED
&
  COMPONENT=MEACOO-
DEFINE CO2 MOLE-FLOW STREAM=LEAN SUBSTREAM=MIXED &
  COMPONENT=CO2
DEFINE HCO3 MOLE-FLOW STREAM=LEAN SUBSTREAM=MIXED &
  COMPONENT=HCO3-
DEFINE CO3 MOLE-FLOW STREAM=LEAN SUBSTREAM=MIXED &
  COMPONENT=CO3--
DEFINE HCOO MOLE-FLOW STREAM=LEAN SUBSTREAM=MIXED &
  COMPONENT=HCOO-
DEFINE MEAIN MOLE-FLOW STREAM=LEANIN SUBSTREAM=MIXED
&
  COMPONENT=MEA
DEFINE MEACIN MOLE-FLOW STREAM=LEANIN
SUBSTREAM=MIXED &
  COMPONENT=MEACOO-
DEFINE HCO3IN MOLE-FLOW STREAM=LEANIN SUBSTREAM=MIXED
&
  COMPONENT=HCO3-
DEFINE CO3IN MOLE-FLOW STREAM=LEANIN SUBSTREAM=MIXED
&
  COMPONENT=CO3--
DEFINE MEAHIN MOLE-FLOW STREAM=LEANIN
SUBSTREAM=MIXED &
  COMPONENT=MEA+
DEFINE CO2IN MOLE-FLOW STREAM=LEANIN SUBSTREAM=MIXED
&
  COMPONENT=CO2
DEFINE LEANLI PARAMETER 2
DEFINE HCOIN MOLE-FLOW STREAM=LEANIN SUBSTREAM=MIXED
&
  COMPONENT=HCOO-
DEFINE DIFF PARAMETER 3
F  LEANL=(MEACOO+HCO3+CO3+CO2)/(MEA+MEAH+MEACOO-HCOO)
F
LEANLI=(MEACIN+HCO3IN+CO3IN+CO2IN)/(MEAIN+MEAHIN+MEACIN-
HCOIN)
F  DIFF=LEANL-LEANLI
SPEC "DIFF" TO "0"
TOL-SPEC ".0001"

```

```

VARY BLOCK-VAR BLOCK=STRP VARIABLE=QN SENTENCE=COL-
SPECS &
  ID1=1
  LIMITS "40000000" "600000000"

DESIGN-SPEC MMEA
  DEFINE OUT MOLE-FLOW STREAM=OUT SUBSTREAM=MIXED &
    COMPONENT=MEA
  DEFINE MEA MOLE-FLOW STREAM=M-MEA SUBSTREAM=MIXED &
    COMPONENT=MEA
  DEFINE PCO2 MOLE-FLOW STREAM=PCO2 SUBSTREAM=MIXED &
    COMPONENT=MEA
  DEFINE S1 MOLE-FLOW STREAM=S-1 SUBSTREAM=MIXED &
    COMPONENT=MEA
  DEFINE BAL PARAMETER 1
F  BAL=MEA-OUT-PCO2-S1
  SPEC "BAL" TO "0"
  TOL-SPEC ".01"
  VARY STREAM-VAR STREAM=M-MEA SUBSTREAM=MIXED &
    VARIABLE=MOLE-FLOW
  LIMITS ".001" "500"

CALCULATOR DELTAT
  DEFINE THOT STREAM-VAR STREAM=LEAN SUBSTREAM=MIXED &
    VARIABLE=TEMP
  DEFINE TCOLD BLOCK-VAR BLOCK=HE1 VARIABLE=TEMP &
    SENTENCE=PARAM
F  TCOLD=THOT-20
  READ-VARS THOT
  WRITE-VARS TCOLD

CALCULATOR HE
  DEFINE HD1 BLOCK-VAR BLOCK=HE1 VARIABLE=QCALC &
    SENTENCE=PARAM
  DEFINE HD2 BLOCK-VAR BLOCK=HE-2 VARIABLE=DUTY &
    SENTENCE=PARAM
F  HD2=-HD1
  READ-VARS HD1
  WRITE-VARS HD2

CALCULATOR LOADINGS
  DEFINE LEANL PARAMETER 2

```

```

DEFINE MEA MOLE-FLOW STREAM=LEAN SUBSTREAM=MIXED &
  COMPONENT=MEA
DEFINE MEAH MOLE-FLOW STREAM=LEAN SUBSTREAM=MIXED &
  COMPONENT=MEA+
DEFINE MEACOO MOLE-FLOW STREAM=LEAN SUBSTREAM=MIXED
&
  COMPONENT=MEACOO-
DEFINE CO2 MOLE-FLOW STREAM=LEAN SUBSTREAM=MIXED &
  COMPONENT=CO2
DEFINE HCO3 MOLE-FLOW STREAM=LEAN SUBSTREAM=MIXED &
  COMPONENT=HCO3-
DEFINE CO3 MOLE-FLOW STREAM=LEAN SUBSTREAM=MIXED &
  COMPONENT=CO3--
DEFINE RICHL PARAMETER 3
DEFINE MEAR MOLE-FLOW STREAM=RICHOUT SUBSTREAM=MIXED
&
  COMPONENT=MEA
DEFINE MEAHR MOLE-FLOW STREAM=RICHOUT
SUBSTREAM=MIXED &
  COMPONENT=MEA+
DEFINE MEACOR MOLE-FLOW STREAM=RICHOUT
SUBSTREAM=MIXED &
  COMPONENT=MEACOO-
DEFINE CO2R MOLE-FLOW STREAM=RICHOUT SUBSTREAM=MIXED
&
  COMPONENT=CO2
DEFINE HCO3R MOLE-FLOW STREAM=RICHOUT
SUBSTREAM=MIXED &
  COMPONENT=HCO3-
DEFINE CO3R MOLE-FLOW STREAM=RICHOUT SUBSTREAM=MIXED
&
  COMPONENT=CO3--
DEFINE HCOO MOLE-FLOW STREAM=LEAN SUBSTREAM=MIXED &
  COMPONENT=HCOO-
DEFINE HCOOR MOLE-FLOW STREAM=RICHOUT
SUBSTREAM=MIXED &
  COMPONENT=HCOO-
DEFINE LEANIN PARAMETER 4
DEFINE CO2I MOLE-FLOW STREAM=LEANIN SUBSTREAM=MIXED &
  COMPONENT=CO2
DEFINE MEAI MOLE-FLOW STREAM=LEANIN SUBSTREAM=MIXED &
  COMPONENT=MEA

```

```

    DEFINE MEACOI MOLE-FLOW STREAM=LEANIN
SUBSTREAM=MIXED &
    COMPONENT=MEACOO-
    DEFINE HCO3I MOLE-FLOW STREAM=LEANIN SUBSTREAM=MIXED
&
    COMPONENT=HCO3-
    DEFINE CO3I MOLE-FLOW STREAM=LEANIN SUBSTREAM=MIXED &
    COMPONENT=CO3--
    DEFINE MEAHI MOLE-FLOW STREAM=LEANIN SUBSTREAM=MIXED
&
    COMPONENT=MEA+
    DEFINE HCOOI MOLE-FLOW STREAM=LEANIN SUBSTREAM=MIXED
&
    COMPONENT=HCOO-
F   LEANL=(CO2+HCO3+CO3+MEACOO)/(MEA+MEAH+MEACOO-HCOO)
F   RICHL=(CO2R+HCO3R+CO3R+MEACOR)/(MEAR+MEAHR+MEACOR-
HCOOR)
C
F   LEANIN=(CO2I+HCO3I+CO3I+MEACOI)/(MEAI+MEAHI+MEACOI-
HCOOI)
F   WRITE(NTERM,*)LEANIN,LEANL,RICHL
EXECUTE LAST

CALCULATOR RD-CO2
    DEFINE RD BLOCK-VAR BLOCK=STRP VARIABLE=REB-DUTY &
    SENTENCE=RESULTS ID1=1
    DEFINE CO2 MASS-FLOW STREAM=PCO2 SUBSTREAM=MIXED &
    COMPONENT=CO2
    DEFINE RDCO2 PARAMETER 1
F   RDCO2=RD/CO2
F   WRITE(NTERM,*)RDCO2
EXECUTE LAST

CALCULATOR REMOVAL
    DEFINE CO2IN MOLE-FLOW STREAM=FLUEGAS SUBSTREAM=MIXED
&
    COMPONENT=CO2
    DEFINE CO2OUT MOLE-FLOW STREAM=PUREGAS
SUBSTREAM=MIXED &
    COMPONENT=CO2
    DEFINE REM PARAMETER 1
F   REM=(CO2IN-CO2OUT)/CO2IN

```

```

F  WRITE(NTERM,*)REM
EXECUTE LAST

CALCULATOR WATER
  DEFINE OUT MOLE-FLOW STREAM=OUT SUBSTREAM=MIXED &
    COMPONENT=H2O
  DEFINE FLUE MOLE-FLOW STREAM=FLUEGAS SUBSTREAM=MIXED
&
  COMPONENT=H2O
  DEFINE MAKEUP MOLE-FLOW STREAM=WMAKEUP
SUBSTREAM=MIXED &
  COMPONENT=H2O
  DEFINE PCO2 MOLE-FLOW STREAM=PCO2 SUBSTREAM=MIXED &
    COMPONENT=H2O
  DEFINE WFRAC MOLE-FRAC STREAM=REFLUX SUBSTREAM=MIXED
&
  COMPONENT=H2O
  DEFINE FLOW BLOCK-VAR BLOCK=B6 SENTENCE=MOLE-FLOW &
    VARIABLE=FLOW ID1=XSH2O
  DEFINE FL PARAMETER 2
F  FL=FLUE+MAKEUP-PCO2-OUT
F  WRITE(NTERM,*)FL
F  FLOW=(FLUE+MAKEUP-PCO2-OUT)/WFRAC
  READ-VARS OUT FLUE MAKEUP PCO2 WFRAC
  WRITE-VARS FLOW

CONV-OPTIONS
  PARAM SPEC-LOOP=OUTSIDE USER-LOOP=OUTSIDE CHECKSEQ=NO

TEAR
  TEAR REFLUX

STREAM-REPOR MOLEFLOW MASSFLOW MOLEFRAC

REACTIONS EQUIL REAC-DIST
  REAC-DATA 1 KBASIS=MOLE-GAMMA
  REAC-DATA 2 KBASIS=MOLE-GAMMA
  REAC-DATA 3 KBASIS=MOLE-GAMMA
  REAC-DATA 4 KBASIS=MOLE-GAMMA
  REAC-DATA 5 KBASIS=MOLE-GAMMA
  K-STOIC 1 A=132.898880 B=-13445.90 C=-22.47730
  K-STOIC 2 A=231.465439 B=-12092.10 C=-36.78160

```


K-STOIC 3 A=216.050430 B=-12431.70 C=-35.48190
 K-STOIC 4 A=-3.0383250 B=-7008.3570 D=-.00313480
 K-STOIC 5 A=-.521350 B=-2545.530
 STOIC 1 H2O -2.0 / H3O+ 1.0 / OH- 1.0
 STOIC 2 CO2 -1.0 / H2O -2.0 / HCO3- 1.0 / H3O+ 1.0
 STOIC 3 HCO3- -1.0 / H2O -1.0 / CO3-- 1.0 / H3O+ 1.0
 STOIC 4 MEA+ -1.0 / H2O -1.0 / MEA 1.0 / H3O+ 1.0
 STOIC 5 MEACOO- -1.0 / H2O -1.0 / MEA 1.0 / HCO3- 1.0

REACTIONS MEA-CO2 REAC-DIST

PARAM SUBROUTINE=KIN4
 REAC-DATA 1 DELT=0.0 KBASIS=MOLE-GAMMA
 REAC-DATA 2 DELT=0.0 KBASIS=MOLE-GAMMA
 REAC-DATA 3 DELT=0.0 KBASIS=MOLE-GAMMA
 REAC-DATA 4 KINETIC
 REAC-DATA 5 KINETIC
 REAC-DATA 6 KINETIC
 REAC-DATA 7 KINETIC
 K-STOIC 1 A=-3.0383250 B=-7008.3570 D=-.00313480
 K-STOIC 2 A=132.8990 B=-13445.90 C=-22.47730
 K-STOIC 3 A=216.0490 B=-12431.70 C=-35.48190
 STOIC 1 H2O -1.0 / MEA+ -1.0 / MEA 1.0 / H3O+ 1.0
 STOIC 2 H2O -2.0 / H3O+ 1.0 / OH- 1.0
 STOIC 3 HCO3- -1.0 / H2O -1.0 / CO3-- 1.0 / H3O+ 1.0
 STOIC 4 CO2 -1.0 / OH- -1.0 / HCO3- 1.0
 STOIC 5 HCO3- -1.0 / CO2 1.0 / OH- 1.0
 STOIC 6 MEA -1.0 / CO2 -1.0 / H2O -1.0 / MEACOO- 1.0 &
 / H3O+ 1.0
 STOIC 7 MEACOO- -1.0 / H3O+ -1.0 / MEA 1.0 / CO2 1.0 &
 / H2O 1.0

;
 ;
 ;
 ;
 ;
 ;
 ;

C.2. Input summary for base case.

Flue Gas			
	Composition	CO2	3.13%
	after saturation	H2O	10.0%
	(mol %)	N2	74.87%
		O2	12.0%
	Water Saturation T		115 °F
	Absorber inlet T		145 °F
	Absorber inlet P		2 psig
	Mole flow		
	(after saturation)		11,377.42 kmol/hr
Solvent			
	Unloaded composition	MEA	11.23 mol%
	(30 wt% MEA, 3.5 wt% Heat stable salts)	H2O	86.142 mol%
		MEA ⁺ H ⁻ COO	1.314 mol%
	Lean loading		0.16
	(mol CO2/mol MEA)		
	Lean solvent T		40 °C
	Solvent rate		10,213.0 kmol/hr
Absorber			
	Packing height		50 ft
	Diameter		20 ft
	Pressure drop		2 psi
	CO2+MEA kinetics		From Dang (2001), corrected
	Packing type		Cascade Mini Rings # 2
Cross exchanger			
	Temp. approach, hot end		20 °F
Stripper			
	Packing height		35 ft
	Diameter		8.5 ft
	Bottom Pressure		26 psi
	Pressure Drop		2 psi
	Reboiler		equilibrium
	Condenser		equilibrium partial condenser, T=120 °F
	Rich solvent feed location		Above segment 2
	Water reflux location		At top
	Packing type		Cascade Mini Rings # 2
	Reactions		All at equilibrium

C.3. ASPEN PLUS process flow diagram

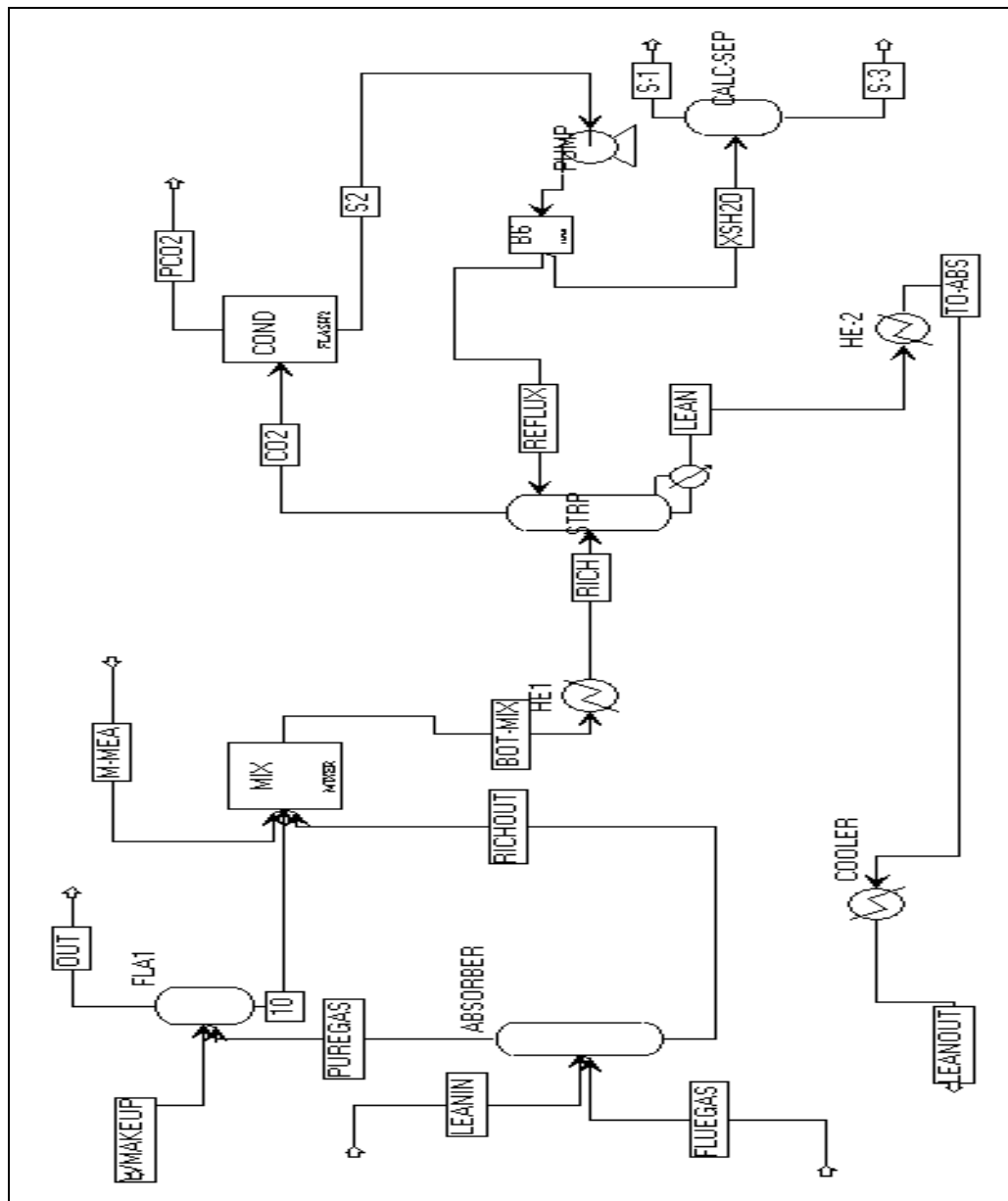


Figure C.1. ASPEN PLUS process flow diagram for absorption/stripping process.

C.4. ASPEN PLUS simulation detailed results for 3% CO₂ base case

Table C.1. Detailed stream results for the base case run, 3.13 % CO₂, 0.1 mol HSS/mol MEA_{tot}, other conditions given in Table 4.2, first column, stream names refer to figure C.1.

	10	13	BOT-MIX	CO2	FLUEGAS
TO	MIX	B6	HE1	COND	ABSORBER
FROM	FLA1	PUMP	MIX	STRP	
Phase	LIQUID	LIQUID	MIXED	VAPOR	VAPOR
Substream: MIXED					
Mole Frac					
H2O	0.9953346	0.9971805	0.8589148	0.6372501	0.1
CO2	1.70E-06	4.89E-04	2.96E-06	0.3619903	0.0313
MEA	1.08E-03	4.22E-06	0.0201001	7.12E-04	0
N2	6.88E-06	1.27E-09	2.99E-06	3.66E-05	0.7487
O2	2.05E-06	6.88E-10	8.76E-07	1.07E-05	0.12
MEA+	1.82E-03	1.16E-03	0.0606639	0	0
MEACOO-	8.99E-04	5.16E-06	0.0436419	0	0
HCO3-	7.77E-04	1.16E-03	3.29E-03	0	0
CO3--	7.19E-05	5.29E-07	3.50E-04	0	0
H3O+	4.01E-11	6.95E-09	5.64E-11	0	0
OH-	7.18E-07	3.99E-09	7.77E-07	0	0
HCOO-	0	0	0.0130345	0	0
Total Flow lbmol/hr	1.0966E+03	1.1249E+03	2.2699E+04	1.8521E+03	2.5083E+04
Total Flow lb/hr	2.0019E+04	2.0394E+04	5.8607E+05	5.0852E+04	7.0214E+05
Total Flow cuft/hr	3.2414E+02	3.3073E+02	1.0184E+04	5.6383E+05	9.7377E+06
Temperature F	1.1860E+02	1.2001E+02	1.2879E+02	2.2112E+02	1.4500E+02
Pressure psi	1.4700E+01	2.3800E+01	1.4700E+01	2.3800E+01	1.6700E+01
Vapor Frac	0.0000E+00	0.0000E+00	5.7141E-07	1.0000E+00	1.0000E+00
Liquid Frac	1.0000E+00	1.0000E+00	1.0000E+00	0.0000E+00	0.0000E+00
Solid Frac	0.0000E+00	0.0000E+00	0.0000E+00	0.0000E+00	0.0000E+00
Enthalpy Btu/lbmol	-1.2247E+05	-1.2237E+05	-1.3234E+05	-1.2635E+05	-1.5210E+04
Enthalpy Btu/lb	-6.7086E+03	-6.7494E+03	-5.1257E+03	-4.6020E+03	-5.4336E+02
Enthalpy Btu/hr	-1.3430E+08	-1.3765E+08	-3.0040E+09	-2.3402E+08	-3.8151E+08
Entropy Btu/lbmol-R	-38.59206	-38.01896	-75.74674	-4.205956	1.162991
Entropy Btu/lb-R	-2.11391	-2.097056	-2.933735	-0.1531876	0.0415464
Density lbmol/cuft	3.382985	3.401306	2.228865	3.28E-03	2.58E-03
Density lb/cuft	61.76059	61.66458	57.54753	0.0901894	0.0721045
Average MW	18.25624	18.12968	25.81922	27.45624	27.99258
Liq Vol 60F cuft/hr				917.7747	20092.31

TO FROM Phase	LEAN	LEANIN	LEANOUT	M-MEA	OUT
	HE-2	ABSORBER		MIX	
	STRP		COOLER		FLA1
	LIQUID	LIQUID	LIQUID	LIQUID	VAPOR
Substream: MIXED Mole Frac H2O CO2 MEA N2 O2 MEA+ MEACOO- HCO3- CO3-- H3O+ OH- HCOO-					
Total Flow lbmol/hr Total Flow lb/hr Total Flow cuft/hr Temperature F Pressure psi Vapor Frac Liquid Frac Solid Frac	0.8603899	0.8608538	0.8608528	0	0.1113768
	2.99E-05	1.68E-08	1.68E-08	0	4.72E-03
	0.0773903	0.0765669	0.0765675	1	7.87E-07
	3.52E-31	0	0	0	0.7618045
Enthalpy Btu/lbmol Enthalpy Btu/lb Enthalpy Btu/hr Entropy Btu/lbmol-R Entropy Btu/lb-R Density lbmol/cuft Density lb/cuft Average MW	5.01E-26	0	0	0	0.1221
	0.0311135	0.0314698	0.03147	0	0
	0.0169037	0.0173736	0.0173737	0	0
	9.92E-04	2.29E-04	2.29E-04	0	0
Liq Vol 60F cuft/hr	3.72E-05	3.60E-04	3.60E-04	0	0
	3.52E-10	4.49E-12	4.49E-12	0	0
	3.34E-06	5.79E-06	5.79E-06	0	0
	0.0131401	0.0131404	0.0131405	0	0
Liq Vol 60F cuft/hr	2.2516E+04	2.2516E+04	2.2516E+04	1.7155E-01	2.4651E+04
	5.5333E+05	5.5333E+05	5.5333E+05	1.0479E+01	6.7698E+05
	9.4395E+03	8.9060E+03	8.9060E+03	1.1116E-01	1.0397E+07
	2.5052E+02	1.0400E+02	1.0400E+02	1.0000E+02	1.1860E+02
Liq Vol 60F cuft/hr	2.6000E+01	2.0000E+01	2.0000E+01	2.5000E+01	1.4700E+01
	0.0000E+00	0.0000E+00	0.0000E+00	0.0000E+00	1.0000E+00
	1.0000E+00	1.0000E+00	1.0000E+00	1.0000E+00	0.0000E+00
	0.0000E+00	0.0000E+00	0.0000E+00	0.0000E+00	0.0000E+00
Liq Vol 60F cuft/hr	-1.2374E+05	-1.2675E+05	-1.2676E+05	-1.1676E+05	-1.2086E+04
	-5.0355E+03	-5.1579E+03	-5.1578E+03	-1.9115E+03	-4.4011E+02
	-2.7863E+09	-2.8540E+09	-2.8540E+09	-2.0031E+04	-2.9794E+08
	-55.60988	-60.33963	-60.33979	-119.6984	0.8039992
Liq Vol 60F cuft/hr	-2.262915	-2.455312	-2.455314	-1.95958	0.0292767
	2.38533	2.528166	2.528162	1.543242	2.37E-03
	58.61817	62.13003	62.13004	94.26696	0.065112
	24.57445	24.57513	24.57518	61.08372	27.46202
Liq Vol 60F cuft/hr				0.1649258	19587.1

TO FROM Phase	PCO2	PUREGAS	REFLUX	RICH	RICHOUT
		FLA1	STRP	STRP	MIX
	COND	ABSORBER	B6	HE1	ABSORBER
	VAPOR	MIXED	LIQUID	LIQUID	LIQUID
Substream: MIXED					
Mole Frac					
H2O	0.0788277	0.1349405	0.9971805	0.8553973	0.8520749
CO2	0.9210515	4.64E-03	4.89E-04	6.65E-04	3.27E-06
MEA	2.20E-09	1.10E-04	4.22E-06	0.0246378	0.0210105
N2	9.34E-05	0.7414204	1.27E-09	2.98E-06	2.79E-06
O2	2.74E-05	0.1188329	6.88E-10	8.75E-07	8.17E-07
MEA+	0	2.84E-05	1.16E-03	0.0596837	0.0636202
MEACOO-	0	2.68E-05	5.16E-06	0.040002	0.04589
HCO3-	0	1.11E-06	1.16E-03	6.51E-03	3.37E-03
CO3--	0	2.36E-07	5.29E-07	7.12E-05	3.33E-04
H3O+	0	1.82E-14	6.95E-09	8.99E-10	5.75E-11
OH-	0	8.75E-10	3.99E-09	6.06E-07	7.33E-07
HCOO-	0	0	0	0.0130258	0.0136962
Total Flow lbmol/hr	7.2589E+02	2.5329E+04	9.9906E+02	2.2714E+04	2.1602E+04
Total Flow lb/hr	3.0458E+04	6.8943E+05	1.8113E+04	5.8607E+05	5.6604E+05
Total Flow cuft/hr	2.0578E+05	1.0930E+07	2.9373E+02	1.0507E+04	9.8591E+03
Temperature F	1.2000E+02	1.3231E+02	1.2001E+02	2.3052E+02	1.2976E+02
Pressure psi	2.1800E+01	1.4700E+01	2.3800E+01	1.0000E+02	1.6700E+01
Vapor Frac	1.0000E+00	9.9947E-01	0.0000E+00	0.0000E+00	0.0000E+00
Liquid Frac	0.0000E+00	5.3477E-04	1.0000E+00	1.0000E+00	1.0000E+00
Solid Frac	0.0000E+00	0.0000E+00	0.0000E+00	0.0000E+00	0.0000E+00
Enthalpy Btu/lbmol	-1.6365E+05	-1.4455E+04	-1.2237E+05	-1.3022E+05	-1.3284E+05
Enthalpy Btu/lb	-3.9003E+03	-5.3108E+02	-6.7494E+03	-5.0469E+03	-5.0697E+03
Enthalpy Btu/hr	-1.1880E+08	-3.6614E+08	-1.2225E+08	-2.9578E+09	-2.8696E+09
Entropy Btu/lbmol-R	0.2328104	0.7502355	-38.01896	-71.10945	-77.67463
Entropy Btu/lb-R	5.55E-03	0.0275631	-2.097056	-2.755953	-2.96436
Density lbmol/cuft	3.53E-03	2.32E-03	3.401306	2.1617	2.191088
Density lb/cuft	0.1480098	0.0630778	61.66458	55.77647	57.41271
Average MW	41.95889	27.21882	18.12968	25.80213	26.20284
Liq Vol 60F cuft/hr	590.2068				

TO	S-1	S-3	S2	TO-ABS	WMAKEUP
FROM			PUMP	COOLER	FLA1
Phase	CALC-SEP	CALC-SEP	COND	HE-2	
	VAPOR	MISSING	LIQUID	LIQUID	LIQUID
Substream: MIXED					
Mole Frac					
H2O	0.9971786	0	0.9971805	0.8608676	1
CO2	1.65E-03	0	4.89E-04	2.36E-07	0
MEA	1.17E-03	0	4.21E-06	0.0767371	0
N2	1.26E-09	0	1.27E-09	0	0
O2	6.87E-10	0	6.88E-10	0	0
MEA+	0	0	1.16E-03	0.0312862	0
MEACOO-	0	0	5.16E-06	0.0173879	0
HCO3-	0	0	1.16E-03	3.98E-04	0
CO3--	0	0	5.29E-07	1.77E-04	0
H3O+	0	0	6.95E-09	2.36E-11	2.85E-09
OH-	0	0	3.99E-09	5.18E-06	2.85E-09
HCOO-	0	0	0	0.0131405	0
Total Flow lbmol/hr	1.2598E+02	0.0000E+00	1.1249E+03	2.2516E+04	4.2000E+02
Total Flow lb/hr	2.2814E+03	0.0000E+00	2.0394E+04	5.5333E+05	7.5664E+03
Total Flow cuft/hr	5.4762E+05	0.0000E+00	3.3073E+02	9.0426E+03	1.2204E+02
Temperature F	1.2000E+02		1.2000E+02	1.5154E+02	1.0000E+02
Pressure psi	1.4297E+00	1.4297E+00	2.1800E+01	2.6000E+01	2.5000E+01
Vapor Frac	1.0000E+00		0.0000E+00	0.0000E+00	0.0000E+00
Liquid Frac	0.0000E+00		1.0000E+00	1.0000E+00	1.0000E+00
Solid Frac	0.0000E+00		0.0000E+00	0.0000E+00	0.0000E+00
Enthalpy Btu/lbmol	-1.0371E+05		-1.2237E+05	-1.2580E+05	-1.2247E+05
Enthalpy Btu/lb	-5.7271E+03		-6.7494E+03	-5.1189E+03	-6.7980E+03
Enthalpy Btu/hr	-1.3066E+07		-1.3765E+08	-2.8324E+09	-5.1437E+07
Entropy Btu/lbmol-R	-5.376186		-38.01919	-58.68465	-38.21263
Entropy Btu/lb-R	-0.2968854		-2.097069	-2.387964	-2.121123
Density lbmol/cuft	2.30E-04		3.401293	2.489953	3.441605
Density lb/cuft	4.17E-03		61.66436	61.19104	62.00148
Average MW	18.10862		18.12968	24.57518	18.01528
Liq Vol 60F cuft/hr	36.64331	0			

TO	XSH2O
FROM	CALC-SEP
Phase	B6
Substream: MIXED	LIQUID
Mole Frac	
H2O	
CO2	0.9971805
MEA	4.89E-04
N2	4.22E-06
O2	1.27E-09
MEA+	6.88E-10
MEACOO-	1.16E-03
HCO3-	5.16E-06
CO3--	1.16E-03
H3O+	5.29E-07
OH-	6.95E-09
HCOO-	3.99E-09
Total Flow lbmol/hr	0
Total Flow lb/hr	1.2584E+02
Total Flow cuft/hr	2.2814E+03
Temperature F	3.6997E+01
Pressure psi	1.2001E+02
Vapor Frac	2.3800E+01
Liquid Frac	0.0000E+00
Solid Frac	1.0000E+00
Enthalpy Btu/lbmol	0.0000E+00
Enthalpy Btu/lb	-1.2237E+05
Enthalpy Btu/hr	-6.7494E+03
Entropy Btu/lbmol-R	-1.5398E+07
Entropy Btu/lb-R	-38.01896
Density lbmol/cuft	-2.097056
Density lb/cuft	3.401306
Average MW	61.66458
Liq Vol 60F cuft/hr	18.12968

Table C.2. Absorber profiles for 3% CO₂ base case.

Segment	T liquid °C	T vapor °C	P (KPa)	Loading	y _{CO2}	L (Kmol/s)	V (Kmol/s)
1	53.093	55.729	101.352	0.1657	0.005	2.9001	3.1915
2	57.530	58.284	102.078	0.1735	0.005	2.918	3.2565
3	58.888	59.051	102.804	0.1823	0.006	2.9201	3.2774
4	59.271	59.234	103.530	0.1922	0.007	2.9157	3.2818
5	59.339	59.216	104.25	0.2033	0.008	2.9088	3.2805
6	59.288	59.110	104.981	0.2157	0.009	2.9005	3.2772
7	59.175	58.949	105.707	0.2294	0.010	2.891	3.2728
8	59.012	58.740	106.433	0.2443	0.011	2.8806	3.2677
9	58.803	58.485	107.159	0.2604	0.013	2.8692	3.262
10	58.546	58.184	107.884	0.2775	0.014	2.8568	3.2556
11	58.242	57.838	108.610	0.2953	0.016	2.8438	3.2488
12	57.889	57.45	109.336	0.3136	0.018	2.8303	3.2414
13	57.490	57.034	110.062	0.3318	0.020	2.8165	3.2337
14	57.050	56.602	110.787	0.3496	0.022	2.8028	3.2257
15	56.579	56.181	111.513	0.3665	0.023	2.7895	3.2176
16	56.089	55.818	112.239	0.3819	0.025	2.7766	3.2096
17	55.597	55.596	112.965	0.3956	0.027	2.764	3.2017
18	55.124	55.672	113.690	0.4072	0.028	2.7523	3.1938
19	54.690	56.355	114.416	0.4169	0.029	2.73	3.1854
20	54.31	58.278	115.142	0.4245	0.030	2.7218	3.1752

Table C.3. Stripper profiles for 3% CO₂ base case.

Segment	T liquid °C	T vapor °C	P (KPa)	Loading	y _{CO2}	L (Kmol/s)	V (Kmol/s)
1	100.429	105.240	164.095	0.323	0.344	0.151	0.246
2	107.186	108.220	164.894	0.393	0.322	3.017	0.239
3	108.556	109.512	165.692	0.383	0.294	3.034	0.254
4	109.824	110.711	166.490	0.371	0.266	3.050	0.267
5	111.001	111.811	167.289	0.359	0.241	3.067	0.280
6	112.074	112.804	168.087	0.347	0.217	3.083	0.293
7	113.037	113.692	168.885	0.335	0.196	3.098	0.305
8	113.896	114.484	169.684	0.324	0.177	3.112	0.316
9	114.661	115.193	170.482	0.313	0.160	3.125	0.327
10	115.347	115.833	171.280	0.303	0.145	3.138	0.337
11	115.967	116.416	172.079	0.292	0.132	3.150	0.346
12	116.533	116.953	172.877	0.283	0.120	3.161	0.355
13	117.055	117.455	173.675	0.273	0.108	3.172	0.363

14	117.544	117.932	174.474	0.263	0.098	3.183	0.371
15	118.007	118.393	175.272	0.253	0.087	3.194	0.379
16	118.450	118.850	176.070	0.243	0.078	3.205	0.386
17	118.881	119.323	176.869	0.232	0.068	3.216	0.394
18	119.306	119.846	177.667	0.220	0.058	3.228	0.402
19	119.731	120.489	178.465	0.206	0.047	3.242	0.410
20	121.399	121.399	179.264	0.160	0.036	2.837	0.419

Table C.4. Base case process heat exchanger duties, normalized to mass of CO₂ removed and relative to the reference value in MJ/Kmol CO₂.

Reboiler duty	1.035
Condenser heat duty	-0.422
Cross exchanger heat duty	0.800
Lean solvent cooler heat duty	-0.374

C.5. Detailed results for 10% CO₂-90% removal case (Figures 5.18 and 5.19)

Table C.5. Detailed material and energy balance for 10% CO₂-90% removal case. McCabe-Thiele diagrams shown in figures 5.18 and 5.19, stream names refer to figure C.1, all other parameters same as 3.13% CO₂ base case.

Stream	10	13	BOT-MIX	CO2	FLUEGAS
To	MIX	B6	HE1	COND	ABSORBER
From	FLA1	PUMP	MIX	STRP	
Phase	LIQUID	LIQUID	MIXED	VAPOR	VAPOR
Substream: MIXED					
Mole Frac					
H2O	9.96E-01	9.98E-01	8.56E-01	5.84E-01	1.01E-01
CO2	3.92E-06	4.89E-04	6.89E-06	4.16E-01	1.00E-01
MEA	5.66E-04	2.99E-06	1.76E-02	5.26E-04	0.00E+00
N2	7.46E-06	1.20E-09	2.75E-06	3.96E-05	7.49E-01
O2	9.24E-07	2.67E-10	3.32E-07	4.78E-06	5.00E-02
MEA+	1.69E-03	9.52E-04	6.36E-02	0.00E+00	0.00E+00
MEACOO-	5.98E-04	3.02E-06	4.59E-02	0.00E+00	0.00E+00
HCO3-	9.91E-04	9.49E-04	4.33E-03	0.00E+00	0.00E+00
CO3--	5.03E-05	3.47E-07	3.11E-04	0.00E+00	0.00E+00
H3O+	7.13E-11	8.05E-09	8.50E-11	0.00E+00	0.00E+00
OH-	4.00E-07	3.29E-09	6.26E-07	0.00E+00	0.00E+00
HCOO-	0.00E+00	0.00E+00	1.27E-02	0.00E+00	0.00E+00
Total Flow lbmol/hr	2.45E+03	3.00E+03	7.86E+04	5.46E+03	2.51E+04
Total Flow lb/hr	4.46E+04	5.43E+04	2.05E+06	1.57E+05	7.23E+05
Total Flow cuft/hr	7.23E+02	8.80E+02	3.58E+04	1.65E+06	9.75E+06
Temperature F	1.19E+02	1.20E+02	1.37E+02	2.16E+02	1.45E+02
Pressure psi	1.47E+01	2.38E+01	1.47E+01	2.38E+01	1.67E+01
Vapor Frac	0.00E+00	0.00E+00	2.60E-07	1.00E+00	1.00E+00
Liquid Frac	1.00E+00	1.00E+00	1.00E+00	0.00E+00	0.00E+00
Enthalpy Btu/lbmol	-1.22E+05	-1.22E+05	-1.33E+05	-1.30E+05	-2.69E+04
Entropy Btu/lbmol-R	-3.84E+01	-3.80E+01	-7.72E+01	-3.59E+00	1.25E+00
Density lb/cuft	6.18E+01	6.17E+01	5.73E+01	9.55E-02	7.42E-02
Average MW	1.82E+01	1.81E+01	2.61E+01	2.88E+01	2.88E+01
Liq Vol 60F cuft/hr				2.87E+03	2.01E+04

Stream	LEAN	LEANIN	LEANOUT	M-MEA	OUT
To	HE-2	ABSORBER		MIX	
From	STRP		COOLER		FLA1
Phase	LIQUID	LIQUID	LIQUID	LIQUID	VAPOR
Substream: MIXED					
Mole Frac					
H2O	8.58E-01	8.59E-01	8.59E-01	0.00E+00	1.11E-01
CO2	4.58E-05	2.36E-08	2.35E-08	0.00E+00	1.08E-02
MEA	7.27E-02	7.16E-02	7.16E-02	1.00E+00	4.08E-07
N2	3.69E-24	0.00E+00	0.00E+00	0.00E+00	8.23E-01
O2	6.30E-26	0.00E+00	0.00E+00	0.00E+00	5.49E-02
MEA+	3.46E-02	3.50E-02	3.50E-02	0.00E+00	0.00E+00
MEACOO-	2.05E-02	2.11E-02	2.11E-02	0.00E+00	0.00E+00
HCO3-	1.28E-03	3.04E-04	3.04E-04	0.00E+00	0.00E+00
CO3--	4.23E-05	4.07E-04	4.07E-04	0.00E+00	0.00E+00
H3O+	3.95E-10	5.13E-12	5.13E-12	0.00E+00	0.00E+00
OH-	2.83E-06	4.97E-06	4.97E-06	0.00E+00	0.00E+00
HCOO-	1.28E-02	1.28E-02	1.28E-02	0.00E+00	0.00E+00
Total Flow lbmol/hr	7.82E+04	7.82E+04	7.82E+04	2.20E-01	2.29E+04
Total Flow lb/hr	1.94E+06	1.94E+06	1.94E+06	1.35E+01	6.24E+05
Total Flow cuft/hr	3.33E+04	3.15E+04	3.15E+04	1.43E-01	9.64E+06
Temperature F	2.50E+02	1.04E+02	1.04E+02	1.00E+02	1.19E+02
Pressure psi	2.60E+01	2.00E+01	2.00E+01	2.50E+01	1.47E+01
Vapor Frac	0.00E+00	0.00E+00	0.00E+00	0.00E+00	1.00E+00
Liquid Frac	1.00E+00	1.00E+00	1.00E+00	1.00E+00	0.00E+00
Enthalpy Btu/lbmol	-1.25E+05	-1.28E+05	-1.28E+05	-1.17E+05	-1.31E+04
Entropy Btu/lbmol-R	-5.79E+01	-6.27E+01	-6.27E+01	-1.20E+02	5.69E-01
Density lb/cuft	5.83E+01	6.17E+01	6.17E+01	9.43E+01	6.47E-02
Average MW	2.48E+01	2.48E+01	2.48E+01	6.11E+01	2.73E+01
Liq Vol 60F cuft/hr				2.12E-01	1.82E+04

Stream	PCO2	PUREGAS	REFLUX	RICH	RICHOUT
To		FLA1	STRP	STRP	MIX
From	COND	ABSORBER	B6	HE1	ABSORBER
Phase	VAPOR	MIXED	LIQUID	LIQUID	LIQUID
Substream: MIXED					
Mole Frac					
H2O	7.89E-02	1.84E-01	9.98E-01	8.52E-01	8.51E-01
CO2	9.21E-01	1.00E-02	4.89E-04	8.76E-04	7.56E-06
MEA	1.56E-09	1.74E-04	2.99E-06	2.26E-02	1.82E-02
N2	8.79E-05	7.56E-01	1.20E-09	2.75E-06	2.60E-06
O2	1.06E-05	5.05E-02	2.67E-10	3.32E-07	3.13E-07
MEA+	0.00E+00	5.53E-05	9.52E-04	6.24E-02	6.55E-02
MEACOO-	0.00E+00	5.19E-05	3.02E-06	4.20E-02	4.74E-02
HCO3-	0.00E+00	2.57E-06	9.49E-04	7.52E-03	4.41E-03
CO3--	0.00E+00	3.75E-07	3.47E-07	7.30E-05	2.99E-04
H3O+	0.00E+00	5.49E-14	8.05E-09	9.80E-10	8.71E-11
OH-	0.00E+00	1.51E-09	3.29E-09	5.27E-07	6.00E-07
HCOO-	0.00E+00	0.00E+00	0.00E+00	1.27E-02	1.31E-02
Total Flow lbmol/hr	2.46E+03	2.49E+04	2.78E+03	7.87E+04	7.61E+04
Total Flow lb/hr	1.03E+05	6.61E+05	5.03E+04	2.05E+06	2.00E+06
Total Flow cuft/hr	6.97E+05	1.09E+07	8.15E+02	3.68E+04	3.50E+04
Temperature F	1.20E+02	1.44E+02	1.20E+02	2.30E+02	1.38E+02
Pressure psi	2.18E+01	1.47E+01	2.38E+01	1.00E+02	1.67E+01
Vapor Frac	1.00E+00	9.99E-01	0.00E+00	0.00E+00	0.00E+00
Liquid Frac	0.00E+00	1.03E-03	1.00E+00	1.00E+00	1.00E+00
Enthalpy Btu/lbmol	-1.64E+05	-2.04E+04	-1.22E+05	-1.31E+05	-1.33E+05
Entropy Btu/lbmol-R	2.32E-01	2.49E-01	-3.80E+01	-7.27E+01	-7.85E+01
Density lb/cuft	1.48E-01	6.04E-02	6.17E+01	5.57E+01	5.72E+01
Average MW	4.20E+01	2.66E+01	1.81E+01	2.60E+01	2.63E+01
Liq Vol 60F cuft/hr	2.00E+03				

Stream	S-1	S-3	S2
To			PUMP
From	CALC-SEP	CALC-SEP	COND
Phase	VAPOR	MISSING	LIQUID
Substream: MIXED			
Mole Frac			
H2O	9.98E-01	0.00E+00	9.98E-01
CO2	1.44E-03	0.00E+00	4.89E-04
MEA	9.57E-04	0.00E+00	2.99E-06
N2	1.19E-09	0.00E+00	1.20E-09
O2	2.67E-10	0.00E+00	2.67E-10
MEA+	0.00E+00	0.00E+00	9.52E-04
MEACOO-	0.00E+00	0.00E+00	3.02E-06
HCO3-	0.00E+00	0.00E+00	9.49E-04
CO3--	0.00E+00	0.00E+00	3.47E-07
H3O+	0.00E+00	0.00E+00	8.05E-09
OH-	0.00E+00	0.00E+00	3.29E-09
HCOO-	0.00E+00	0.00E+00	0.00E+00
Total Flow lbmol/hr	2.21E+02	0.00E+00	3.00E+03
Total Flow lb/hr	4.00E+03	0.00E+00	5.43E+04
Total Flow cuft/hr	9.35E+05	0.00E+00	8.80E+02
Temperature F	1.20E+02		1.20E+02
Pressure psi	1.47E+00	1.47E+00	2.18E+01
Vapor Frac	1.00E+00		0.00E+00
Liquid Frac	0.00E+00		1.00E+00
Enthalpy Btu/lbmol	-1.04E+05		-1.22E+05
Entropy Btu/lbmol-R	-5.42E+00		-3.80E+01
Density lb/cuft	4.28E-03		6.17E+01
Average MW	1.81E+01		1.81E+01
Liq Vol 60F cuft/hr	6.42E+01	0.00E+00	

Stream	TO-ABS	WMAKEUP	XSH2O
To	COOLER	FLA1	CALC-SEP
From	HE-2		B6
Phase	LIQUID	LIQUID	LIQUID
Substream: MIXED			
Mole Frac			
H2O	8.59E-01	1.00E+00	9.98E-01
CO2	5.07E-07	0.00E+00	4.89E-04
MEA	7.19E-02	0.00E+00	2.99E-06
N2	0.00E+00	0.00E+00	1.20E-09
O2	0.00E+00	0.00E+00	2.67E-10
MEA+	3.48E-02	0.00E+00	9.52E-04
MEACOO-	2.11E-02	0.00E+00	3.02E-06
HCO3-	5.63E-04	0.00E+00	9.49E-04
CO3--	1.79E-04	0.00E+00	3.47E-07
H3O+	3.37E-11	2.85E-09	8.05E-09
OH-	4.30E-06	2.85E-09	3.29E-09
HCOO-	1.28E-02	0.00E+00	0.00E+00
Total Flow lbmol/hr	7.82E+04	4.20E+02	2.21E+02
Total Flow lb/hr	1.94E+06	7.57E+03	4.00E+03
Total Flow cuft/hr	3.20E+04	1.22E+02	6.48E+01
Temperature F	1.59E+02	1.00E+02	1.20E+02
Pressure psi	2.60E+01	2.50E+01	2.38E+01
Vapor Frac	0.00E+00	0.00E+00	0.00E+00
Liquid Frac	1.00E+00	1.00E+00	1.00E+00
Enthalpy Btu/lbmol	-1.26E+05	-1.22E+05	-1.22E+05
Entropy Btu/lbmol-R	-6.08E+01	-3.82E+01	-3.80E+01
Density lb/cuft	6.06E+01	6.20E+01	6.17E+01
Average MW	2.48E+01	1.80E+01	1.81E+01
Liq Vol 60F cuft/hr			

Table C.6. Absorber profiles for 10% CO₂-90% removal case.

Segment	T liquid °C	T vapor °C	P (KPa)	Loading	y _{CO2}	L (Kmol/s)	V (Kmol/s)
1	56.155	62.392	101.353	0.195	0.011	10.132	3.136
2	66.784	69.595	102.079	0.202	0.012	10.321	3.423
3	71.917	72.975	102.804	0.209	0.014	10.405	3.620
4	74.006	74.310	103.530	0.217	0.017	10.427	3.713
5	74.741	74.715	104.256	0.227	0.020	10.419	3.744
6	74.895	74.699	104.982	0.238	0.023	10.395	3.746
7	74.772	74.459	105.708	0.250	0.027	10.363	3.735
8	74.480	74.064	106.433	0.264	0.031	10.323	3.717
9	74.050	73.529	107.159	0.279	0.036	10.277	3.692
10	73.483	72.851	107.885	0.296	0.042	10.226	3.664
11	72.768	72.020	108.611	0.313	0.048	10.169	3.631
12	71.895	71.027	109.336	0.331	0.054	10.109	3.594
13	70.851	69.866	110.062	0.349	0.060	10.046	3.554
14	69.632	68.537	110.788	0.366	0.067	9.982	3.511
15	68.237	67.048	111.514	0.382	0.073	9.917	3.467
16	66.672	65.420	112.239	0.397	0.079	9.853	3.420
17	64.942	63.701	112.965	0.410	0.085	9.791	3.373
18	63.048	62.000	113.691	0.422	0.090	9.728	3.326
19	60.976	60.595	114.417	0.433	0.095	9.665	3.277
20	58.684	60.212	115.142	0.442	0.100	9.594	3.225

Table C.7. Stripper profiles for 10% CO₂-90% removal case.

Segment	T liquid °C	T vapor °C	P (KPa)	Loading	y _{CO2}	L (Kmol/s)	V (Kmol/s)
1	96.923	102.139	164.095	0.323	0.416	0.378	0.688
2	104.607	105.121	164.894	0.411	0.397	10.251	0.634
3	105.119	105.710	165.692	0.409	0.387	10.267	0.649
4	105.690	106.389	166.490	0.406	0.375	10.287	0.663
5	106.368	107.178	167.289	0.402	0.361	10.313	0.679
6	107.160	108.072	168.087	0.397	0.344	10.343	0.700
7	108.060	109.053	168.885	0.391	0.324	10.379	0.725
8	109.049	110.096	169.684	0.383	0.302	10.421	0.754
9	110.099	111.169	170.482	0.374	0.278	10.467	0.787
10	111.176	112.240	171.280	0.364	0.254	10.517	0.823
11	112.248	113.283	172.079	0.354	0.230	10.570	0.862
12	113.287	114.278	172.877	0.342	0.206	10.624	0.903
13	114.274	115.215	173.675	0.330	0.183	10.679	0.944
14	115.200	116.092	174.474	0.317	0.162	10.734	0.986

15	116.059	116.913	175.272	0.304	0.141	10.789	1.027
16	116.858	117.692	176.070	0.291	0.122	10.844	1.067
17	117.599	118.446	176.869	0.277	0.104	10.899	1.107
18	118.293	119.208	177.667	0.262	0.087	10.956	1.147
19	118.948	120.031	178.465	0.246	0.070	11.015	1.187
20	121.007	121.007	179.264	0.190	0.052	9.850	1.229

Table C.8. Process heat exchanger duties, normalized to mass of CO₂ removed and relative to the reference value in MJ/Kmol CO₂, 10% CO₂-90% removal.

Reboiler duty	0.96
Condenser heat duty	-0.307
Cross exchanger heat duty	0.756
Lean solvent cooler heat duty	-0.440

C.6. Hints on convergence of the model

The absorber RATEFRAC model presents serious convergence problems. When a converged case is available, a new case needs to be obtained from the first one, by successive small changes in the inputs. The following indications must be followed in order to achieve convergence.

1. Once a converged case is available, never reinitialize the simulation.
2. When copying a simulation to a new directory, copy all the five files associated with it (.apw, .bkp, .for, .appdf, .his); by opening only the apw file, all the previous run history is not loaded. As a consequence the simulation will not converge.

3. Always save the same simulation with two different names. In case one is lost, the user will not have to restart from the scratch.
4. When the simulation diverges, do not save it: close ASPEN PLUS and re-open the file. If the simulation is saved, convergence will not be obtained any more.

Typical inputs that require particularly small steps in order to maintain convergence are the solvent and flue gas flow rate, composition and temperature, the heights of the columns and the pressure of the columns.

If a new simulation needs to be started from an input file, the following steps can be followed to obtain one converged case.

1. In the same flowsheet, separate absorber from stripper, breaking the rich solvent stream.
2. Use the “hide” option for all CALCULATOR blocks and DESIGN-SPECIFICATION blocks that are involved with convergence of the integrated absorber-stripper. In this way the simulation is defined to treat absorber and stripper independently.
3. Reinitialize simulation.
4. Start with a very short absorber, by setting the height on ABSORBER→COLUMNS→1→PackSpecs→1→Specifications and setting the height of a segment in the subroutine interaction vector, found in ABSORBER→User Subroutines→User Kinetics→ parameter 3. This parameter provides the subroutine with the height per segment.
5. If one case works at low height, save the simulation and proceed with small steps toward the wanted height. Run and save every simulation and never reinitialize.

APPENDIX D

High CO₂ Base Case for Absorption/Stripping Model

The model developed uses ASPEN RATEFRAC for both absorber and stripper. The absorber is modeled with kinetic reactions, the stripper with all equilibrium reactions. Equilibrium is calculated with an Electrolyte-NRTL model, regressed on the data of Jou et al. (1995), using the Henry's constant of CO₂ in H₂O. The kinetic model uses the following expression for the flux.

$$N_{CO_2} = \sqrt{(AF)k_{2,MEA}[MEA]_i \frac{D_{CO_2}}{\gamma_{CO_2}} (a_{CO_2,i} - a_{CO_2,i}^*)} \quad (1)$$

The driving force is activity based, with activities calculated by the Electrolyte-NRTL model. The square root dependence on rate constant and concentration of MEA at the interface is consistent with an interface-pseudo-first-order approximation. The rate constant for the CO₂+MEA reaction ($k_{2,MEA}$) is the value of Hikita (1977), given in equation 2; AF is an adjustment factor, given in equation 3, to match wetted wall data from Dang (2001).

$$\text{Log}_{10} k_{2,MEA} = 10.99 - \frac{2152}{T(^{\circ}K)} \quad (2)$$

$$\ln AF = -11.32 + \frac{4050.6}{T(^{\circ}K)} \quad (3)$$

The diffusivity of CO₂ is calculated with a Stokes-Einstein correlation, given by equation 4 (Pacheco, 1998).

$$D_{CO_2} = D_{CO_2,water} \left(\frac{\mu_{water}}{\mu_{solution}} \right)^{0.545} \quad (4)$$

The viscosity of solution is calculated with a correlation by Weiland et al. (1996), which includes temperature, MEA concentration and CO₂ loading dependences.

Table D.1. Input summary for the high CO₂ base case.

Flue Gas			
	Composition (mol %)	CO ₂	12.57%
	(from EPA-600/2-75-006	H ₂ O	7.77%
	January 1975, Table 4)	N ₂	74.80%
		O ₂	4.86%
	Water Saturation T		45 °C
	Absorber inlet T		55 °C
	Absorber inlet P		111.325 Kpa
	Mole flow		
	(after saturation)		11,000 kmol/hr
Solvent			
	Unloaded composition	MEA	11.23 mol%
	(30 wt% MEA)	H ₂ O	88.77 mol%
	Lean loading		0.21
	(mol CO ₂ /mol MEA)		
	Lean solvent T		40 °C
	CO₂ removal		90%
	(solvent rate calculated to get specified removal)		
Absorber			
	Packing height		15 meters
	Diameter		7 meters
	Pressure drop		10 Kpa
	CO₂+MEA kinetics		From Dang (2001)
	Packing type		Cascade Mini Rings #2
Cross exchanger			
	Temp. approach, hot end		10 °C
Stripper			
	Packing height		10 meters
	Diameter		4.5 meters
	Bottom Pressure		172.12 KPa
	Pressure Drop		10 KPa
	Reboiler		equilibrium
	Condenser		equilibrium partial condenser, T=50 °C
	Rich solvent feed location		0.5 meters from top
	Water reflux location		At top
	Packing type		Cascade Mini Rings #2
	Reactions		All at equilibrium

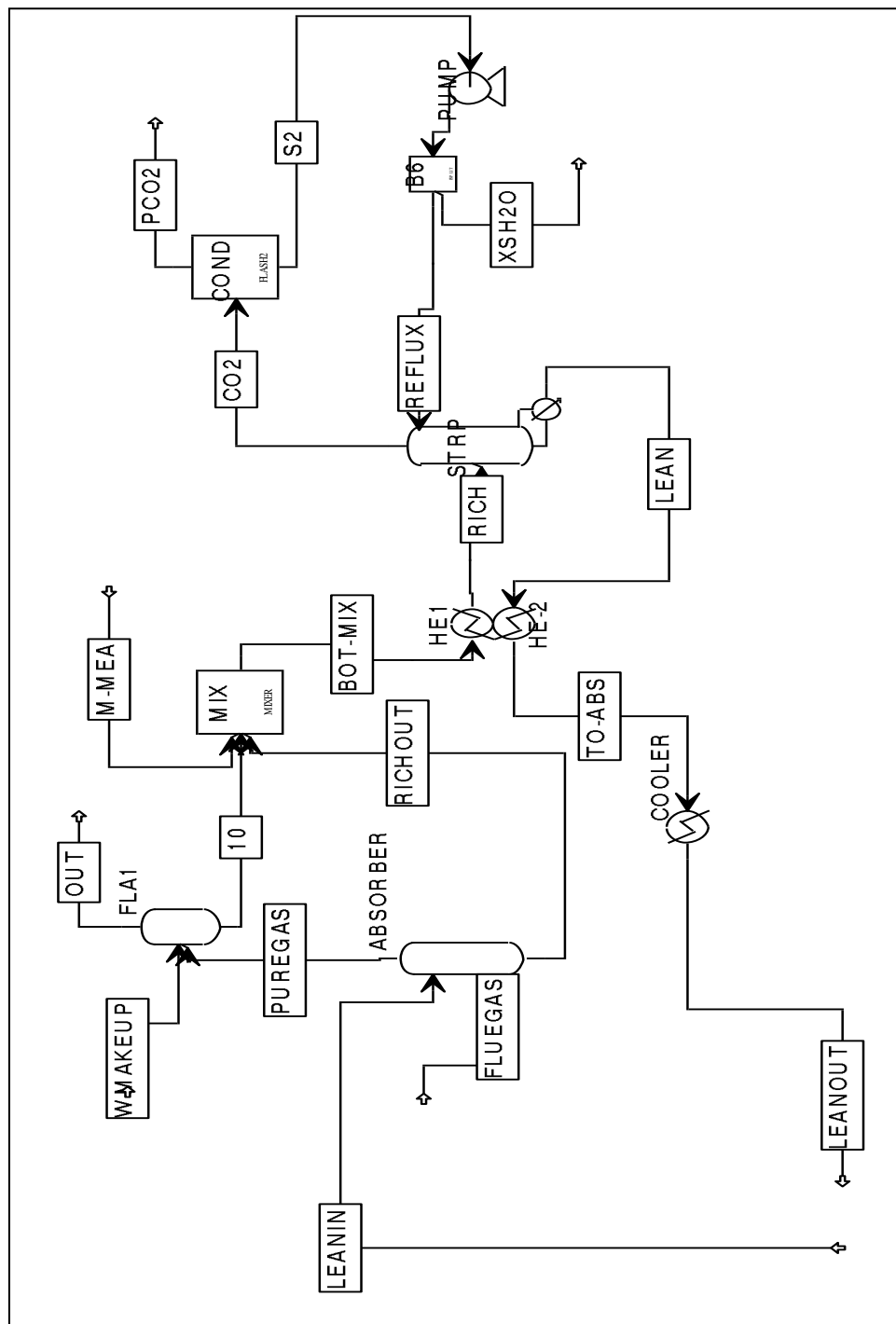


Figure D.1. ASPEN PLUS process flow diagram for absorption/stripping base case.

Table D.2. Material and energy balance.

Stream name	10	13	BOT-MIX	CO2	FLUEGAS
To	MIX	B6	HE1	COND	ABSORBER
From	FLA1	PUMP	MIX	STRP	
Phase	LIQUID	LIQUID	LIQUID	VAPOR	VAPOR

Substream: MIXED

Mole Frac

H2O	9.968E-01	9.981E-01	8.825E-01	6.416E-01	9.411E-02
CO2	4.954E-06	4.703E-04	6.373E-06	3.579E-01	1.235E-01
MEA	3.773E-04	2.032E-06	1.414E-02	4.405E-04	0
N2	7.489E-06	1.296E-09	2.959E-06	3.780E-05	7.347E-01
O2	9.029E-07	2.820E-10	3.487E-07	4.455E-06	4.774E-02
MEA+	1.406E-03	7.193E-04	5.193E-02	0	0
MEACOO-	3.842E-04	1.524E-06	4.587E-02	0	0
HCO3-	9.500E-04	7.174E-04	5.094E-03	0	0
CO3--	3.582E-05	2.015E-07	4.781E-04	0	0
H3O+	8.940E-11	9.625E-09	8.394E-11	0	0
OH-	3.062E-07	2.779E-09	7.868E-07	0	0
Total Flow kmol/sec	3.290E-01	5.803E-01	1.217E+01	9.521E-01	3.056E+00
Total Flow kg/sec	5.977E+00	1.050E+01	3.054E+02	2.603E+01	8.934E+01
Total Flow cum/sec	6.042E-03	1.063E-02	3.205E-01	1.824E+01	7.480E+01
Temperature K	3.213E+02	3.232E+02	3.297E+02	3.766E+02	3.282E+02
Pressure N/sqm	1.014E+05	1.621E+05	1.014E+05	1.621E+05	1.113E+05
Vapor Frac	0	0	0	1	1
Liquid Frac	1	1	1	0	0
Solid Frac	0	0	0	0	0
Enthalpy J/kmol	-2.847E+08	-2.843E+08	-3.069E+08	-2.934E+08	-7.044E+07
Entropy J/kmol-K	-1.599E+05	-1.584E+05	-3.098E+05	-1.782E+04	5.398E+03
Density kg/cum	9.892E+02	9.871E+02	9.527E+02	1.427E+00	1.194E+00
Average MW	1.817E+01	1.809E+01	2.510E+01	2.734E+01	2.924E+01

Stream name	LEAN	LEANIN	LEANOUT	M-MEA	OUT
To	HE-2	ABSORBER		MIX	
From	STRP		COOLER		FLA1
Phase	LIQUID	LIQUID	LIQUID	LIQUID	VAPOR

Substream: MIXED

Mole Frac

H2O	8.863E-01	8.868E-01	8.868E-01	0.000E+00	1.115E-01
CO2	2.570E-05	2.653E-08	2.651E-08	0.000E+00	1.364E-02
MEA	6.653E-02	6.544E-02	6.546E-02	1.000E+00	2.713E-07
N2	1.208E-22	0	0	0	8.215E-01
O2	1.460E-25	0	0	0	5.337E-02
MEA+	2.362E-02	2.418E-02	2.417E-02	0	0
MEACOO-	2.212E-02	2.265E-02	2.264E-02	0	0
HCO3-	1.355E-03	3.382E-04	3.381E-04	0	0
CO3--	6.629E-05	5.881E-04	5.880E-04	0	0
H3O+	2.799E-10	4.404E-12	4.402E-12	0	0
OH-	4.312E-06	6.488E-06	6.490E-06	0	0
Total Flow kmol/sec	1.213E+01	1.213E+01	1.213E+01	3.846E-06	2.733E+00
Total Flow kg/sec	2.898E+02	2.898E+02	2.898E+02	2.349E-04	7.468E+01
Total Flow cum/sec	2.977E-01	2.820E-01	2.820E-01	1.556E-07	7.195E+01
Temperature K	3.918E+02	3.132E+02	3.132E+02	3.109E+02	3.213E+02
Pressure N/sqm	1.721E+05	1.379E+05	1.379E+05	1.724E+05	1.014E+05
Vapor Frac	0	0	0	0	1
Liquid Frac	1	1	1	1	0
Solid Frac	0	0	0	0	0
Enthalpy J/kmol	-2.882E+08	-2.949E+08	-2.949E+08	- 2.716E+08	-3.166E+07
Entropy J/kmol-K	-2.324E+05	-2.521E+05	-2.521E+05	- 5.012E+05	2.453E+03
Density kg/cum	9.733E+02	1.027E+03	1.028E+03	1.510E+03	1.038E+00
Average MW	2.389E+01	2.389E+01	2.389E+01	6.108E+01	2.733E+01

Stream name	PCO2	PUREGAS	REFLUX	RICH	RICHOUT
To		FLA1	STRP	STRP	MIX
From	COND	ABSORBER	B6	HE1	ABSORBER
Phase	VAPOR	MIXED	LIQUID	LIQUID	LIQUID

Substream: MIXED

Mole Frac

H2O	8.445E-02	1.928E-01	9.981E-01	8.789E-01	8.793E-01
CO2	9.154E-01	1.248E-02	4.703E-04	6.144E-04	6.686E-06
MEA	1.170E-09	1.257E-04	2.032E-06	1.875E-02	1.448E-02
N2	9.690E-05	7.460E-01	1.296E-09	2.957E-06	2.833E-06
O2	1.142E-05	4.847E-02	2.820E-10	3.485E-07	3.333E-07
MEA+	0	5.799E-05	7.194E-04	5.093E-02	5.332E-02
MEACOO-	0	5.351E-05	1.524E-06	4.220E-02	4.720E-02
HCO3-	0	3.517E-06	7.174E-04	8.494E-03	5.171E-03
CO3--	0	4.841E-07	2.015E-07	1.126E-04	4.693E-04
H3O+	0	8.047E-14	9.625E-09	9.222E-10	8.494E-11
OH-	0	1.775E-09	2.779E-09	7.390E-07	7.690E-07
Total Flow kmol/sec	3.715E-01	3.009E+00	5.759E-01	1.217E+01	1.184E+01
Total Flow kg/sec	1.553E+01	7.971E+01	1.042E+01	3.054E+02	2.994E+02
Total Flow cum/sec	6.685E+00	8.266E+01	1.055E-02	3.296E-01	3.146E-01
Temperature K	3.232E+02	3.356E+02	3.232E+02	3.818E+02	3.300E+02
Pressure N/sqm	1.483E+05	1.013E+05	1.621E+05	6.895E+05	1.113E+05
Vapor Frac	1	0.9987606	0	0	0
Liquid Frac	0	1.24E-03	1	1	1
Solid Frac	0	0	0	0	0
Enthalpy J/kmol	-3.798E+08	-5.055E+07	-2.843E+08	-3.024E+08	-3.076E+08
Entropy J/kmol-K	1.062E+03	7.865E+02	-1.584E+05	-2.913E+05	-3.141E+05
Density kg/cum	2.323E+00	9.642E-01	9.871E+02	9.264E+02	9.517E+02
Average MW	4.181E+01	2.649E+01	1.809E+01	2.509E+01	2.529E+01

Stream name	S2	TO-ABS	WMAKEUP	XSH2O
To	PUMP	COOLER	FLA1	
From	COND	HE-2		B6
Phase	LIQUID	LIQUID	LIQUID	LIQUID

Substream: MIXED

Mole Frac

H2O	9.981E-01	8.868E-01	1.000E+00	9.981E-01
CO2	4.703E-04	3.696E-07	0	4.703E-04
MEA	2.032E-06	6.572E-02	0	2.032E-06
N2	1.296E-09	0.000E+00	0	1.296E-09
O2	2.820E-10	0.000E+00	0	2.820E-10
MEA+	7.193E-04	2.386E-02	0	7.193E-04
MEACOO-	1.524E-06	2.269E-02	0	1.524E-06
HCO3-	7.174E-04	5.960E-04	0	7.174E-04
CO3--	2.015E-07	2.788E-04	0	2.015E-07
H3O+	9.626E-09	2.438E-11	2.846E-09	9.625E-09
OH-	2.778E-09	6.014E-06	2.846E-09	2.779E-09
Total Flow kmol/sec	5.803E-01	1.213E+01	5.292E-02	4.325E-03
Total Flow kg/sec	1.050E+01	2.898E+02	9.534E-01	7.824E-02
Total Flow cum/sec	1.063E-02	2.865E-01	9.599E-04	7.927E-05
Temperature K	3.232E+02	3.411E+02	3.109E+02	3.232E+02
Pressure N/sqm	1.483E+05	1.721E+05	1.724E+05	1.621E+05
Vapor Frac	0	0	0	0
Liquid Frac	1	1	1	1
Solid Frac	0	0	0	0
Enthalpy J/kmol	-2.843E+08	-2.925E+08	-2.849E+08	-2.843E+08
Entropy J/kmol-K	-1.584E+05	-2.447E+05	-1.600E+05	-1.584E+05
Density kg/cum	9.871E+02	1.011E+03	9.932E+02	9.871E+02
Average MW	1.809E+01	2.389E+01	1.802E+01	1.809E+01

Table D.3. Absorber profiles.

	Liquid temperature	Vapor temperature	Pressure	CO ₂ loading	y _{CO2}	y _{H2O}	Liquid flow	Vapor flow
Height from top (meters)	°C	°C	kPa				kmol/hr	kmol/hr
0.75	55.6369319	62.4793988	101.325	0.216	0.013	0.193	44874.5	10833.3
1.5	67.300933	70.5691065	101.851	0.223	0.014	0.273	45802.1	12068.3
2.25	73.3173421	74.5454205	102.378	0.231	0.015	0.324	46255.2	13032.3
3	75.7893723	76.1191023	102.904	0.240	0.018	0.345	46386.9	13524.7
3.75	76.6183101	76.5598823	103.43	0.250	0.021	0.351	46358.2	13699.8
4.5	76.7407879	76.4872779	103.957	0.261	0.024	0.348	46250.9	13720.2
5.25	76.5318856	76.1487973	104.483	0.274	0.028	0.342	46098.2	13668.9
6	76.1253439	75.6298195	105.009	0.289	0.033	0.333	45912.2	13579.5
6.75	75.5601373	74.9516678	105.536	0.305	0.039	0.322	45698.1	13464.4
7.5	74.8390083	74.1115827	106.062	0.322	0.045	0.309	45459.2	13328.0
8.25	73.951555	73.0989355	106.588	0.340	0.052	0.295	45199.4	13172.4
9	72.8842066	71.9024454	107.114	0.358	0.059	0.278	44923.4	12999.4
9.75	71.625451	70.5137815	107.641	0.375	0.067	0.261	44637.3	12811.5
10.5	70.1687598	68.9290158	108.167	0.392	0.075	0.243	44347.0	12611.4
11.25	68.5130125	67.1480602	108.693	0.407	0.083	0.223	44057.8	12402.6
12	66.6593118	65.1727506	109.22	0.421	0.090	0.203	43773.0	12187.9
12.75	64.6035284	63.0069833	109.746	0.432	0.098	0.183	43492.9	11969.5
13.5	62.32472	60.6688049	110.272	0.443	0.104	0.163	43213.9	11747.4
14.25	59.7688043	58.2401836	110.799	0.452	0.111	0.142	42927.0	11518.7
15	56.8223597	56.0235785	111.325	0.460	0.117	0.120	42613.0	11275.5

Table D.4. Stripper profiles.

	Liquid temperature	Vapor temperature	Pressure	CO ₂ loading	y _{CO2}	Y _{H2O}	Liquid flow	Vapor flow
Height from top (meters)	°C	°C	kPa				kmol/hr	kmol/hr
0.5	99.2570778	103.459283	162.12		0.358	0.642	2252.3	3427.7
1	104.887298	105.894988	162.646	0.429	0.335	0.664	46069.6	3282.1
1.5	106.073351	107.039859	163.173	0.420	0.310	0.689	46273.1	3463.5
2	107.208989	108.1396	163.699	0.411	0.285	0.714	46484.4	3627.5
2.5	108.306023	109.183537	164.225	0.401	0.260	0.739	46700.2	3794.3
3	109.34165	110.154303	164.752	0.391	0.237	0.762	46915.2	3962.7
3.5	110.299074	111.043087	165.278	0.381	0.216	0.783	47125.3	4128.7
4	111.171742	111.84949	165.804	0.371	0.196	0.803	47327.7	4289.1
4.5	111.961242	112.578897	166.331	0.360	0.178	0.821	47521.2	4442.0
5	112.674273	113.239903	166.857	0.350	0.161	0.837	47705.6	4586.6
5.5	113.320087	113.842439	167.383	0.341	0.146	0.852	47881.8	4723.2
6	113.908744	114.39664	167.909	0.331	0.133	0.866	48051.2	4852.4
6.5	114.450092	114.912365	168.436	0.322	0.120	0.878	48215.7	4975.5
7	114.953198	115.399227	168.962	0.312	0.108	0.890	48377.3	5093.9
7.5	115.426866	115.867157	169.488	0.302	0.097	0.901	48538.5	5209.2
8	115.877963	116.327651	170.015	0.292	0.086	0.912	48702.8	5323.0
8.5	116.314075	116.796547	170.541	0.281	0.075	0.923	48873.7	5437.8
9	116.741884	117.299058	171.067	0.269	0.064	0.934	49056.3	5555.9
9.5	117.168065	117.88046	171.594	0.255	0.052	0.946	49258.0	5680.3
10	118.627577	118.627577	172.12	0.210	0.039	0.958	43669.1	5815.5

Table D.5. Heat exchanger duties (values in KW).

Reboiler duty	69992.910
Condenser heat duty	-26749.978
Cross exchanger heat duty	52946.720
Lean solvent cooler heat duty	-28550.745

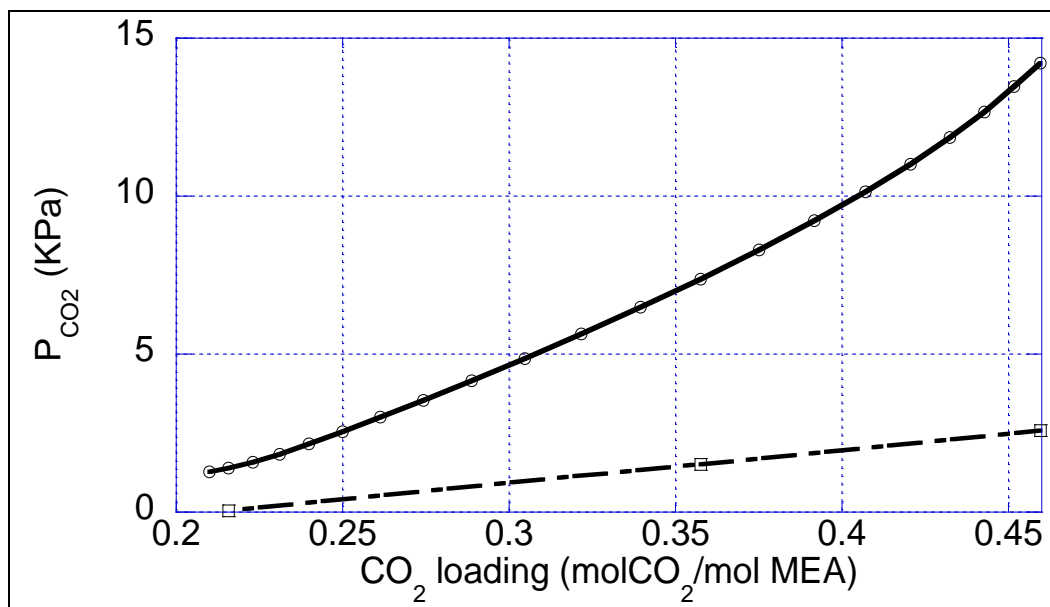


Figure D.2. Absorber McCabe-Thiele diagram.

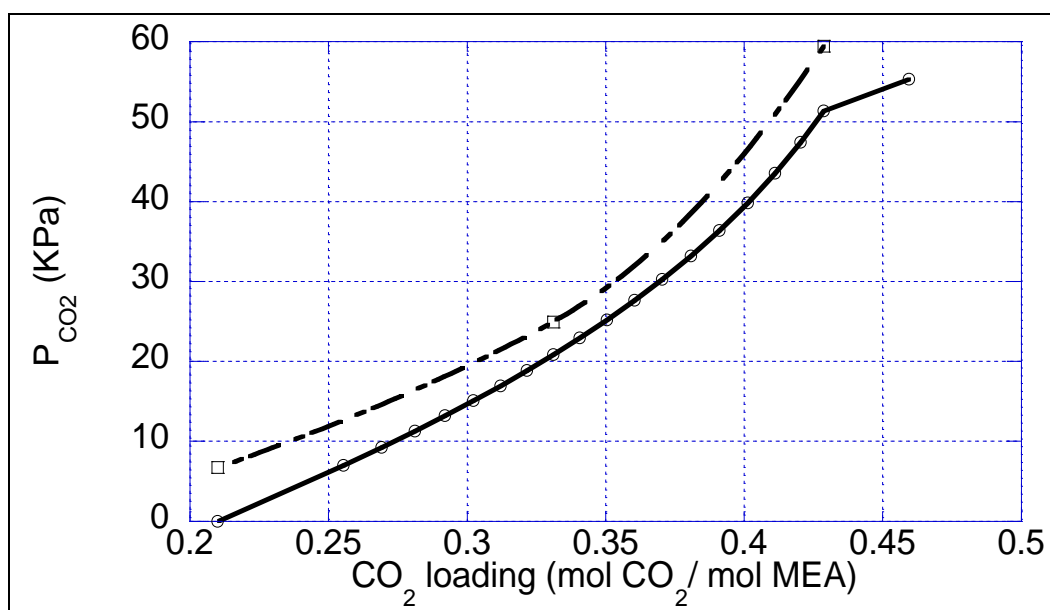


Figure D.3. Stripper McCabe-Thiele diagram.

Table D.6. Tabular data for Figures D.2 and D.3.

Absorber			Stripper		
Loading	P _{CO2} Op. line	P _{CO2} [*] Eq. line	Loading	P _{CO2} Op. line	P _{CO2} [*] Eq. line
	KPa	Kpa		Kpa	KPa
0.210	1.270				
0.216	1.389	0.045	0.460	55.282	
0.223	1.582		0.027	51.334	59.448
0.231	1.837		0.033	47.411	
0.240	2.157		0.019	43.553	
0.250	2.544		0.051	39.859	
0.261	3.004		0.064	36.399	
0.274	3.541		0.082	33.208	
0.289	4.159		0.105	30.288	
0.305	4.859		0.134	27.623	
0.322	5.636		0.170	25.183	
0.340	6.480		0.216	22.932	
0.358	7.375	1.510	0.271	20.834	24.928
0.375	8.298		0.361	18.851	
0.392	9.225		0.190	16.944	
0.407	10.136		0.510	15.077	
0.421	11.015		0.622	13.206	
0.432	11.857		0.758	11.283	
0.443	12.670		0.931	9.246	
0.452	13.472		1.162	7.009	
0.460	14.212	2.577	1.506	0.000	6.729

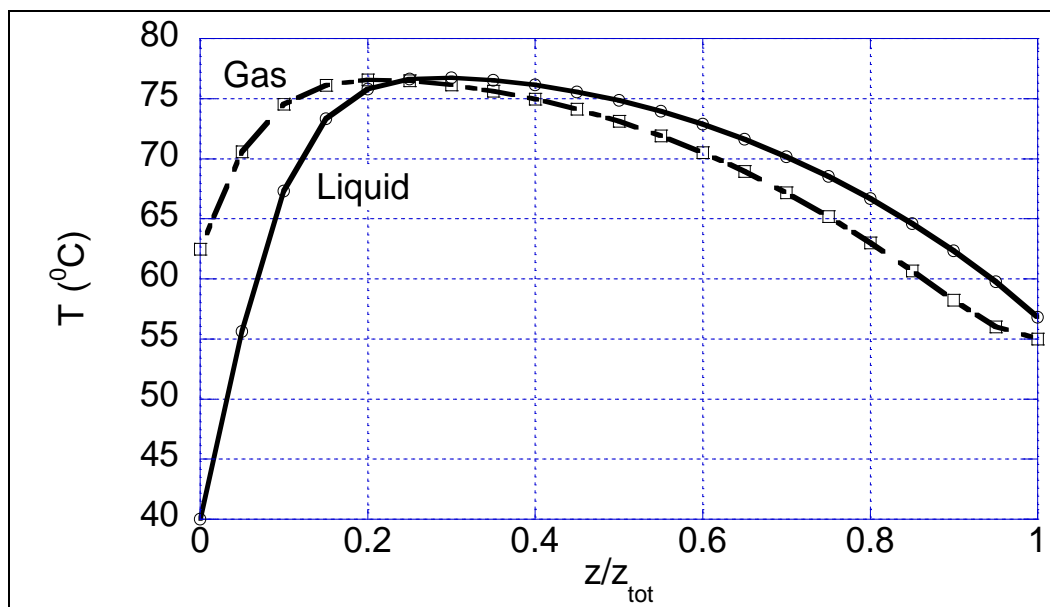


Figure D.4. Gas and liquid temperature profiles in the absorber.

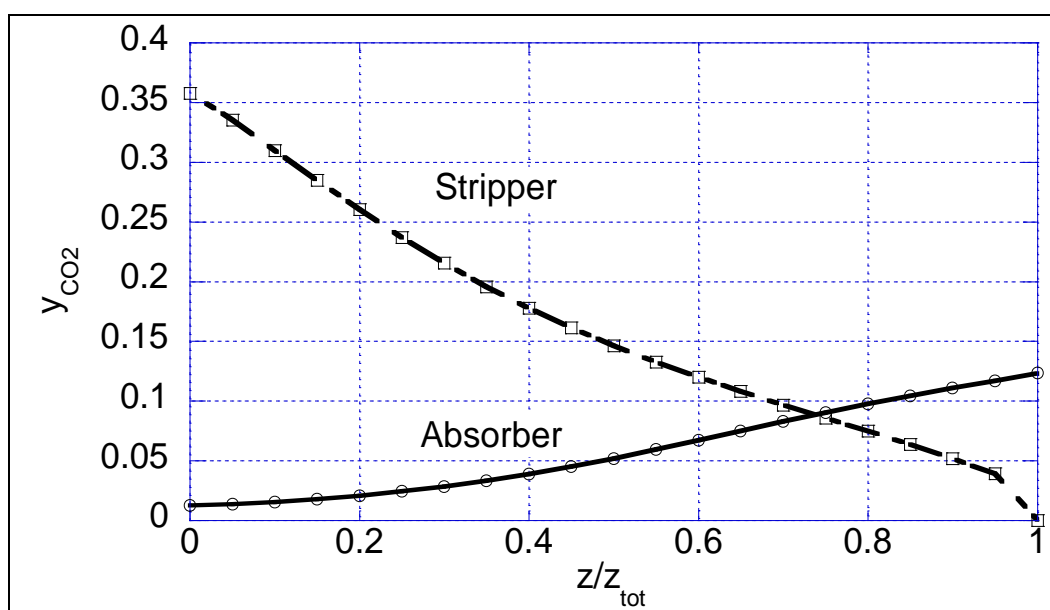


Figure D.5. CO₂ mole fraction profiles in absorber and stripper.

APPENDIX E

Detailed Simulation Results

Table E.1. Detailed simulation results for runs in Chapter 5.

	mol% CO ₂ in flue gas	% Removal	wt% MEA _{tot}	Z _{absorber} /Z _{base case}	Z _{stripper} /Z _{base case}	X _{HSS} /X _{MEA,tot}	P _{reboiler} (atm)	L/G _{mass}	Lean Loading	Rich Loading	Q _{rel}
Table 5.1	3%	85%	33.5%	1.0	1.0	0.1	1.7	0.6326	0.11	0.4171	1.490
	3%	85%	33.5%	1.0	1.0	0.1	1.7	0.6839	0.13	0.4152	1.269
	3%	85%	33.5%	1.0	1.0	0.1	1.7	0.7351	0.15	0.4132	1.145
	3%	85%	33.5%	1.0	1.0	0.1	1.7	0.7801	0.16	0.4115	1.085
	3%	85%	33.5%	1.0	1.0	0.1	1.7	0.8628	0.18	0.4083	1.050
	3%	85%	33.5%	1.0	1.0	0.1	1.7	0.9118	0.19	0.4064	1.053
	3%	85%	33.5%	1.0	1.0	0.1	1.7	0.9678	0.20	0.4043	1.063
	3%	85%	33.5%	1.0	1.0	0.1	1.7	1.0318	0.21	0.4020	1.078
	3%	85%	33.5%	1.0	1.0	0.1	1.7	1.2991	0.24	0.3934	1.143
Table 5.2	3%	85%	33.5%	1.0	1.0	0.1	1.7	1.7749	0.27	0.3829	1.255
	3%	85%	33.5%	0.6	1.0	0.1	1.7	3.29	0.26	0.321	1.87
	3%	85%	33.5%	1.0	1.0	0.1	1.7	0.91	0.19	0.406	1.06
	3%	85%	33.5%	1.6	1.0	0.1	1.7	0.82	0.20	0.440	0.95
	3%	90%	33.5%	0.8	1.0	0.1	1.7	3.37	0.28	0.343	1.69
	3%	90%	33.5%	1.0	1.0	0.1	1.7	1.18	0.19	0.368	1.25
	3%	90%	33.5%	1.6	1.0	0.1	1.7	0.85	0.19	0.435	0.97
	10%	90%	33.5%	0.8	1.0	0.1	1.7	5.42	0.29	0.417	1.11
	10%	90%	33.5%	1.0	1.0	0.1	1.7	2.68	0.19	0.442	0.96
5.3	10%	90%	33.5%	1.6	1.0	0.1	1.7	2.61	0.20	0.460	0.90
	3%	85%	33.5%	1.0	0.285	0.1	1.7	1.174	0.23	0.399	1.142
	3%	85%	33.5%	1.0	0.428	0.1	1.7	1.031	0.21	0.402	1.110
	3%	85%	33.5%	1.0	0.714	0.1	1.7	0.967	0.2	0.404	1.079
Table 5.4	3%	85%	33.5%	1.0	1.0	0.1	1.7	0.912	0.19	0.406	1.064
	3%	85%	20%	1.0	1.0	0	1.7	1.25	0.22	0.451	1.201
	3%	85%	20%	1.0	1.0	0.05	1.7	1.279	0.21	0.448	1.197
	3%	85%	20%	1.0	1.0	0.10	1.7	1.321	0.2	0.444	1.196
	3%	85%	20%	1.0	1.0	0.15	1.7	1.314	0.18	0.441	1.195
	3%	85%	20%	1.0	1.0	0.20	1.7	1.319	0.16	0.437	1.198
	3%	85%	20%	1.0	1.0	0.25	1.7	1.39	0.15	0.432	1.203
	3%	85%	30%	1.0	1.0	0	1.7	0.97	0.23	0.431	1.093
	3%	85%	30%	1.0	1.0	0.05	1.7	0.951	0.21	0.427	1.084
	3%	85%	30%	1.0	1.0	0.10	1.7	0.99	0.2	0.421	1.074
	3%	85%	30%	1.0	1.0	0.15	1.7	0.988	0.18	0.416	1.067
	3%	85%	30%	1.0	1.0	0.20	1.7	0.996	0.16	0.41	1.063
	3%	85%	30%	1.0	1.0	0.25	1.7	1.021	0.14	0.402	1.066
	3%	85%	36%	1.0	1.0	0	1.7	0.928	0.23	0.407	1.087
	3%	85%	36%	1.0	1.0	0.05	1.7	0.86	0.2	0.402	1.069
	3%	85%	36%	1.0	1.0	0.10	1.7	0.896	0.19	0.396	1.053
	3%	85%	36%	1.0	1.0	0.15	1.7	0.951	0.18	0.387	1.043
	3%	85%	36%	1.0	1.0	0.20	1.7	0.871	0.14	0.381	1.04
	3%	85%	36%	1.0	1.0	0.25	1.7	0.894	0.12	0.372	1.033

Table 5.5	3%	85%	33.5%	1.0	1.0	0.1	0.5	1.93	0.28	0.384	2.102
	3%	85%	33.5%	1.0	1.0	0.1	1.77	0.863	0.18	0.408	1.05
	3%	85%	33.5%	1.0	1.0	0.1	2.04	0.81	0.17	0.411	1.019
	3%	85%	33.5%	1.0	1.0	0.1	2.43	0.78	0.16	0.413	0.974
	3%	85%	33.5%	1.0	1.0	0.1	3.06	0.71	0.14	0.415	0.928
	3%	85%	33.5%	1.0	1.0	0.1	3.40	0.68	0.13	0.416	0.909
	3%	85%	33.5%	1.0	1.0	0.1	3.74	0.66	0.12	0.417	0.892

Nomenclature

a_j	activity of component j (dimensionless)
$a_{\text{CO}_2}^*$	activity of CO_2 in equilibrium with the interface composition
a_{tot}	total packing area per unit volume (1/m)
a_w	wetted packing area per unit volume (1/m)
D	column diameter (m)
D_j	diffusivity of species j in solution (m^2/s)
g_{ji}	energy of interaction for Electrolyte-NRTL model (KJ/Kmol)
eff	stage efficiency
eff_m	modified stage efficiency
E_A	Activation energy (KJ/mol)
f_j	fugacity of species j in solution (atm)
f_j^0	fugacity at a pure component reference state (atm)
f_j^*	fugacity at infinite dilution reference state (atm)
G	gas flow rate in absorber (Kmol/s)
G	Gibb's free energy of mixture (KJ/mol)
G^E	Excess Gibb's free energy
H	Enthalpy of mixture (KJ/mol)
$\Delta H_{\text{abs}, \text{CO}_2}$	Heat of absorption (KJ/mol)
$\Delta H_{\text{vap}, \text{H}_2\text{O}}$	Heat of vaporization of H_2O (KJ/mol)
H^E	Excess enthalpy (KJ/mol)
H_{CO_2}	Henry's constant of CO_2 (atm/M)
$[j]$	concentration of species j (mol/liter)
$[j]_{\text{bulk}}$	concentration of species j at liquid bulk (mol/litr)
$[j]_i$	concentration of species j at the interface (mol/liter)

I_x	Ionic strength of solution (dimensionless)
k_2	rate constant of second order reactions (liter/mol s)
k_g	gas phase mass transfer coefficient (mol/atm cm ² s)
k_g^I	liquid phase mass transfer coefficient with partial pressure driving force (mol/atm cm ² s)
k_l^0	liquid phase physical mass transfer coefficient (m/s)
K	equilibrium constant
K_g	overall mass transfer coefficient with partial pressure driving force (mol/atm cm ² s)
L	Liquid flow (Kmol/s)
N_{CO_2}	Flux of CO ₂ (mol/cm ² s)
n_{CO_2}	moles of CO ₂ reacted in a segment (kmol/s)
P	total pressure (atm)
$P_{CO_2}^{* \text{ bulk}}$	partial pressure of CO ₂ in equilibrium with liquid bulk (atm)
$P_{CO_2}^{* i}$	partial pressure of CO ₂ in equilibrium with interface composition (atm)
$P_{CO_2,i}$	partial pressure of CO ₂ at the interface (atm)
Q_r	Reboiler duty (MJ)
Q_{rel}	Relative reboiler duty (dimensionless)
R	Universal gas constant (8.314 KJ/Kmol K)
S	Column cross sectional area (m ²)
S	Entropy of mixture (KJ/mol ⁰ K)
S^E	Excess entropy (KJ/mol ⁰ K)
T	Temperature (⁰ K)
V	vapor flow rate in stripper (Kmol/s)
w_j	mass fraction of species j
x_j	liquid mole fraction of species j
y_j	gas mole fraction of species j

z	height of a segment (m)
Z	height of packing in a column (m)
α	non-randomness factor for Electrolyte-NRTL model
α	CO ₂ loading
β	heat stable salts loading
δ	boundary layer thickness
γ_j	activity coefficient of species j with reference state at pure component
γ_j^*	activity coefficient of species j with reference state at infinite dilution
γ_j^∞	infinite dilution activity coefficient with reference state of pure component
σ	standard deviation
ν_j	stoichiometric coefficient of component j
τ	interaction parameter for Electrolyte-NRTL model

References

- Al-Baghli, N.A., Pruess, S.A., Yesavage, V.F., Selim, M.S., "A rate-based model for the design of gas absorbers for the removal of CO₂ and H₂S using aqueous solutions of MEA and DEA", *Fluid Phase Equilibria.*, 185, 31-43, 2001.
- Alvarez-Fuster, C., Midoux, N., Laurent, A., Charpentier, J.C., « Chemical Kinetics of the Reaction of Carbon Dioxide with Amines in Pseudo m-nth Order Conditions in Aqueous and Organic Solutions», *Chem. Eng. Sci.*, 35, 1717-1723, 1980.
- Austgen, D.M., A Model for Vapor-Liquid Equilibrium for Acid gas-Alkanolamine-Water Systems. Ph.D dissertation, The University of Texas at Austin, 1989.
- Austgen, D.M., Rochelle, G.T., Chen, C.C., « A Model for Vapor-Liquid Equilibria for Aqueous Acid Gas-Alkanolamine Systems Using the Electrolyte-NRTL Equation», *Ind. Eng. Chem. Res.*, 28(7), 1060, 1989.
- Bishnoi, S., Physical and Chemical Solubility of Carbon Dioxide in aqueous methyldietanolamine. Master Report, the University of Texas at Austin, 1998.
- Bishnoi, S., Carbon Dioxide Absorption and Solution Equilibrium in Piperazine Activated Methyldietanolamine. Ph.D. dissertation, The University of Texas at Austin, 2000.
- Blauwhoff, P.M.M., Versteeg, G.F., Van Swaaij, "A Study on the Reaction Between CO₂ and Alkanolamines in Aqueous Solutions", *Chem. Eng. Sci.*, 39,2,207, 1984.
- Carey, T.R., Rate-Based Modeling of Acid Gas Absorption and Stripping Using Aqueous Alkanolamine Solutions. Master Thesis, The University of Texas at Austin, 1990.

Chen, C.C., Britt, H.I., Boston, J.F., Evans, L.B., "Extension and Application of the Pitzer Equation for Vapor-Liquid Equilibrium for Aqueous Electrolyte Systems with Molecular Solutes", *AIChE J.*, 25(5), 820, 1979.

Chen, C.C., Evans, L.B., "A Local Composition Model for the Excess Gibbs Energy of Aqueous Electrolyte Systems", *AIChE, J.*, 32(3), 444-454, 1986.

Chen, C.C., Britt, H.I., Boston, J.F., Evans, L.B., "Local Composition Model for Excess Gibbs Energy of Electrolyte Systems, Part I: Single Solvent, Single Completely Dissociated Electrolyte", *AIChE, J.*, 28(4), 588-596, 1982.

Clarke, J.K.A., "Kinetics of Absorption of Carbon Dioxide in Monoethanolamine Solutions at Short Contact Times", *I & EC Fundamentals* 3(3), 239-245, 1964.

Cullinane, J.T., Carbon Dioxide Absorption in Aqueous Mixtures of Potassium Carbonate and Piperazine. Master Thesis, The University of Texas at Austin, 2002.

Dang, H., CO₂ Absorption Rate and Solubility in Monoethanolamine/Piperazine/Water. Master Thesis, the University of Texas at Austin, 2001.

Danckwerts, P.V., Sharma, M.M., "The Absorption of Carbon Dioxide into Solutions of Alkalis and Amines", *Chemical Engineer*, 10, CE244, 1966.

Dantus, M., Rochelle, G.T., "Modeling CO₂ Capture from Flue Gas, A Report for Work done from 6/1/99 to 10/31/99", The University of Texas at Austin, 1999.

Deming, W.E., *Statistical Adjustment of Data*, Wiley, New York (1943).

Hikita, H., Asai, S., Ishikawa, H., Honda, M., "The Kinetics of Reactions of Carbon Dioxide with Monoethanolamine, Diethanolamine and Triethanolamine by a Rapid Mixing Method", *Chem. Eng. J.*, 13, 7-12, 1977.

Holmes, J.W., Spears, M.L., Bullin, J.A., "Sweetening LPG's with amines", *Chem. Eng. Prog.*, 80(5), 47-50, 1984.

Jou., F.Y., Mather, A.E., Otto, F.D., "The Solubility of CO₂ in a 30 Mass Percent Monoethanolamine Solution", *Can. J. Chem. Eng.*, 73, 140-147, 1995.

King, C.J., "Turbulent liquid phase mass transfer at a free gas-liquid interface", *Ind. Eng. Chem. Fund.*, 5, 1, 1-8, 1966.

- Kohl, A.L., Nielsen, R.B., *Gas Purification*, 5th edition, Houston, 1997.
- Lee, J.I., Otto, F.D., Mather, A.E., "Equilibrium Between Carbon Dioxide and Aqueous Monoethanolamine Solutions", *Appl. Chem. Biotechnol.*, 26, 541-549, 1976.
- Lewis, W.K., Whitman, W.G., "Principles of Gas Absorption", *Ind. Eng. Chem.*, 16, 12, 1924.
- Littel, R.J., Versteeg, G.F., Van Swaaij, W.P.M., "Kinetics of CO₂ with Primary and Secondary Amines in Aqueous Solutions-I. Zwitterion Deprotonation Kinetics for DEA and DIPA in Aqueous Blends of Alkanolamines", *Chem. Eng. Sci.*, 47, 2027-2035, 1992.
- Littel, R.J., Versteeg, G.F., Van Swaaij, W.P.M., "Kinetics of CO₂ with Primary and Secondary Amines in Aqueous Solutions-II. Influence of Temperature on Zwitterion Formation and Deprotonation Rates", *Chem. Eng. Sci.*, 47, 2037-2045, 1992.
- Liu, Y., Zhang, L., Watanasiri, S., "Representing Vapor-Liquid Equilibrium for an Aqueous MEA-CO₂ System Using the Electrolyte Nonrandom-Two-Liquid Model", *Ind. Eng. Chem. Res.*, 38, 2080-2090, 1999.
- Mock, B., Evans, L.B., Chen, C.C., "Thermodynamic Representation of Phase Equilibria of Mixed-Solvent Electrolyte Systems", *AIChE J.*, 32(10), 1655-1664, 1986.
- Mshewa, M.M. Carbon Dioxide Desorption/Absorption with Aqueous Mixtures of Methyldiethanolamine and Diethanolamine at 40 to 120 °C. Ph.D. Dissertation, The University of Texas at Austin, 1995.
- Onda, K., Takeuchi, H., Okumoto, Y., "Mass transfer coefficients between gas and liquid phases in packed columns", *Journal of Chemical Engineering of Japan*, 56,1, 1968.
- Pacheco, M.A., Mass Transfer, Kinetics and Rate-Based Modeling of Reactive Absorption. Ph.D. Dissertation, The University of Texas at Austin, 1998.
- Penny, D.E., Ritter, T.J., "Kinetic Study of the Reaction between Carbon Dioxide and Primary Amines", *J. Chem. Soc., Faraday Trans.*, 79, 2103-2109 (1983).

Pinsent, B.R.W., Pearson, L., and Roughton, F.J.W., "The kinetics of combination of CO₂ with NH₃," *Trans. Faraday Soc.*, 52, 1594 (1956).

Posey, M.L. Thermodynamic Model for Acid Gas Loaded Aqueous Alkanolamine Solutions. Ph.D. Dissertation, The University of Texas at Austin, 1996.

Renon, H., Prausnitz, J.M., "Local Compositions in Thermodynamic Excess Functions for Liquid Mixtures. *AICHE J.*, 14(1), 135, 1968.

Rochelle, G.T., "Process Synthesis and Innovation in Flue Gas desulfurization", EPRI-FP-463-SR, 1977.

Rochelle, G.T., Bishnoi, S., Chi, S., Dang, H., "Research Needs for CO₂ Capture from Flue Gas by Aqueous Absorption/Stripping", Final report, U.S. Dept. of Energy, Federal Energy Technology Center, P.O. No. DE-AF26-99FT01029, 2001.

Rowley, R.L., Diffusion coefficients in aqueous alkanolamines., GRI/GPA Research Report RR-163. GPA Project 911, GRI Contract #5092-260-2356., 1999.

Scaufaire, P., Richards, D., Chen, C.C., "Ionic Activity Coefficients of Mixed-Solvent Electrolyte Systems", *AICHE J.*, submitted (1989).

Sherwood, T.K., Pigford, R.L., Wilke, C.R., *Mass Transfer*, McGraw-Hill, New York (1975).

Shethna, H.K., Towler, G.P., "Design of Mixed-Solvent Processes for Chemisorption with Ultrahigh Recovery", *Ind. Eng. Chem. Res.*, 36(12), 5037-5320, 1997.

Shoeld, M. Purification and separation of gaseous mixtures. U.S. Patent 1,971,798, 1934.

Versteeg, G.F., van Swaaij, W.P.M., "Solubility and Diffusivity of Acid Gases (CO₂, N₂O) in Aqueous Alkanolamine Solutions", *J. Chem. Eng. Data*, 33, 29, 1988.

Wang, Y.W., Xu, S., Otto, F.D., Mather, A.E., "Solubility of N₂O in alkanolamines and in mixed solvents", *Chem. Eng. J.*, 48, 31-40 (1992).

Weiland, R.H., "Physical Properties of MEA, DEA, MDEA and MDEA-Based Blends Loaded with CO₂", GRI/GPA Research Report RR-152. GPA project 911, 1996.

Weiland, R.H., “Reaction Kinetics of CO₂ with MEA, DEA and MDEA and in MDEA-Based Blends”, GPA/GRI research report, GPA project number 911, 1996.

Won, K.W., Scherffius, J.R., Condorelli, P., “Improved Econamine FG Processsm and Economic Evaluation”, Fluor Daniel internal paper, 1999.

Zhang, D.D., Ng, H.J., “Modeling of liquid hydrocarbon sweetening with amine solutions”, Proc., Annu. Conv. – Gas Process. Assoc., 75th, 22-26, 1996.

Vita

Stefano Freguia was born August 7, 1977 in Desio, Italy, the son of Ermenegildo Freguia and Giovanna Crippa. He enrolled at Politecnico di Milano, in Milan, Italy, in 1996, after completing his secondary education at Liceo Scientifico Marie Curie in Meda, Italy. After three years of attendance at Politecnico di Milano, he was awarded a European Union scholarship to participate in an exchange program with The University of Texas at Austin, where he completed his senior year. He began his graduate studies at The University of Texas at Austin in August, 2000.

Full time employment has been accepted with Fluor Corp. after graduation in Aliso Viejo, California.

Permanent Address: Via Bari, 1 20030 Camnago (MI), Italy

This thesis was typed by the author.